Multiscale Mapping of Transcriptomic Signatures for Cardiotoxic Drugs

Supplementary Information

Jens Hansen,[1,2] Yuguang Xiong,[1,2] Mustafa Siddiq,[1,2] Priyanka Dhanan,[1,2] Bin Hu,[1,2] Bhavana Shewale,[1,3] Arjun S. Yadaw,[1,2] Gomathi Jayaraman,[1,2] Rosa Tolentino,[1,2] Yibang Chen,[1,2] Pedro Martinez, [1,2] Kristin G. Beaumont,[4] Robert Sebra,[4] Dusica Vidovic,[5] Stephan C. Schürer,[5] Joseph Goldfarb,[1,2] James Gallo,[2,6] Marc R. Birtwistle,[1,7] Eric A. Sobie,[1,2] Evren U. Azeloglu,[1,2,8] Seth Berger,[9] Angel Chan,[1,10] Christoph Schaniel,[1,11] Nicole C. Dubois,*[,1,3] Ravi Iyengar*[,1,2]

1 Mount Sinai Institute for Systems Biomedicine, Icahn School of Medicine at Mount Sinai, New York, NY 10029, USA
2 Department of Pharmacological Sciences, Icahn School of Medicine at Mount Sinai, New York, NY 10029, USA
3 Department of Cell, Developmental and Regenerative Biology, Icahn School of Medicine at Mount Sinai, New York, NY 10029, USA
4 Department of Genetics and Genomic Sciences, Icahn School of Medicine at Mount Sinai, New York, NY 10029, USA
5 Institute for Data Science and Computing, University of Miami, Coral Gables, FL 33146, USA
6 School of Pharmacy and Pharmaceutical Sciences, University of Buffalo SUNY System, Buffalo, NY 14260, USA
7 Chemical and Biomolecular Engineering, Clemson University, Clemson, SC, 29634, USA
8 Department of Medicine, Division of Nephrology, Icahn School of Medicine at Mount Sinai, New, York, NY 10029, USA
9 Center for Genetic Medicine Research, Children's National Research Institute, Washington DC USA, 20012, Washington, DC 20012, USA
10 Cardiology Division, Department of Medicine, Memorial Sloan Kettering Cancer Center New York, NY 10065, USA
11 Department of Medicine, Division of Hematology and Medical Oncology, Tisch Cancer Institute, Icahn School of Medicine at Mount Sinai, New York, NY 10029, USA

*These authors jointly supervised this work.

Address correspondence to
Jens Hansen - jens.hansen@mssm.edu
or
Nicole Dubois - nicole.dubois@mssm.edu
or
Ravi Iyengar - ravi.iyengar@mssm.edu

Supplementary Note 1

Organization of Supplementary Information in two parts

The supplementary information is organized in two parts. The first part contains the supplementary notes 1 and 2, most supplementary figures and supplementary tables. The second part contains supplementary figures with very detailed information that can span multiple pages. For the first investigation of our supplementary information, we suggest to focus (and eventually print) only the first part (pages 1 - 78) that includes referenced page positions for the figures of the second part.

Part 1: Pages 1-78: Main Supplementary Information

- Page 2: Supplementary Note 1
- Pages 2-10: Supplementary Note 2
- Pages 11-75: Most Supplementary Figures
- Pages 76-78: Supplementary Tables

Part 2: Pages 79-341: Supplementary Figures with very detailed information

- Pages 79-93: Supplementary Figure 11
- Pages 94-97: Supplementary Figure 12
- Pages 98-111: Supplementary Figure 14B
- Pages 112-125: Supplementary Figure 14C
- Pages 126-139: Supplementary Figure 14D
- Pages 140-154: Supplementary Figure 14E
- Pages 155-173: Supplementary Figure 17
- Pages 174-182: Supplementary Figure 29

Supplementary Note 2

Drug-selective gene expression profiles allow for identification of SCPs which agree with prior knowledge of SCPs associated with cardiac diseases and drug effects

Up- and downregulated genes in each cell line/drug combination were subjected to enrichment analysis using the Molecular Biology of the Cell Ontology (MBCO) [28] and Fisher's exact test. Predicted subcellular processes (SCPs) were ranked by decreasing significance for each list of genes and SCP level. We will refer to these ranks as enrichment ranks.

As outlined in the main text, the SVD-based identification of drug-selective gene expression profiles greatly increased the number of predicted SCPs that are up- or downregulated in at least two of three, three of four, four of five or four of six cell lines (i.e., ≥ 66%) by the same drugs (Supplementary Fig. 15A). The median overlap between downregulated level-1, -2, -3, -4 SCPs among the top 5, 5, 10 and 5 predicted SCPs increased from 2 to 3.5, 1 to 3, 1 to 4 and 0 to 1, respectively. The median overlap between upregulated level-1, -2, -3, -4 SCPs among the top 5, 5, 10 and 5 predicted SCPs increased from 1 to 3, 0 to 3, 1 to 4 and 0 to 1, respectively. These results depend on the complete SVD-pipeline, since removal of the first eigenarray alone improved the median number of drug-selective overlapping up- or downregulated SCPs in only one case (upregulated level-2 SCPs, from 0 to 1).

Analysis of drug-selective gene expression profiles enabled identification of enrichment patterns that were obscured within the complete gene expression profiles. For example, our decomposition pipeline allowed identification of SCPs that were selectively downregulated by the group of anthracyclines that have high rates of cardiotoxicity [100]. These SCPs are involved in iron metabolism and single protein turn-over (Supplementary Fig. 14/B/C/D/E). They form parent-child relationships within three MBCO branches (Supplementary Fig. 15B). The observed downregulation of 'Cellular iron storage' is in agreement with the suggested interference of anthracyclines with iron metabolism [101] and ferroptosis as a disease mechanism involved in heart failure [38]. The clinical relevance of our unbiased findings from transcriptomic data is suggested by the use of iron chelators as supportive therapy [42], though the protective effect of iron chelators might involve mechanisms that are not primarily targeting iron homeostasis [43]. Identified down-regulation of SCPs involved in protein degradation might explain cardiotoxicity by interference with sarcomere turn-over [30], as supported by the cardiotoxic effects of proteasome inhibitors [102]. The almost exclusive downregulation of these SCPs by anthracyclines could not be documented using the complete gene expression profiles (Supplementary Fig. 15C).

SCPs predicted from the drug-selective gene expression profiles of other drugs often describe functions that are supported by prior knowledge as well, based on transcriptomic and orthogonal methodologies.

For example, enrichment analysis of nilotinib-selective gene expression profiles leads to a more consistent prediction of upregulated SCPs involved in centrosome and mitotic spindle dynamics as well as mitosis compared to analysis of nilotinib's complete gene expression profiles (Supplementary Fig. 14B/C/D). Similar results were obtained for the kinase inhibitors imatinib, ponatinib, sorafenib and regorafenib. In agreement, previous morphological analysis documents centrosome aberrations and mitotic spindle defects induced by treatment of primary human fibroblasts with imatinib or nilotinib [103]. Centrosome defects were also observed in disease-unaffected cells from patients treated with imatinib, nilotinib, sorafenib, sunitinib, dasatinib and bosutinib [104].

There are two MBCO level-3 SCPs that refer to increased cholesterol synthesis activity, 'Cholesterol synthesis' and 'Cholesterol-sensitive control of SREBP activation'. Though multiple drugs upregulate these SCPs at varying ranks, analysis of lapatinib-selective gene

expression profiles predicts upregulation of both SCPs at top enrichment ranks (5x rank 1 and ranks 2, 3, 4, 5, 6, respectively) (Supplementary Fig. 14D). In agreement, mevalonate pathway activity was found to be increased in lapatinib-resistant and lapatinib + trastuzumab–resistant cells [105]. Resistance was reversed by statin treatment that inhibits cholesterol synthesis.

SCPs associated with cardiotoxic and non-cardiotoxic responses to TKI treatment describe cellular dysfunctions involved in drug-independent cardiomyopathy development.

In the main text, we briefly describe SCPs involved in muscle contraction and sarcomere renewal, energy metabolism and ferroptosis. Here, we discuss identified and additional pathways in more detail.

Our F1 score and AUC statistics generate lists of SCPs that are up- or downregulated by cardiotoxic or non-cardiotoxic TKIs. Within each toxicity group combined up- and downregulated SCPs were ranked by decreasing AUC. We will refer to these ranks as AUC ranks to distinguish them from the enrichment ranks that are described above.

As already indicated in the main results section, we distinguish between SCPs whose activity for an association with a cardiotoxic response reaches sufficient levels after TKI treatment or is already sufficient at baseline levels. The first set of SCPs was identified by screening for those SCPs that are up- or downregulated at higher ranks by cardiotoxic TKIs, as compared to non-cardiotoxic TKIs. Treatment with a cardiotoxic TKI might change the SCP activity beyond a threshold that separates non-association from association with a cardiotoxic response. Treatment with a non-cardiotoxic TKI might move the SCP activity across the threshold in the opposite direction, changing its status from sufficient to insufficient for association with a cardiotoxic response. Both sets of SCPs can be organized based on the SCP activity that favors a cardiotoxic response. SCPs upregulated by cardiotoxic TKIs and downregulated by non-cardiotoxic TKIs are SCPs whose higher activity could favor a cardiotoxic response (‘bad SCPs’). In contrast, SCPs downregulated by cardiotoxic TKIs and upregulated by non-cardiotoxic TKIs are SCPs whose lower activity could favor a cardiotoxic response (‘good SCPs’). We use this classification in comparing the inferred SCPs from this data set to previously published data, since presence or absence of sufficient SCP activity is associated with presence or absence of cardiomyopathy development. We followed this principle in our figures as well. For SCPs that are upregulated by cardiotoxic and downregulated by non-cardiotoxic TKIs we use the colors red and orange, respectively (Supplementary Figs. 17 and 18). For SCPs downregulated by cardiotoxic and upregulated by non-cardiotoxic TKIs we use the colors blue and light blue, respectively. The same color scheme was applied in our network-based visualization that integrates identified SCPs into the MBCO parent-child hierarchy and groups SCPs participating in similar functions into the same module (Fig. 2C, Supplementary Fig. 19).

For both TKI groups we focused on the top 10 level-1, 10 level-2, 25 level-3 and 10 level-4 SCPs based on increasing AUC ranks (Supplementary Fig. 18). Six level-1, two level-2, eleven level-3 and four level-4 of those SCPs were predicted to be relevant for cardiotoxicity and regulated by both TKI groups in the opposite direction. In these cases, both TKI groups link the same SCP activities (i.e., higher or lower) to be associated with a cardiotoxic response. This approach was mostly successful. We only obtained conflicting results for one level-4 SCP that was downregulated by both TKI groups.

Identified SCPs were mapped back to the TKIs that increase or decrease their activity. To document which TKIs contributed to the identification of an SCP we show which cardiotoxic (Supplementary Fig. 20) or non-cardiotoxic (Supplementary Fig. 21) TKIs up- or downregulate an identified SCP at specified enrichment ranks.

Sarcomere dynamics

SCPs involved in muscle contractility were discussed in the main section. Here we want to add some more details. Identified level-1 SCP ‘Cellular contraction’, its level-3 grandchild SCPs ‘Thin myofilament organization’, ‘Myofibril formation’ and the level-4 SCPs ‘Actin filament depolymerization’ and ‘Myoglobin synthesis’ (Fig. 2B, Supplementary Fig. 19), are all involved in dynamics and turnover of the sarcomere, as already described in the main results section. The identified SCPs whose lower activities favor a cardiotoxic response, belong to those SCPs that were identified with evidence for both the cardiotoxic and non-cardiotoxic group: four of five SCPs were downregulated by cardiotoxic TKIs and at the same time upregulated by non-cardiotoxic TKIs (Supplementary Fig. 18). In addition, the level-2 SCP ‘Myofibril formation and organization’, a child of ‘Cellular contraction’ is identified (Supplementary Fig. 19), because it is downregulated by the non-cardiotoxic TKIs (Supplementary Fig. 18). Overall, all cardiotoxic TKIs, except vandetinib and trastuzumab downregulate (Supplementary Fig. 20), while 13 of 17 non-cardiotoxic TKIs upregulate (Supplementary Fig. 21) at least one of the contractility-related SCPs in one to six or one to five cell lines, respectively. Four of six SCP genes of the SCP ‘Thin myofilament organization’ that are inhibited by cardiotoxic and induced by non-cardiotoxic TKIs are components of tropomyosin or inhibitory troponin. Both complexes interact to block the binding of the myosin head to the thin myofilament during muscle contraction. This mechanism is also targeted by the new drug mavacamten that was recently approved by the FDA to treat obstructive HCM [33], suggesting clinical relevance of our findings.

Electrical transmission

Four cardiotoxic TKIs, trametinib, trastuzumab, lapatinib and bevacizumab upregulate ‘Potassium transmembrane transport’ in three of four (enrichment ranks 2, 3, 9), two of three (7, 10), two of five (7, 10) and one of four (17) cell lines (Fig. 2B, Supplementary Fig. 20), respectively. The SCP with an AUC rank of 7 (Fig. 2B, Supplementary Fig. 18) is predicted based on potassium channels, transporters and components of the sodium potassium ATPase

(Supplementary Data 11). Among the SCP genes is *SUR2A* coding for a regulatory subunit of the cardiac ATP-sensitive potassium channel involved in genetic DCM [106].

The level-3 SCP 'Gap junction organization' is predicted with an AUC rank of 24 for the cardiotoxic TKIs (Fig. 2B, Supplementary Fig. 18). It is downregulated by the cardiotoxic TKI dabrafenib in one of five (enrichment rank 24), pazopanib in two of six (1, 3), ponatinib in three of six (15, 16, 17), vandetinib in one of three (9) and vevacizumab in four of four (13, 2x14, 15) treated cell lines (Supplementary Fig. 20). In agreement, multiple connexins that form the building block of gap junctions are downregulated in explanted heart from patients with idiopathic cardiomyopathy [107].

Energy metabolism

We identified multiple SCPs that suggest interference with cardiac energy metabolism as a major trigger for TKI-induced cardiotoxicity.

The level-2 SCPs 'Mitochondrial energy production', 'Fatty acid metabolism', 'Carbohydrate metabolism and transport' and 'Post-translational protein modification in Mitochondria' were upregulated by cardiotoxic TKIs with the AUC ranks one to four, respectively (Supplementary Fig. 18). Their upregulated level-3 child SCPs 'Citric acid cycle' and 'Desaturation of fatty acids' were predicted with AUC ranks 1 and 11, respectively (Fig. 2B, Supplementary Figs. 18, 19). Three of these level-2 and -3 SCPs map to ventricular cardiomyocytes in the adult heart (Fig. 3A, Supplementary Fig. 23) as the cell type with the highest energy requirement. These SCPs that interact with each other to ensure energy supply were almost exclusively predicted based on their induction by pazopanib (Supplementary Fig. 20), a TKI with a high rate of cardiotoxicity (>10%) (Supplementary Data 3). Genes of these SCPs induced by pazopanib are involved in the citric acid cycle and oxidative phosphorylation, fatty acid activation, elongation and desaturation as well as glucose import, release from glycogen and degradation (Supplementary Data 11).

Many studies document an overall reduction in oxidative phosphorylation during heart failure [34], in agreement with the enrichment results obtained in adult and hiPSC-derived DCM and adult HCM cardiomyocytes (Fig. 3B, Supplementary Fig. 24). Nevertheless, compensatory upregulation of oxidative phosphorylation was suggested for a large DCM subgroup that is caused by truncating titin variants [35-37]. Another prominent molecular phenotype observed in these studies is a shift from fatty acid oxidation towards glycolysis. Upregulated genes mapping to carbohydrate catabolism and fatty acid anabolism might support such interpretation of our data as well, though the level-3 and -4 child SCPs that specifically describe these functions, were not among the top predictions. For the non-cardiotoxic TKIs, we predict the level-2 SCP 'Carbohydrate metabolism and transport' and its level-3 child 'Glycolysis and Gluconeogenesis' at ranks 1 and 25, respectively (Supplementary Figs. 18 and 19), based on a set of partly overlapping genes (Supplementary Data 11B and C), further supporting glucose utilization as a cellular function whose higher activity favors a cardiotoxic response to TKI-treatment.

Polyunsaturated fatty acids (PUFAs) generated by genes mapping to the upregulated SCP "Fatty acid desaturation" (Supplementary Data 11C) [39,40] can be deoxygenized by lipoxygenases, resulting in cardiotoxic PUVA hydroperoxides [38]. PUVA hydroperoxides are a main stimulator of ferroptosis, a potentially major mechanism involved in heart failure.

The involvement of ferroptosis in drug-induced cardiomyopathy was also predicted for the cardiotoxic anthracyclines based on the downregulation of 'Cellular iron storage' (Supplementary Figs. 14D, 15B), as discussed above. However, upregulated transporter activities involved in import of iron-containing molecules, such as transferrin or haptoglobin-hemoglobin complexes, are predicted as part of the level-3 SCP 'Cellular iron uptake and export' for the non-cardiotoxic TKIs with AUC rank 23 (Supplementary Fig. 18). These seemingly contradictory results could indicate that it is the balance in cellular iron content rather than an increase or decrease of iron levels that is associated with cardiotoxicity.

The level-3 SCP 'Serine and glycine metabolism' was identified for cardiotoxic and non-cardiotoxic TKIs as an SCP whose higher activity indicates a cardiotoxic response with the AUC ranks 19 and 5, respectively (Supplementary Fig. 18). Seven cardiotoxic (Supplementary Fig. 20) and twelve non-cardiotoxic (Supplementary Fig. 21) TKIs up- and downregulate this SCP, respectively, in one to six cell lines. Dabrafenib, a TKI with a cardiotoxicity frequency between 1 and 10%, upregulated this SCP in all five cell lines with top enrichment ranks (3x1, 2, 3), followed by pazopanib (ranks 2x2, 3, 4, 5) (Supplementary Fig. 20). Identified SCP genes are involved in serine and glycine biosynthesis (Supplementary Data 11C). Stimulation of serine biosynthesis in hiPSC-derived cardiomyocytes from patients with genetic DCM rescues contractile dysfunction in-vitro by increasing the glucose flux into the citric acid cycle and oxidative phosphorylation [108]. The seemingly contradictory findings could indicate a compensatory upregulation of mRNAs coding for serine and glycine metabolism proteins or suggest that levels of serine could be a driver of energy balance in cardiomyocytes. These hypotheses needs to be experimentally verified.

Two level-3 SCPs involved in cholesterol synthesis and another SCP predicted based on genes involved in cholesterol export (Supplementary Data 11C) were up- and downregulated by the cardiotoxic TKIs, with the AUC ranks 15, 22 and 23, respectively (Fig. 2B, Supplementary Fig. 18). Both synthesis SCPs were also downregulated by non-cardiotoxic drugs, with the AUC ranks 3 and 24. Our results link higher intracellular cholesterol levels, either based on increased synthesis or decreased export, to a cardiotoxic response. While six cardiotoxic (Supplementary Fig. 20) and eleven non-cardiotoxic (Supplementary Fig. 21) TKIs induce the described pathway activities in opposite directions with varying enrichment ranks, it is, in particular, the cardiotoxic TKI lapatinib that upregulates both cholesterol synthesis SCPs with top enrichment ranks (5x1 and 2, 3, 4, 5, 6). Our observations agree with the results of a meta-analysis documenting a cardioprotective effect of statin treatment against chemotherapy-induced cardiomyopathy [44], though statins might induce multiple cardioprotective mechanisms besides inhibition of HMG-CoA reductase, the rate-controlling enzyme in cholesterol synthesis [109].

Since lapatinib resistance of breast cancer cells due to increased cholesterol synthesis could be reversed *in-vitro* by statin treatment [105], our results might suggest a potential effect of statin treatment on lapatinib's cardiotoxicity as well. Potential detrimental effects of statin treatment in heart failure [110] and involvement of cholesterol biosynthesis intermediates in the antioxidant defense against ferroptosis [38] might indicate the need for correct balance of cholesterol homeostasis and TKI-selective supportive statin therapy.

Cellular antioxidant systems

The level-1 and -2 SCPs 'Cellular redox homeostasis' and 'Cellular antioxidant defense systems' in parent-child relationships (Supplementary Fig. 19) were predicted with AUC ranks 2 and 5 (Supplementary Fig. 18), respectively. Both were downregulated by vandetinib in three of three (enrichment ranks 3, 4, 5 and 3, 4, 7) and bevacizumab in two of four (6, 7 and 7, 8) treated cell lines (Supplementary Fig. 20). Multiple animal models document involvement of oxidative stress in heart failure and oxidative stress biomarkers are increasingly used in the monitoring of heart failure patients [111]. Reduction of oxidative stress is a protective mechanism against ferroptosis [38], a cardiotoxic mechanism that is also suggested based on other identified SCPs.

Posttranslational protein modification and translational quality control

The cardiotoxic TKI dabrafenib upregulates the level-1 SCP 'Posttranslational protein modification' and its level-2 child SCP 'Posttranslational protein modification and quality control during secretory pathway' (Supplementary Fig. 19) in two of five treated cell lines (both enrichment ranks 1, 2) (Supplementary Fig. 20). Both SCPs were predicted for the cardiotoxic drugs with AUC ranks of 1 and 7, respectively (Supplementary Fig. 18). Many of the upregulated SCP genes participate in protein folding, quality control and stress response in the endoplasmic reticulum (ER) (Supplementary Data 11B). Their upregulation could be a response to protein accumulation in the ER that can be differentiated into two phases [112]. The initial physiological ER stress response of the heart addresses the accumulation of proteins in the ER, while in case of prolonged stress a pathological response triggers autophagy and apoptosis.

Cellular signaling pathways

Among the identified signaling pathways were PDGF, Natriuretic receptor, HIF-1 alpha, Oncostatin M and Hippo signaling (Fig. 2B, Supplementary Fig. 18).

PDGF signaling was identified as an SCP that favors a non-cardiotoxic response with the AUC rank 14 (Fig. 2B, Supplementary Fig. 18) and preferentially maps to cardiac fibroblasts and smooth muscle cells in the adult human heart (Fig. 3A, Supplementary Fig. 23). It is downregulated by seven cardiotoxic TKIs in one to six cell lines (Supplementary Fig. 20). Ponatinib (cardiotoxicity 1-10%), trastuzumab (>10%) and sorafenib (1-10%) downregulated

the SCP in all treated cell lines (enrichment ranks 4, 3x6, 13; 2, 4, 5, 11 and 5, 6, 10, 15, respectively). In agreement with our results, PDGF and PDGF signaling in the heart increase during disease states and are generally considered to play an important role during cardioprotection [113], as supported by the PDGF-induced increase in cell survival and contractility of engineered cardiac tissue [114,115].

The level-4 SCPs 'Atrial -', 'Brain-' and 'C-type natriuretic receptor signaling' and their level-3 parent SCP 'Natriuretic peptide receptor signaling' (Supplementary Fig. 19) were identified to favor a non-cardiotoxic response (Supplementary Fig. 18). They were upregulated by six, four, two and six overlapping non-cardiotoxic drugs in one to four cell lines, respectively (Supplementary Fig. 21). The SCP 'Atrial natriuretic peptide receptor signaling' was additionally downregulated by the three cardiotoxic TKIs lapatinib, ponatinib and vandetanib in one of their treated cell lines (enrichment ranks 4, 4 and 2, respectively). Induced genes contain the ligands *NPPA*, *NPPB* and *NPPC* as well as receptor genes (Supplementary Data 11C and D). Though our data was generated *in vitro*, the classification into cardiotoxic and non-cardiotoxic drugs is based on clinical data. A potential explanation for the identified association could be that both secreted ANP and BNP have a protective effect on cardiac preload, afterload and cardiovascular growth [116]. The endopeptidase neprilysin degrades several endogenous vasoactive peptides including natriuretic peptides [117]. Treatment schemes of patients with chronic heart failure that combine neprilysin and angiotensin II receptor inhibition achieve better results than treatment with an angiotensin converting enzyme (ACE) inhibitor [45,46], suggesting clinical relevance of our findings [117].

We identified genes involved in the inhibition of HIF-1 alpha signaling (Supplementary Data 11C) as associated with a non-cardiotoxic response with the AUC rank 20 (Fig. 2B, Supplementary Fig. 18). They were downregulated by the two cardiotoxic TKIs dabrafenib and pazopanib in two (enrichment ranks 8, 8) and three (1, 6, 6) of five treated cell lines, respectively (Supplementary Fig. 20). In agreement, only short-term HIF-1 signaling in acute stress situations has a cardioprotective effect, while continuously active HIF-1 signaling might be harmful [118], suggesting an explanation of why its inhibition under long-term TKI treatment might improve cardiac outcomes.

A similar effect was described for Oncostatin M (OSM) receptor signaling that favors a cardiotoxic response (Supplementary Fig. 18), since it is downregulated by two non-cardiotoxic TKIs in two and four cell lines (Supplementary Fig. 21). Stimulation of OSM signaling cascades mitigates cardiac damage in acute stress conditions, while its chronic activation contributes to the development of heart failure [119].

The level-3 SCP 'Hippo signaling' was downregulated by cardiotoxic TKIs with an AUC rank of 13 (Fig. 2B, Supplementary Fig. 18). Pazopanib downregulates this SCP in three of five treated cell lines (enrichment ranks 1, 2x6) (Supplementary Fig. 20). It preferentially maps to cardiac fibroblasts in the adult human heart (Supplementary Fig. 23). Five of six downregulated genes inhibit the Hippo downstream transcription factor YAP1 (Supplementary Data 11C). Consistent

with this finding, increased YAP activity and expression of hypertrophic target genes was also observed in HCM patient tissue and a HCM murine model [120].

Extracellular matrix organization

Fibrillar collagen constitutes the most abundant protein in the cardiac extracellular matrix (ECM) which provides structural organization for the correct alignment of cardiomyocytes, generates myocardial stiffness and helps in force transmission [121]. Diffuse interstitial fibrosis, a histopathological feature observed in non-ischemic cardiomyopathies or hypertensive heart disease is characterized by excessive deposition of type I and III collagen, by changing ratios of type I to type III collagen and by an increase in collagen crosslinking. The degree of collagen crosslinking, but not total collagen deposition correlates with surrogate parameters (e.g., myocardial stiffness) or hospitalization in patients with hypertensive heart disease [47,48]. In agreement, 'Collagen fiber cross-linking' is downregulated by eleven non-cardiotoxic TKIs in one to six cell lines (Supplementary Fig. 21), identified with the AUC rank 7 and consequently categorized as an SCP that favors a cardiotoxic response (Supplementary Fig. 18). Downregulation of the SCP 'Elastin cross-linking and assembly' (AUC rank 16) is predicted based on genes shared with the collagen-cross linking SCP. The SCP 'Collagen fibril organization by fibril-associated bridges' that contains the FACIT collagens is upregulated by eleven non-cardiotoxic TKIs in one to six cell lines (Supplementary Fig. 21) and was identified with the AUC rank 17 as an SCP whose higher activity favors a non-cardiotoxic response (Supplementary Fig. 18). The reduced expression of FACIT collagen during progressive liver cirrhosis is associated with a loss of flexibility [122]. Whether FACIT collagen can exhibit a similar effect on the cardiac wall needs to be investigated.

Water transmembrane transport

Down- and upregulation of aquaporins that are the main components of the level-3 SCP 'Water transmembrane transport' is predicted with AUC ranks of 9 and 2 for cardiotoxic and non-cardiotoxic TKIs, respectively (Fig. 2B, Supplementary Fig. 18). Three cardiotoxic drugs, dabrafenib, pazopanib and ponatinib, downregulate the SCP in two of three (enrichment ranks 6, 7), one of five (4) and two of six (6, 9) treated cell lines (Supplementary Fig. 20). The induced and repressed SCP genes, aquaporins 1, 3, 7 and 10 (Supplementary Data 11C) might be related to their function in transmembrane transport of water (AQP1, 3, 7, 10), CO_2 and NO (AQP1) or urea and the energy substrate glycerol (AQP 3, 7, 10) [123].

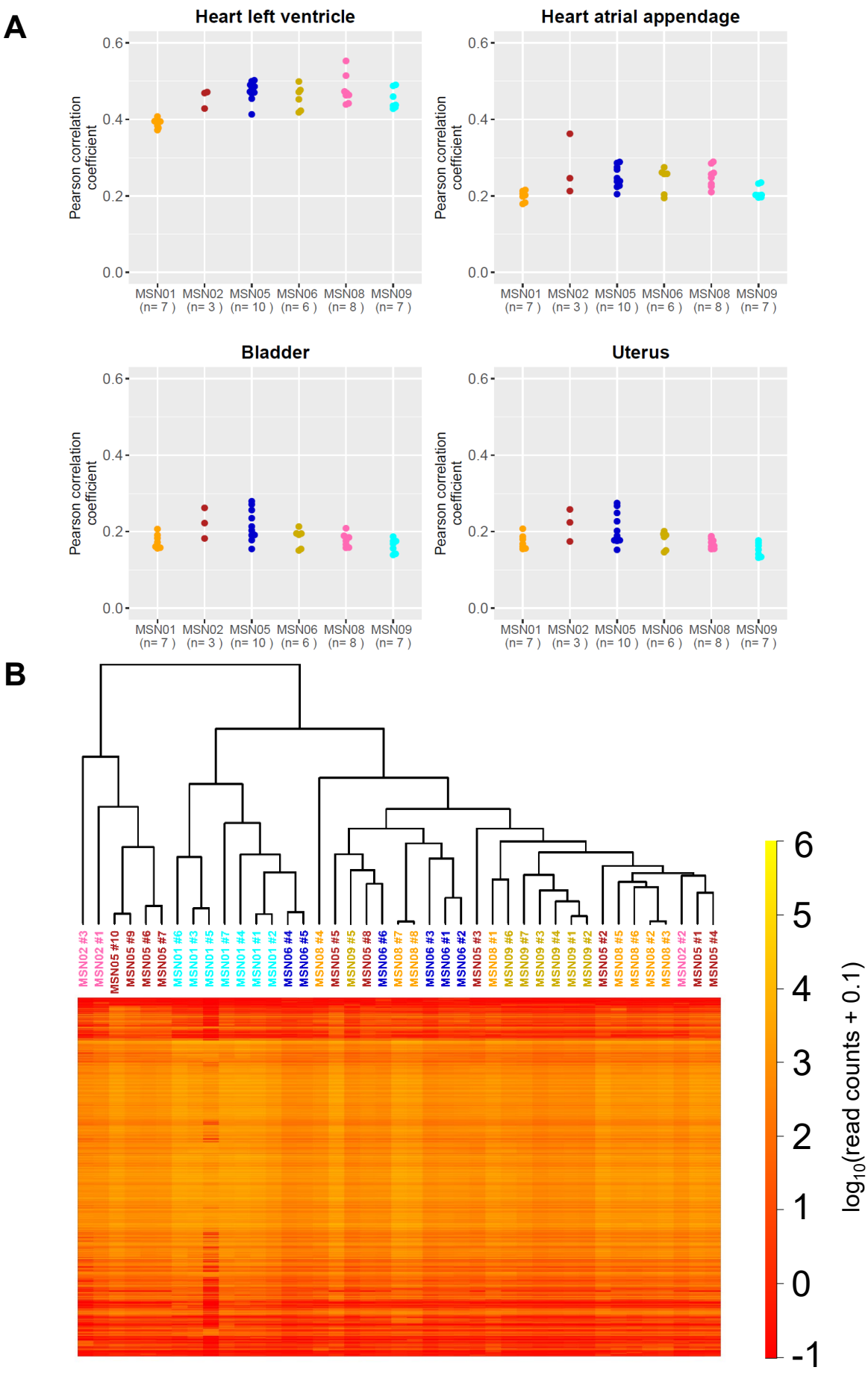

Supplementary Fig. 1

Supplementary Fig. 1. Basal gene expression of six hiPSC-derived cardiomyocyte cell lines map to the human heart and show cell line specificity. (A) Raw read counts of vehicle-treated replicates [16] were correlated with median gene expression levels for each tissue in the GTEx database. Pearson correlation coefficients are shown for each replicate of all cell lines and the top four tissues with the highest correlation coefficients. Numbers of replicates are provided in parentheses. **(B)** Gene expression raw counts obtained in all replicates of vehicle-treated cell lines [16] were subjected to pairwise correlation analysis, followed by hierarchical clustering. Visualized matrix shows the $\log_{10}$(read counts + 0.1). Rows and columns were re-arranged according to clustering results. Replicates of the same cell line are colored with the same color.

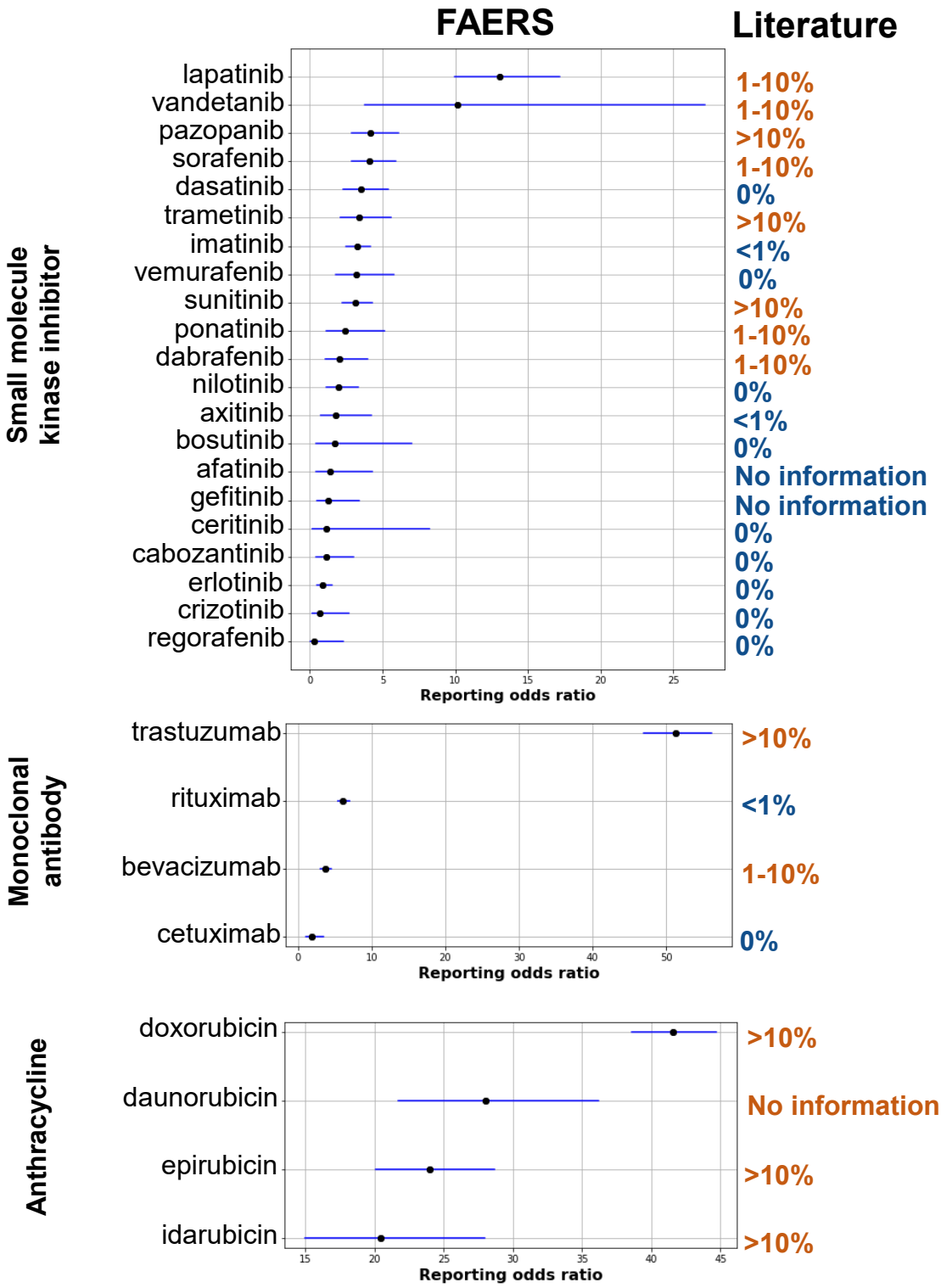

Supplementary Fig. 2

Supplementary Fig. 2. Cardiac toxicity of kinase inhibitors and monoclonal antibodies curated from the FAERS database. Risk profiles were curated from the FAERS database. Horizontal lines indicate 95% confidence intervals. Blue and orange comments describe published cardiotoxicity levels as outlined in Supplementary Data 3.

A

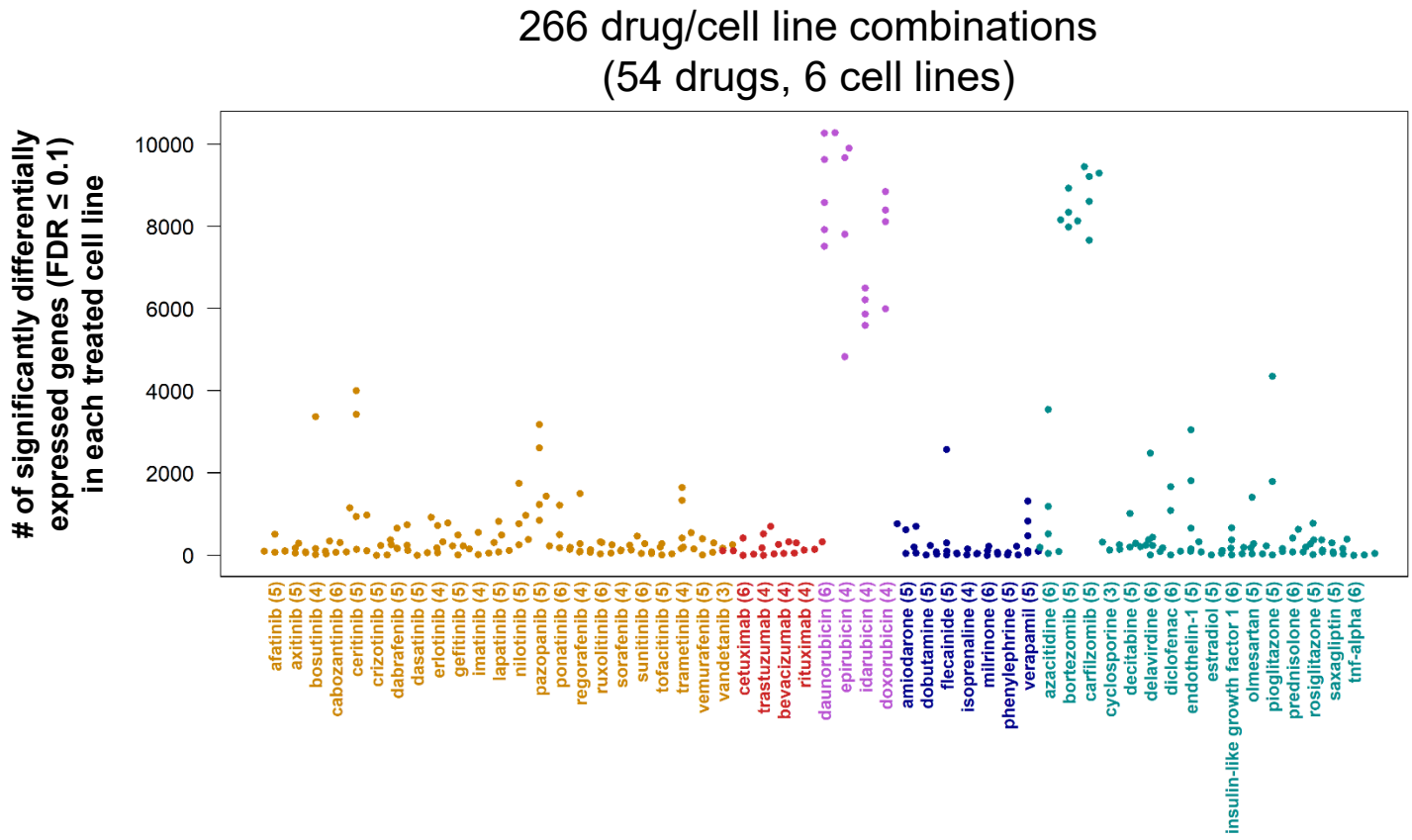

23 Small molecule kinase inhibitors
4 Monoclonal antibodies
4 Anthracyclines
7 Cardiac-acting drugs
16 Non-cardiac-acting drugs

27 Tyrosine kinase inhibitors (TKIs)

Supplementary Fig. 3

B

Gene expression profiles of 266 drug/cell combinations

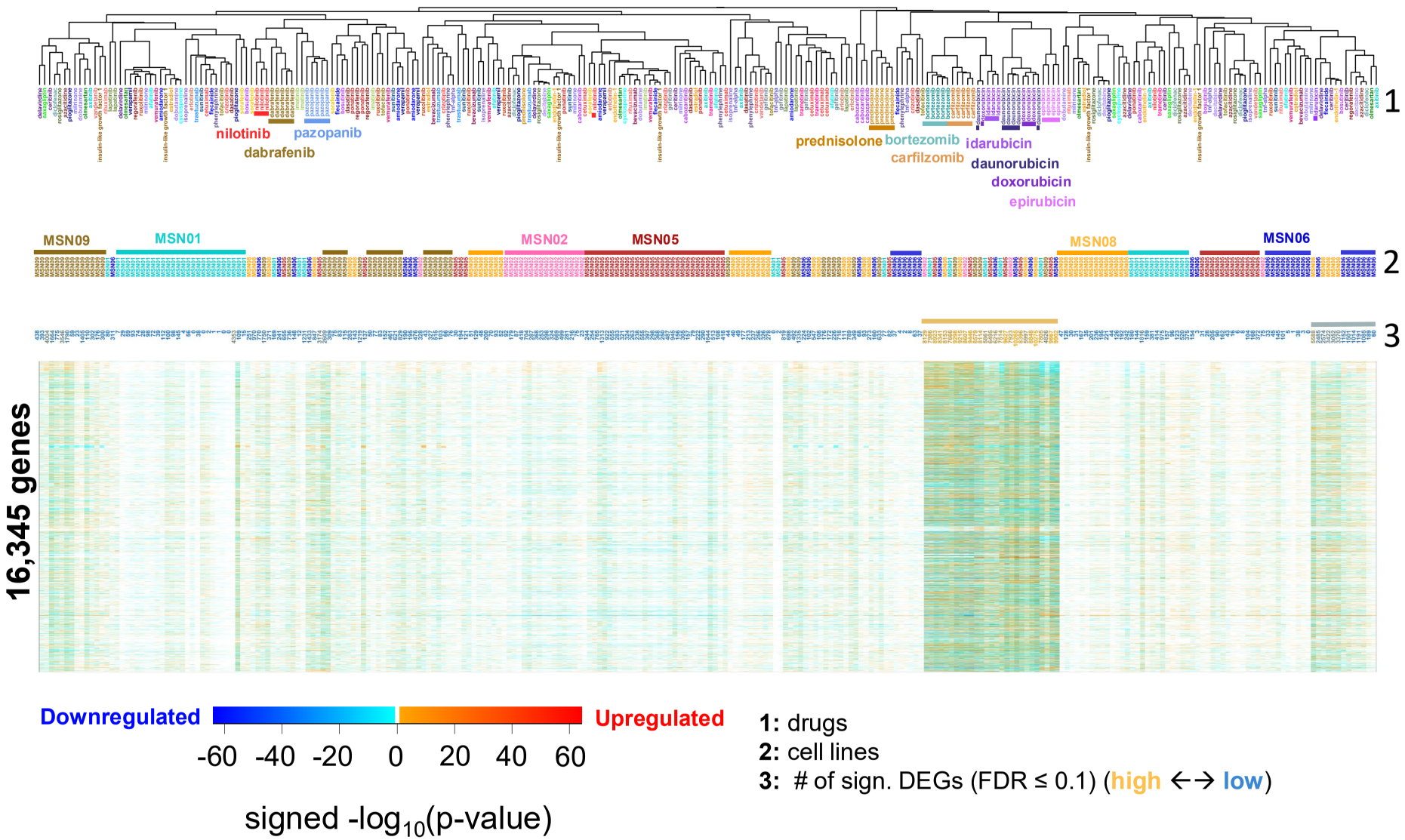

Supplementary Fig. 3

Supplementary Fig. 3. Drug-induced gene expression profiles in six hiPSC-derived cardiomyocyte cell lines. (A) Three to six hiPSC-derived cardiomyocyte cell lines were stimulated with one out of 54 drugs or vehicle for 48h, followed by bulk RNAseq and identification of 266 lists of DEGs. The number of DEGs induced by the different drugs in the different cell lines showed great variation (FDR ≤ 10%). Total numbers of treated cell lines for each drug are shown in parentheses next to the drug labels. **(B)** Significance p-values were transformed into $-\log_{10}$(p-values) and defined to be positive or negative for up- or downregulated genes, respectively. Pairwise correlation analysis followed by hierarchical clustering, documents that only a few gene expression profiles are determined by the drug used for treatment (1), while most profiles are determined by the treated cell line (2) or the number of significant DEGs (3). Fig. 1B shows the same dendrogram.

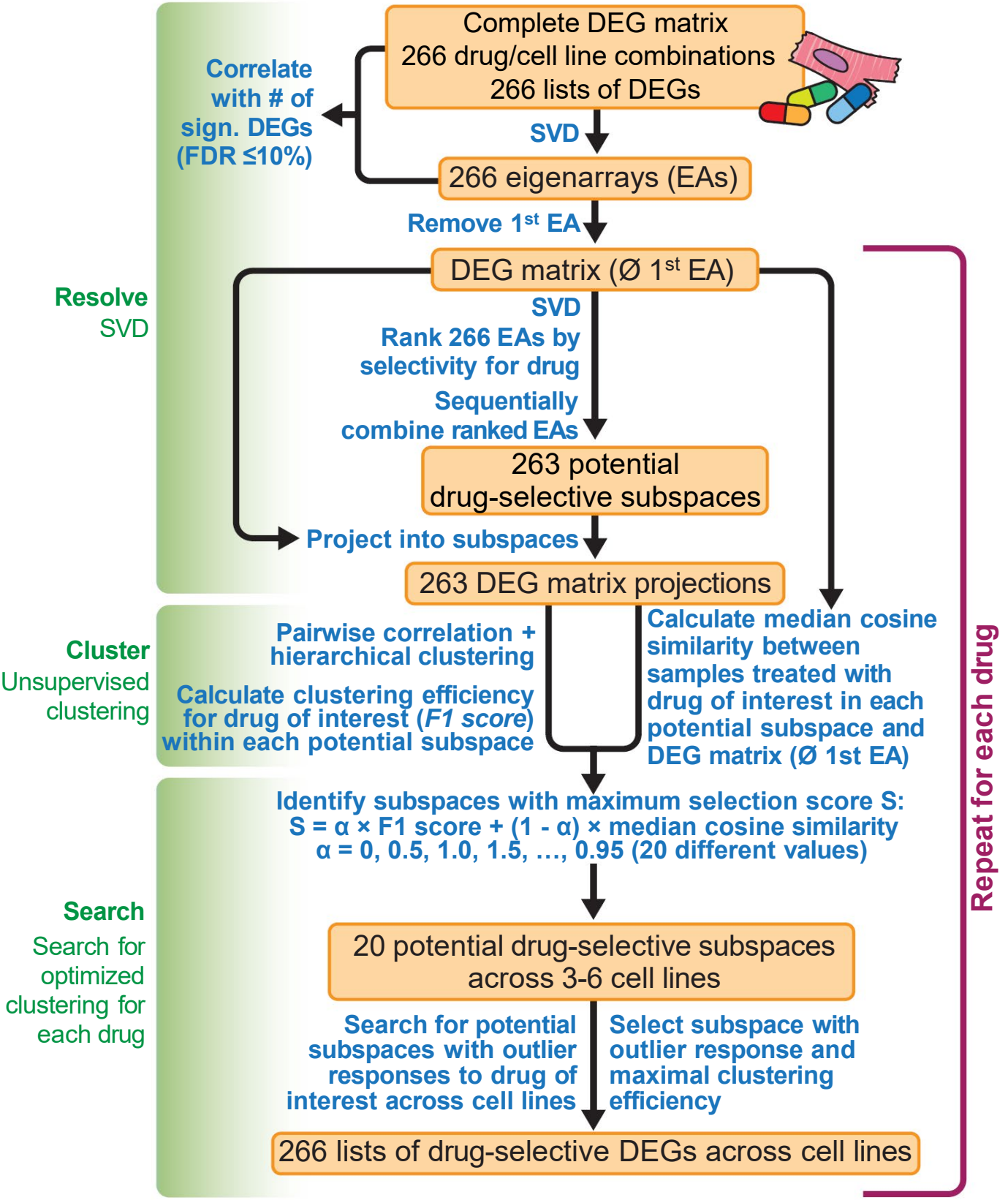

Supplementary Fig. 4. Computational pipeline for the identification of drug-selective and outlier gene expression responses. Our pipeline subjects drug-induced DEGs to Singular Value Decomposition (SVD) to identify drug-selective gene expression profiles and cell lines that respond differently to a drug of interest than the other cell lines. See methods for details. &: and; Ø: without. Flow chart is used with permission from Mount Sinai Health System, licensed under CC BY.

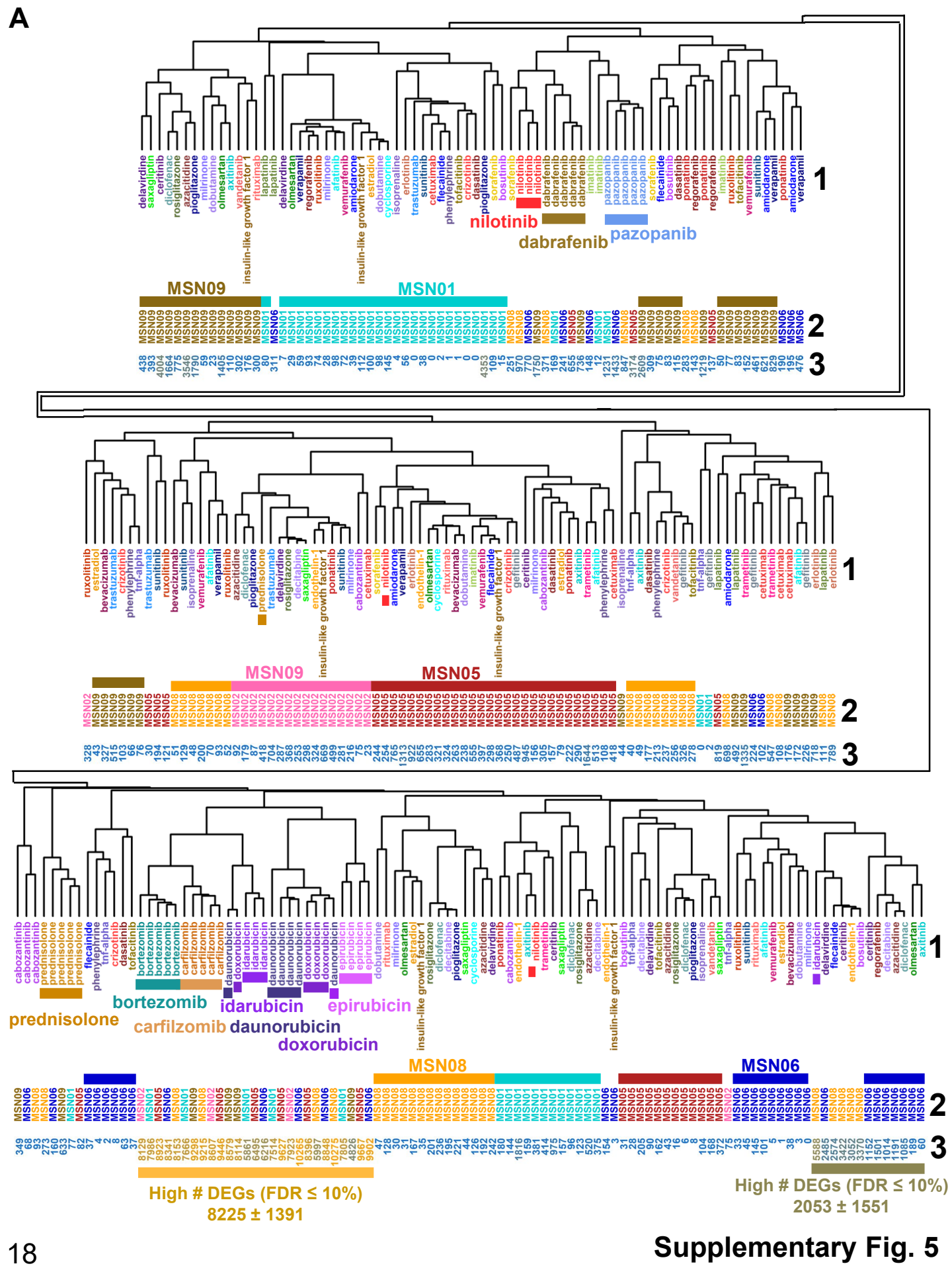

Supplementary Fig. 5

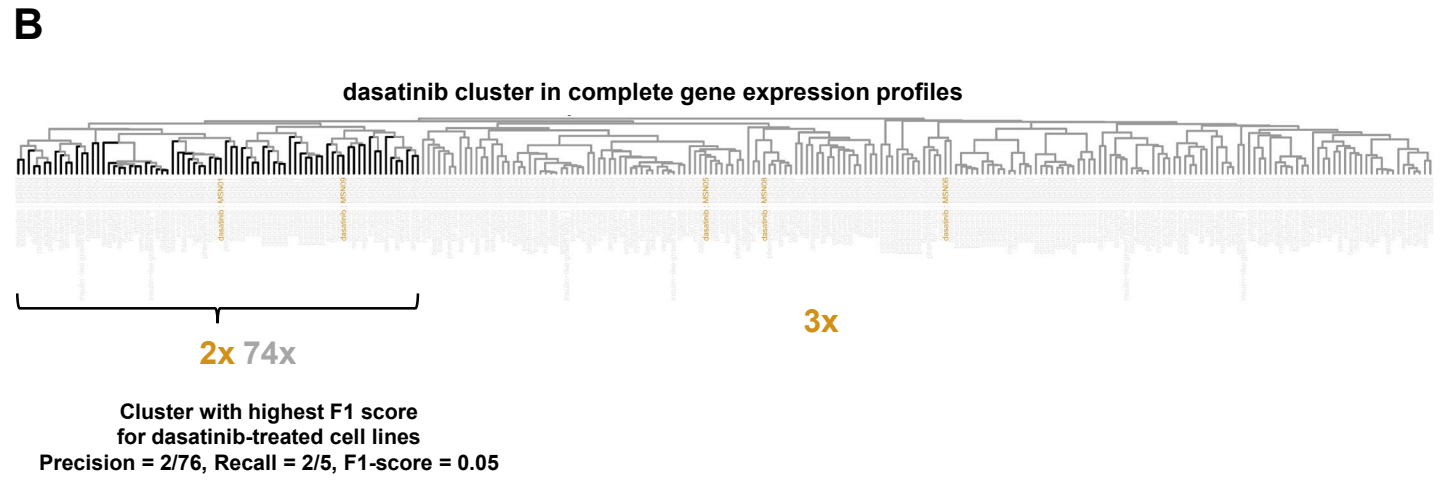

Supplementary Fig. 5

Supplementary Fig. 5. Clustering efficiency of drug-induced gene expression profiles in six hiPSC-derived cardiomyocyte cell lines. (A) To allow detailed investigation of the clustering results we visualized dendrogram and dendrogram labels of Supplementary Fig. 3B at larger sizes. Fig. 1B shows the same dendrogram with a focus on the drugs. **(B)** For each drug, we calculated one F1 score for each cluster that can be obtained by cutting the dendrogram at any height and contains at least two cell line/drug combinations. The F1 score is the harmonic mean of the precision (how many cell line/drug combinations within a cluster were treated with the drug) and the recall (how many cell line/drug combinations treated with the drug were in that cluster). The cluster with the highest F1 score that was selected for further analysis in this example is labeled black.

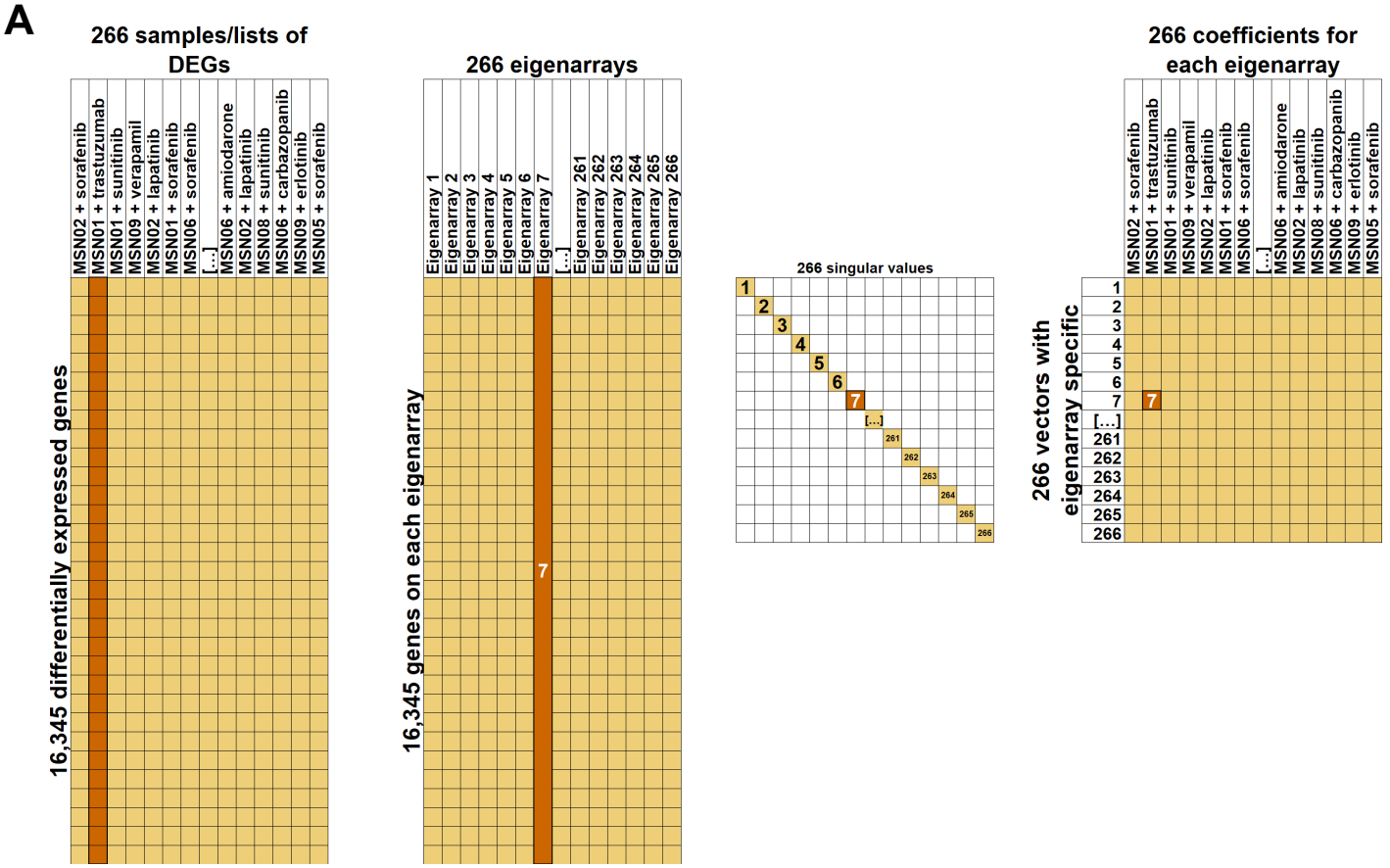

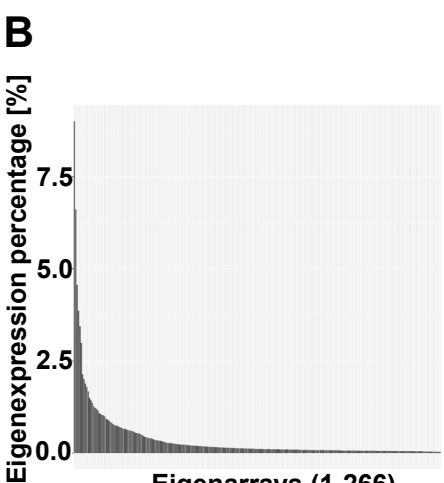

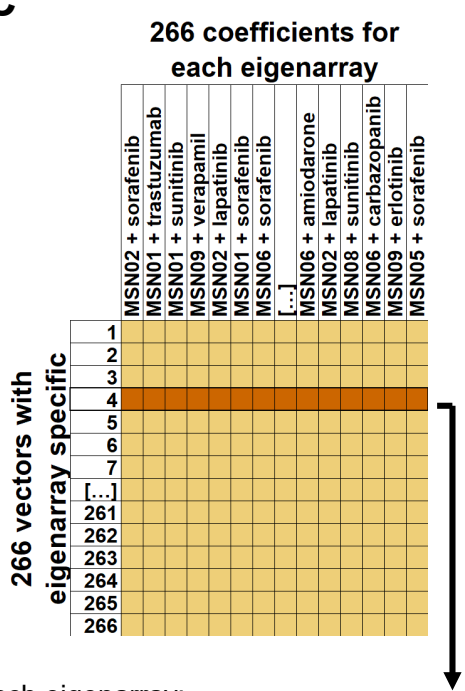

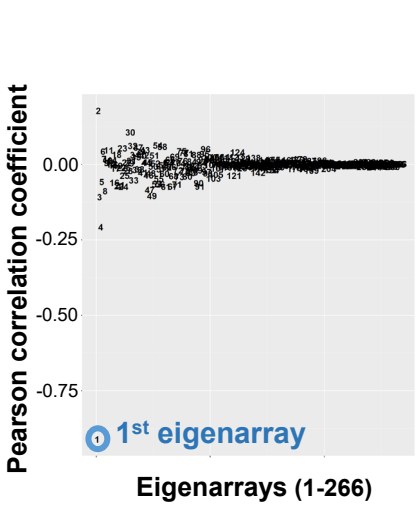

For each eigenarray:
Correlate coefficients of that eigenarray with # of significantly differentially expressed genes in each sample.

Supplementary Fig. 6

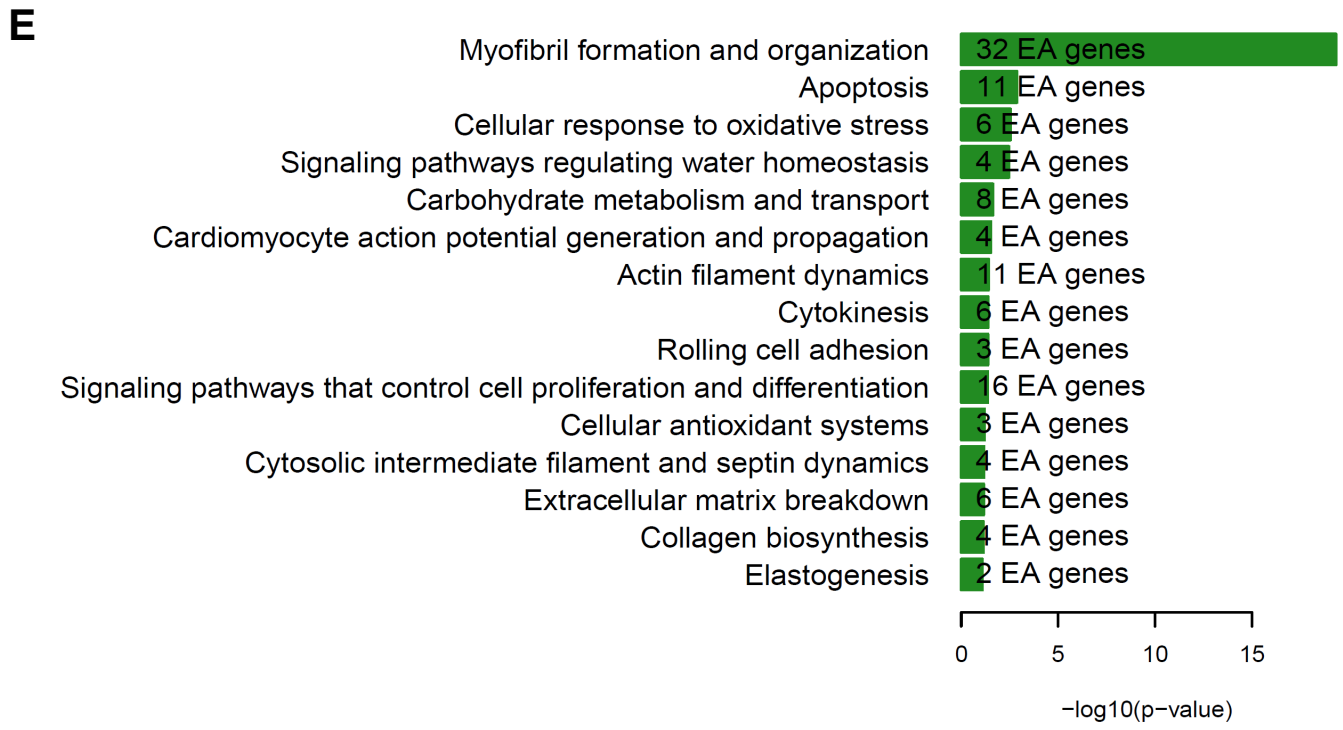

Supplementary Fig. 6

Supplementary Fig. 6. Identification of drug-selective gene expression responses using Singular Value Decomposition. (A) Singular value decomposition (SVD) decomposes the input data matrix into a matrix of left singular vectors or eigenarrays, a diagonal matrix of singular or eigenexpression values and a matrix of right singular vectors. Each cell line/drug combination gene expression vector in the full matrix is a linear combination of all eigenarrays. Cell line/drug combination specific coefficients of this linear combination are documented in the matrix of right singular vectors. The eigenexpression values in the diagonal document how much each eigenarray contributes to the complete gene expression dataset of all cell line/drug combinations and need to be considered for the linear combination as well. To calculate the contribution of the seventh eigenarray to the complete gene expression profile induced by trametinib in cell line MSN09 it must be multiplied with highlighted eigenexpression value and the highlighted coefficient, both labeled with seven. **(B)** SVD of the gene expression matrix identified 266 orthonormal eigenarrays that are sorted by their relative contribution to the total variance. **(C)** For each eigenarray, we calculated the Pearson correlation between the cell line/drug combination-specific coefficients and the number of significant DEGs in the corresponding complete gene expression profiles. **(D)** Our results document a high correlation with the number of significant DEGs for the first eigenarray. **(E)** Pathway enrichment analysis of the top 600 genes of the first eigenarray identifies muscle contraction.

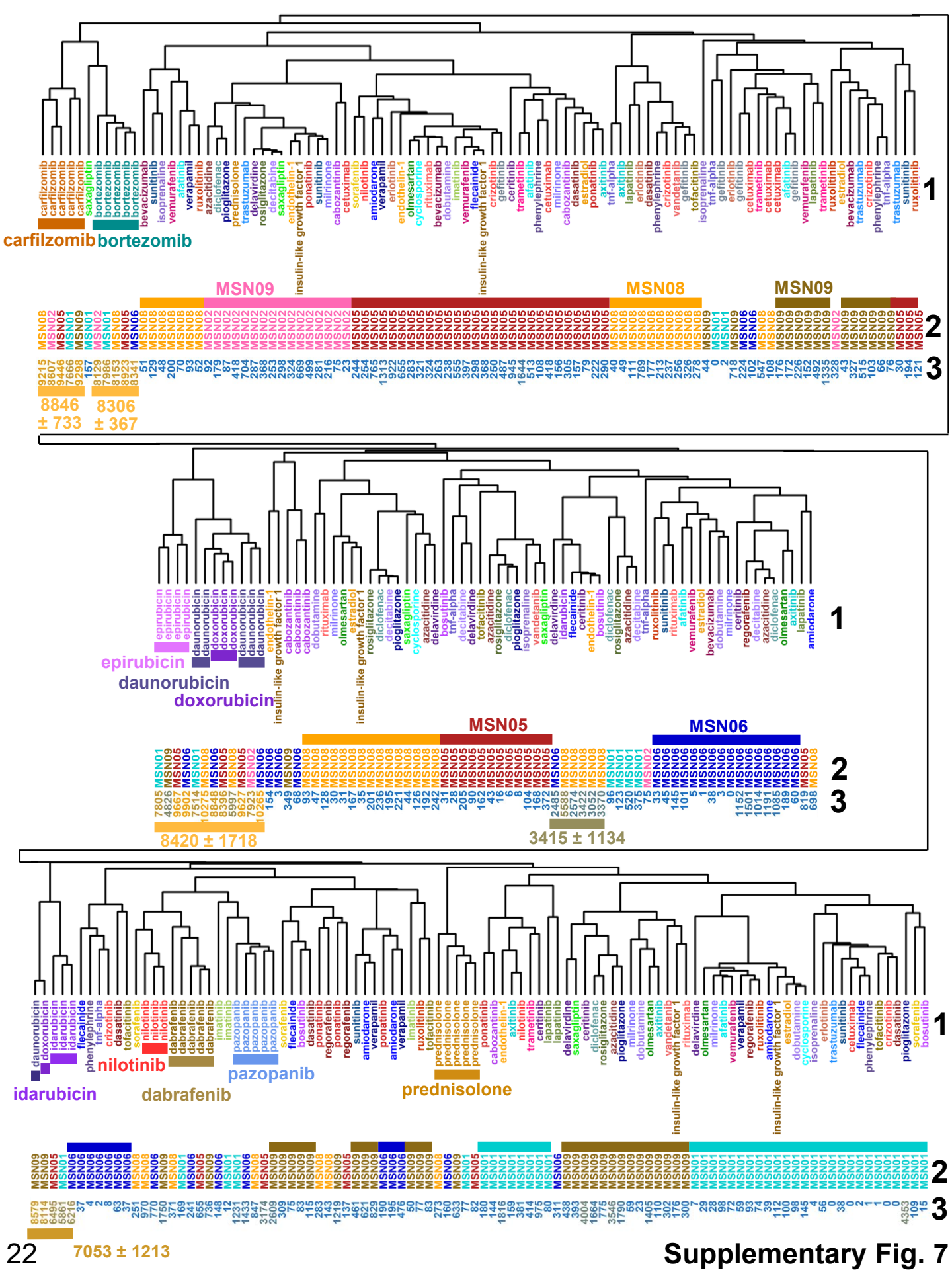

Supplementary Fig. 7

Supplementary Fig. 7. Clustering of DEGs after removal of first eigenarray. Removal of the first eigenarray from the complete DEG matrix disrupts hierarchical clustering by the number of significant DEGs (3).

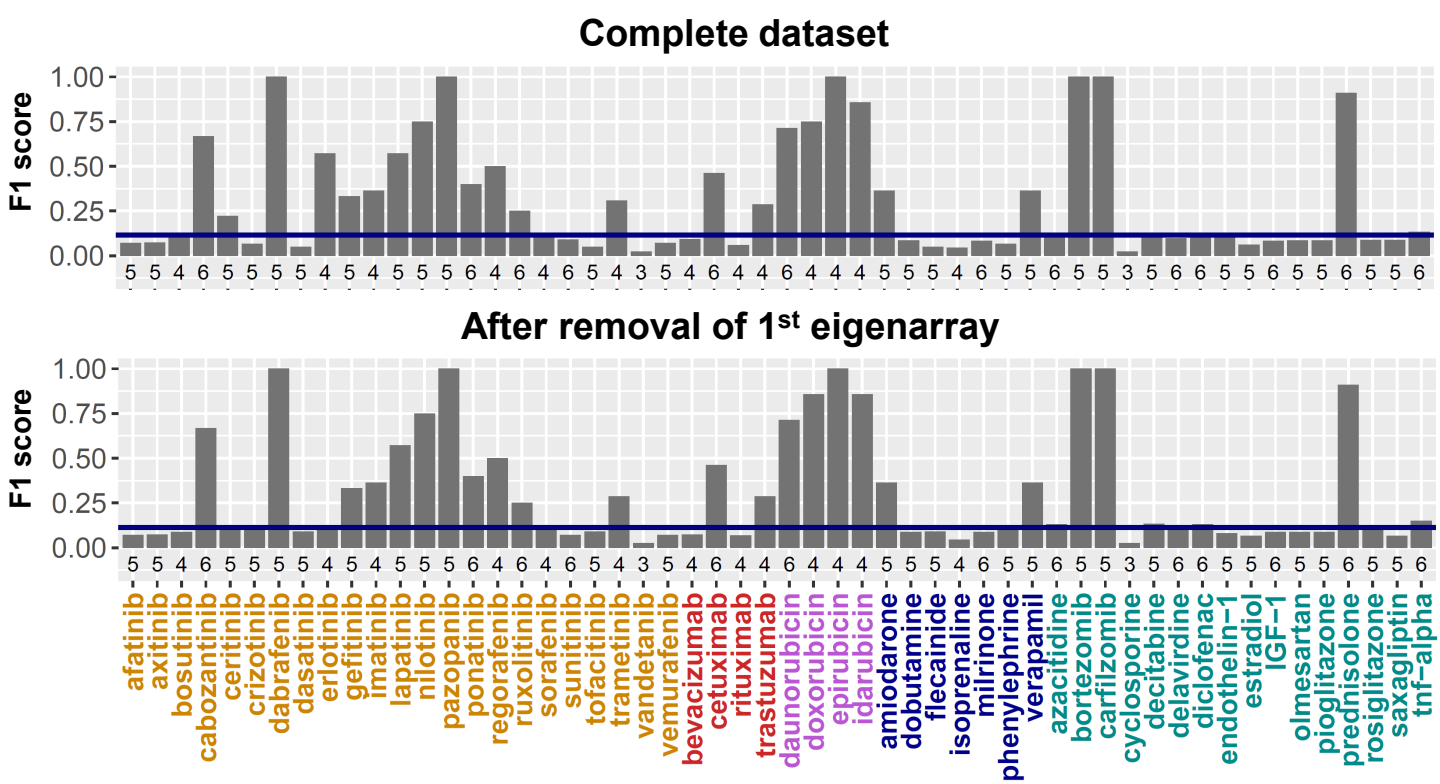

Supplementary Fig. 8

Supplementary Fig. 8. Clustering efficiency after removal of the first eigenarray. DEG matrix after removal of the first eigenarray was subjected to pairwise correlation analysis and hierarchical clustering, followed by calculation of the highest F1 scores for each drug (bottom figure). Numbers of treated cell lines are shown below the bars. To allow easier comparison, we added the F1 scores calculated for each drug using the complete DEG profiles (top figure) that is also shown in Fig. 1C.

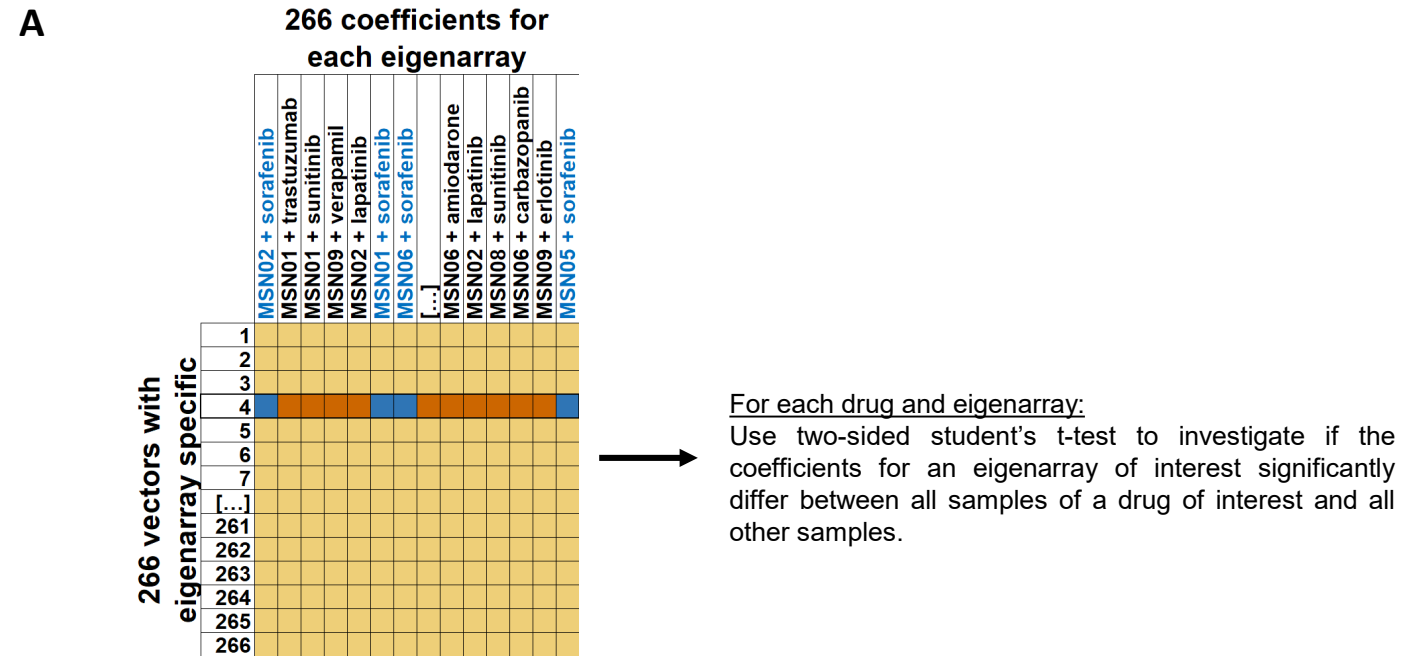

Supplementary Fig. 9

B

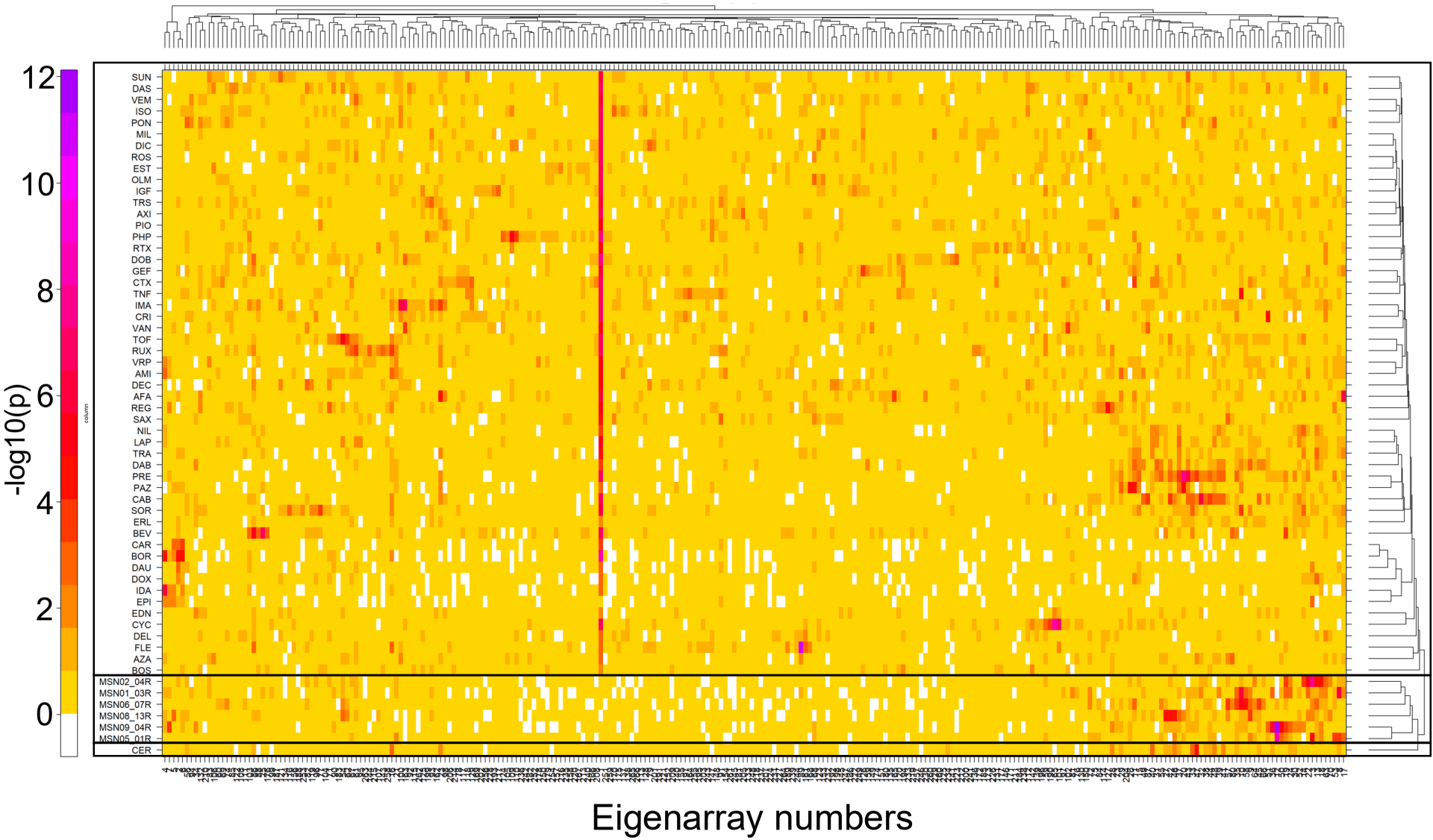

Supplementary Fig. 9

Supplementary Fig. 9. Cell-line- and drug-selective effects are captured by different eigenarrays. (A) For each eigenarray and drug, we analyzed if the coefficients that are related to the gene expression profiles for that drug on that eigenarray significantly differ from all other coefficients on that eigenarray. Consequently, we calculated one p-value for each drug-eigenarray combination. Similarly, we calculated one p-value for each cell line-eigenarray combination. **(B)** All p-values were transformed into -$\log_{10}$(p-values) and used to calculate pairwise correlation coefficients between all drugs and cell lines, followed by hierarchical clustering. The initial heatmap of -$\log_{10}$(p-values) was rearranged according to the clustering results. Grouping of the six cell lines into a single separated cluster (boxed) suggests that the eigenarray decomposition allows differentiation of cell-line-specific effects from drug-specific effects.

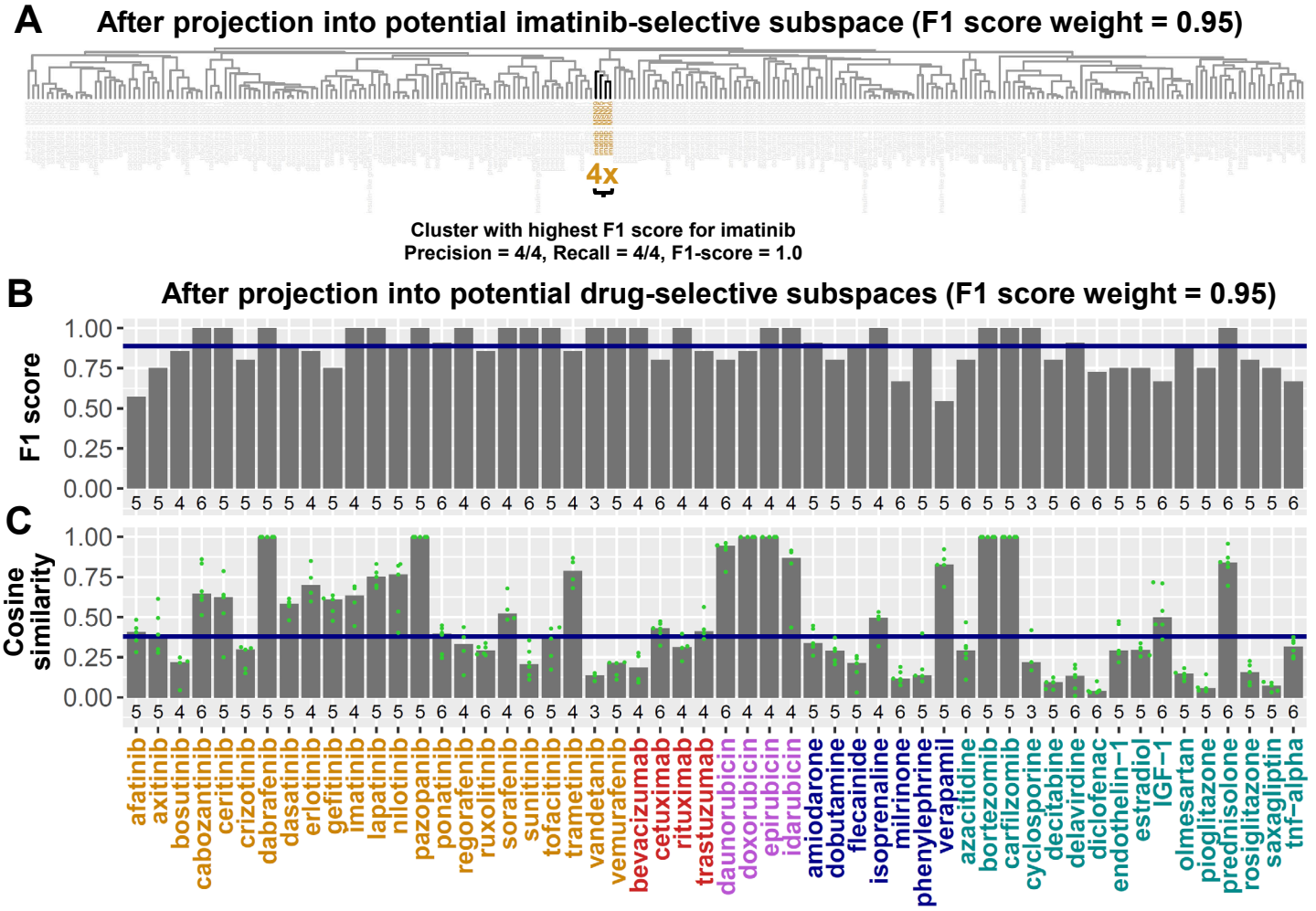

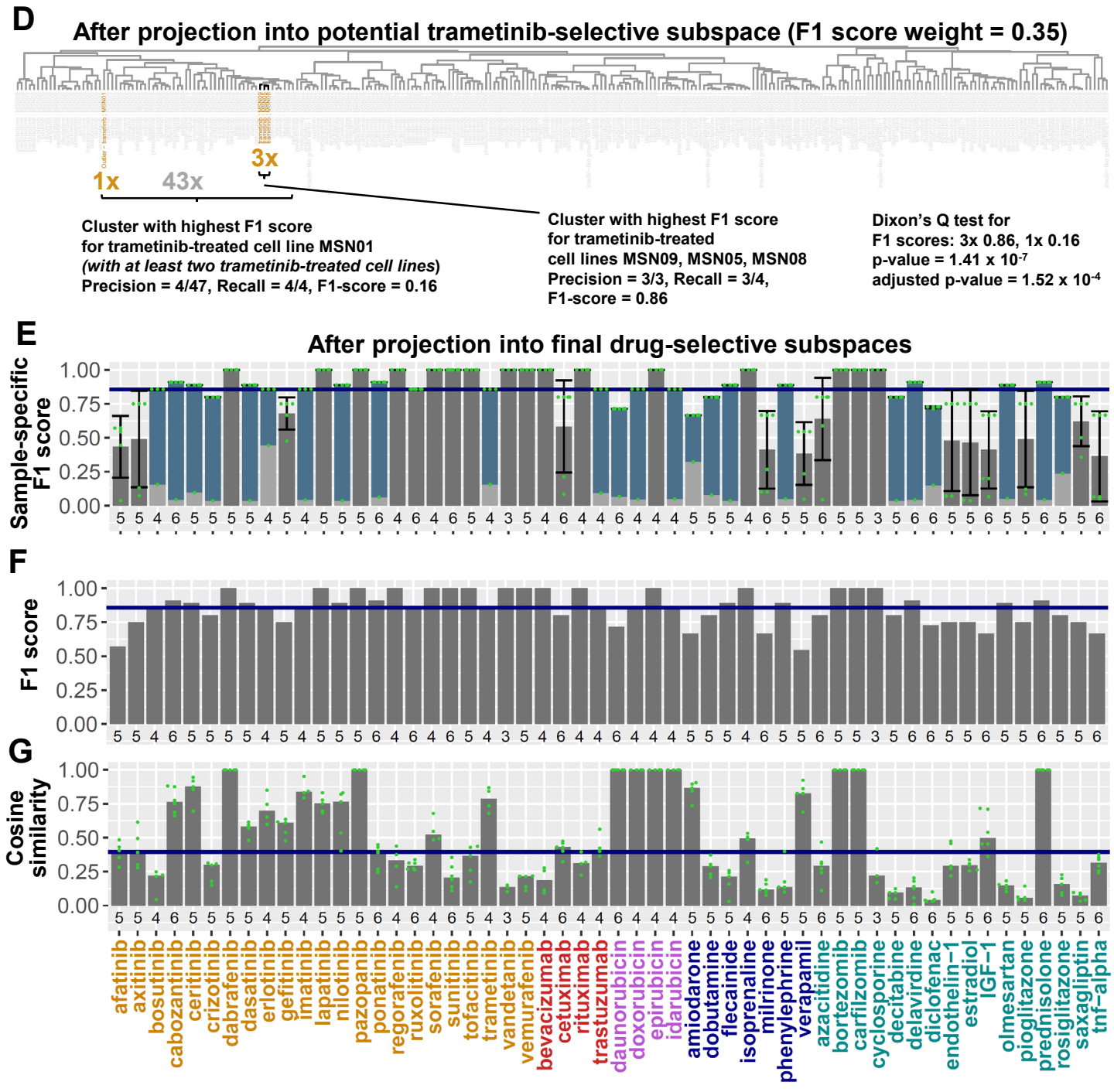

Supplementary Fig. 10

Supplementary Fig. 10. Identification of drug-selective gene expression profiles and outlier responses. (A) For each drug, we ranked all eigenarrays by their ability to separate the coefficients associated with cell line/drug combinations treated with that drug from all other coefficients, i.e., we ranked them by increasing p-values. The top 3 to 266 eigenarrays were combined to yield 264 potential drug-selective subspaces. Gene expression profiles after removal of the first eigenarray were projected into the subspaces, followed by pairwise correlation, hierarchical clustering and F1 score calculation for the drug

of interest. The example shows the F1 score calculation for imatinib after projection of the data into one of the potential imatinib-selective subspaces. **(B/C)** Cosine similarities between the projected gene expression profiles and the gene expression profiles after removal of the first eigenarray were calculated for each drug. For each potential drug-selective subspace, we calculated weighted averages between the F1 score and the median cosine similarity with changing relative contributions as defined by 20 different F1 score weights (ranging from 0.00 to 0.95 in steps of 0.05). Each F1 score weight allowed us to select one drug-selective subspace, i.e., that subspace with the highest weighted mean or selection score. Shown are **(B)** F1 scores and **(C)** single (green dots) as well as median (bars) cosine similarities obtained based on an F1 score weight of 0.95. Blue lines indicate median heights of all bars. Numbers of treated cell lines are shown below the bars. **(D)** For each drug, we screened all 20 potential drug-selective subspaces (that are defined by different F1 score weights) for subspaces where one cell line/drug combination shows a different transcriptomic response to the drug of interest than all other cell line/drug combinations. We calculated cell line/drug combination-specific F1 scores, using the same approach described above, except that the cell line/drug combination of interest has to be part of the corresponding cluster. Dixon's Q test applied to cell line/drug combination-specific F1 scores was used to identify outliers (adj. p-value ≤ 0.05). **(E)** F1-scores of non-outlier cell line/drug combinations in the final drug-selective subspaces were averaged. Blue and dark gray bars indicate averaged F1 scores for drugs with and without identified outliers, respectively. Error bars show standard deviations for non-outlier cell line/drug combinations. F1 scores identified for outlier cell line/drug combinations are visualized separately (light gray bars). Green dots show individual drug-selective F1-scores. The larger the difference between the top of the blue and light gray bars, the larger the difference in F1 scores between regular and outlier responses. The blue line indicates the median height of blue and dark gray bars. Numbers of treated cell lines are shown below the bars. **(F)** Projection of gene expression profiles into the final drug-selective subspaces leads to a great increase in drug-specific F1 scores. Notice that the F1 scores are the maximum cell line/drug combination-specific F1-scores shown in E. This figure is the same as figure 1D. **(G)** Cosine similarities (green dots) and median cosine similarities (bars) between complete DEG profiles and DEG profiles in final drug-selective subspaces are shown. The blue line shows the median height of all bars.

Supplementary Fig. 11: Clustering results for each drug after removal of the first eigenarray and in the final drug-selective subscpaces. See pages 79 - 93.

Supplementary Fig. 12: Identification of outlier responses. See pages 94 - 97.

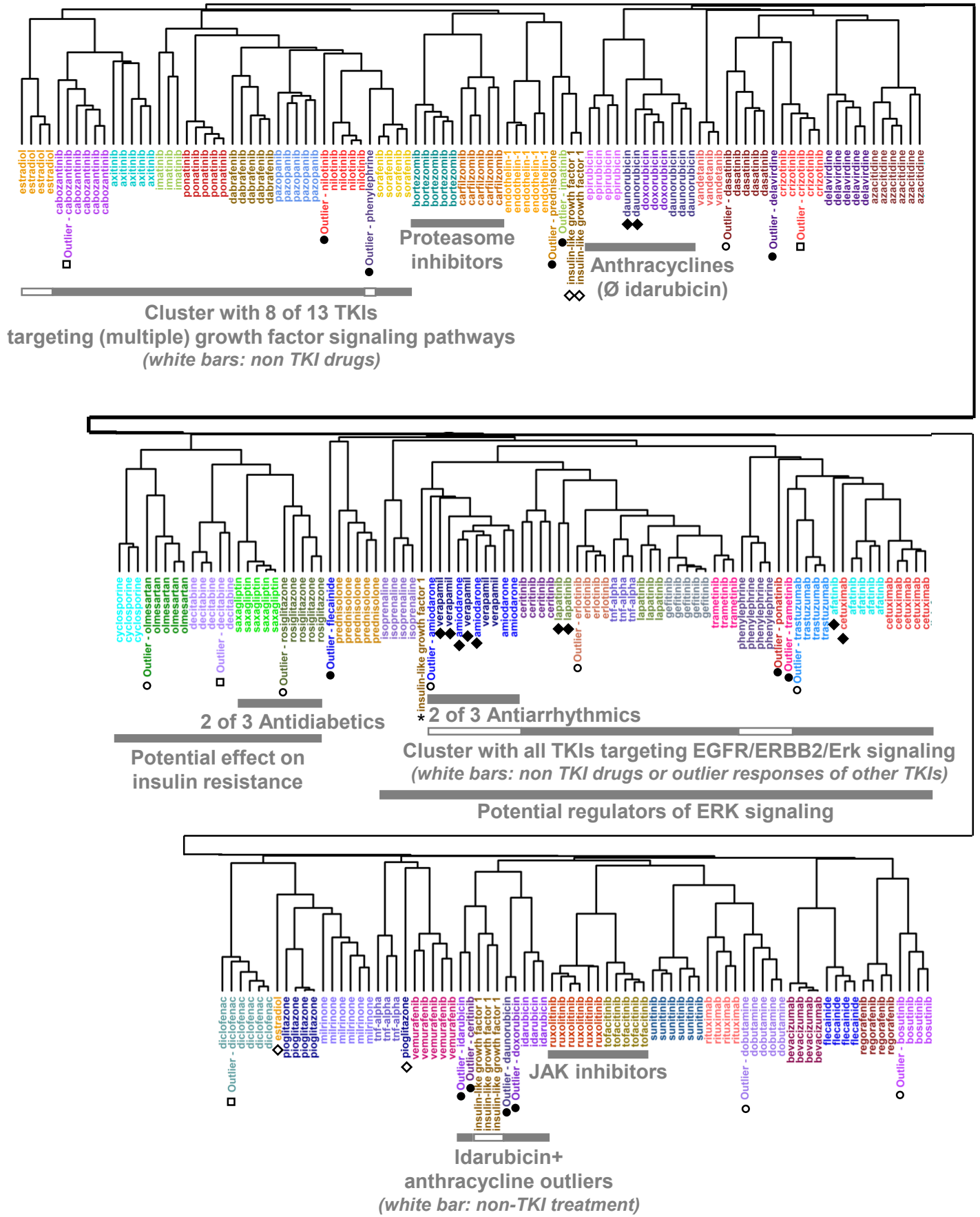

Supplementary Fig. 13

Supplementary Fig. 13. Clustering of merged drug-selective gene expression profiles. Drug-selective gene expression profiles obtained after projection of the complete gene expression matrix into drug-selective subspaces were merged, followed by pairwise correlation and hierarchical clustering. Outlier cell line/drug combinations are labeled with 'Outlier'. Closed circles label outlier responses that show great outlier characteristics in this dendrogram as well, and do not cluster together with the other cell line/drug combinations treated with the same drugs. Open circles label outlier responses with minor outlier characteristics in this dendrogram, i.e., those outliers that are grouped together with the cell line/drug combinations treated with the same drug in a larger cluster, but get separated from them after sub-clustering. Closed squares label outlier responses that are grouped together with the cell line/drug combinations treated with the same drug. Asterisks label cell line/drug combinations that do not cluster together with the other cell line/drug combinations treated with the same drug and were not identified as outlier responses. Bars label clusters that are composed of cell line/drug combinations from different drugs with closely related potential mechanisms. Fig. 1E shows the same dendrogram, drug labels and most of the bars.

A

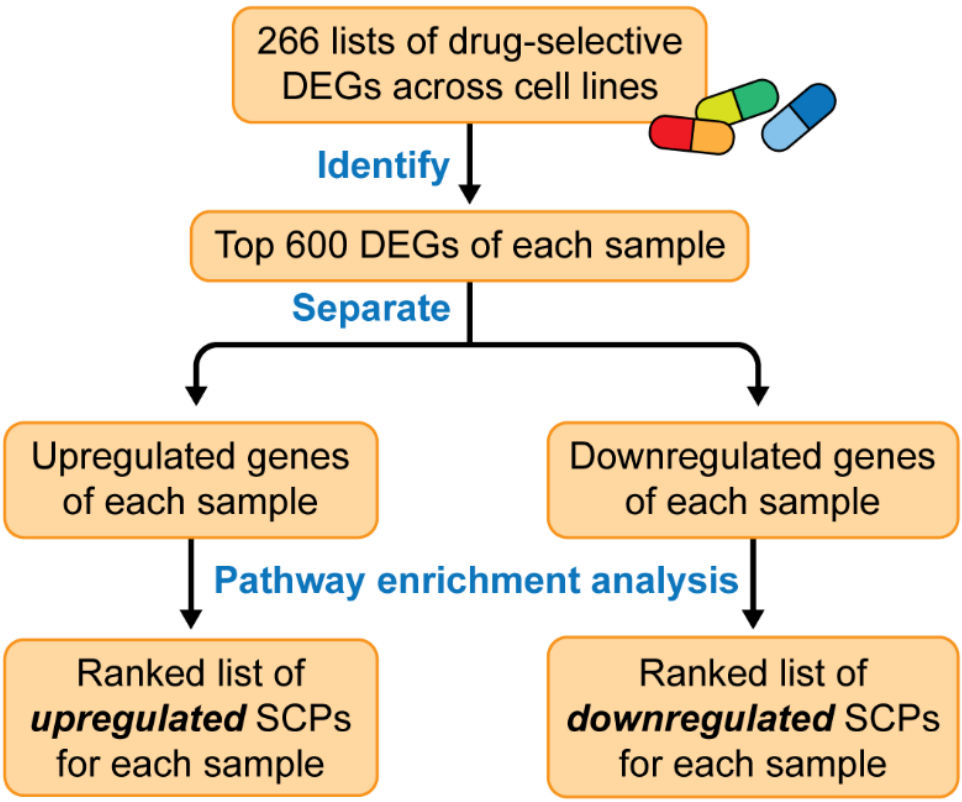

Supplementary Fig. 14

Supplementary Fig. 14. Top Subcellular Processes predicted from complete gene expression profiles, after removal of first eigenarray and from drug-selective gene expression profiles. (A) Complete, decomposed gene expression profiles and gene expression profiles after removal of the first eigenarray were subjected to pathway enrichment analysis using the Molecular Biology of the Cell Ontology and Fisher's Exact Test to identify up- and downregulated subcellular processes (SCPs). Flow chart is used with permission from Mount Sinai Health System, licensed under CC BY.

Supplementary Figs. 14B-E: Top Subcellular Processes predicted from complete gene expression profiles, after removal of first eigenarray and from drug-selective gene expression profiles.

14B: MBCO level-1 SCPs: pages 98 - 111
14C: MBCO level-2 SCPs: pages 112 - 125
14D: MBCO level-3 SCPs: pages 126 - 139
14E: MBCO level-3 SCPs: pages 140 - 154

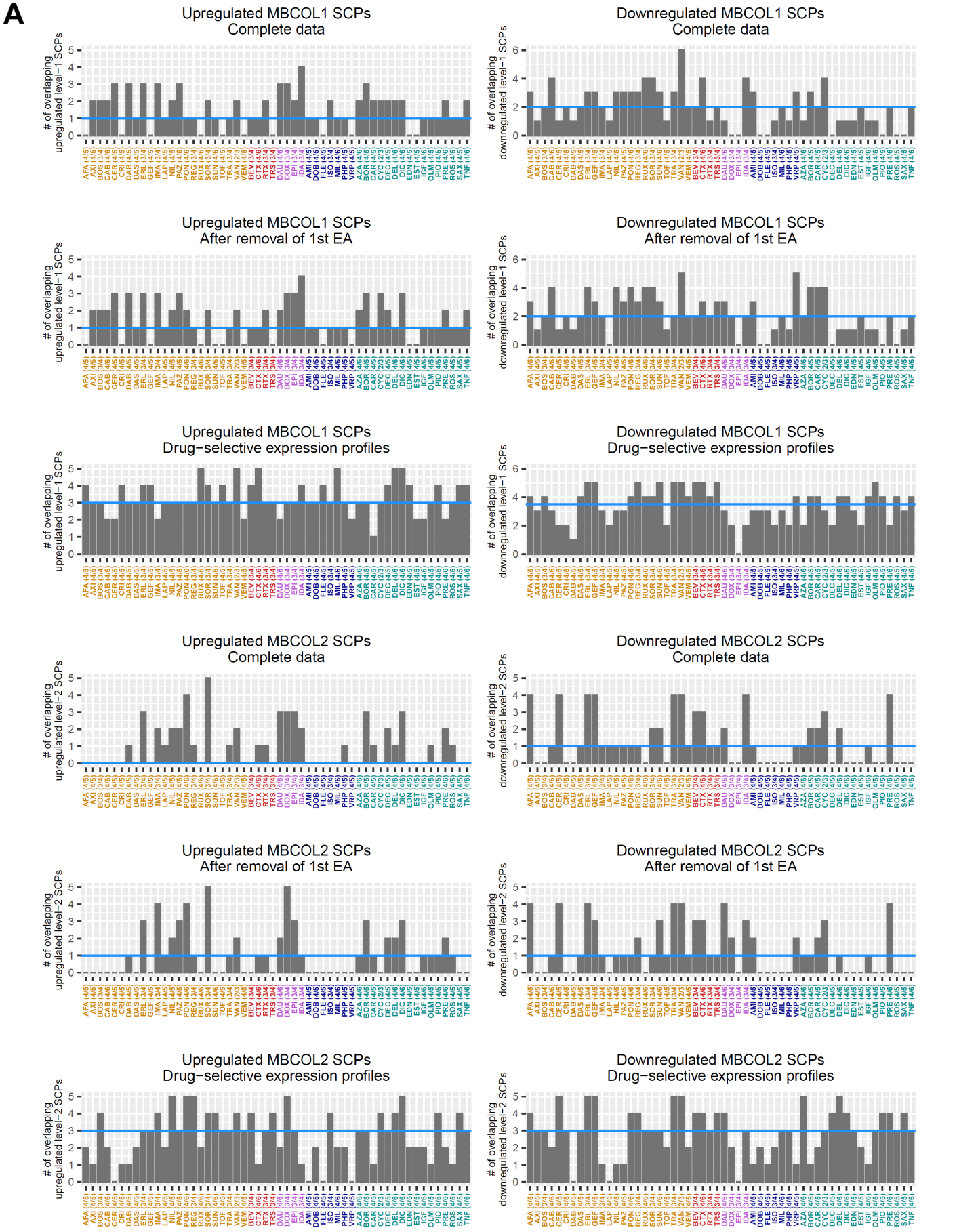

Supplementary Fig. 15

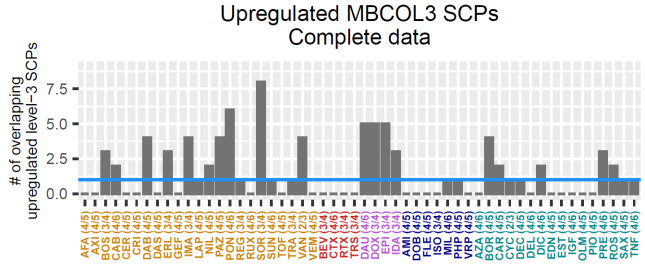

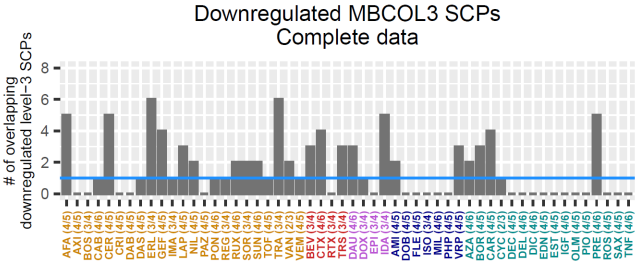

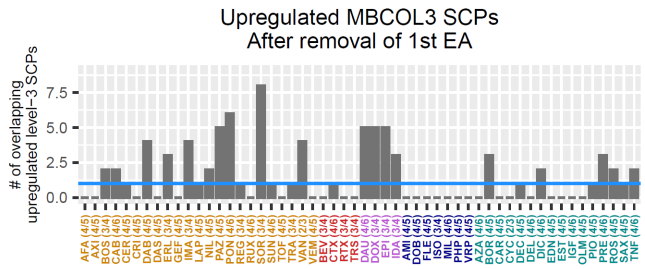

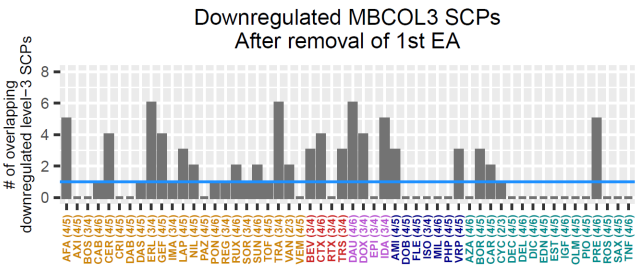

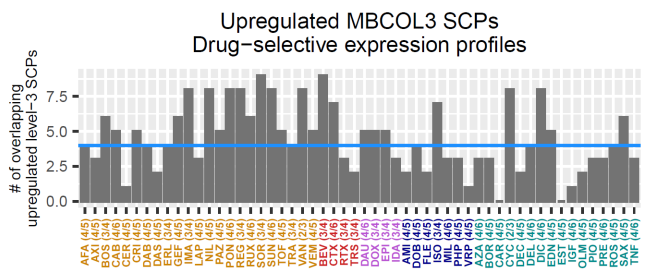

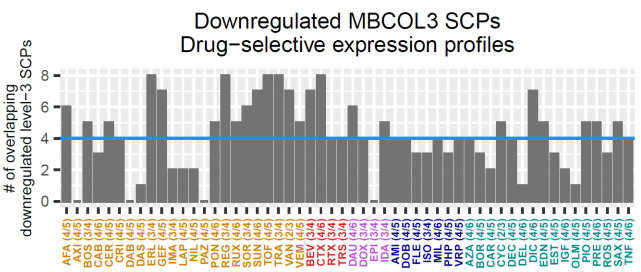

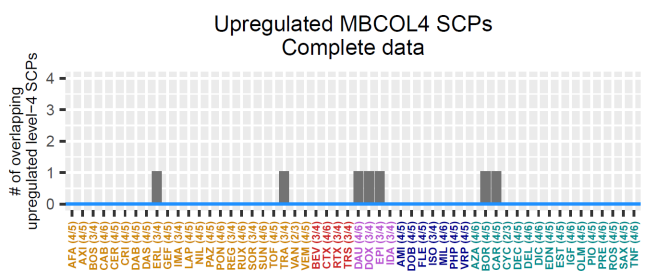

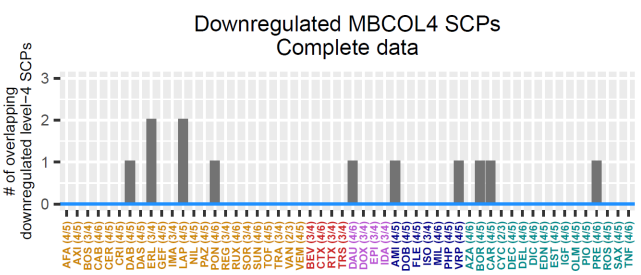

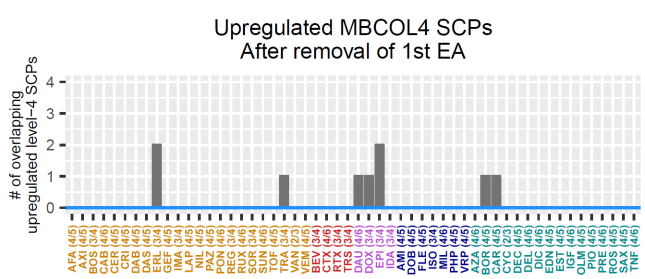

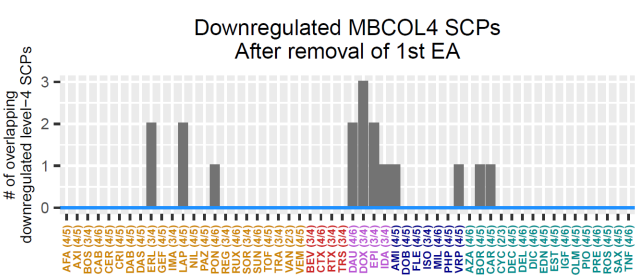

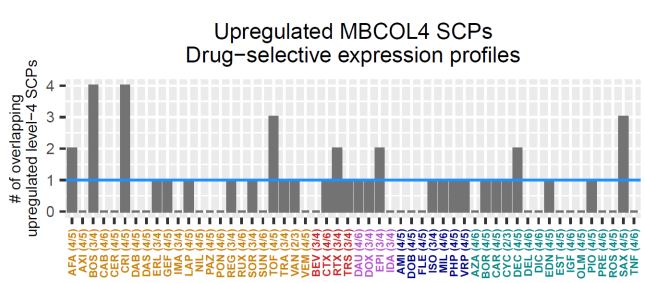

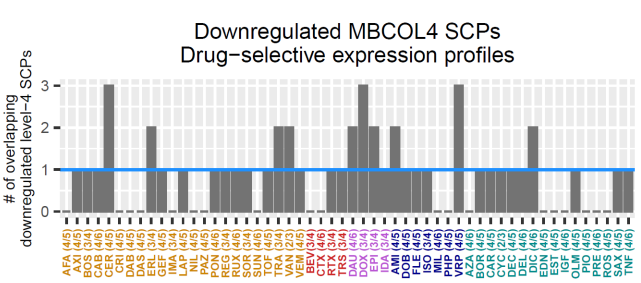

Supplementary Fig. 15

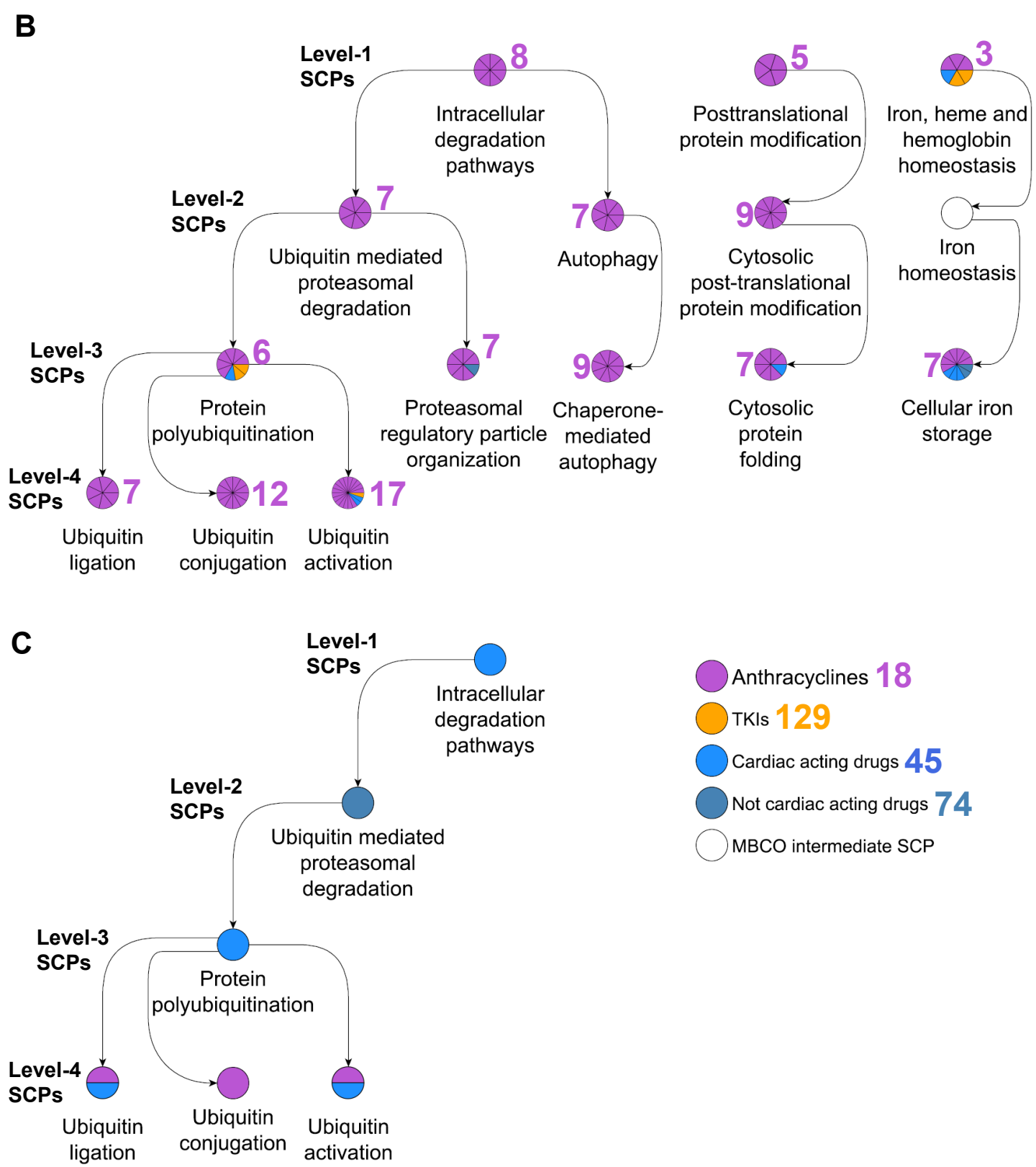

Supplementary Fig. 15

Supplementary Fig. 15. SVD decomposition increases the consistency of identified SCPs by the same drug across different cell lines and reveals potentially cardiotoxic SCPs. (A) We analyzed, for each drug, how many up- or downregulated level-1, -2, -3 and -4 SCPs were predicted in at least 66% of all treated cell lines with a maximum rank of five, five, ten and five, respectively. The minimum numbers that equal or exceed 66% and the total numbers of treated cell lines are given as nominators and denominators, respectively, in brackets after the drug abbreviations. The blue line documents the median of overlapping SCP counts. For drug abbreviations see Supplementary Data 3. **(B)** The top five, five, ten and five level-1, -2, -3 and -4 SCPs predicted from downregulated genes in the drug-selective gene expression profiles were integrated into the MBCO hierarchy. Selected SCPs in parent-child relationships (arrows) are shown. Any drug that downregulates an SCP is added as a new pie slice colored according to the drug's class. Purple numbers next to the SCPs indicate the number of anthracycline-treated cell line/drug combinations for which the SCP was predicted (i.e., the number of purple slices). Numbers next to the drug classes in the legend indicate how many cell line/drug combinations were treated with drugs of that class in total. **(C)** The top five, five, ten and five level-1, -2, -3 and -4 SCPs predicted from downregulated genes in the complete gene expression profiles were integrated into the MBCO hierarchy, as described in B. The same SCPs are shown, if predicted.

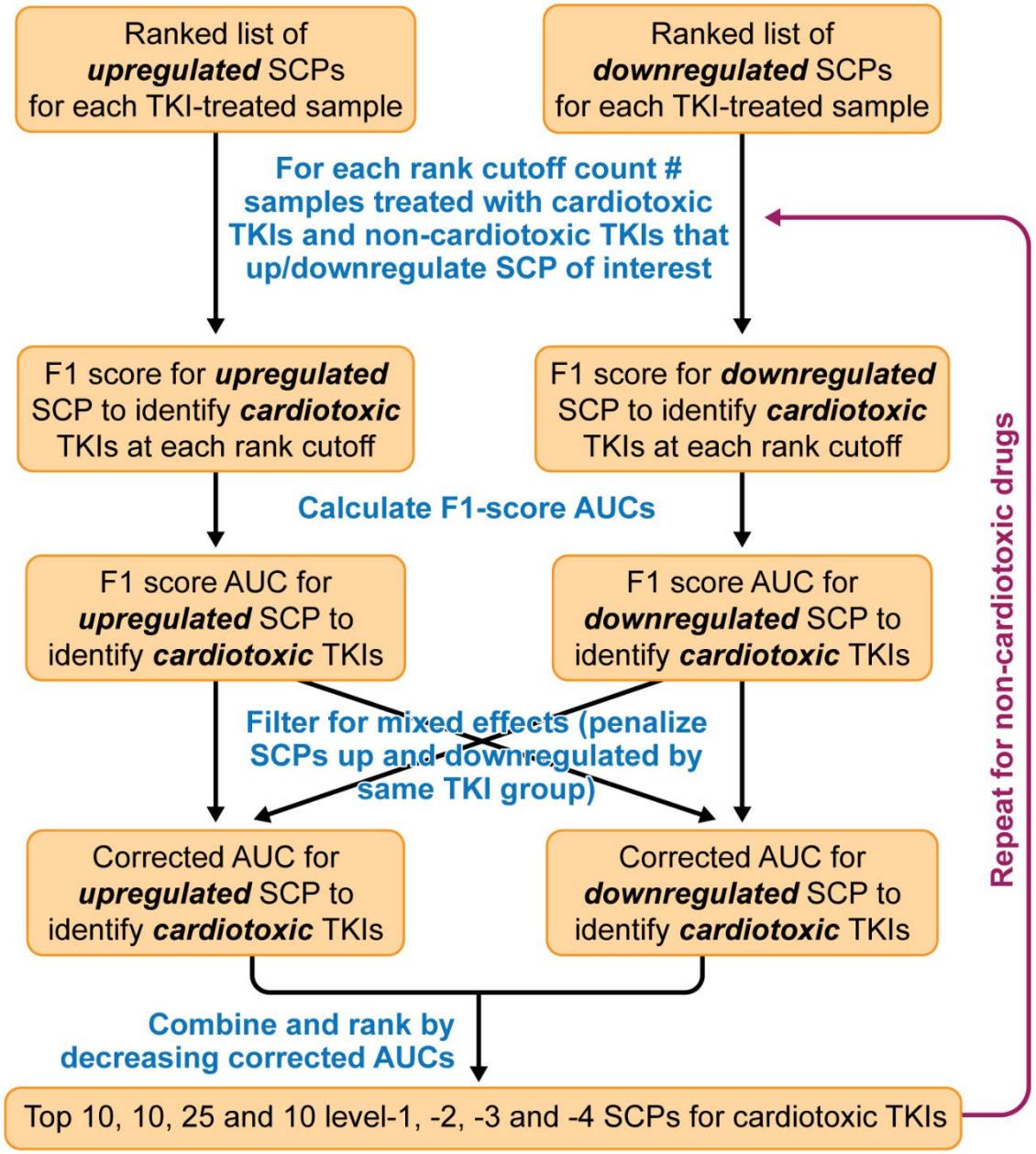

Supplementary Fig. 16

Supplementary Fig. 16. Identification of SCPs associated with cardiotoxic and non-cardiotoxic TKIs. SCPs that were predicted from pathway enrichment analysis of drug-selective gene expression profiles were subjected to our computational pipeline that searches for SCPs associated with a cardiotoxic or non-cardiotoxic response to TKI treatment. See methods for details. Flow chart is used with permission from Mount Sinai Health System, licensed under CC BY.

Supplementary Fig. 17. F1 score and Area Under the Curve statistics. See pages 155 - 173.

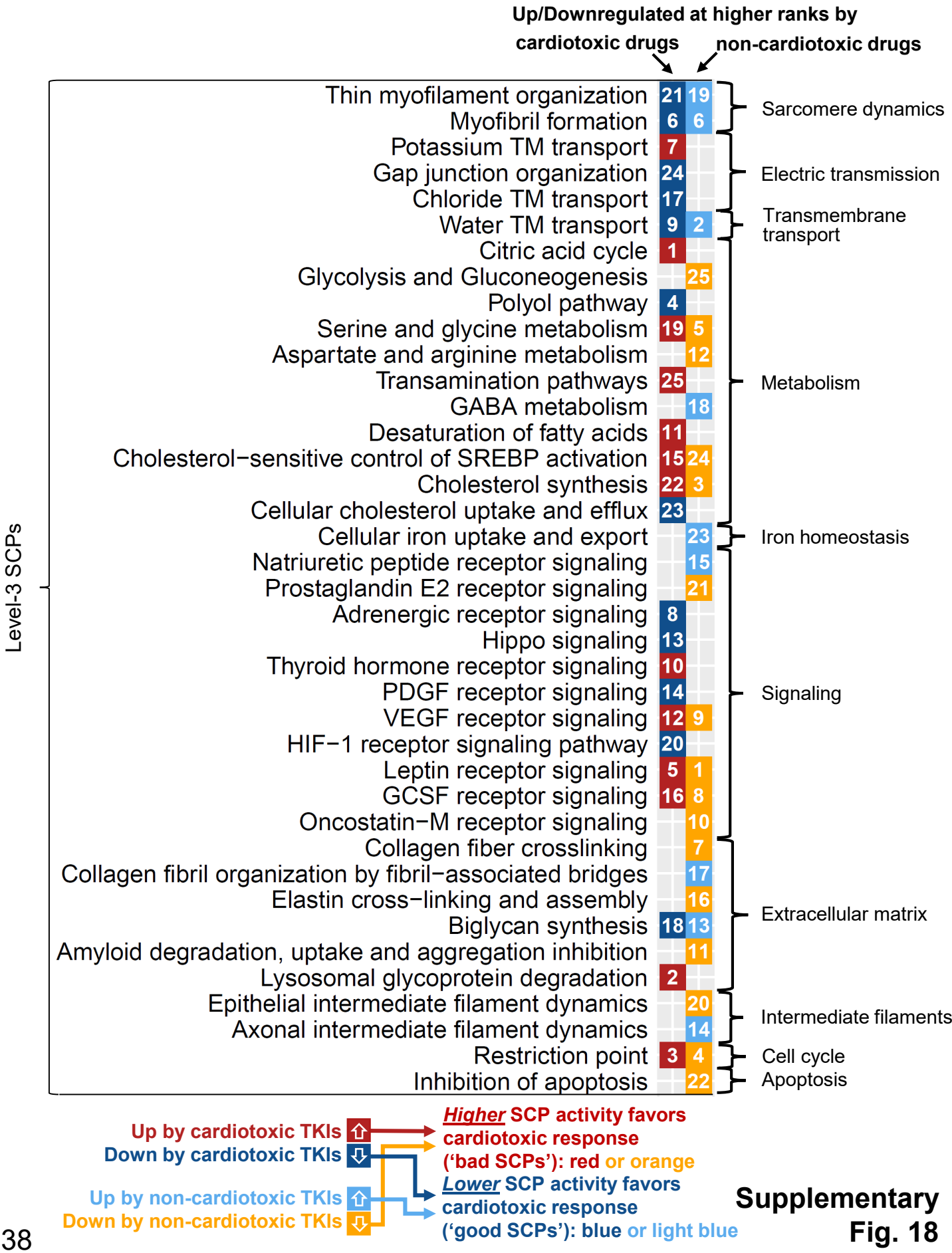

Supplementary Fig. 18

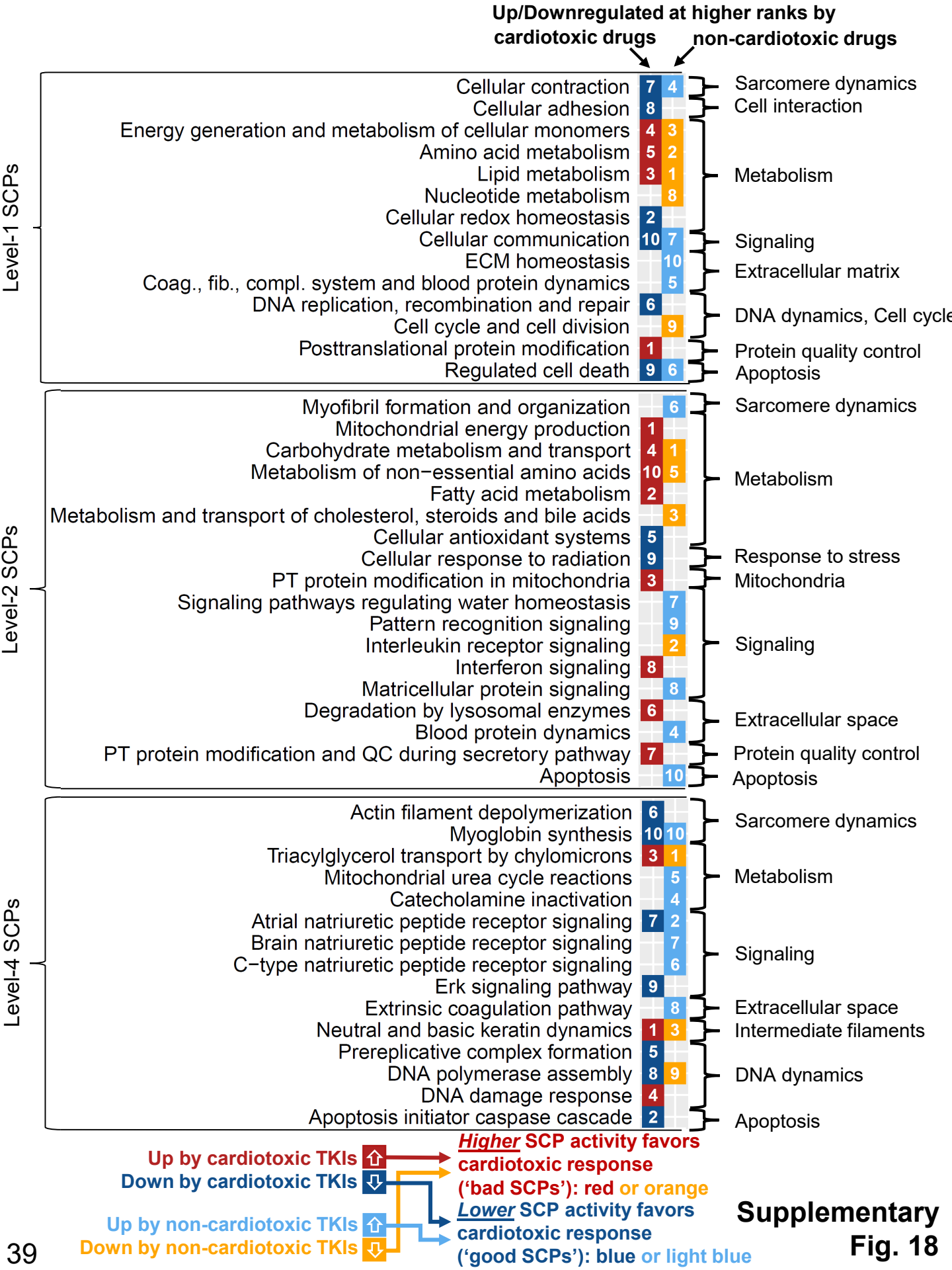

Supplementary Fig. 18

Supplementary Fig. 18. SCPs associated with cardiotoxic and non-cardiotoxic responses. Predicted up- and downregulated subcellular processes (SCPs) of the same level were ranked by significance for each drug and cell line. We searched for those SCPs that are up- or downregulated at higher significance ranks by cardiotoxic or non-cardiotoxic TKIs. Identified SCPs were ranked by their selectivity for either cardiotoxic or non-cardiotoxic drugs (white numbers). To simplify our findings, we defined that SCPs that are upregulated by cardiotoxic drugs (red) or downregulated by non-cardiotoxic drugs (orange) are associated with a cardiotoxic response after upregulation or at baseline level, respectively. For these SCPs a higher activity favors a cardiotoxic response. Similarly, we defined that SCPs downregulated by cardiotoxic (dark blue) or upregulated by non-cardiotoxic drugs (light blue) are associated with a non-cardiotoxic response after downregulation or at baseline level, respectively. For these SCPs a lower activity favors a cardiotoxic response. Shown are the top 25, 10, 10 and 10 predicted level-3, -1, -2 and -4 SCPs for cardiotoxic and non-cardiotoxic TKIs. The level-3 SCPs that are up- or downregulated by cardiotoxic TKIs are also shown in Fig. 2B.

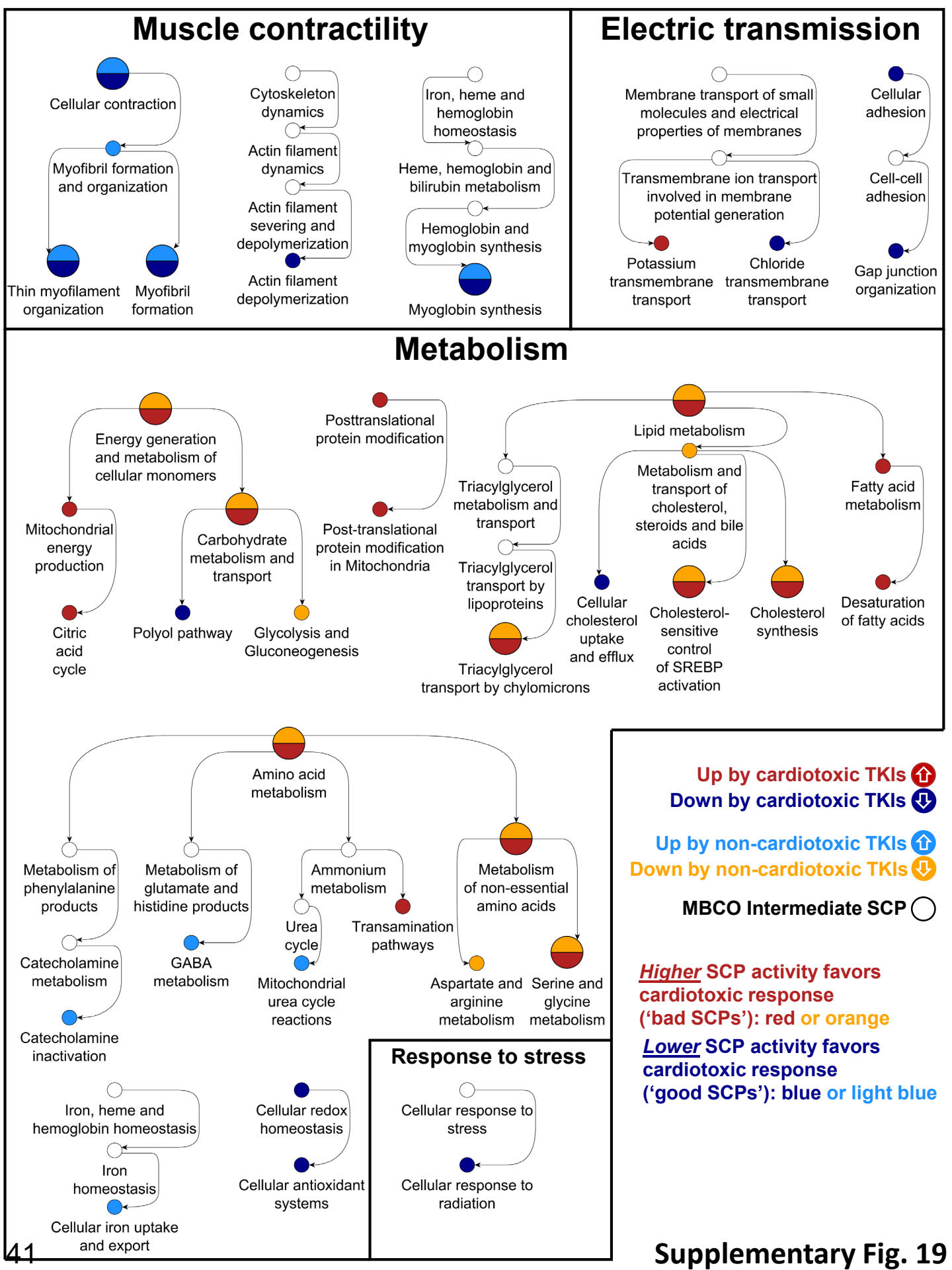

Supplementary Fig. 19

Signaling

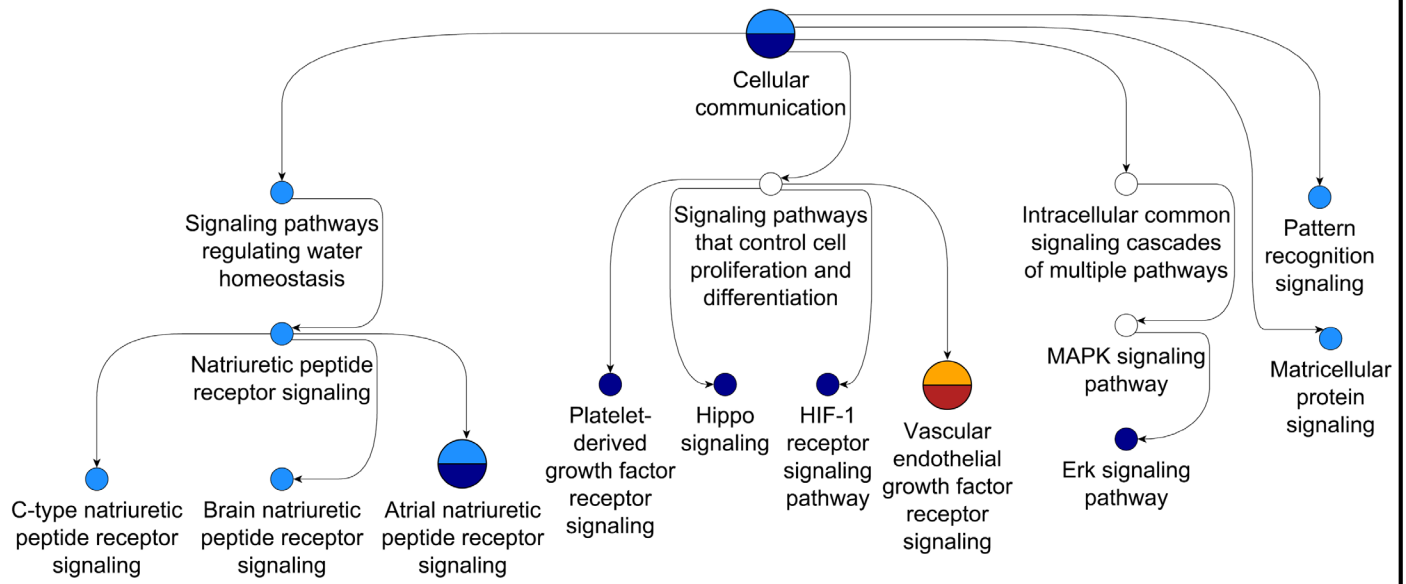

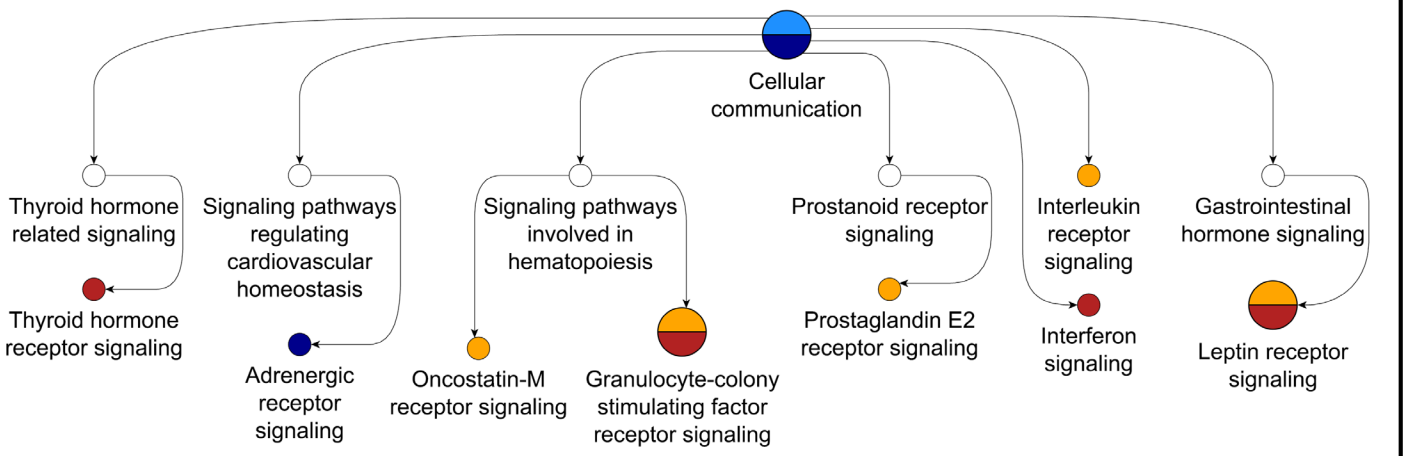

Extracellular matrix and intracellular degradation

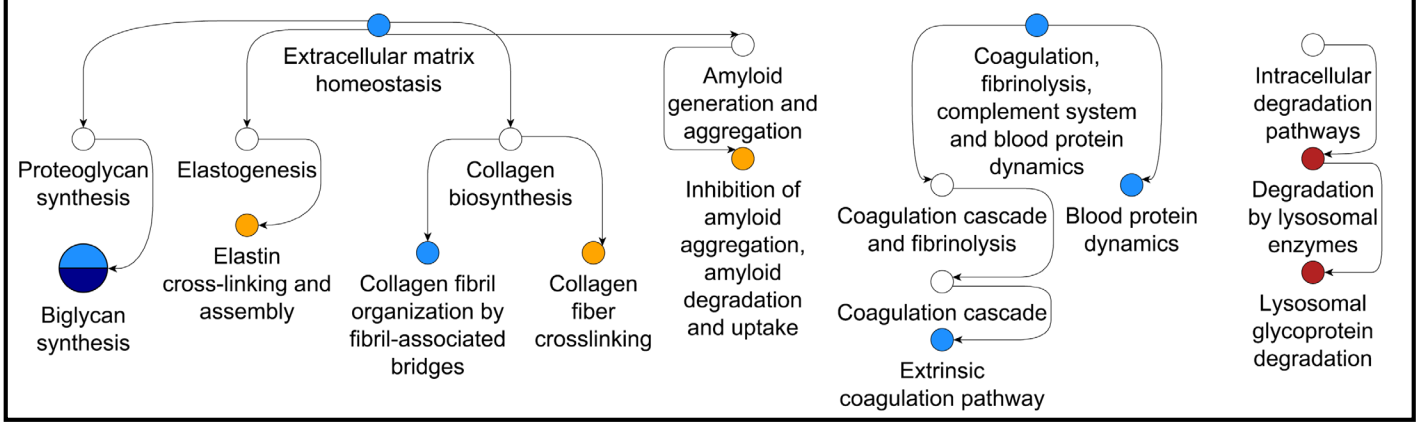

Up by cardiotoxic TKIs
Down by cardiotoxic TKIs
Up by non-cardiotoxic TKIs
Down by non-cardiotoxic TKIs
MBCO Intermediate SCP

Supplementary Fig. 19

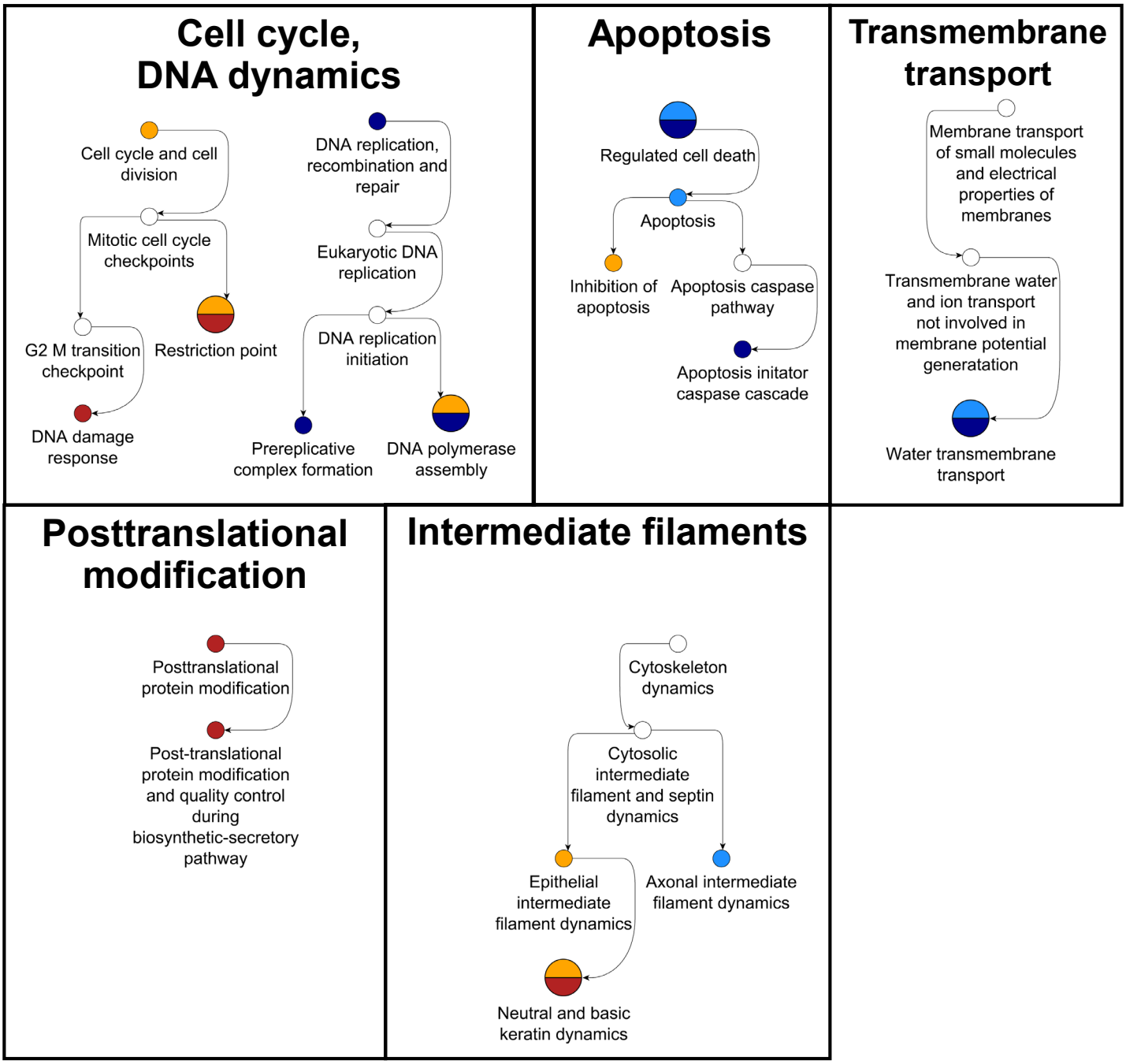

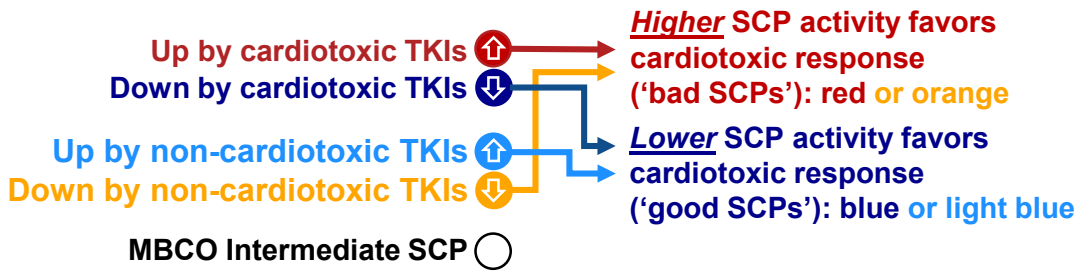

Supplementary Fig. 19

Supplementary Fig. 19. Integration of identified SCPs into the MBCO hierarchy. Up- and downregulated SCPs associated with a cardiotoxic or non-cardiotoxic response were integrated into the MBCO hierarchy. Arrows point from parent to child SCPs. Each tree starts with a level-1 SCP and then consecutively connects it to predicted level-2, -3 and -4 SCPs. Not predicted SCPs that are ancestors of predicted SCPs are in white. Red/orange: SCPs whose higher activity favors a cardiotoxic response, Dark blue/light blue: SCPs whose lower activity favors a cardiotoxic response. The muscle contractility SCPs, and selected SCPs involved in Energy metabolism are also shown in Fig. 2C.

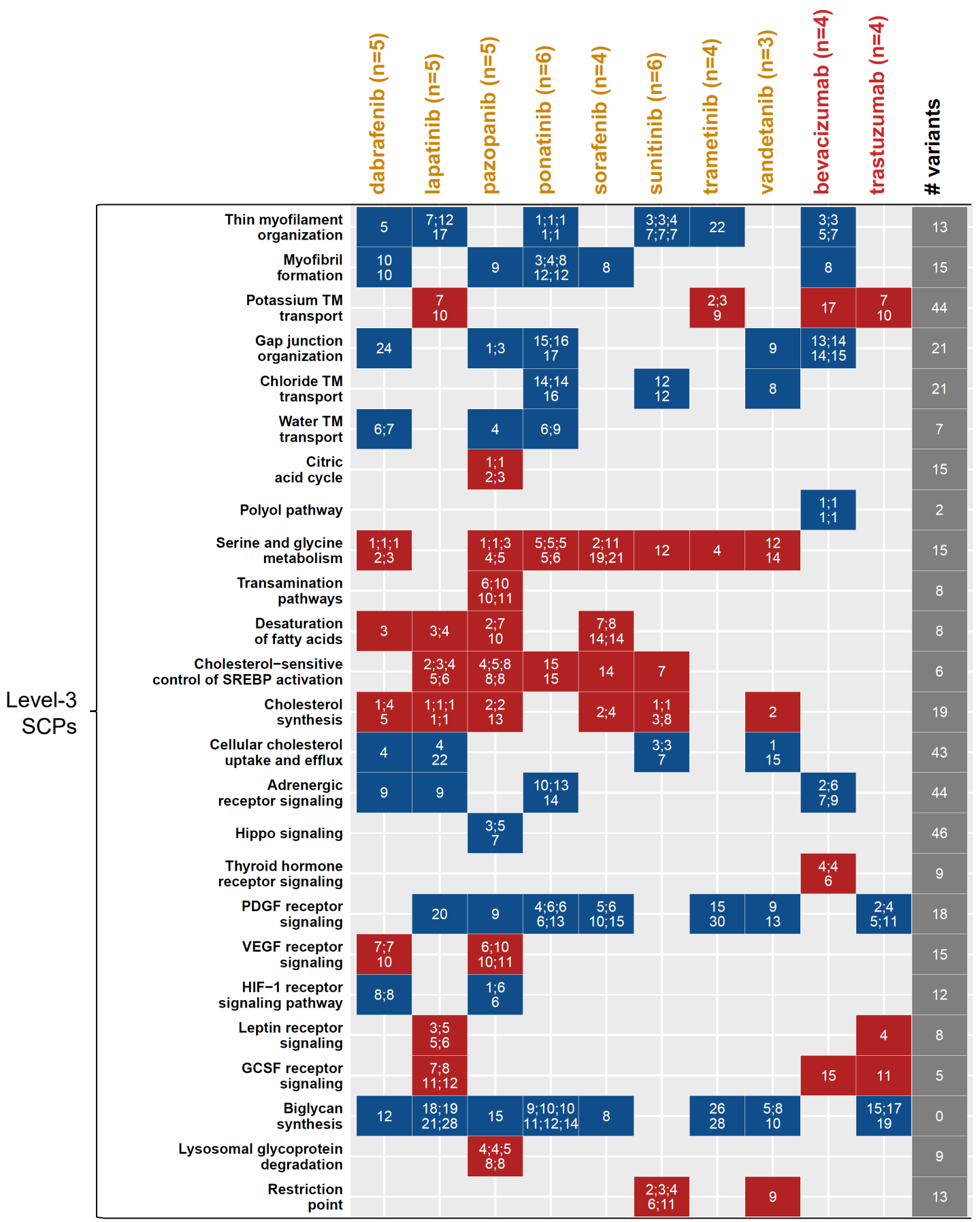

Supplementary Fig. 20

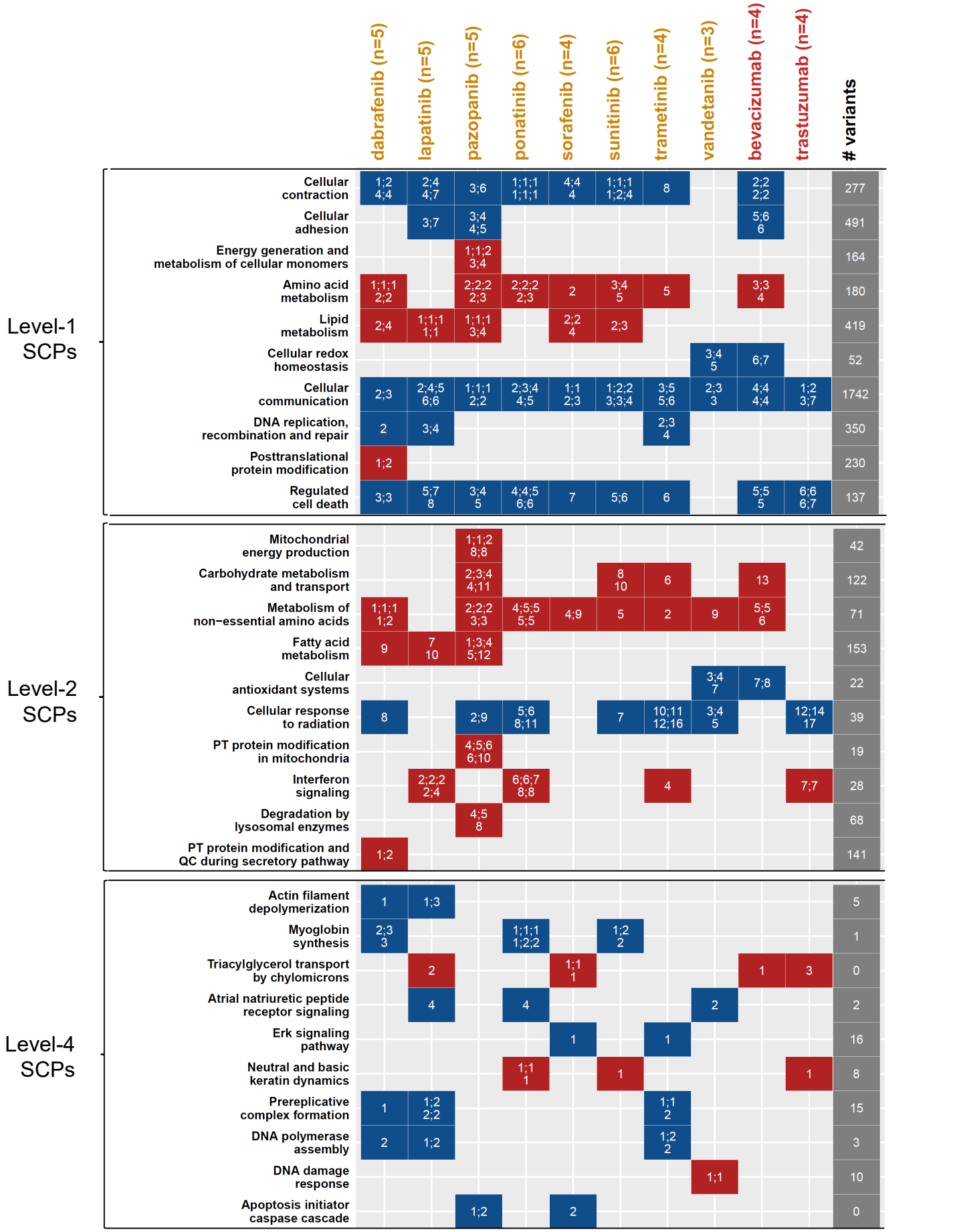

Supplementary Fig. 20

Supplementary Fig. 20. Regulation of identified SCPs by each cardiotoxic TKI. SCPs that were up- or downregulated at higher ranks by cardiotoxic TKIs were mapped back to the individual drugs that upregulated (red) or repressed (dark blue) them. Numbers indicate significance ranks as shown in Suppl. Figs. 14B/C/D/E for level-1, -2, -3 and -4 SCPs. Only ranks that were below the maximum rank cutoff in our F1 score and AUC statistics are shown (20, 20, 30, 20 for level-1, -2, -3 and -4 SCPs). Numbers in parentheses after drug labels indicate total numbers of treated cell lines for each TKI. Number of genomic variants that are underrepresented in the general population and map to SCP genes are shown in the last column. See methods for details. Note that this representation gives an estimation of the recall for each SCP, but does not allow conclusions about the precision that was favored during identification of SCPs associated with a cardiotoxic response. Drug labels of small molecule kinase inhibitors and monoclonal antibodies are colored orange and red, respectively.

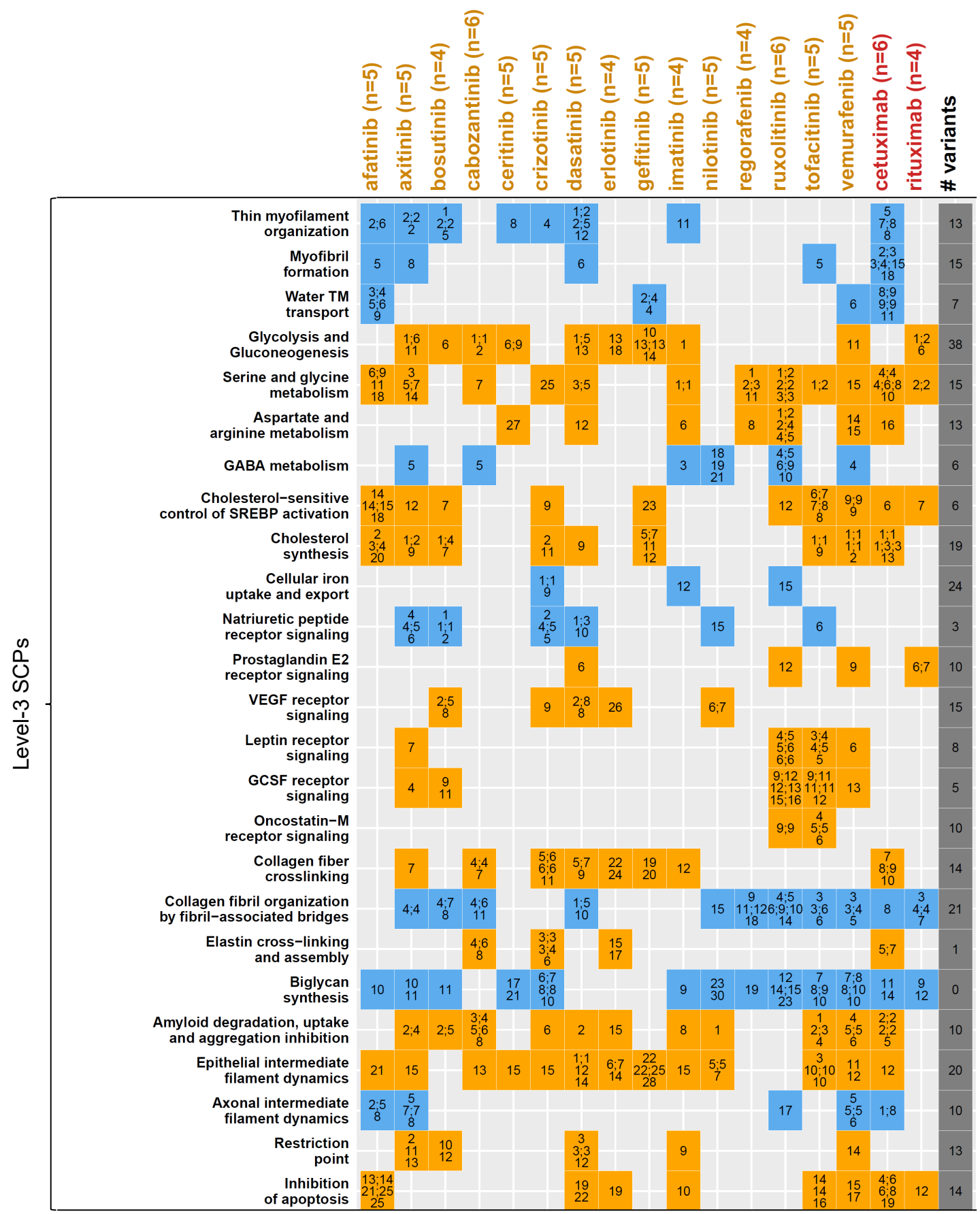

Up by non-cardiotoxic TKIs ('good SCPs')

Down by non-cardiotoxic TKIs ('bad SCPs')

Supplementary Fig. 21

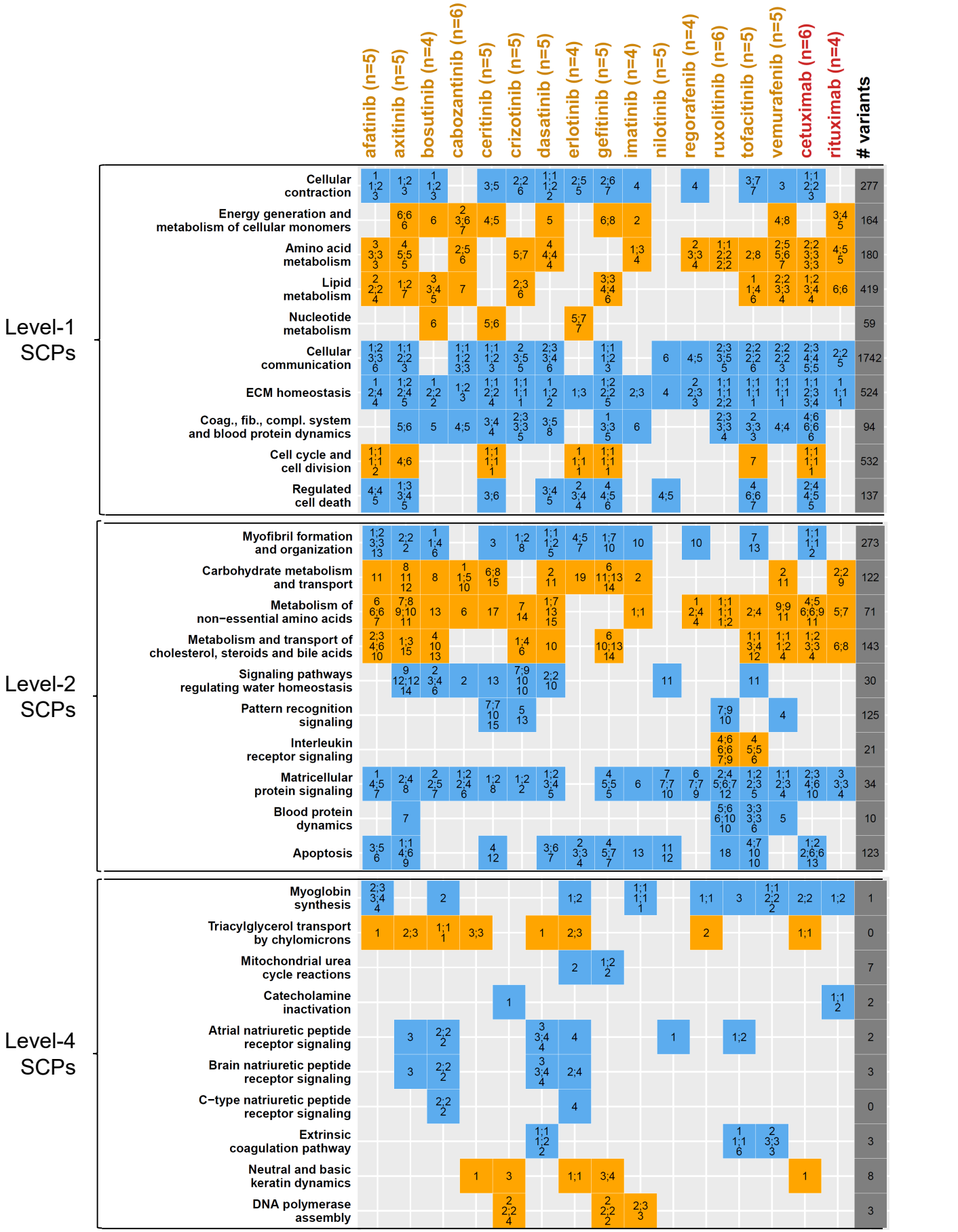

Up by non-cardiotoxic TKIs ('good SCPs')

Down by non-cardiotoxic TKIs ('bad SCPs')

Supplementary Fig. 21

Supplementary Fig. 21. Regulation of identified SCPs by each non-cardiotoxic TKI. SCPs that were up- or downregulated at higher ranks by non-cardiotoxic TKIs were mapped back to the individual drugs that down- (orange) or upregulated (light blue) them. Numbers indicate significance ranks as shown in Suppl. Figs. 14B/C/D/E for level-1, -2, -3 and -4 SCPs. Only ranks that were below the maximum rank cutoff in our F1 score and AUC statistics are shown (20, 20, 30, 20 for level-1, -2, -3 and -4 SCPs). Numbers after drug indicates total numbers of treated cell lines for each TKI. Number of genomic variants that are underrepresented in the general population and map to SCP genes are shown in the last column. See methods for details. Note that this representation gives an estimation of the recall for each SCP, but does not allow conclusions about the precision that was favored during identification of SCPs associated with a non-cardiotoxic response. Drug labels of small molecule kinase inhibitors and monoclonal antibodies are colored orange and red, respectively.

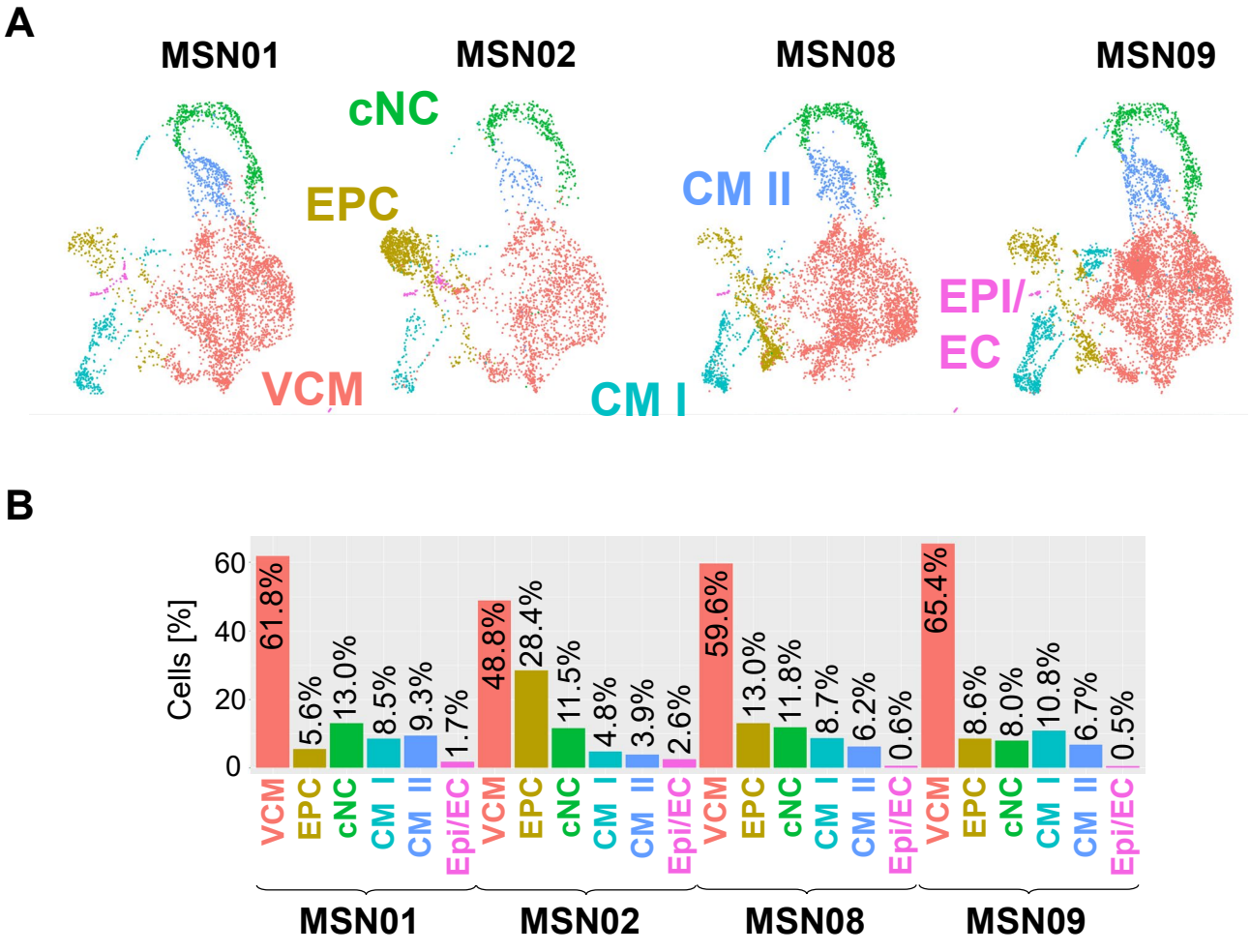

C

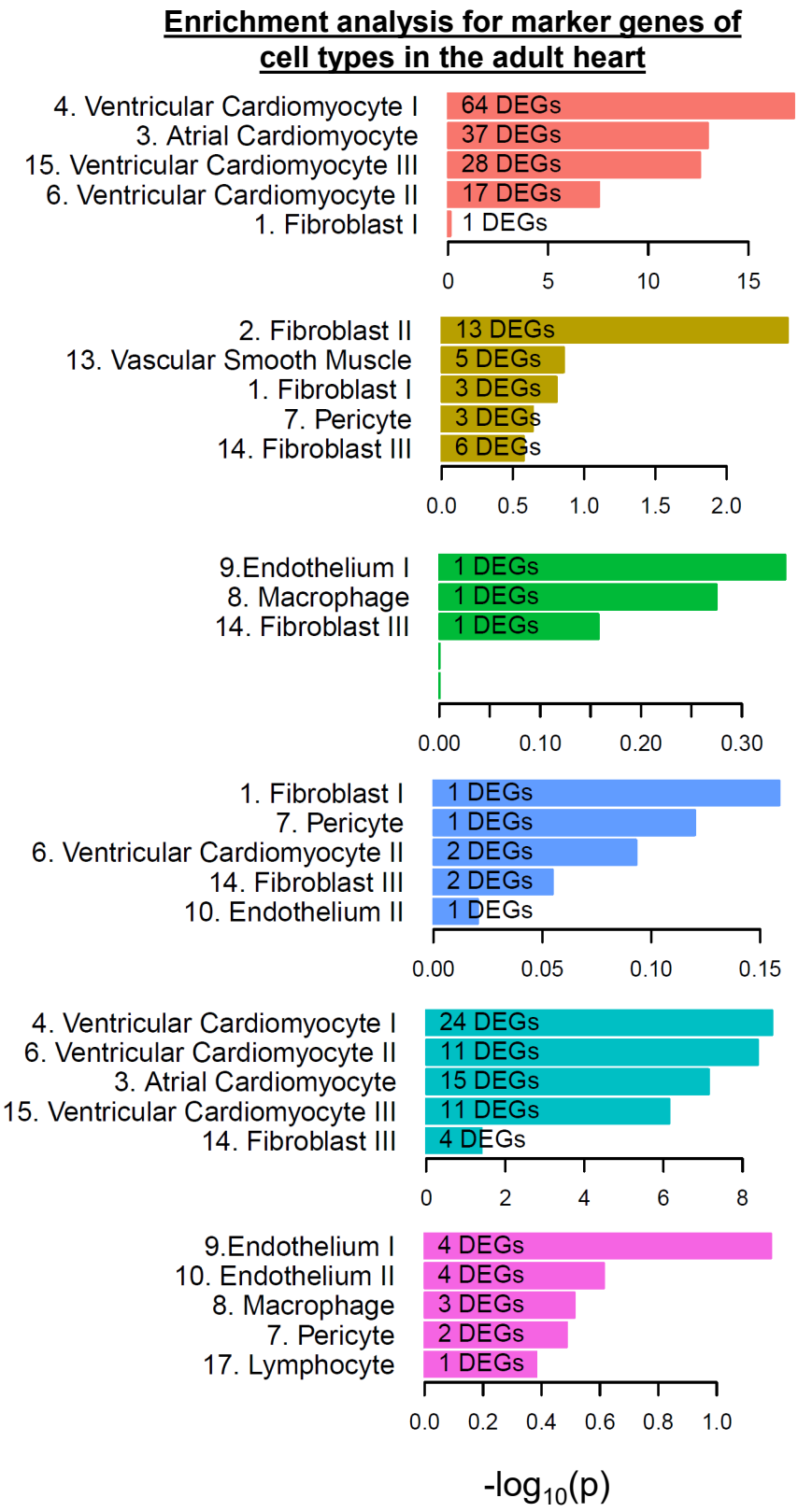

Supplementary Fig. 22

D

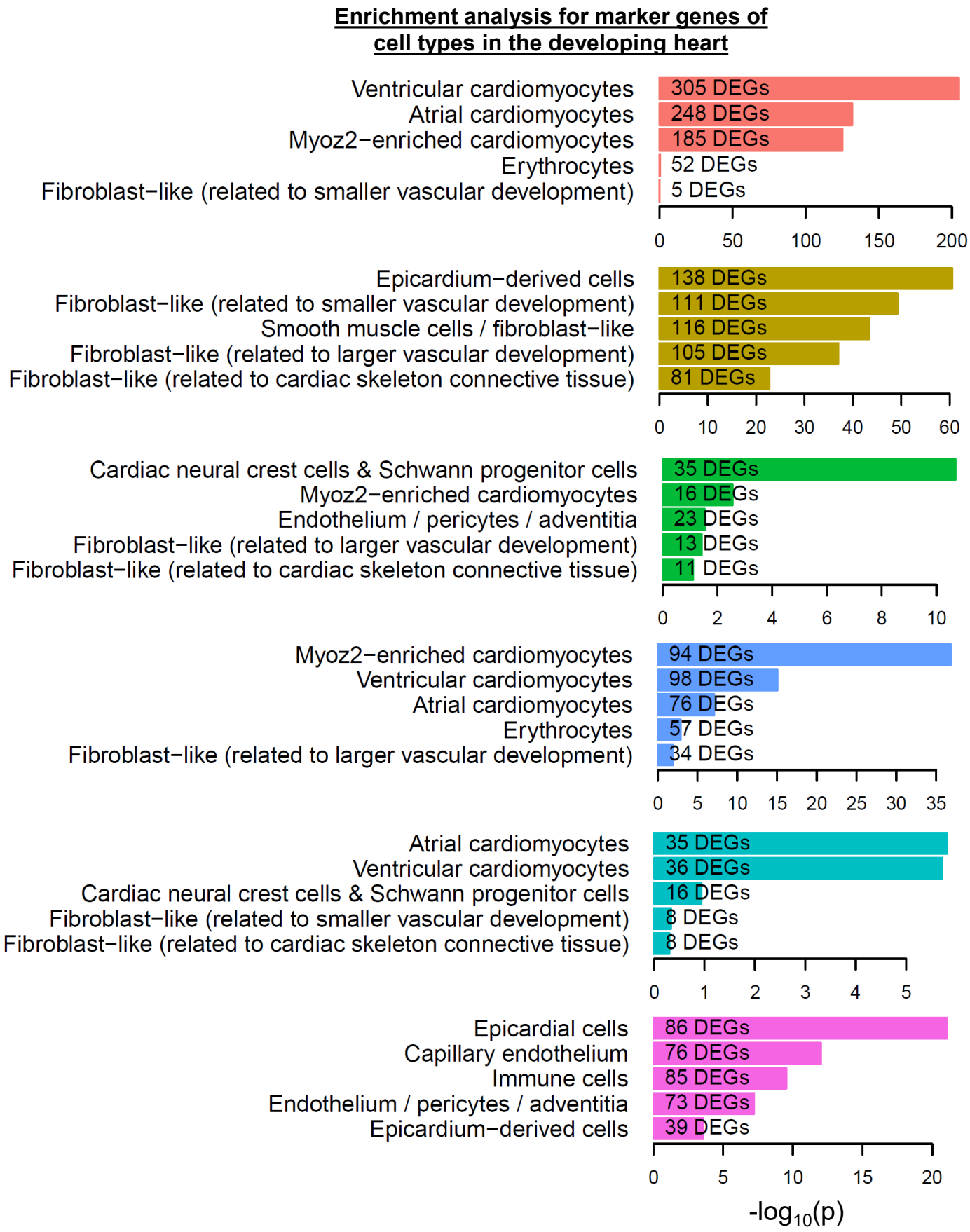

Supplementary Fig. 22

Supplementary Fig. 22. Single cell RNAseq identifies five different cellular subtypes. (A) Single cell RNAseq analysis of four of our six different hiPSC-derived cardiomyocyte cell lines identifies one ventricular cardiomyocyte (VCM) subtype, two additional cardiomyocyte subtypes (CM I and CM II), one epicardial-cell-derived subtype (EPC), one cardiac neural crest (cNC) subtype and one epicardial (EPI) or endothelial (EC) cell subtype. **(B)** Cell counts of the identified subtypes document that most of our cells are ventricular cardiomyoyctes in all four cell lines. A and B are updated versions of two supplemental figures in our previous publication [16]. **(C)** Subtype-specific marker genes were subjected to pathway enrichment analysis using cell type marker genes identified from single nucleus RNAseq of the human adult heart or **(D)** cell type marker genes identified from single nucleus RNAseq of the human fetal heart. Enrichment results were used for cell type annotations shown in (A).

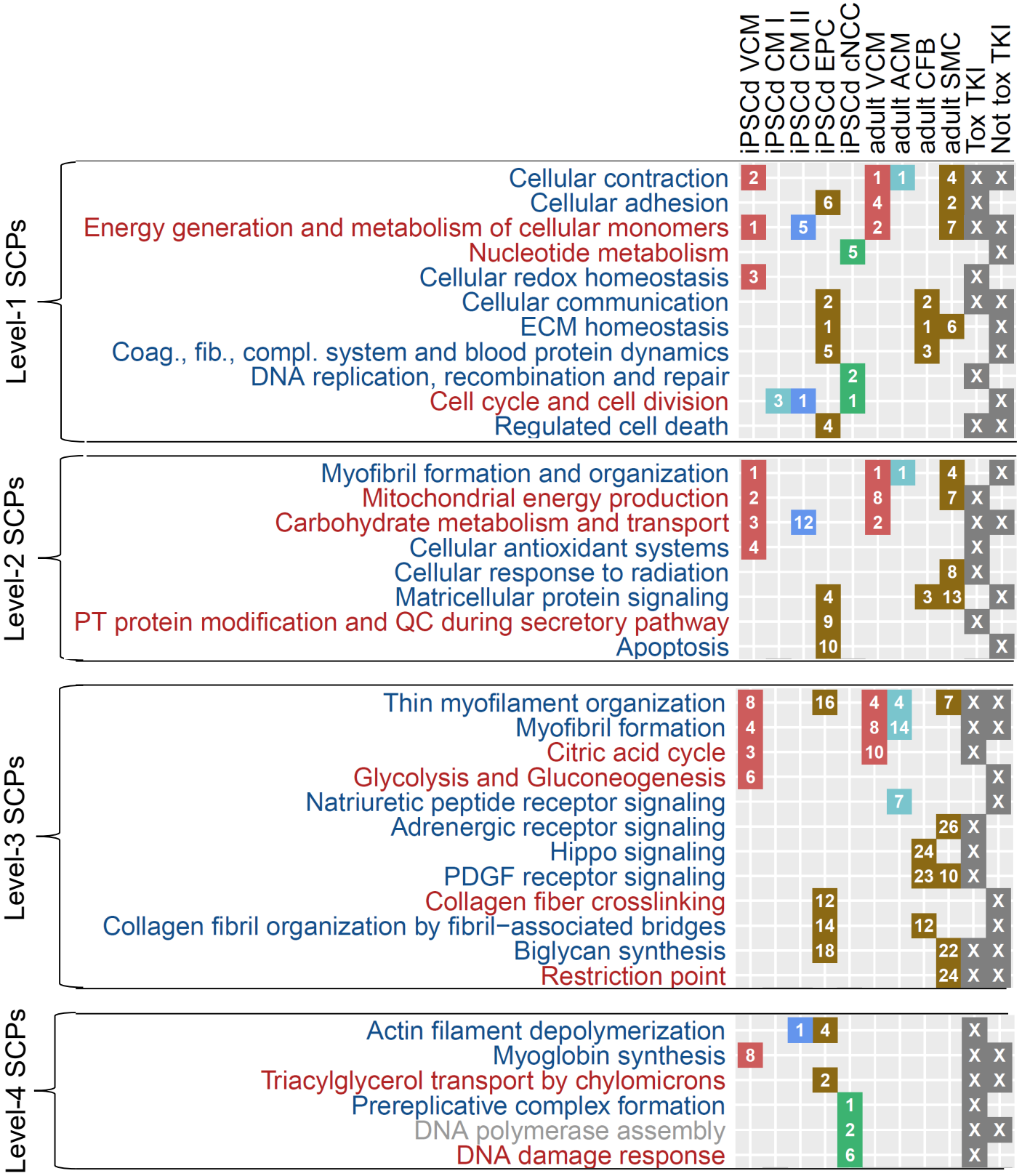

Supplementary Fig. 23

Supplementary Fig. 23. SCPs can be mapped to cellular cardiac cell types. Subtype marker genes identified by single cell RNAseq analysis of our four cell lines [16] were subjected to enrichment analysis using MBCO and Fisher's exact test. Significant SCPs (nominal p-value ≤ 0.05) were ranked by significance (numbers in the diagram). Similarly, we subjected cell type marker genes obtained from single nucleus RNAseq of the adult human heart [29] to pathway enrichment analysis. The last two columns indicate if the SCP was identified based on cardiotoxic and/or non-cardiotoxic TKIs. SCPs whose higher and lower activity is associated with a cardiotoxic response are in red and blue, respectively. Results for level-3 SCPs identified based on cardiotoxic TKIs are also shown in main figure 3A.

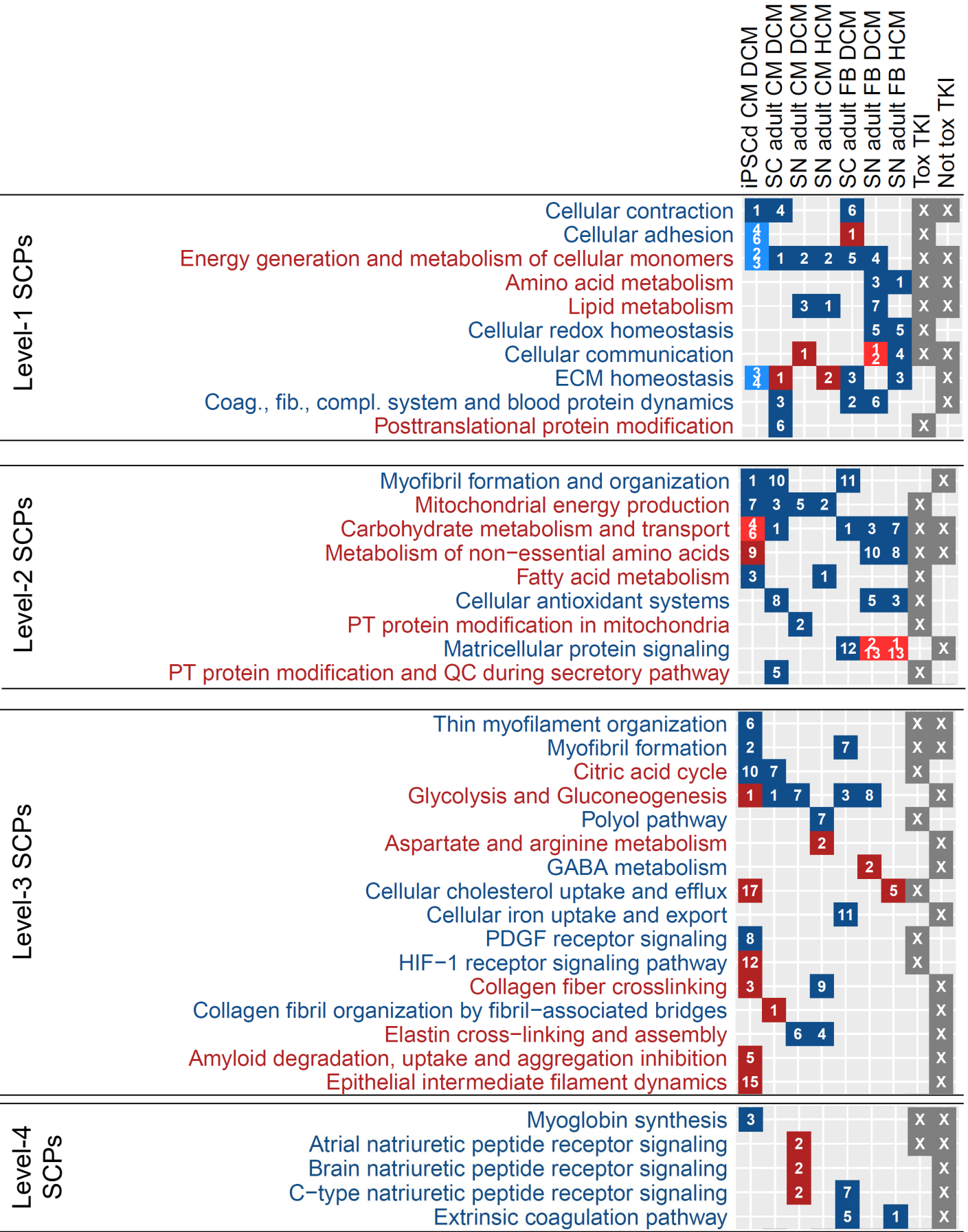

Supplementary Fig. 24

Supplementary Fig. 24. SCPs indicative of TKI-induced cardiotoxicity partially overlap with prior knowledge obtained from single cell and single nucleus RNAseq studies. DEGs in heart cells from patients with DCM or HCM obtained by single cell (SC) [13] and nucleus (SN) [14] RNAseq, respectively, as well as in hiPSC-derived cardiomyocytes from infant DCM patients (GSE184899) were subjected to pathway enrichment analysis using MBCO and Fisher's exact test. Significantly up- or downregulated SCPs of each cell type (nominal p-value ≤ 0.05) were ranked by significance (numbers in the diagram). Only SCPs that overlap with SCPs for which higher (red) or lower (blue) activity favors a cardiotoxic response are shown. The last two columns indicate whether the SCP was identified based on cardiotoxic and/or non-cardiotoxic TKIs. iPSCd: iPSC-derived, CM: cardiomyocyte, FB: Cardiac fibroblast. Results for level-3 SCPs that were predicted based on cardiotoxic TKIs are also shown in main Figure 3B.

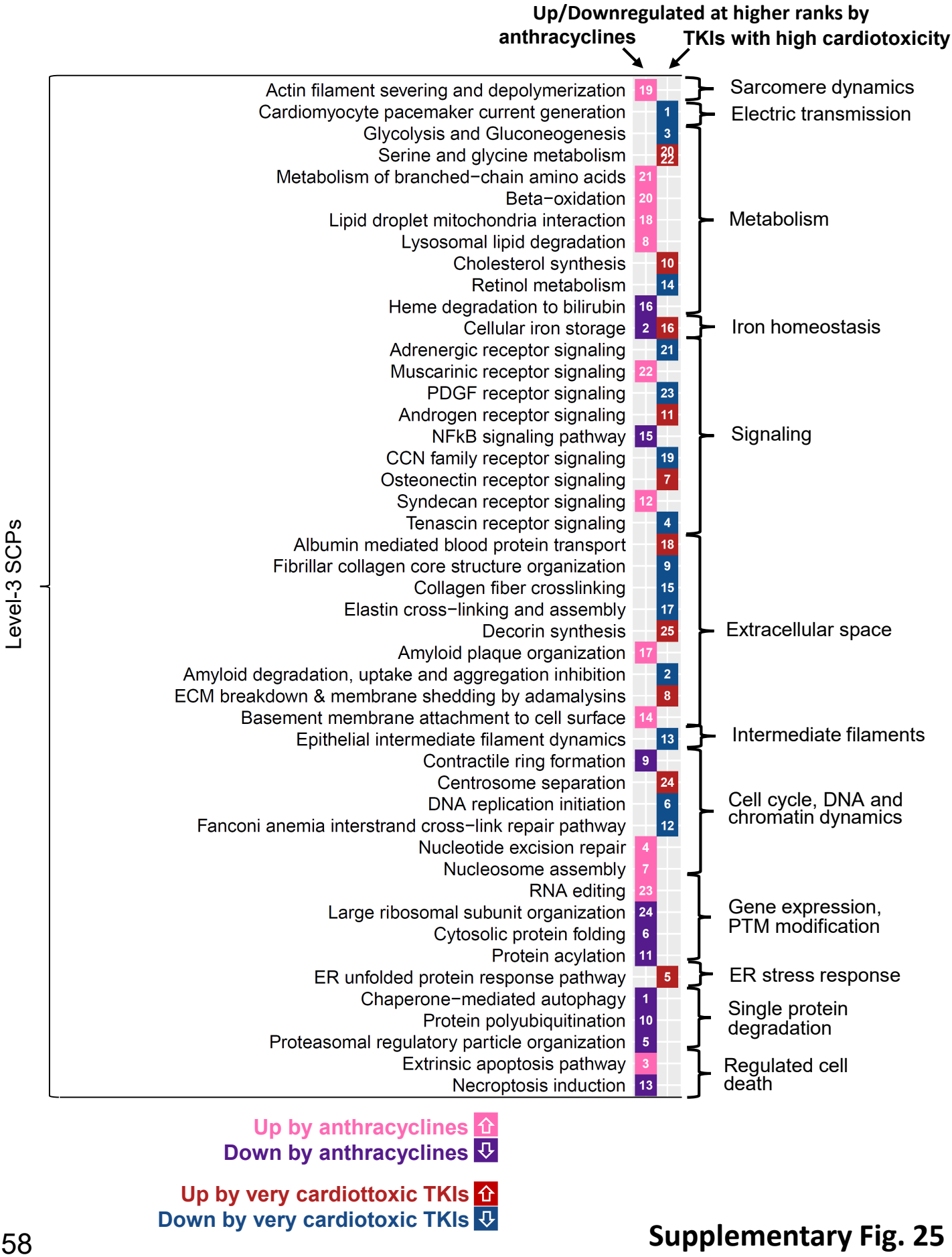

Supplementary Fig. 25

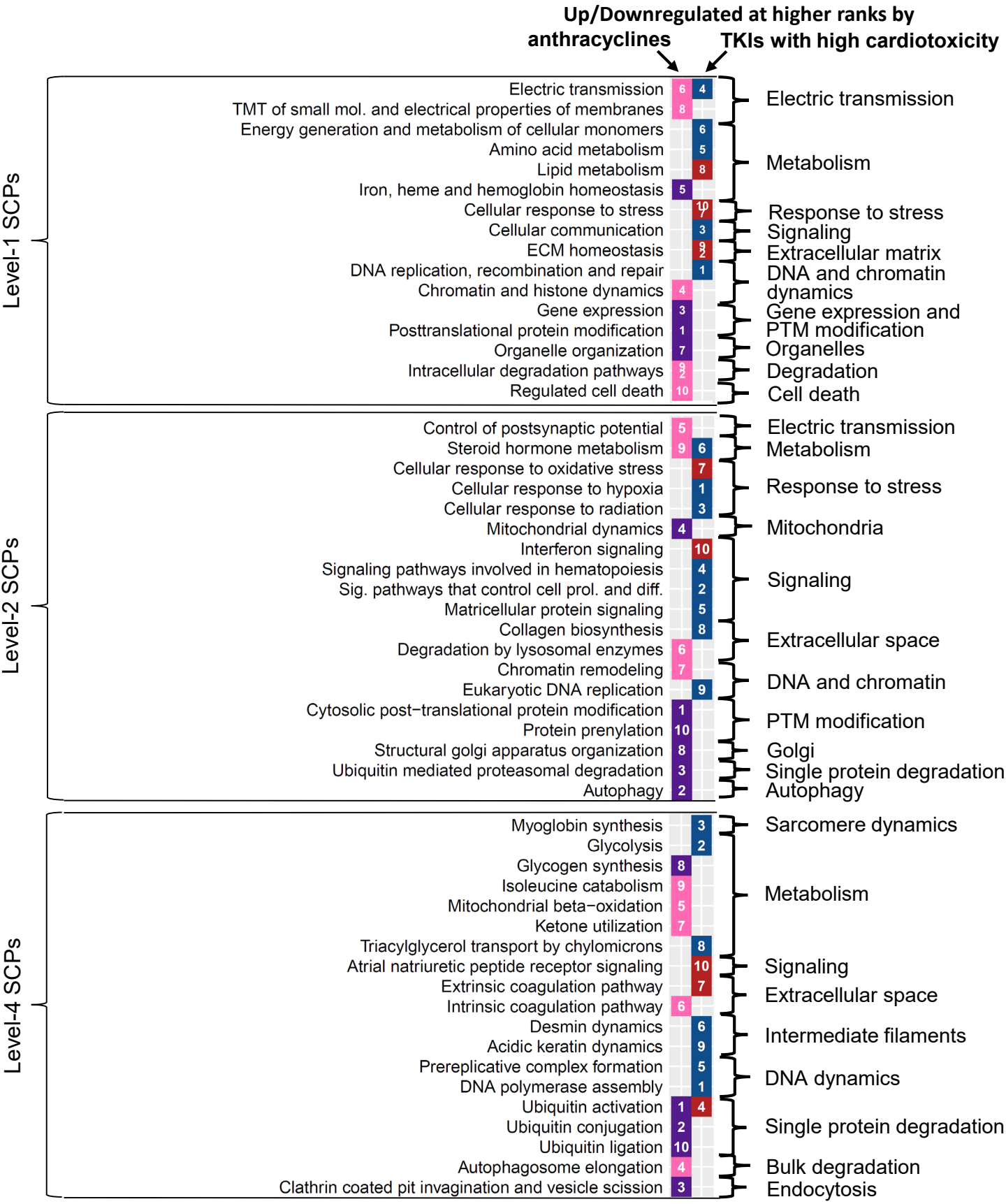

Supplementary Fig. 25

Supplementary Fig. 25. SCPs associated with responses to anthracycline and highly cardiotoxic TKIs. Predicted up- and downregulated subcellular processes (SCPs) of the same level were ranked by significance for each drug and cell line. We searched for those SCPs that are up- or downregulated at higher significance ranks by anthracyclines or highly cardiotoxic TKIs (cardiotoxicity frequency > 10%). Identified SCPs were ranked by their selectivity for either anthracyclines or TKIs (white numbers). Shown are the top 25, 10, 10 and 10 predicted level-3, -1, -2 and -4 SCPs for both drug groups. The level-3 SCPs that are up- or downregulated by anthracyclines are also shown in Fig. 2D. PTM: post-translational modification.

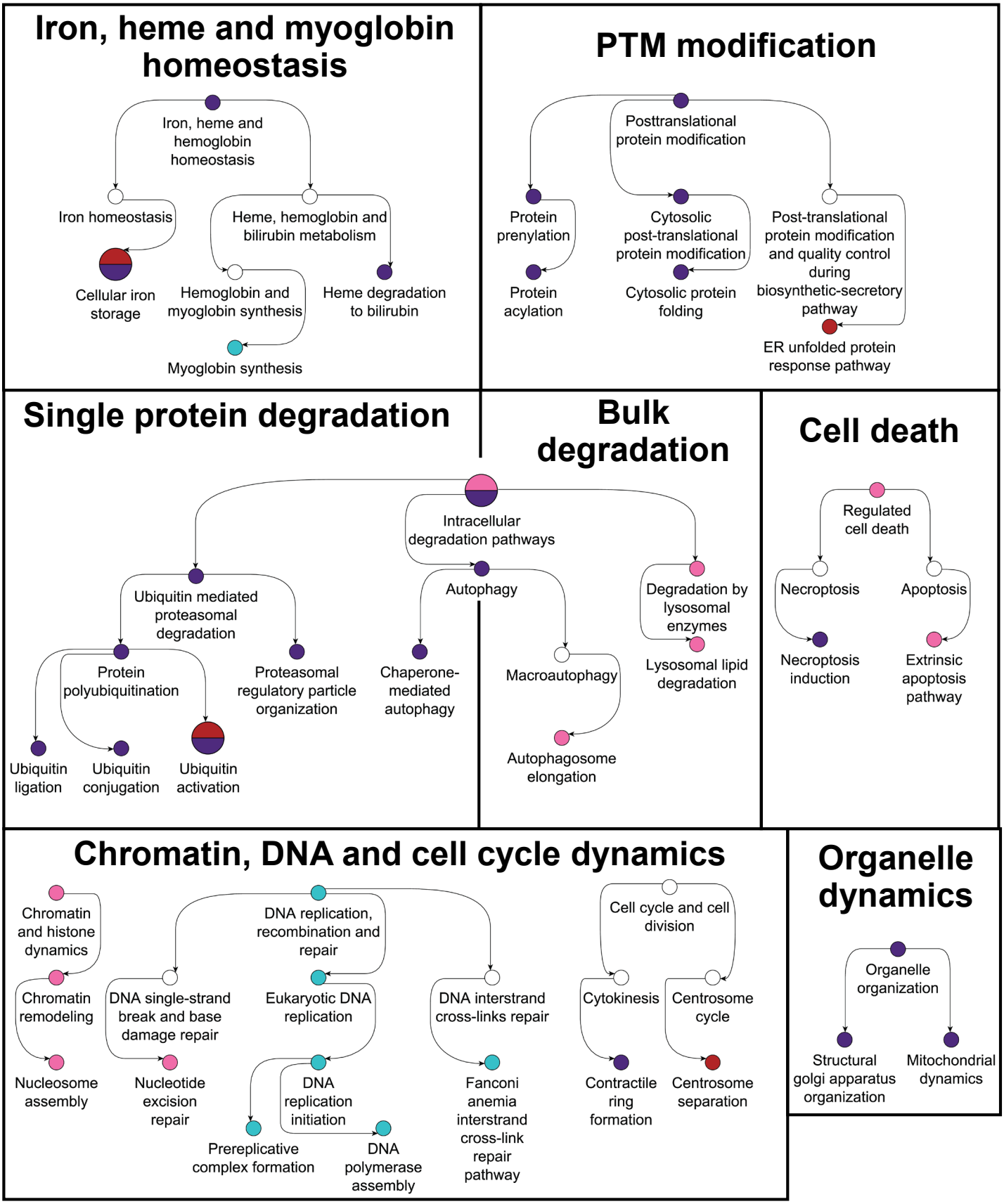

Supplementary Fig. 26

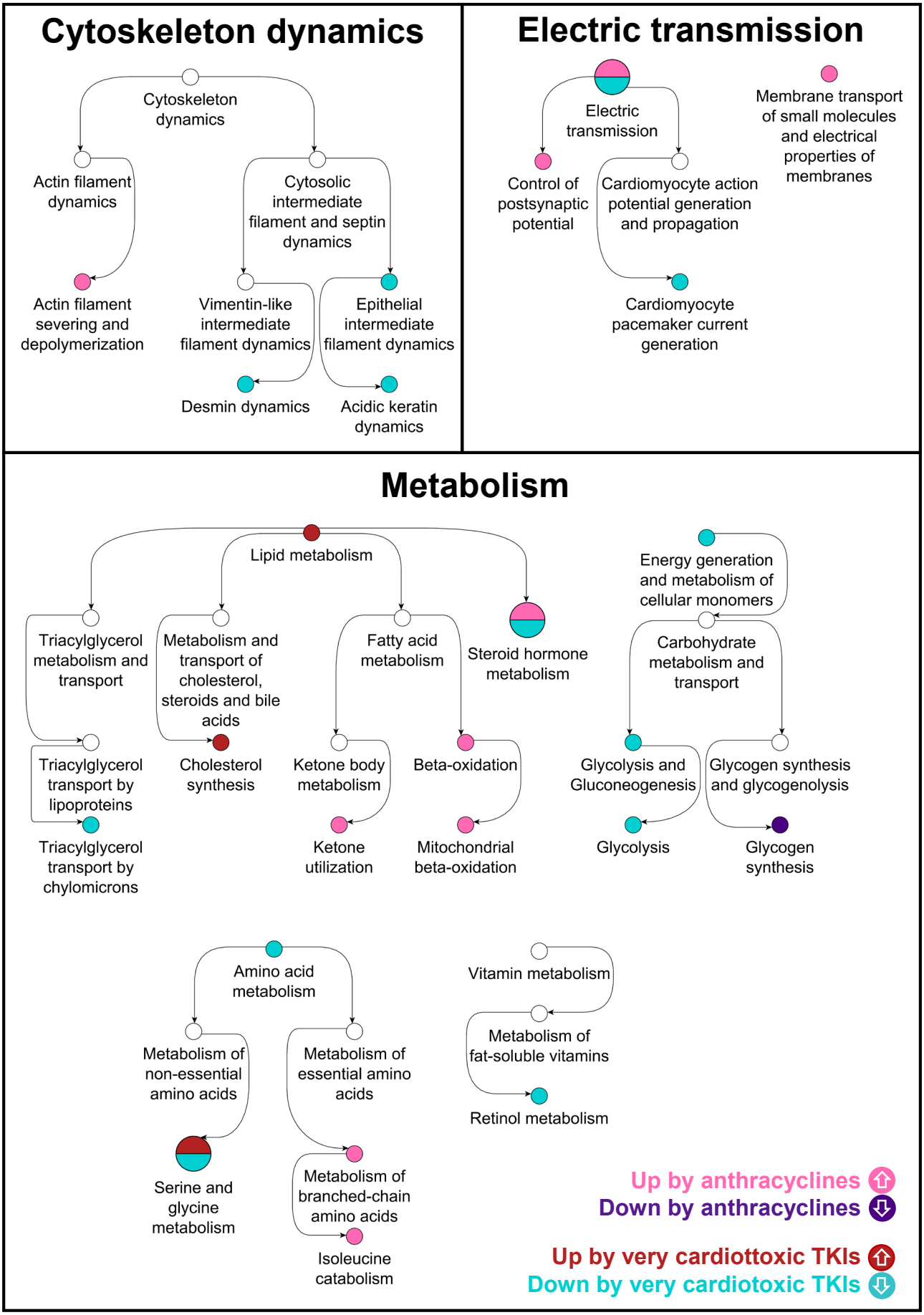

Supplementary Fig. 26

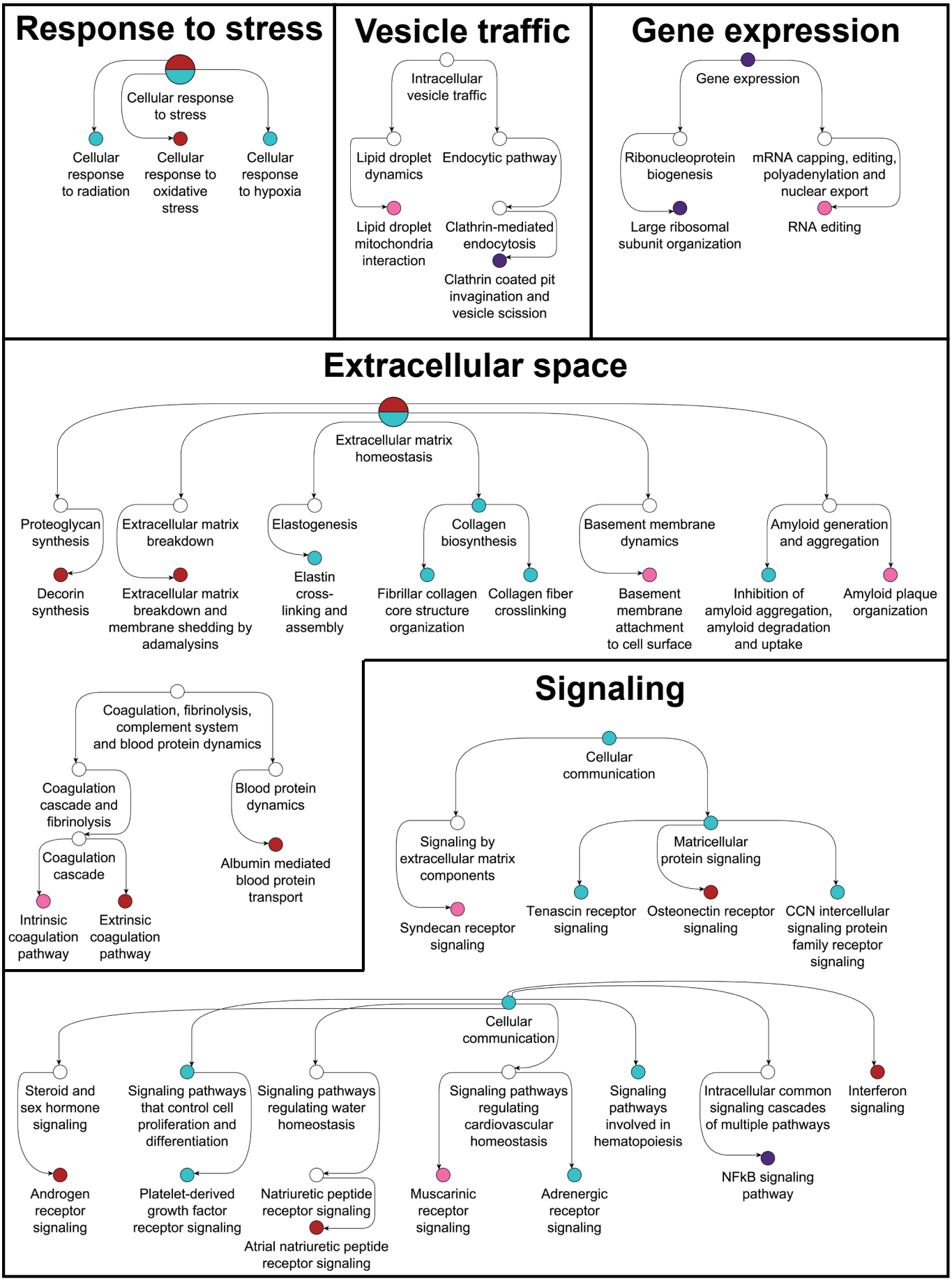

Up by anthracyclines ⇧ Up by very cardiottoxic TKIs ⇧

Down by anthracyclines ⇩ Down by very cardiotoxic TKIs ⇩

Suppl. Fig. 26

Supplementary Fig. 26. Integration of identified SCPs into the MBCO hierarchy. Up- and downregulated SCPs associated with anthracycline or highly cardiotoxic TKI treatment were integrated into the MBCO hierarchy. Arrows point from parent to child SCPs. Each tree starts with a level-1 SCP and then consecutively connects it to predicted level-2, -3 and -4 SCPs. Non-predicted SCPs that are ancestors of predicted SCPs are in white. Most of the SCPs on the first page are also shown in main figure 2E. PTM: post-translational modification.

A.

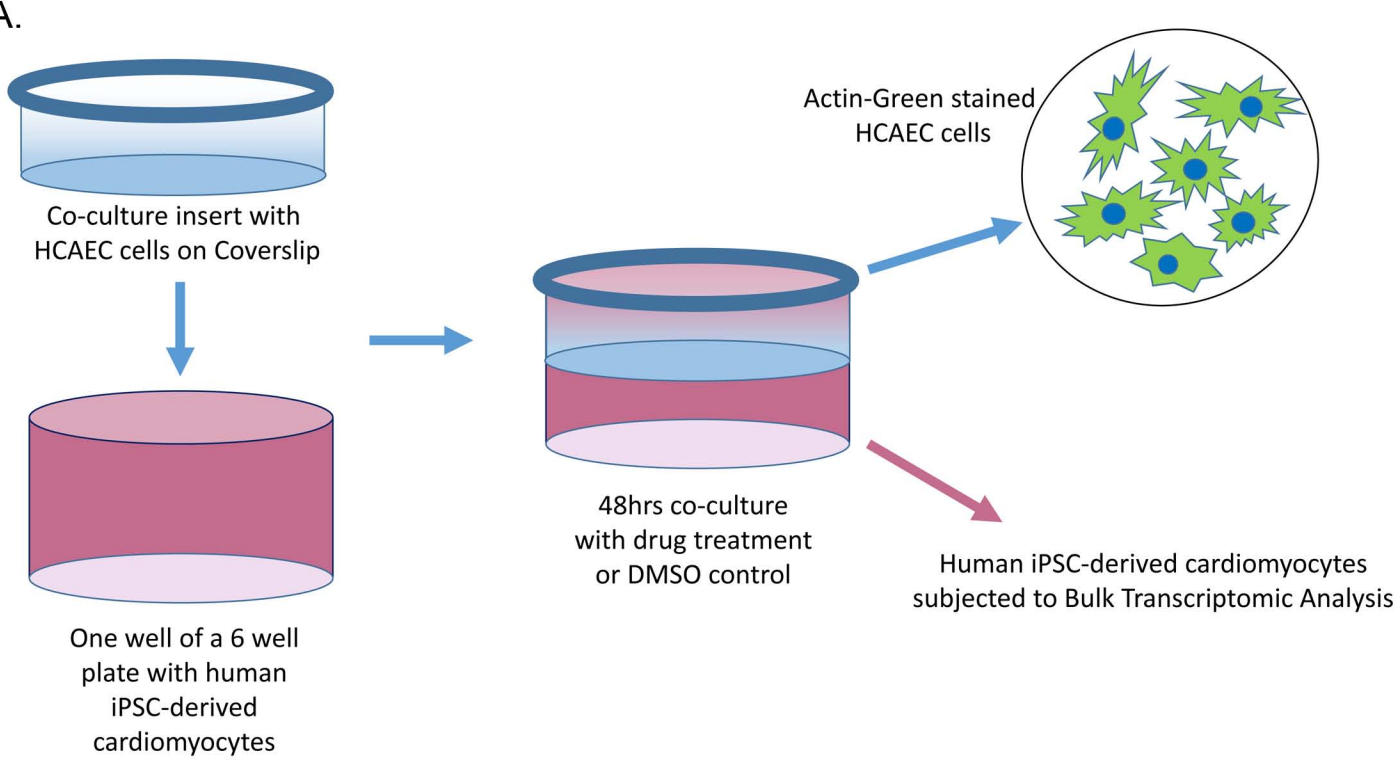

B. Human Coronary Artery Endothelial Cells (HCAEC) stained with Actin-Green

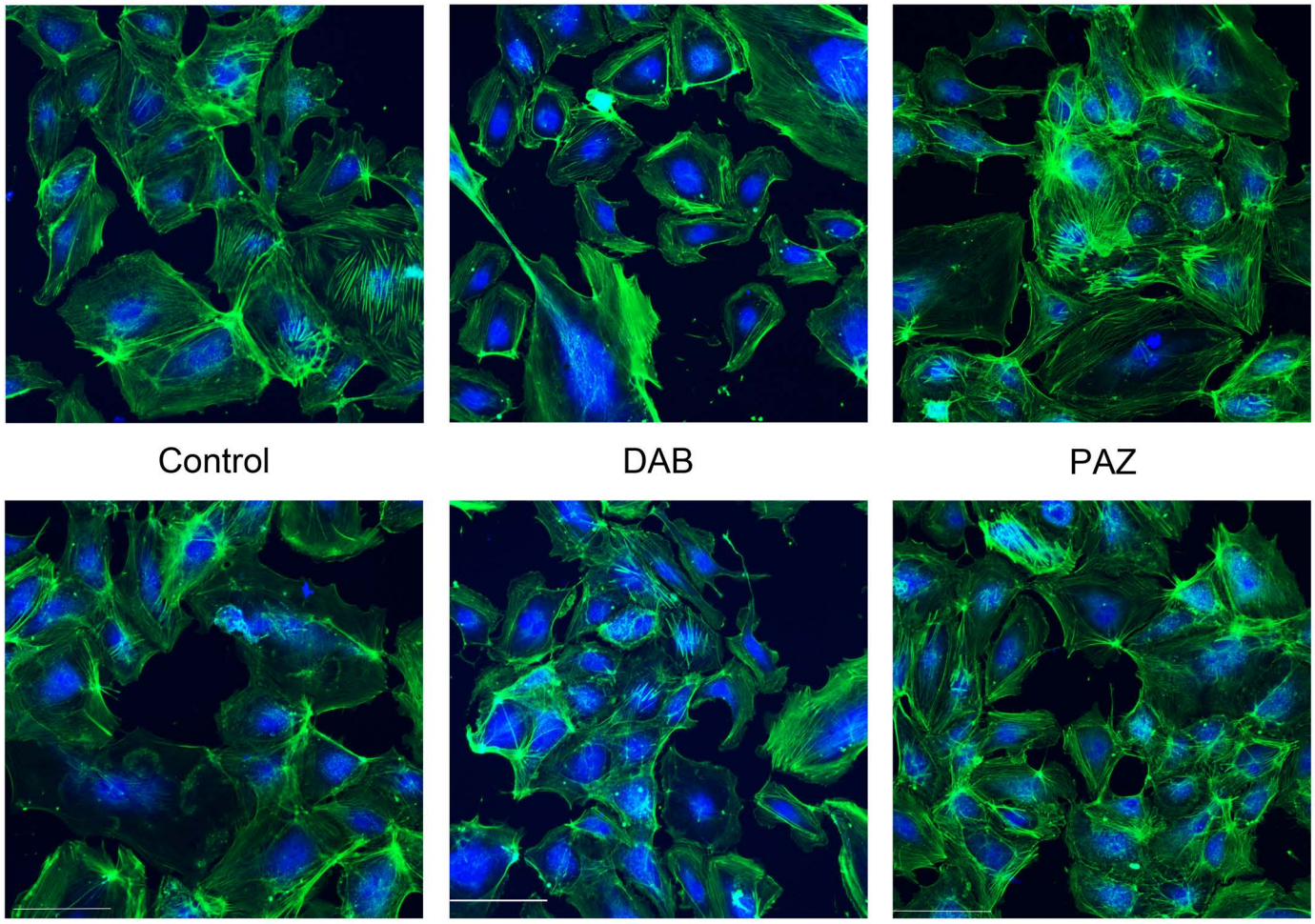

Supplementary Figure 27

Supplementary Fig. 27. Cardiomyocyte-endothelial cell cocultures. (A) iPSC-derived cardiomyocyte (CM) cell lines MSN08 and MSN09 were incubated for 24 hours with or without human coronary artery endothelial cells (HCAEC). HCAEC were seeded on a well insert consisting of a glass coverslip and a porous filter allowing communication between HCAEC and iPSC-CM. Pazopanib, dabrafenib or control vehicles were added to the media, followed by an additional 48 hours before cardiomyocyte harvesting and HCAEC fixation. Cardiomyocytes were subjected to bulk transcriptomic sequencing. **(B)** ACTIN green staining of HCAEC documents endothelial cell phenotypes.

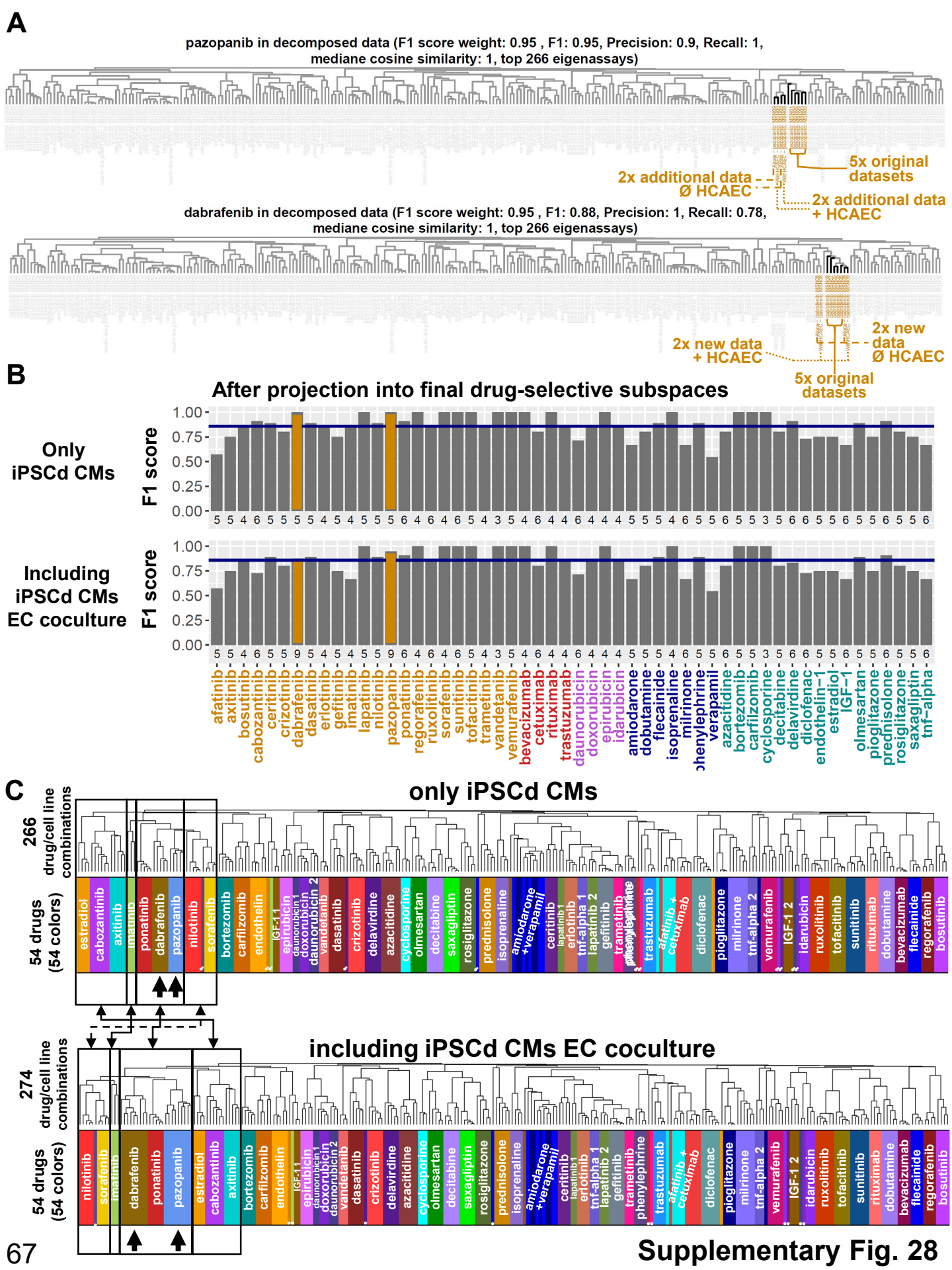

Supplementary Fig. 28

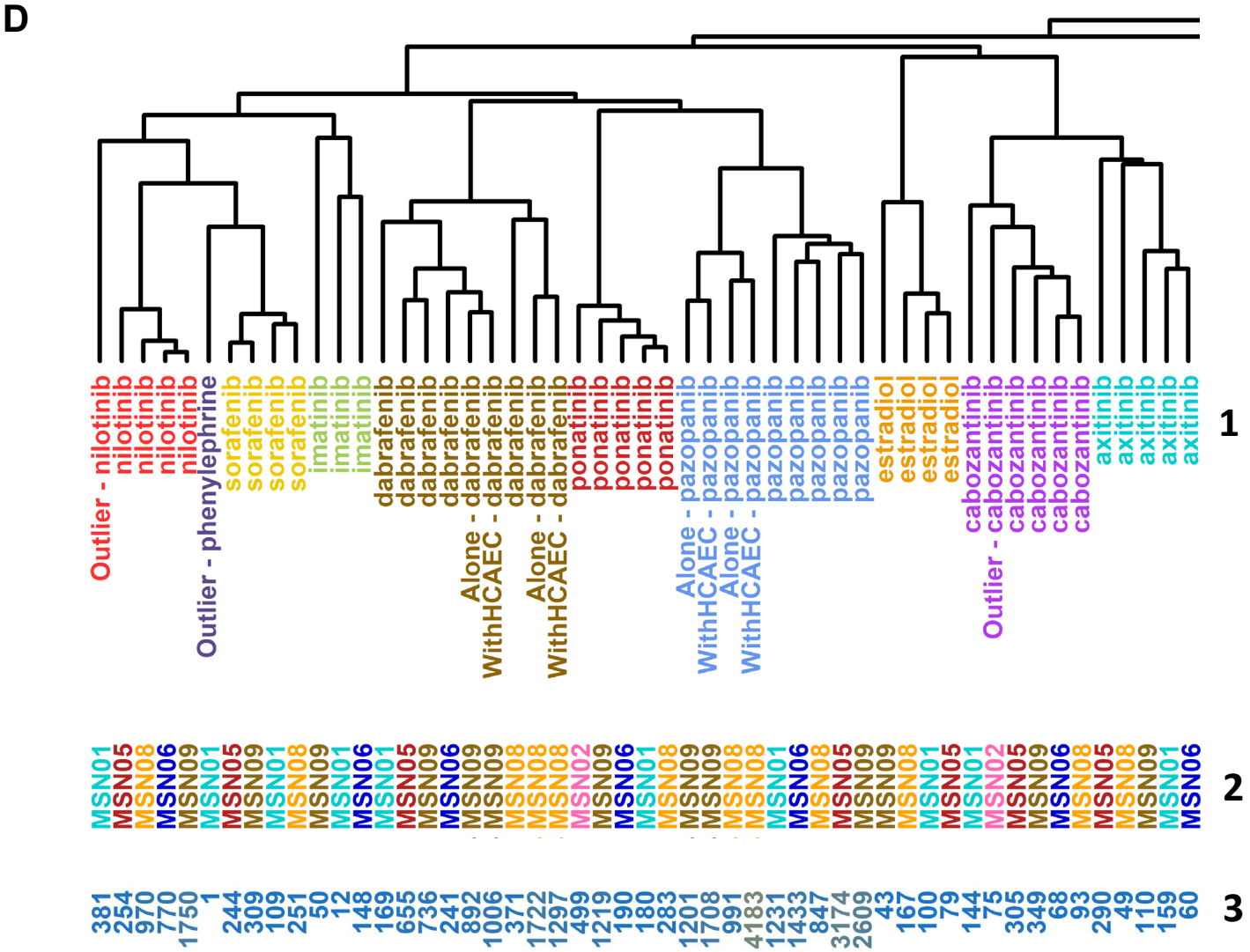

Supplementary Fig. 28

Supplementary Fig. 28. Projection of DEGs from cardiomyocyte-endothelial cell co-culture experiments into drug-selective subspaces. DEGs induced by pazopanib or dabrafenib with or without HCAEC coculture were calculated in cell lines MSN08 and MSN09. The generated additional eight lists of DEGs were merged with the original 266 lists. **(A)** Projection of the combined 274 lists of DEGs into the pazopanib- or dabrafenib-selective subspaces (that were identified using only the original data of 266 lists of DEGs) revealed close clustering of the new pazopanib and dabrafenib-treated cell lines with the existing cell lines treated with the same drugs. A different clustering behavior of the new data generated with or without HCAEC coculture was not observed. **(B)** Comparison of the F1 scores obtained for each drug within its selective subspace, obtained either after projecting the 266 (upper panel) or 274 (lower panel) lists of DEGs, shows only minor differences. Orange bars highlight F1 scores for pazopanib and dabrafenib. The upper panel is identical with the panels shown in Figure 1D and Suppl. Figure 10B. **(C)** All drug-selective DEGs, generated by projecting either the original 266 (upper panel) or the extended 274 (lower panel) lists of DEGs were merged, followed by pairwise correlation and hierarchical clustering. The new data caused small rearrangements in the clustering behavior of nine drugs that cluster close to pazopanib and dabrafenib. Boxes frame treatments that got rearranged against each other. The upper panel is identical with the one shown in Figure 1E. **(D)** The figure shows drug treatments (1), cell lines (2) and number of significant DEGs (3) mapping to the dendrogram area that is framed in C, lower panel.

Supplementary Fig. 29. Top Subcellular Processes predicted from complete gene expression profiles, after removal of first eigenarray and from drug-selective gene expression profiles of all dabrafenib or pazopanib-treated samples. See pages 174 - 182.

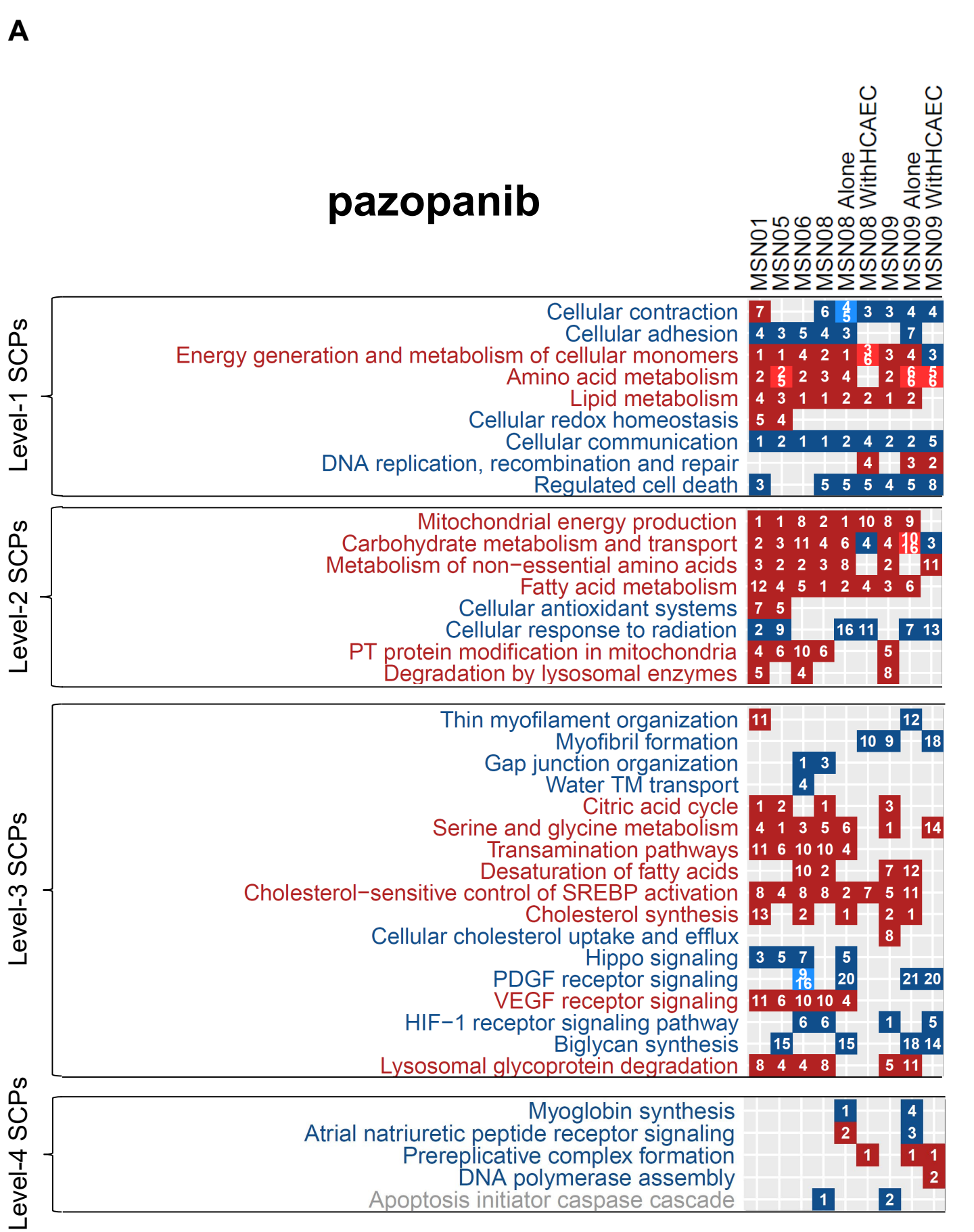

Supplementary Fig. 30

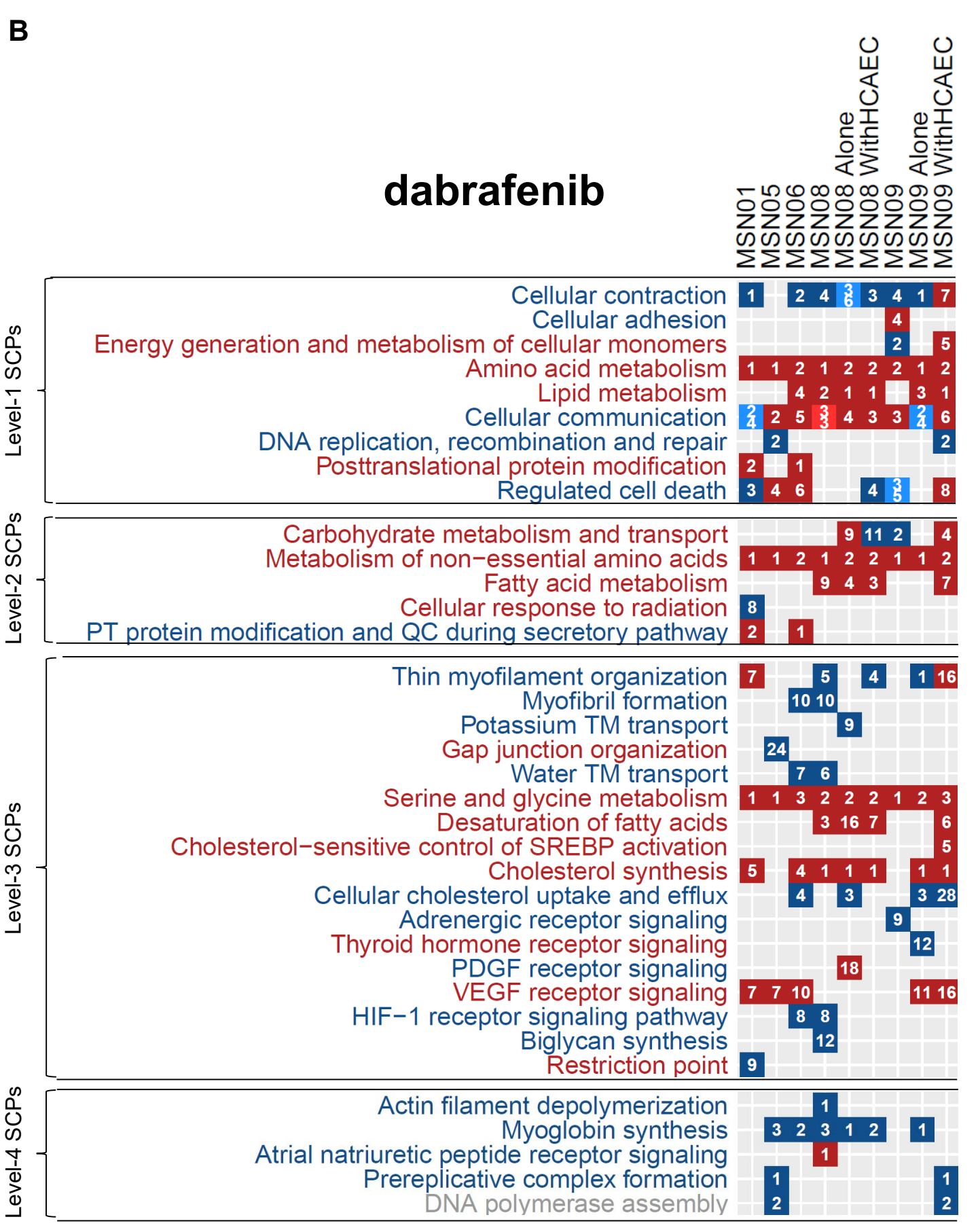

Supplementary Fig. 30

Supplementary Fig. 30. Coculture with HCAEC has only minor influence on up or down regulation of cardiotoxic pathways. (A) Enrichment results (p-value ≤ 0.05) of DEGs induced by pazopanib were filtered for pathways for which a higher (red SCP names) or lower (blue SCP names) activity favors a cardiotoxic response, as predicted from the cardiotoxic drugs. Gray labels an SCP with conflicting results. Since our F1 score and AUC statistics only considered SCPs with a maximum p-value of 0.05 and a maximum significance rank of 20, 20, 30 and 20 for level-1, -2, -3 and -4 SCPs, we filtered the pazopanib-induced pathways using the same criteria. Numbers show enrichment ranks in indicated cell lines. Ranks on a red or blue field indicate up- or downregulation. Bright red fields indicate up- and downregulation with the upper and lower rank in that field, respectively. Reversely, light blue fields indicate down- and upregulation with the upper and lower rank in that field, respectively. Original datasets are only labeled with the stimulated cell lines, additional datasets are further labeled with 'Alone' or 'With HCAEC', if they were obtained from cardiomyocytes cultured without or with HCAEC, respectively. **(B)** The figure shows described results obtained for dabrafenib treatments.

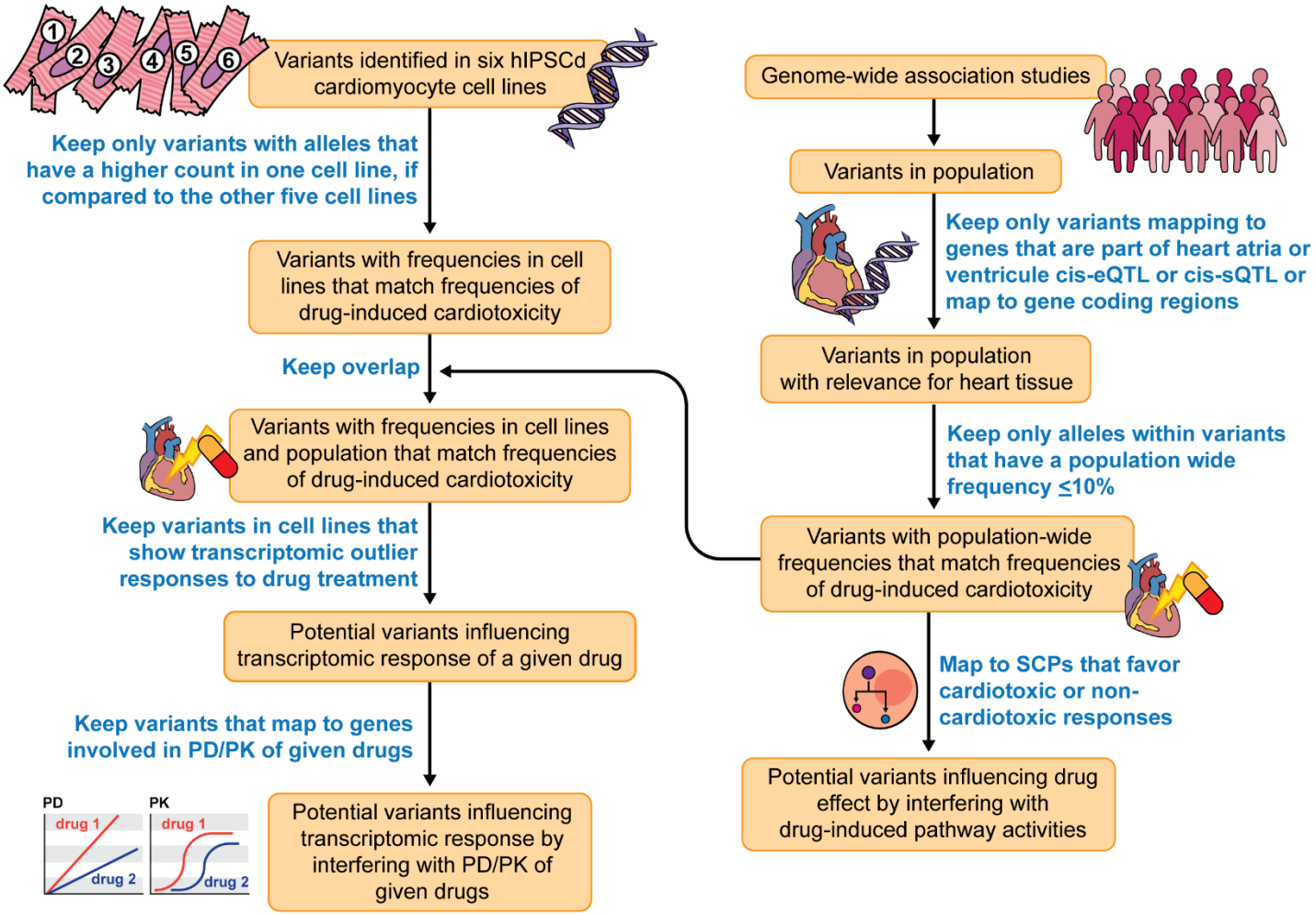

Supplementary Fig. 31

Supplementary Fig. 31. Computational pipeline for the identification of potential genomic variants associated with anthracycline- and TKI-induced cardiotoxicity. The flow chart shows the steps involved in our pipeline for the identification of genomic variant candidates associated with drug-induced cardiotoxicity. See methods for details. Flow chart is used with permission from Mount Sinai Health System, licensed under CC BY.

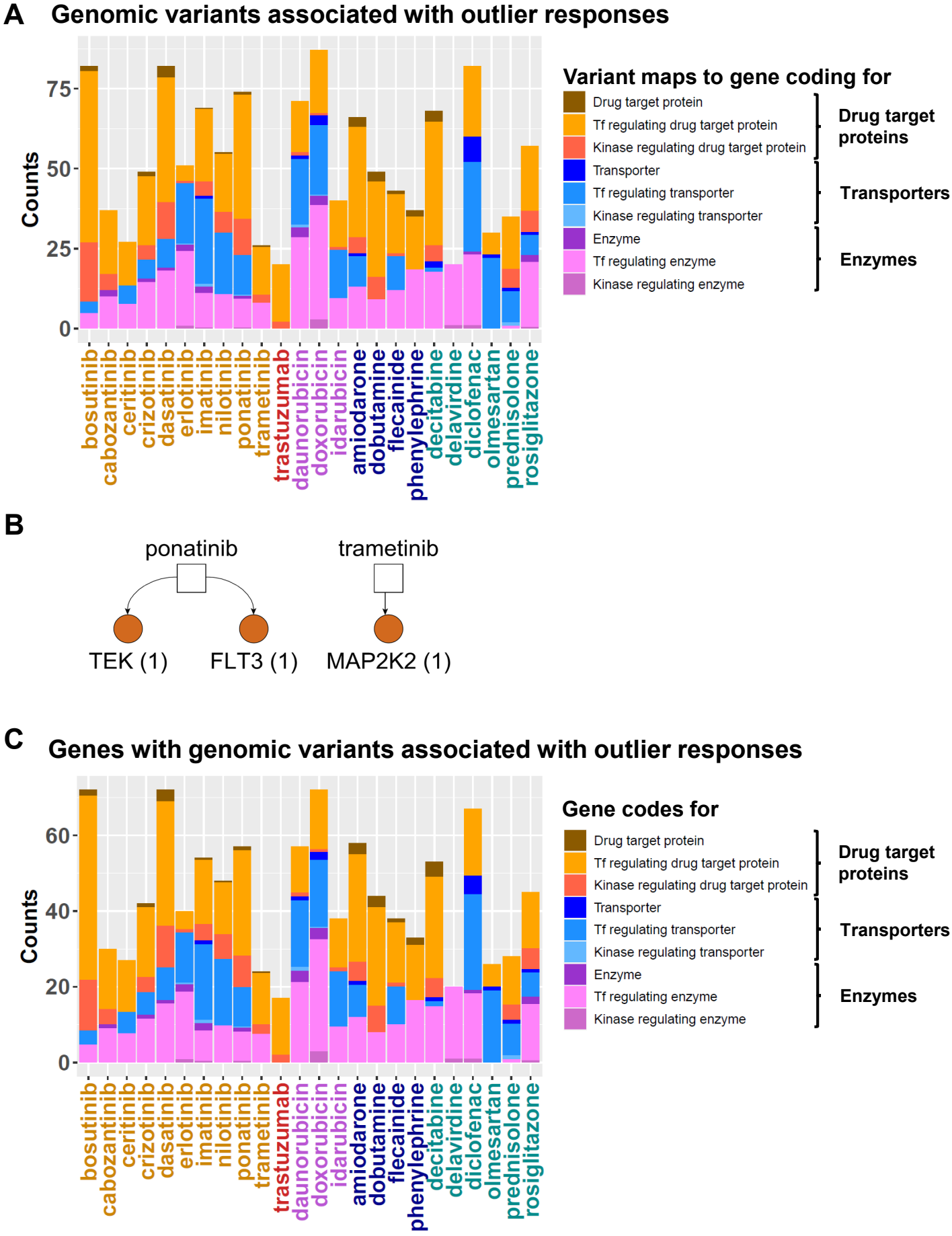

Supplementary Fig. 32

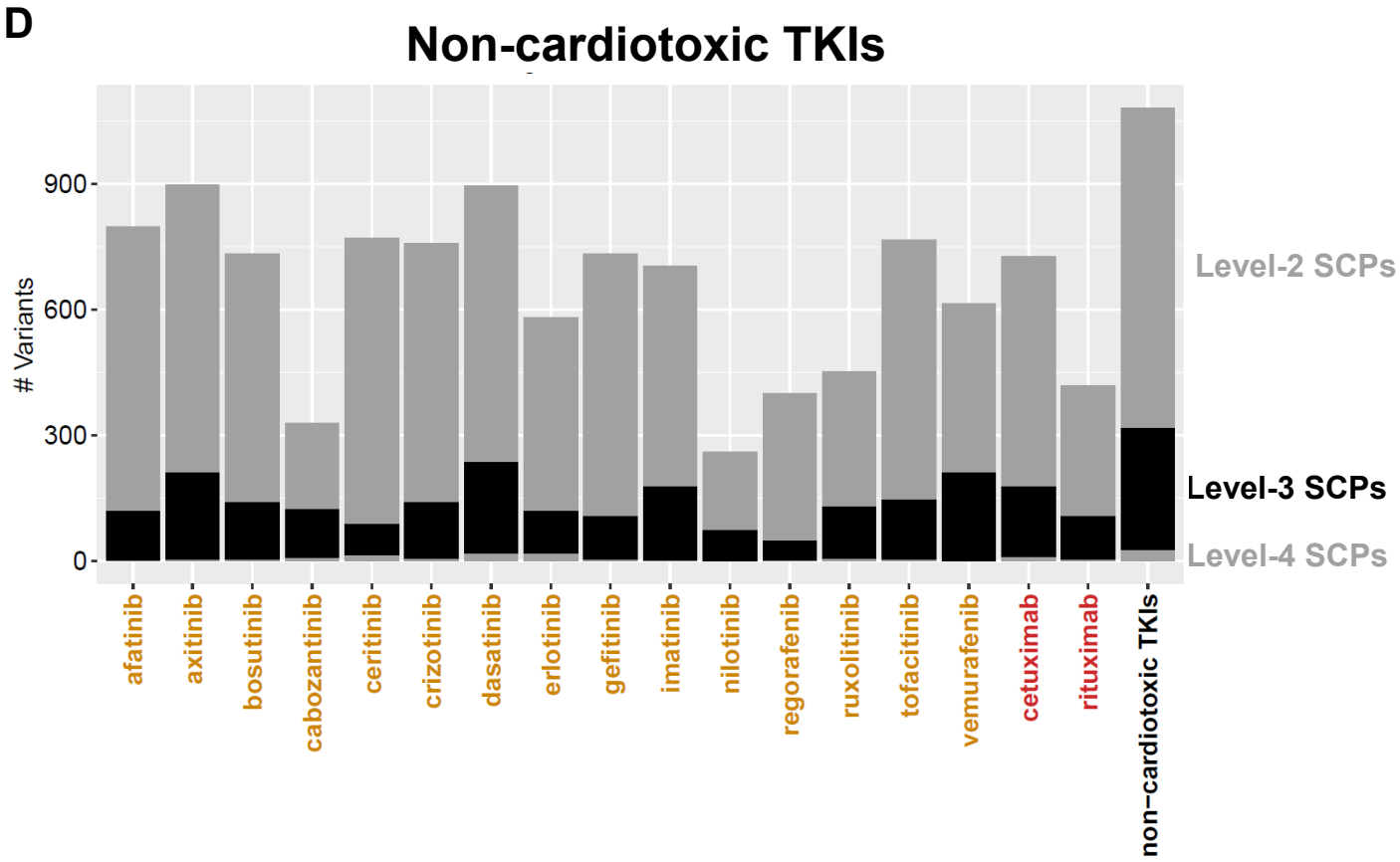

Supplementary Fig. 32

Supplementary Fig. 32. Identification of potential genomic variants associated with anthracycline- and TKI-induced cardiotoxicity. (A) Genomic variants that our algorithm identified as potential regulators of genes involved in a drug's pharmacodynamics (PD) or -kinetics (PK) are shown for all identified small molecule kinase inhibitors (orange), monoclonal antibodies against kinases (red), anthracyclines (purple), cardiac (blue) and non-cardiac (turquoise) acting drugs. The results for the cardiotoxic TKIs and anthracyclines are also shown in Fig. 4E. **(B)** Three example genes each targeted by one identified variant (numbers in brackets) and code for drug target proteins are shown. **(C)** Since multiple variants map to the same genes, we also counted the number of genes with at least one variant. **(D)** Variants passing our population-wide criteria were mapped to up- or downregulated level-2, -3 and -4 SCPs that we predicted to be up- or downregulated at higher ranks by non-cardiotoxic TKIs. Variants that are part of identified SCPs of multiple levels are only counted for the lowest level SCPs (with the highest level numbers) to prevent double counting. See Fig. 4G for results obtained for cardiotoxic TKIs.

(A) Metadata

1. **Materials/Reagents:** Company name, Catalogue and lot numbers

PRODUCT	COMPANY NAME	CAT #	Storage	Usable life
DMEM (500 mL)	Life Technologies	11965-118	+4°C	M
IMDM	Life Technologies	12440-053	+4°C	M
DMEM/F12	Life Technologies	11330057	+4°C	M
Penicillin/Streptomycin (100x)	Life Technologies	15140-122	+4°C	M
Sodium-Pyruvate (100 mM)	Life Technologies	11360-070	+4°C	M
L-Glutamine (200 mM)	Life Technologies	25030-081	+4°C	M
Non-Essential Amino Acids (100x)	Life Technologies	11140-050	+4°C	M
Fetal Bovine Serum (FBS; 500 mL)	Corning	35-011-CV	+4°C	M
EDTA	Corning	46-034-CI	RT	M
KnockOut Serum Replacement	Life Technologies	10828-028	-20°C +4°C	M
mTeSR™: 1) mTeSR™ Basal medium 2) mTeSR™ 1.5X Supplement	STEMCELL Technologies	05850	+4°C -20°C	M
2-Mercaptoethanol	MP Biomedicals	194705	RT	N/A
TrypLE Express (1X)	Life Technologies	12605010	+4°C	M
ReLeSR™	STEMCELL Technologies	05872	RT	M
Gelatin	Sigma	G1890	RT	M
Matrigel	Corning	254248	-20°C +4°C	M
Dulbecco's phosphate-buffered saline (DPBS)	Life Technologies	14190-136	+4°C	M
DMSO	Fisher Scientific	BP2311	RT	M
FGF2	R&D Systems	223-FB-10	-20°C +4°C	M
Thiazovivin	Millipore	420220	-20°C +4°C	M
Irradiated MEFs (Mouse Embryonic Fibroblasts)	Global Stem	GSC-6001G	Liquid Nitrogen	M
mRNA Reprogramming Kit	Stemgent	00-0071	-70°C	M
microRNA Booster Kit	Stemgent	00-0073	-70°C	M
B18R	Stemgent	03-0071	-70°C	M
Pluriton Supplement (2500x)	Stemgent	01-0061	-80°C	M
Pluriton Medium (500 mL)	Stemgent	01-0015	-20°C +4°C	M
Stemfect RNA Transfection Kit: 1) Stemfect Transfection Buffer 2) Stemfect Transfection Reagent	Stemgent	00-0069	+4°C	M

PureLink™ Genomic DNA Mini Kit	Life Technologies	K1820-001	RT	N/A
e-Myco™ plus Mycoplasma PCR Detection KIT	iNtRON Biotechnology	25235	-20°C	M
50 ml conical tube	BD FALCON	352098	RT	N/A
15 ml conical tube	BD FALCON	352099	RT	N/A
75 cm^2 Cell Culture Flask	Corning	430641	RT	N/A
50 mL Rapid Flow Conical Filter with a 0.2 µm aPES membrane	Thermo Scientific	564-0020	RT	N/A
6 well Tissue Culture (TC) plate	Corning	353046	RT	N/A
2 ml Aspirating pipettes	BD FALCON	357558	RT	N/A
5 ml Serological Pipettes	BD FALCON	357543	RT	N/A
10 ml Serological Pipettes	BD FALCON	357551	RT	N/A
Hemocytomter	Thermo Scientific	0267110	RT	N/A
1 mL filter tips	USA Scientific	1126-7810	RT	N/A
200 µL filter tips	USA Scientific	1120-8810	RT	N/A
20 µL filter tips	USA Scientific	1123-1810	RT	N/A
0.1-10 µL filter tips	USA Scientific	1121-3810	RT	N/A
Cryovials	Nunc	377367	RT	N/A
Cryo 1°C freezing container	Nalgene	5100-0001	RT	N/A
2-Propanol	Thermo Scientific	A417-4	RT	N

M; according to manufacture's shelf-life information; RT, room temperature

2. **Subject(s):** subject ID (de-identified), age, gender/sex, race/ethnicity

3. **Fibroblast(s):** subject ID (de-identified), passage number, dates of each passage, date of biopsy, date of initial plating, date of freezing.

4. **Microscopy pictures:** subject ID (de-identified), passage number, date, microscope name (company, catalogue number), magnification.

(B) Materials used for co-culture experiments

HCAEC	PromoCell	Catalog# C-12221
Endothelial Cell Growth Medium MV Kit	PromoCell	Catalog# C-22120
DetachKit (Trypsin/EDTA)	PromoCell	Catalog# C-41210
ActinGreen 488 Ready Probes Reagent	ThermoFisher	Catalog# R37110
Poly-L-lysine hydrobromide	Sigma-Aldrich	Catalog# P1274
Glass circular coverslips (18mm)	FisherScientific	Catalog# 12-545-86
Nunc Polycarbonate Cell Culutre Inserts in 6-well plates – Pore size of 0.4µm	ThermoFisher	Catalog# 140640
Paraformaldehyde 32% aqueous solution	Electron Microscopy Services	Catalog# 15714S
ProLong Gold Antifade Mountant with DAPI	ThermoFisher	Catalog# P36931

Supplementary Table 1. Description of materials used in this study. **(A)** This table lists the materials used for the initial experiments. It is taken from the Supplementary Information for Schaniel et al. (Stem Cell Reports. 2021 Dec 14;16(12):3036-3049, pages 9 and 10) [16], since the two studies were conducted concurrently. **(B)** This table lists additional materials used for the coculture experiments.

afatinib after removal of 1st eigenarray , F1: 0.07 , Precision: 0.04 , Recall: 0.4

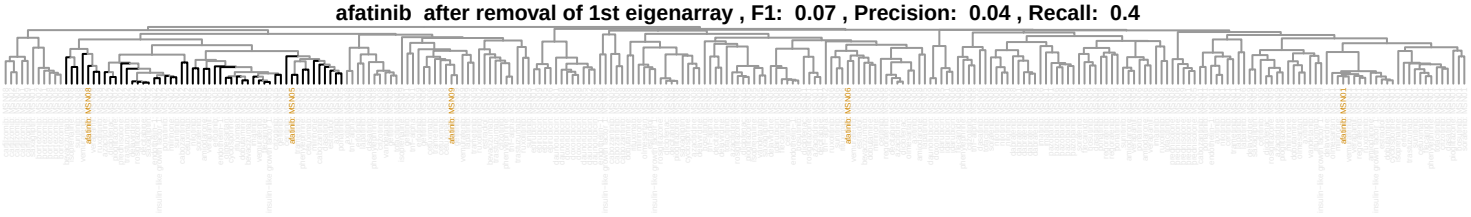

afatinib in decomposed data (F1 score weight: 0.95 , F1: 0.57, Precision: 1, Recall: 0.4,
mediane cosine similarity: 0.41, top 23 eigenarrays)

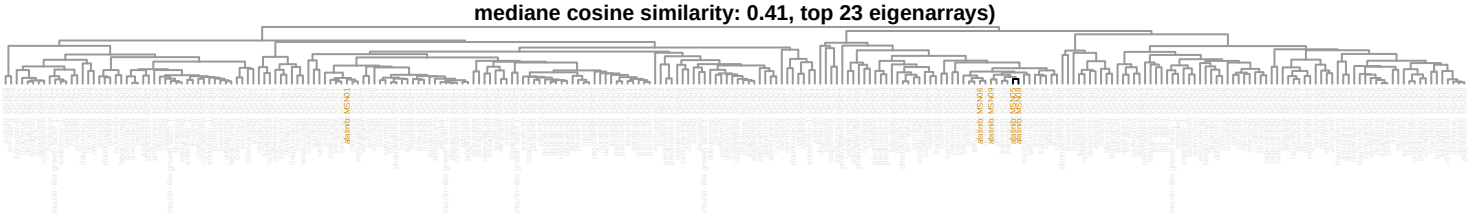

axitinib after removal of 1st eigenarray , F1: 0.07 , Precision: 0.04 , Recall: 0.4

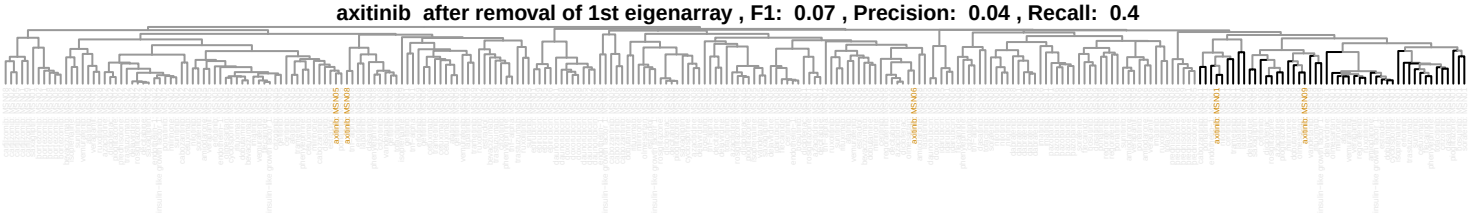

axitinib in decomposed data (F1 score weight: 0.95 , F1: 0.75, Precision: 1, Recall: 0.6,
mediane cosine similarity: 0.39, top 50 eigenarrays)

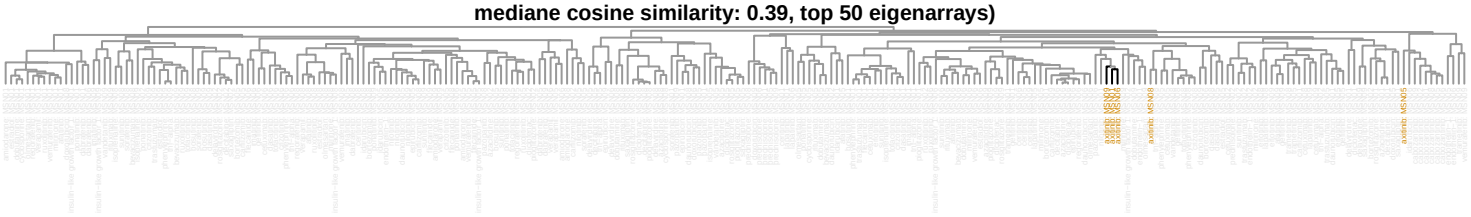

bosutinib after removal of 1st eigenarray , F1: 0.09 , Precision: 0.05 , Recall: 0.5

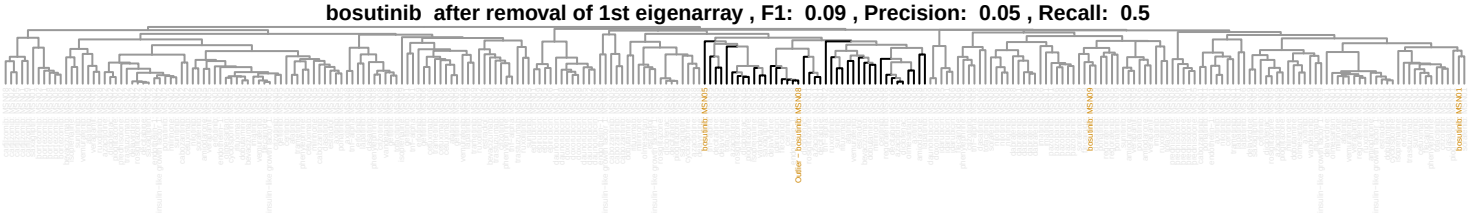

bosutinib in decomposed data (F1 score weight: 0.65 , F1: 0.86, Precision: 1, Recall: 0.75,
mediane cosine similarity: 0.22, top 24 eigenarrays)

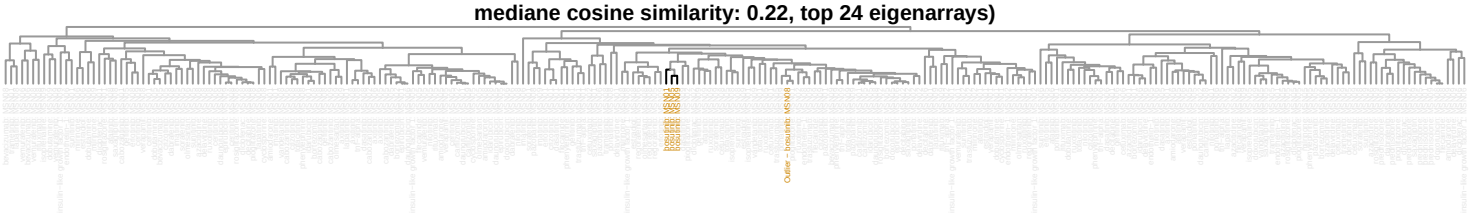

cabozantinib after removal of 1st eigenarray , F1: 0.67 , Precision: 1 , Recall: 0.5

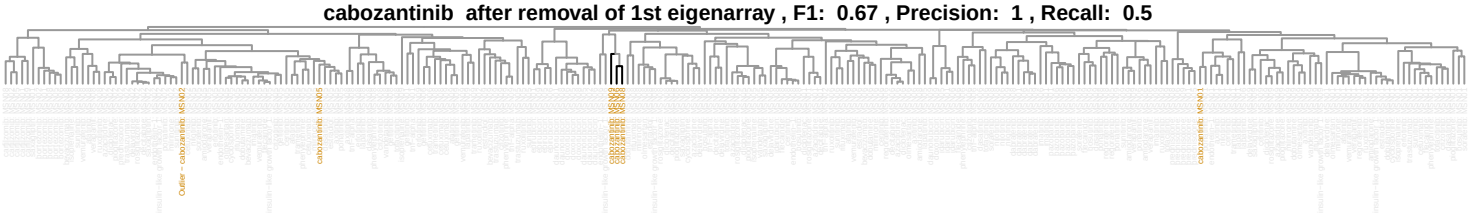

cabozantinib in decomposed data (F1 score weight: 0.5 , F1: 0.91, Precision: 1, Recall: 0.83,
mediane cosine similarity: 0.76, top 57 eigenarrays)

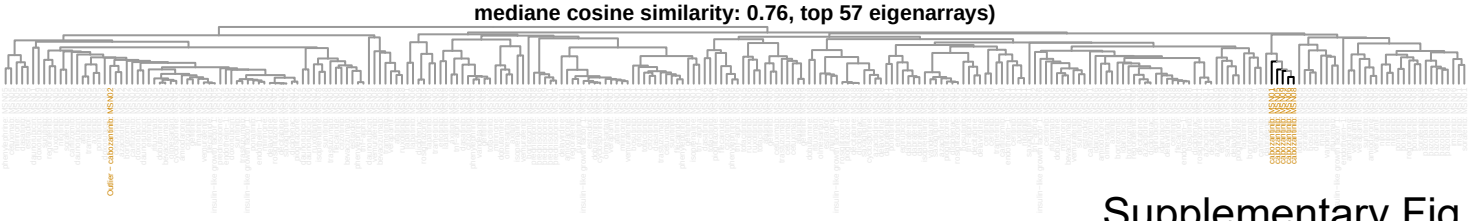

Supplementary Fig. 11

ceritinib after removal of 1st eigenarray , F1: 0.12 , Precision: 0.07 , Recall: 0.4

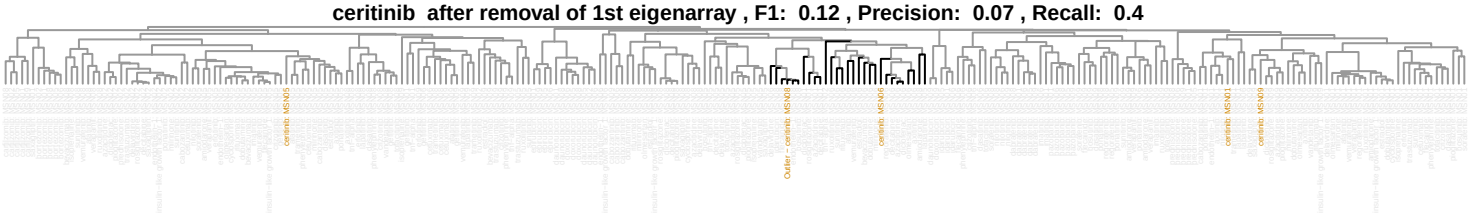

ceritinib in decomposed data (F1 score weight: 0.15 , F1: 0.89, Precision: 1, Recall: 0.8,
mediane cosine similarity: 0.88, top 86 eigenarrays)

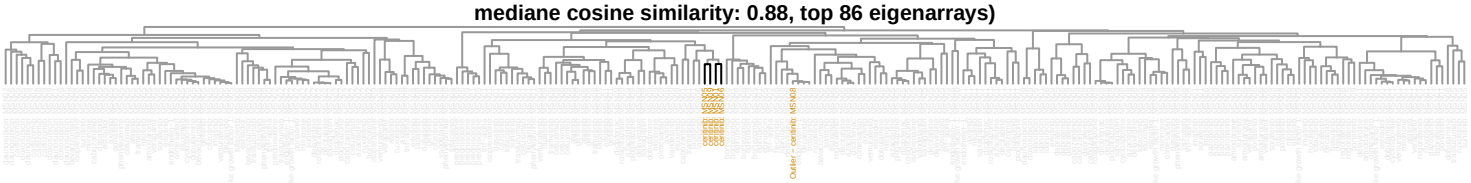

crizotinib after removal of 1st eigenarray , F1: 0.1 , Precision: 0.06 , Recall: 0.4

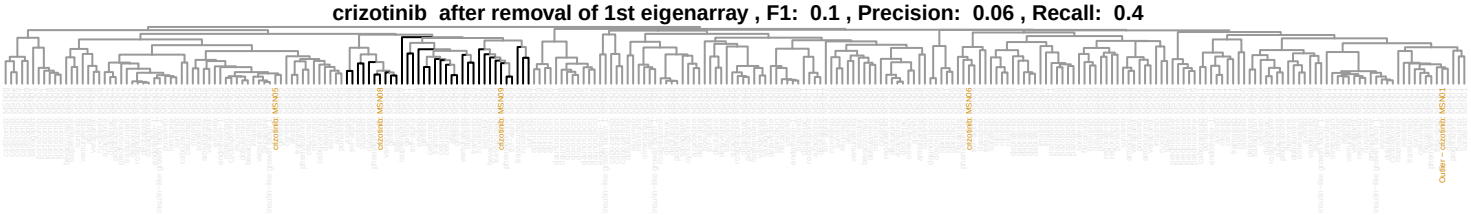

crizotinib in decomposed data (F1 score weight: 0.6 , F1: 0.8, Precision: 0.8, Recall: 0.8,
mediane cosine similarity: 0.3, top 23 eigenarrays)

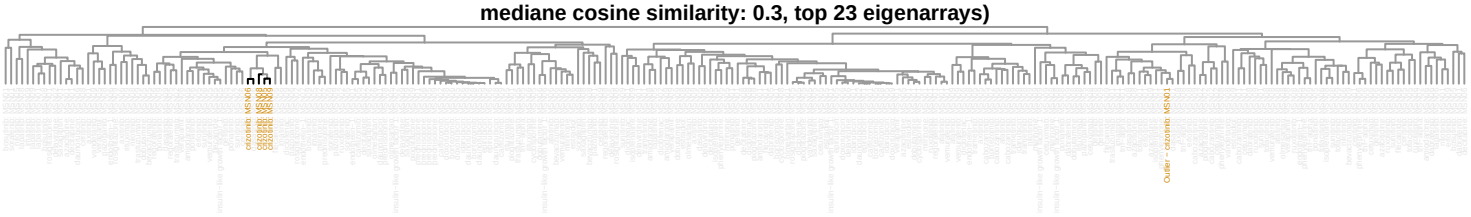

dabrafenib after removal of 1st eigenarray , F1: 1 , Precision: 1 , Recall: 1

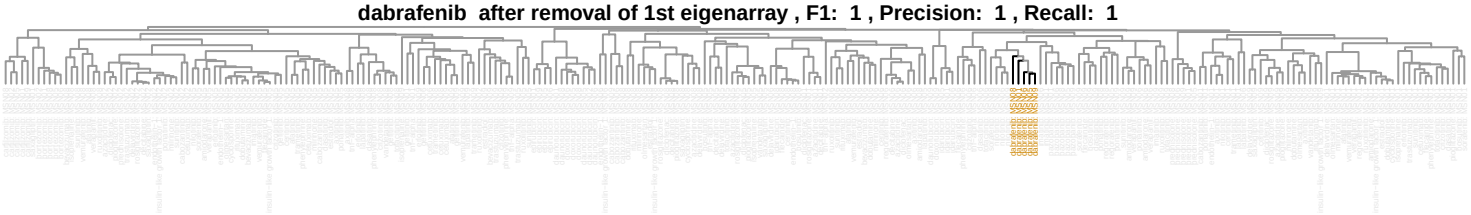

dabrafenib in decomposed data (F1 score weight: 0.95 , F1: 1, Precision: 1, Recall: 1,
mediane cosine similarity: 1, top 266 eigenarrays)

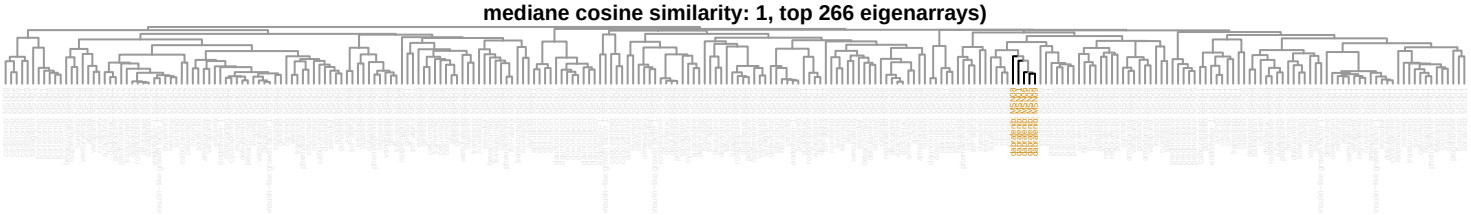

dasatinib after removal of 1st eigenarray , F1: 0.09 , Precision: 0.05 , Recall: 0.4

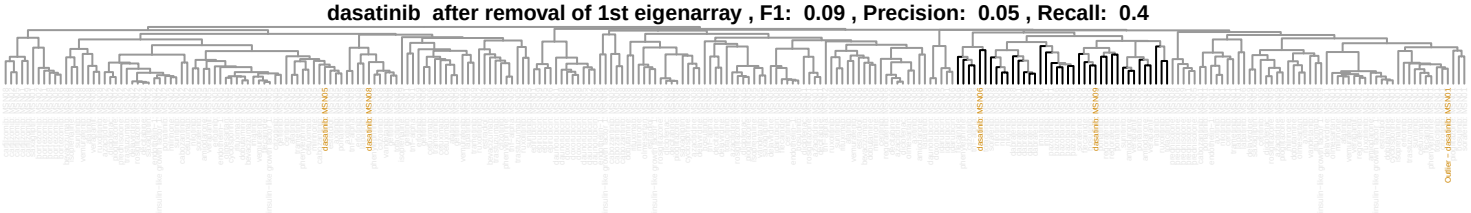

dasatinib in decomposed data (F1 score weight: 0.6 , F1: 0.89, Precision: 1, Recall: 0.8,
mediane cosine similarity: 0.58, top 43 eigenarrays)

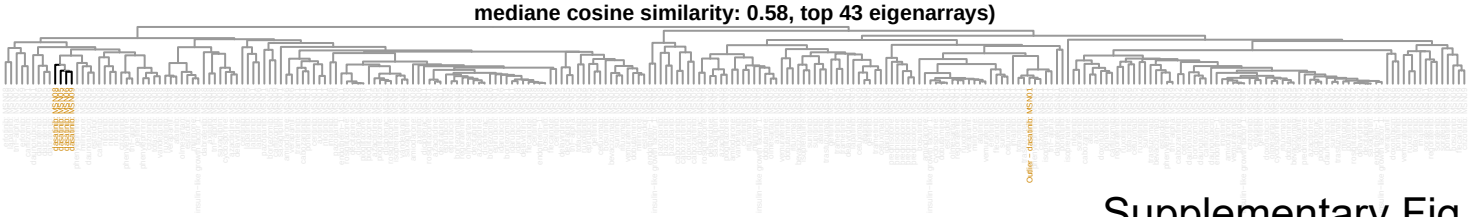

Supplementary Fig. 11

erlotinib after removal of 1st eigenarray , F1: 0.11 , Precision: 0.06 , Recall: 0.5

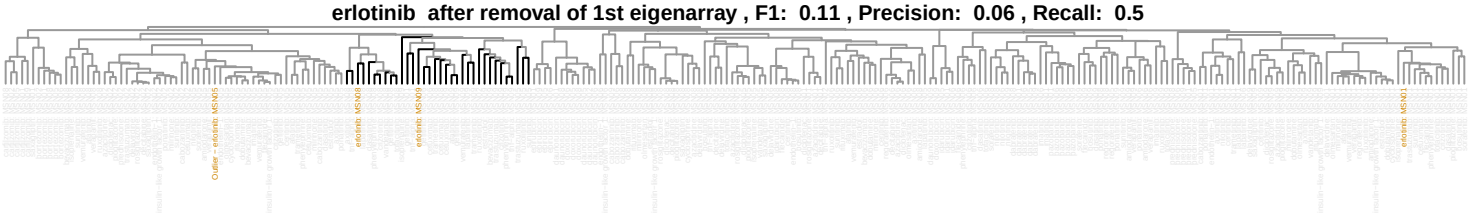

erlotinib in decomposed data (F1 score weight: 0.55 , F1: 0.86, Precision: 1, Recall: 0.75, mediane cosine similarity: 0.7, top 25 eigenarrays)

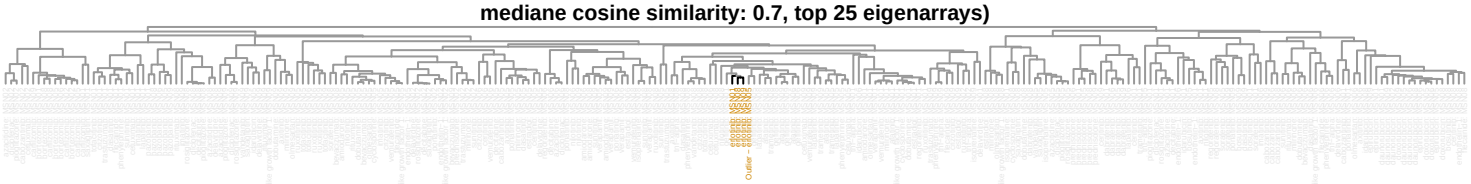

gefitinib after removal of 1st eigenarray , F1: 0.33 , Precision: 0.23 , Recall: 0.6

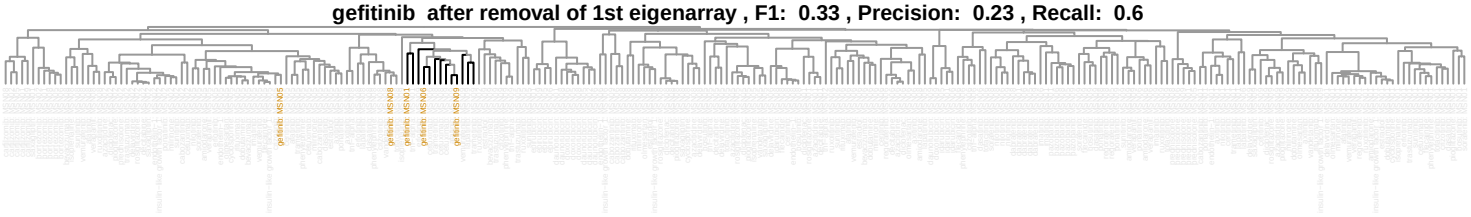

gefitinib in decomposed data (F1 score weight: 0.95 , F1: 0.75, Precision: 1, Recall: 0.6, mediane cosine similarity: 0.61, top 16 eigenarrays)

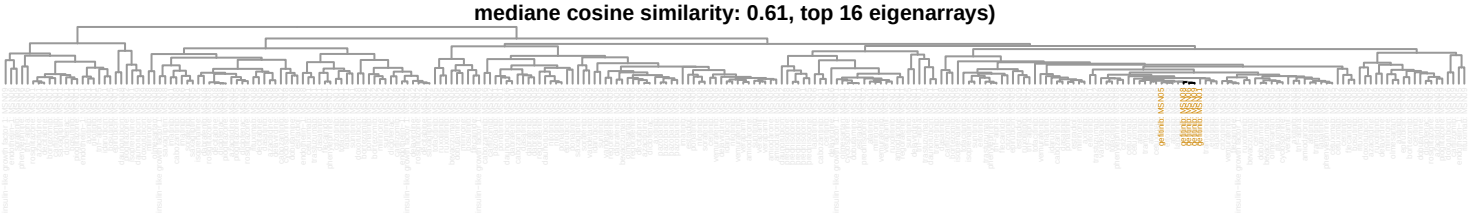

imatinib after removal of 1st eigenarray , F1: 0.36 , Precision: 0.29 , Recall: 0.5

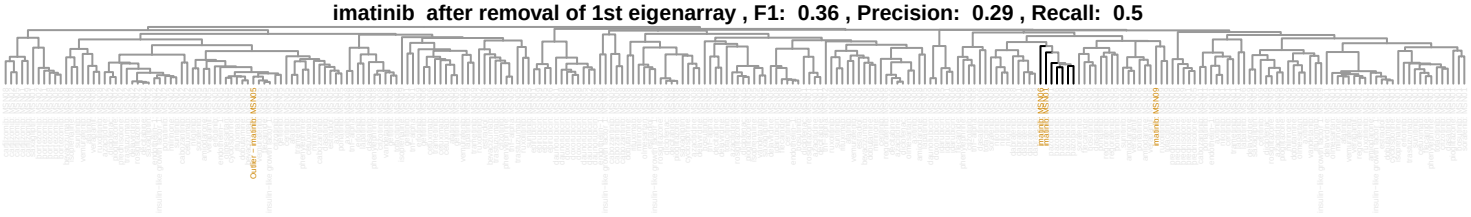

imatinib in decomposed data (F1 score weight: 0.4 , F1: 0.86, Precision: 1, Recall: 0.75, mediane cosine similarity: 0.84, top 146 eigenarrays)

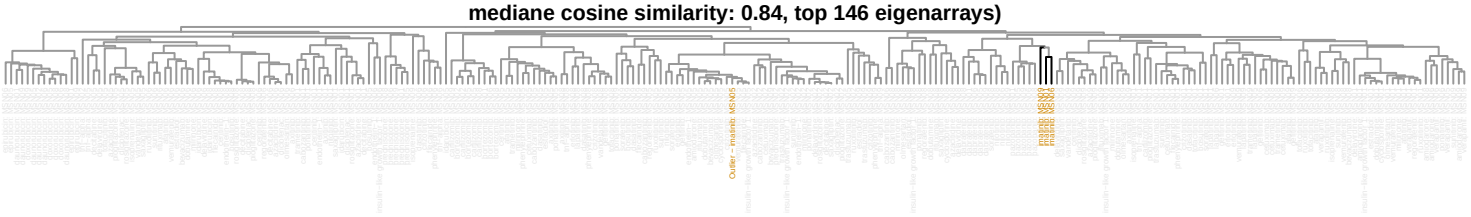

lapatinib after removal of 1st eigenarray , F1: 0.57 , Precision: 1 , Recall: 0.4

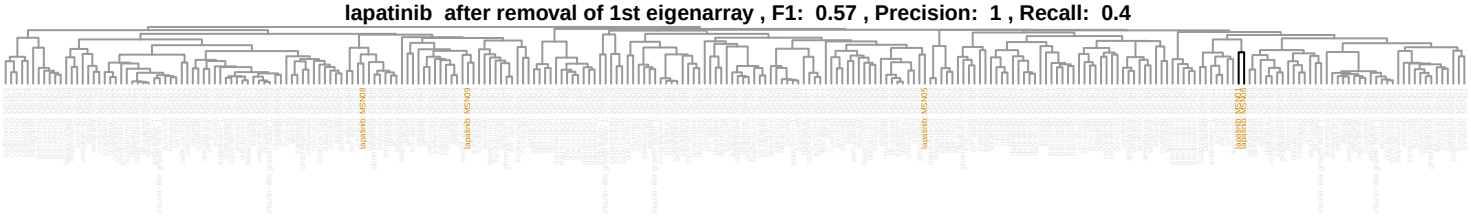

lapatinib in decomposed data (F1 score weight: 0.95 , F1: 1, Precision: 1, Recall: 1, mediane cosine similarity: 0.75, top 37 eigenarrays)

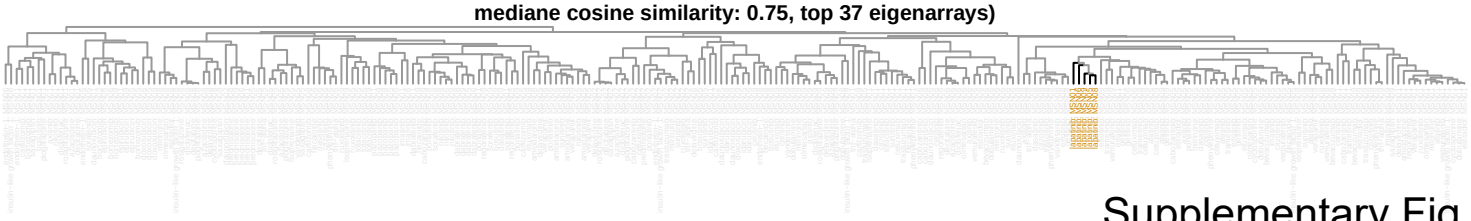

Supplementary Fig. 11

nilotinib after removal of 1st eigenarray , F1: 0.75 , Precision: 1 , Recall: 0.6

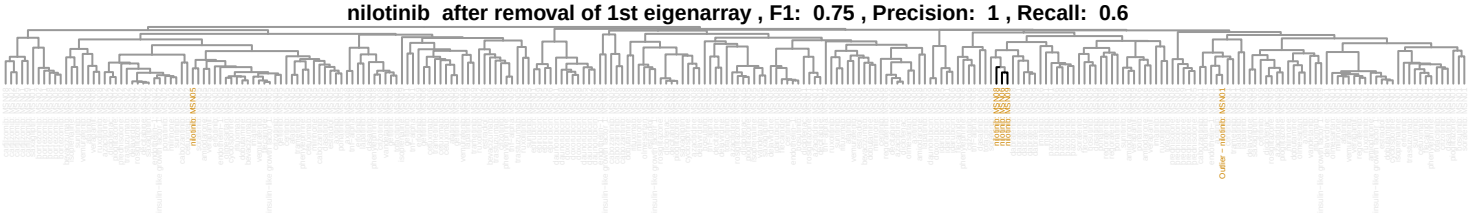

nilotinib in decomposed data (F1 score weight: 0.65 , F1: 0.89, Precision: 1, Recall: 0.8, mediane cosine similarity: 0.77, top 21 eigenarrays)

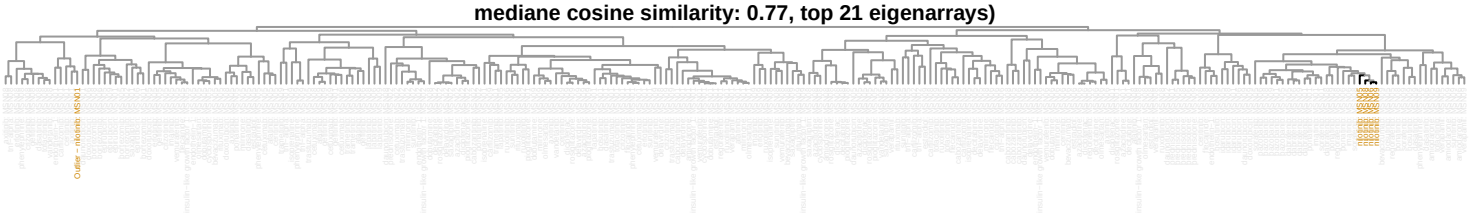

pazopanib after removal of 1st eigenarray , F1: 1 , Precision: 1 , Recall: 1

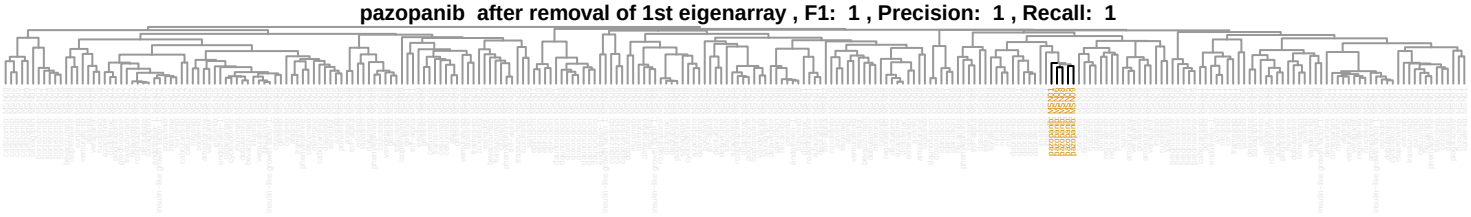

pazopanib in decomposed data (F1 score weight: 0.95 , F1: 1, Precision: 1, Recall: 1, mediane cosine similarity: 1, top 266 eigenarrays)

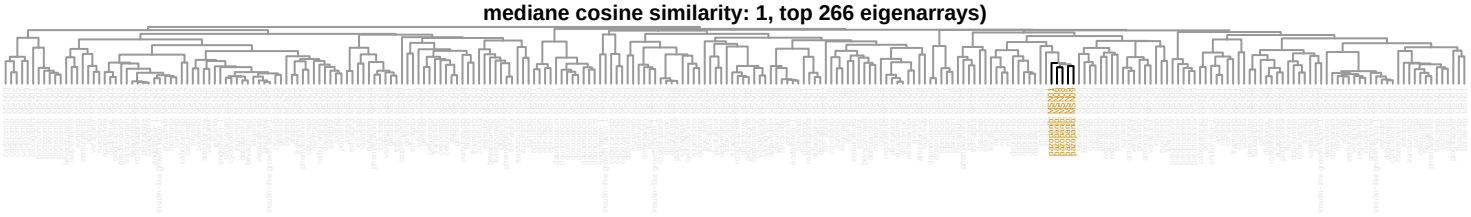

ponatinib after removal of 1st eigenarray , F1: 0.4 , Precision: 0.5 , Recall: 0.33

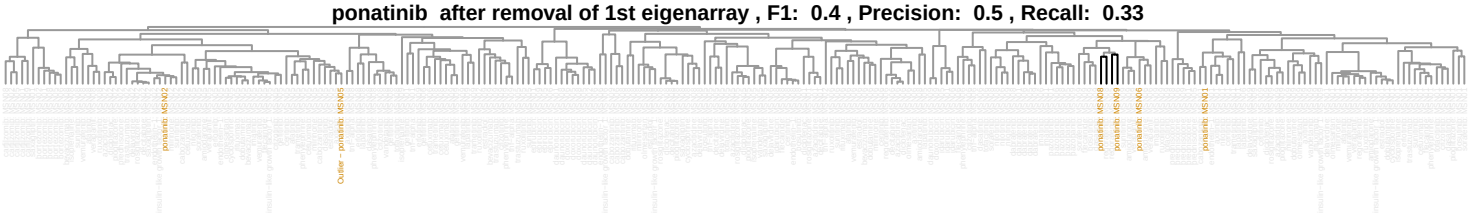

ponatinib in decomposed data (F1 score weight: 0.7 , F1: 0.91, Precision: 1, Recall: 0.83, mediane cosine similarity: 0.4, top 15 eigenarrays)

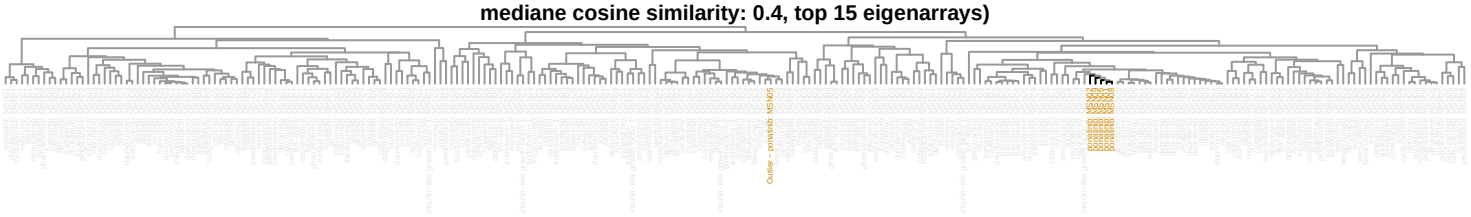

regorafenib after removal of 1st eigenarray , F1: 0.5 , Precision: 0.5 , Recall: 0.5

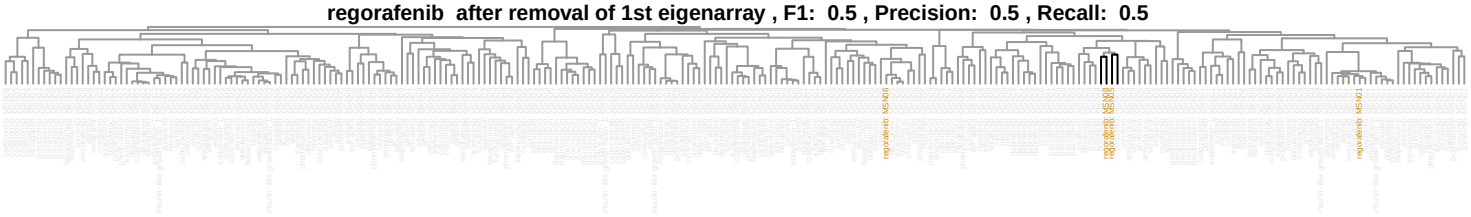

regorafenib in decomposed data (F1 score weight: 0.95 , F1: 1, Precision: 1, Recall: 1, mediane cosine similarity: 0.33, top 16 eigenarrays)

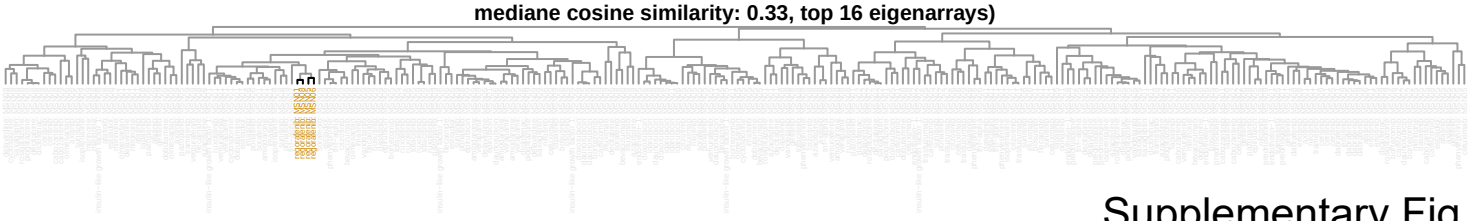

ruxolitinib after removal of 1st eigenarray , F1: 0.25 , Precision: 0.2 , Recall: 0.33

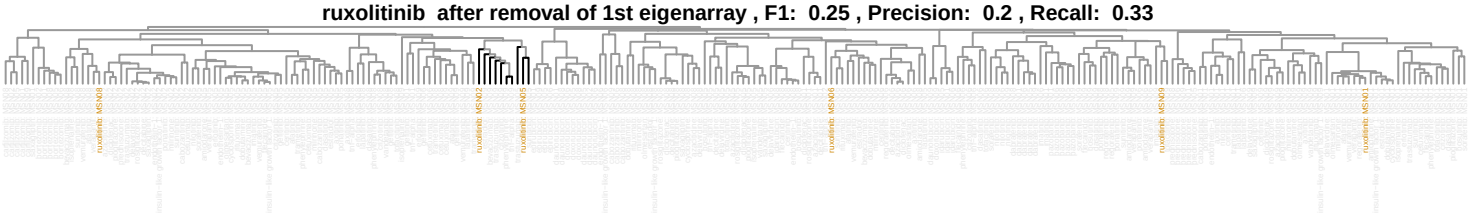

ruxolitinib in decomposed data (F1 score weight: 0.95 , F1: 0.86, Precision: 0.75, Recall: 1,
mediane cosine similarity: 0.29, top 12 eigenarrays)

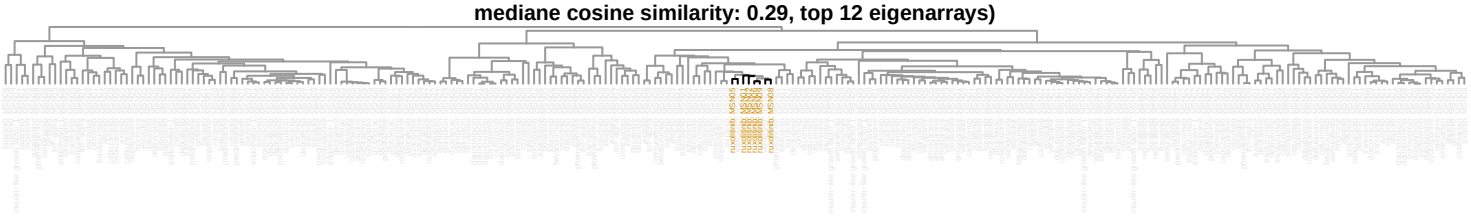

sorafenib after removal of 1st eigenarray , F1: 0.11 , Precision: 0.06 , Recall: 0.5

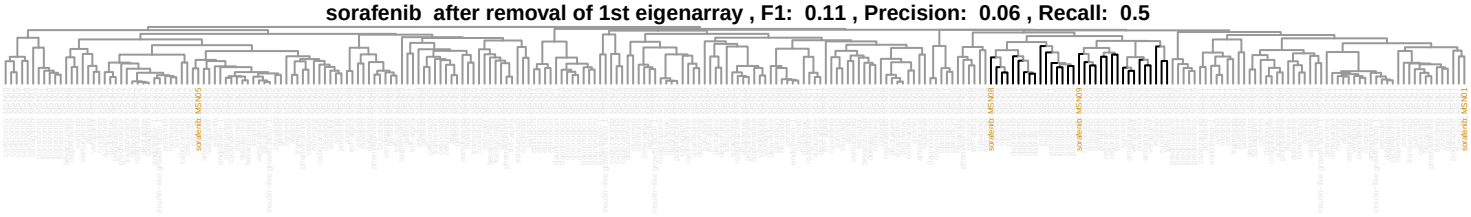

sorafenib in decomposed data (F1 score weight: 0.95 , F1: 1, Precision: 1, Recall: 1,
mediane cosine similarity: 0.52, top 19 eigenarrays)

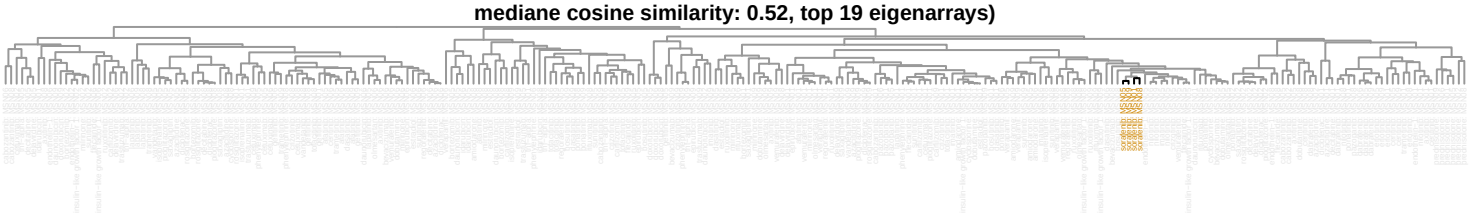

sunitinib after removal of 1st eigenarray , F1: 0.07 , Precision: 0.04 , Recall: 0.33

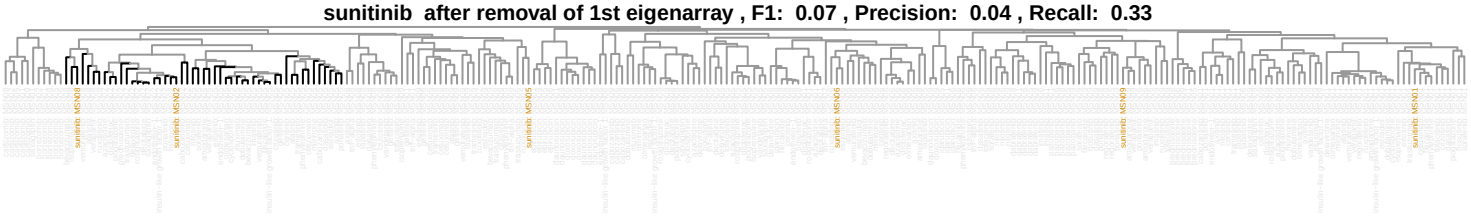

sunitinib in decomposed data (F1 score weight: 0.95 , F1: 1, Precision: 1, Recall: 1,
mediane cosine similarity: 0.2, top 14 eigenarrays)

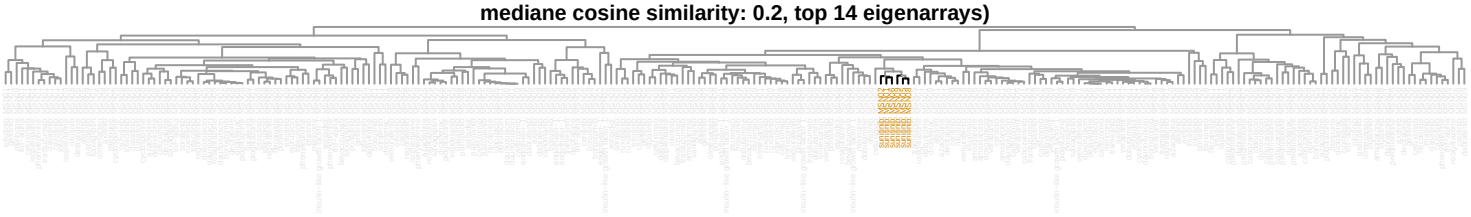

tofacitinib after removal of 1st eigenarray , F1: 0.09 , Precision: 0.05 , Recall: 0.4

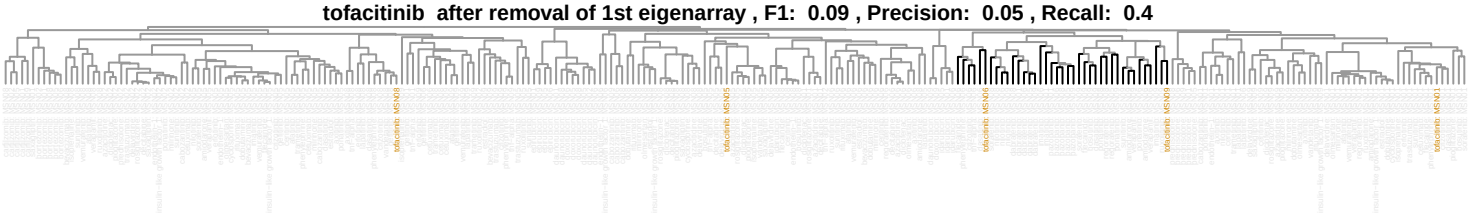

tofacitinib in decomposed data (F1 score weight: 0.95 , F1: 1, Precision: 1, Recall: 1,
mediane cosine similarity: 0.37, top 12 eigenarrays)

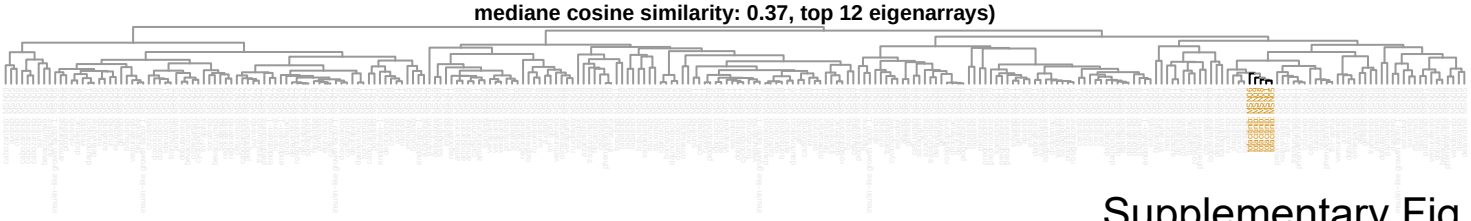

Supplementary Fig. 11

trametinib after removal of 1st eigenarray , F1: 0.29 , Precision: 0.2 , Recall: 0.5

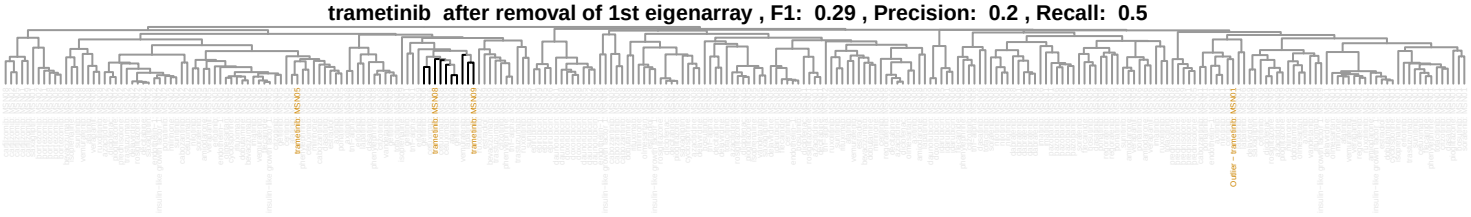

trametinib in decomposed data (F1 score weight: 0.35 , F1: 0.86, Precision: 1, Recall: 0.75,
mediane cosine similarity: 0.79, top 31 eigenarrays)

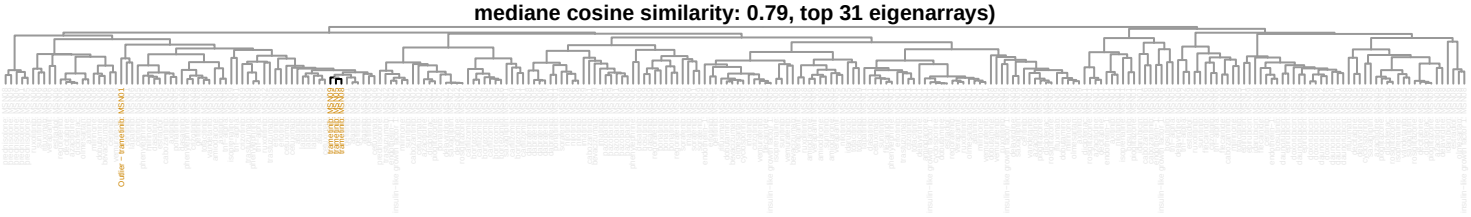

vandetanib after removal of 1st eigenarray , F1: 0.02 , Precision: 0.01 , Recall: 0.67

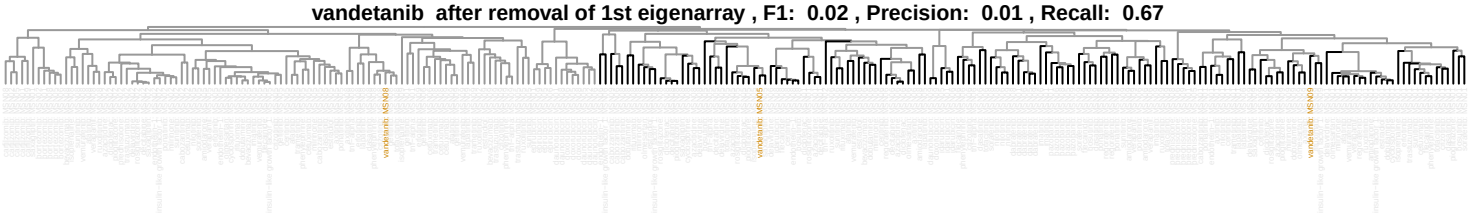

vandetanib in decomposed data (F1 score weight: 0.95 , F1: 1, Precision: 1, Recall: 1,
mediane cosine similarity: 0.14, top 16 eigenarrays)

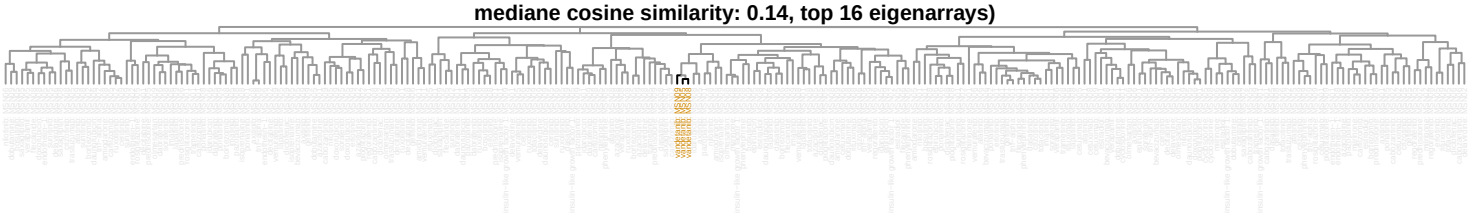

vemurafenib after removal of 1st eigenarray , F1: 0.07 , Precision: 0.04 , Recall: 0.4

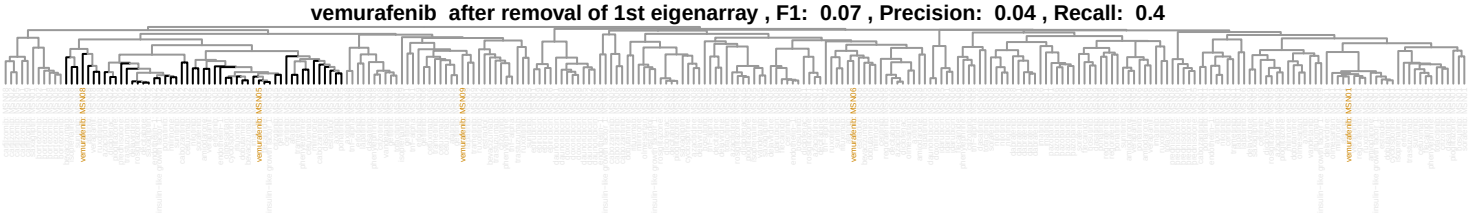

vemurafenib in decomposed data (F1 score weight: 0.95 , F1: 1, Precision: 1, Recall: 1,
mediane cosine similarity: 0.21, top 19 eigenarrays)

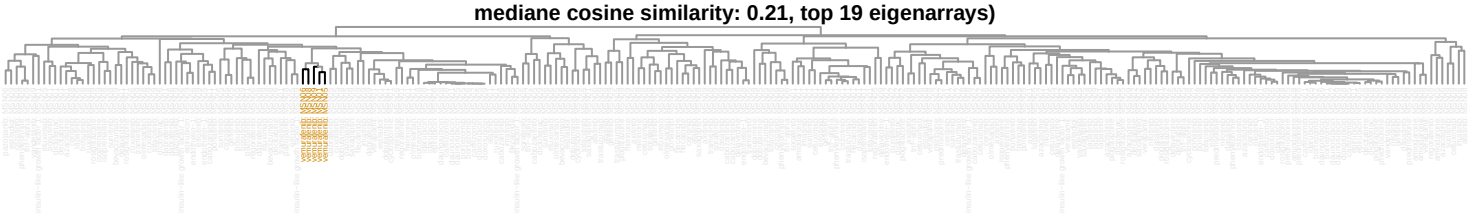

bevacizumab after removal of 1st eigenarray , F1: 0.07 , Precision: 0.04 , Recall: 0.5

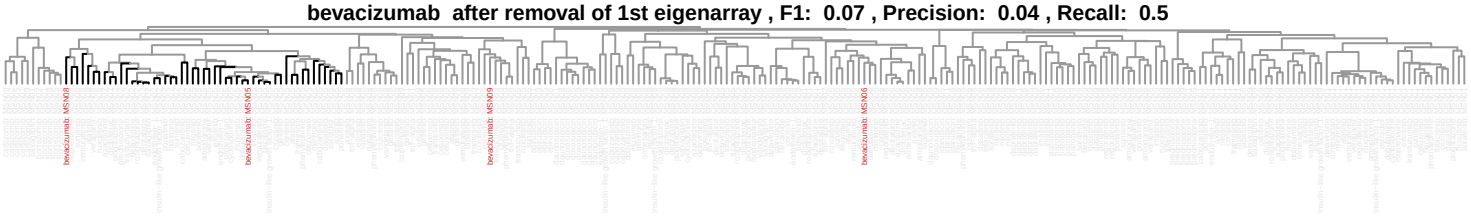

bevacizumab in decomposed data (F1 score weight: 0.95 , F1: 1, Precision: 1, Recall: 1,
mediane cosine similarity: 0.19, top 8 eigenarrays)

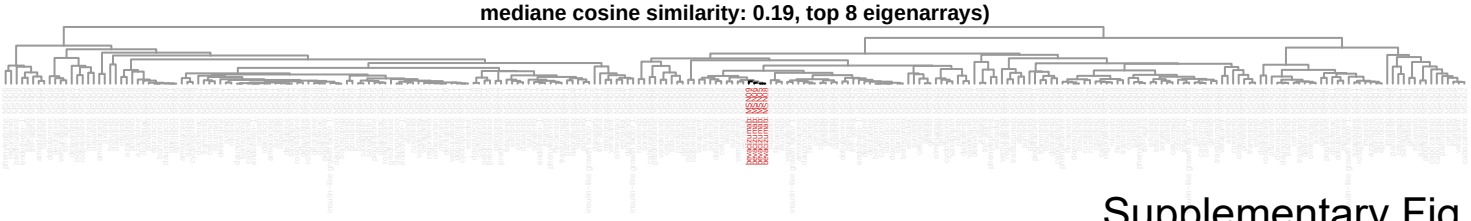

Supplementary Fig. 11

cetuximab after removal of 1st eigenarray , F1: 0.46 , Precision: 0.43 , Recall: 0.5

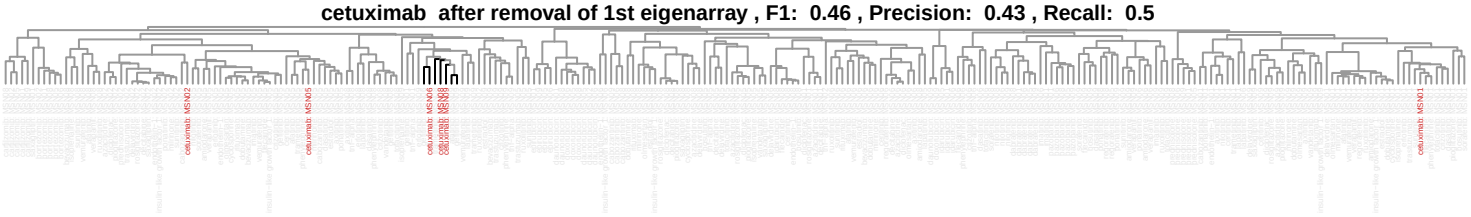

cetuximab in decomposed data (F1 score weight: 0.95 , F1: 0.8, Precision: 1, Recall: 0.67,
mediane cosine similarity: 0.43, top 23 eigenarrays)

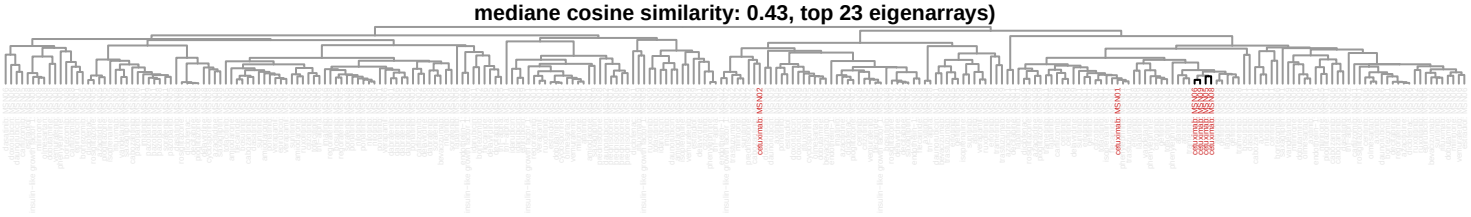

rituximab after removal of 1st eigenarray , F1: 0.07 , Precision: 0.04 , Recall: 0.5

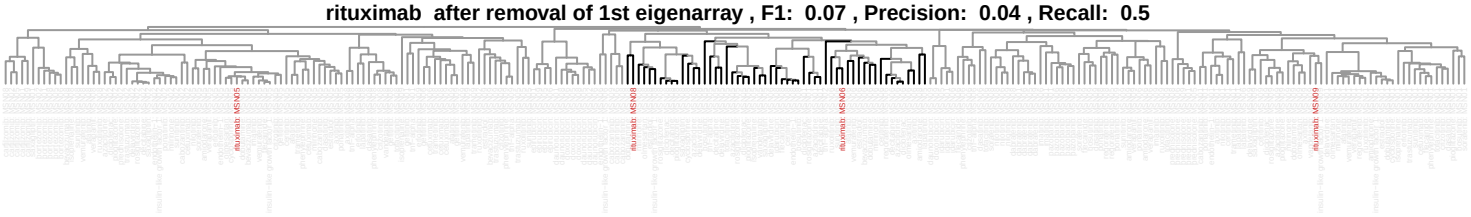

rituximab in decomposed data (F1 score weight: 0.95 , F1: 1, Precision: 1, Recall: 1,
mediane cosine similarity: 0.31, top 44 eigenarrays)

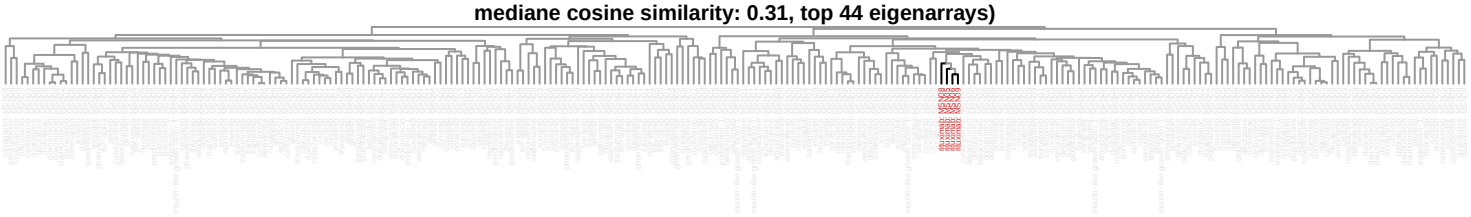

trastuzumab after removal of 1st eigenarray , F1: 0.29 , Precision: 0.2 , Recall: 0.5

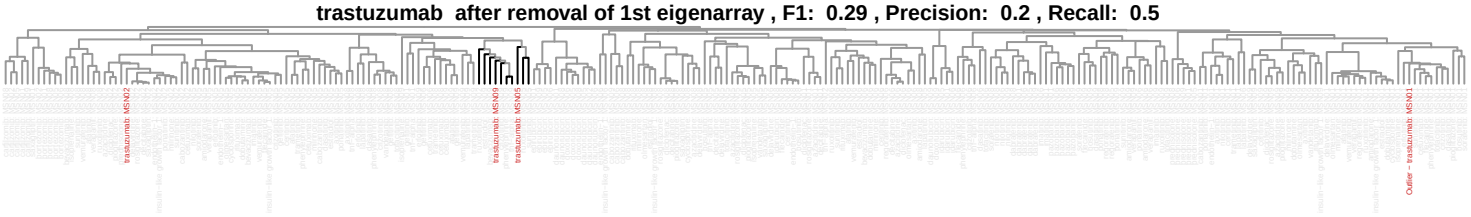

trastuzumab in decomposed data (F1 score weight: 0.65 , F1: 0.86, Precision: 1, Recall: 0.75,
mediane cosine similarity: 0.41, top 29 eigenarrays)

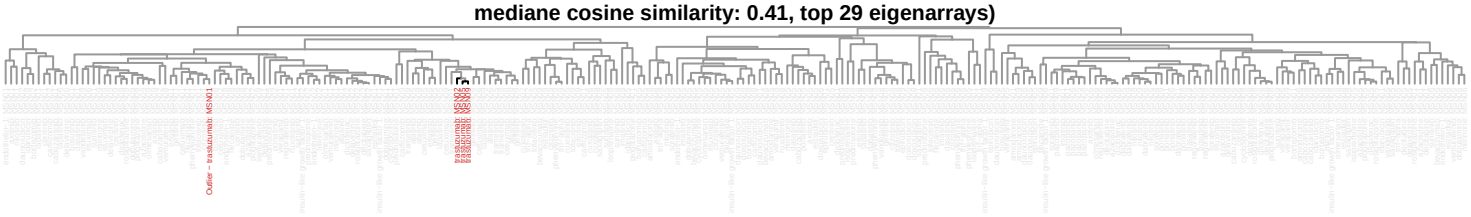

daunorubicin after removal of 1st eigenarray , F1: 0.71 , Precision: 0.62 , Recall: 0.83

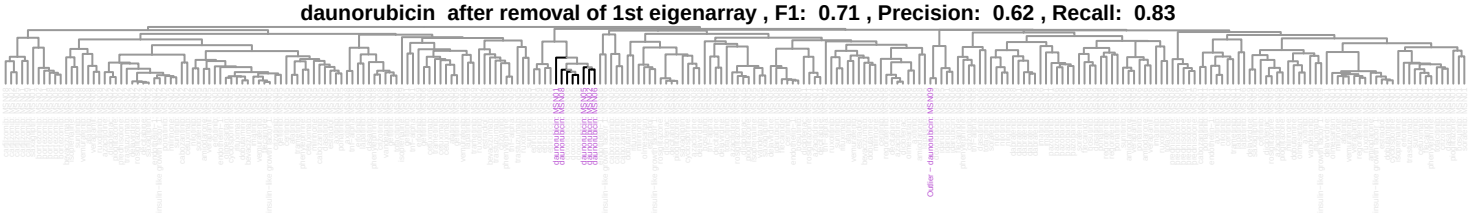

daunorubicin in decomposed data (F1 score weight: 0 , F1: 0.71, Precision: 0.62, Recall: 0.83,
mediane cosine similarity: 1, top 266 eigenarrays)

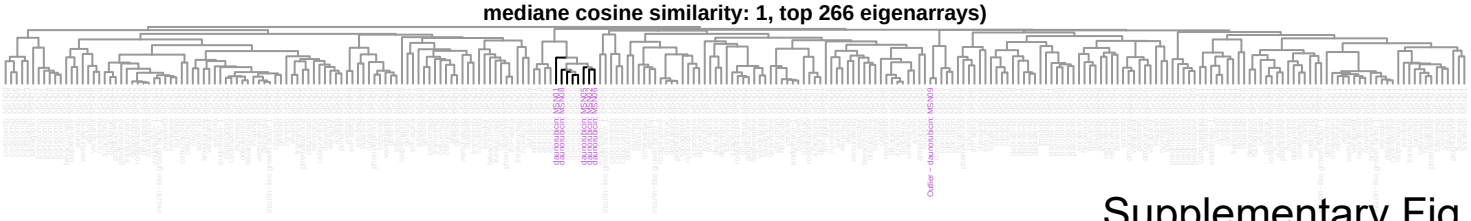

Supplementary Fig. 11

doxorubicin after removal of 1st eigenarray , F1: 0.86 , Precision: 1 , Recall: 0.75

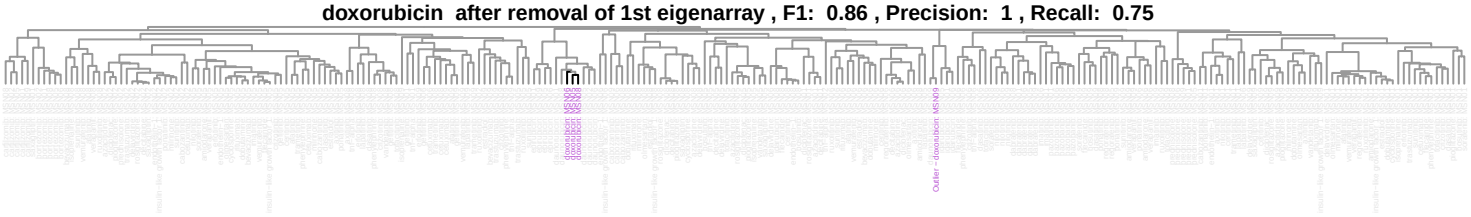

doxorubicin in decomposed data (F1 score weight: 0 , F1: 0.86, Precision: 1, Recall: 0.75, mediane cosine similarity: 1, top 266 eigenarrays)

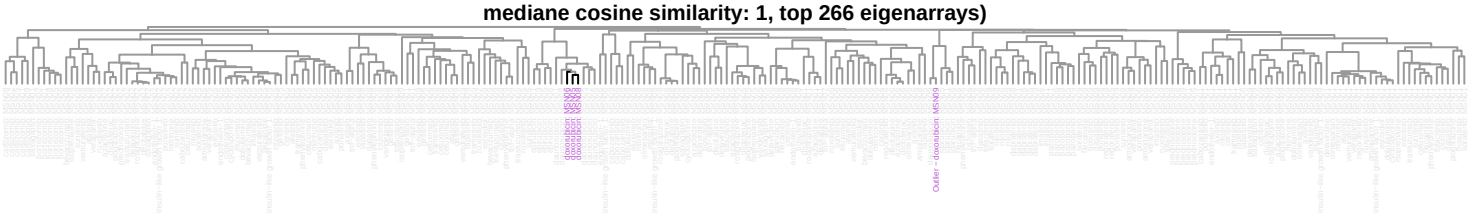

epirubicin after removal of 1st eigenarray , F1: 1 , Precision: 1 , Recall: 1

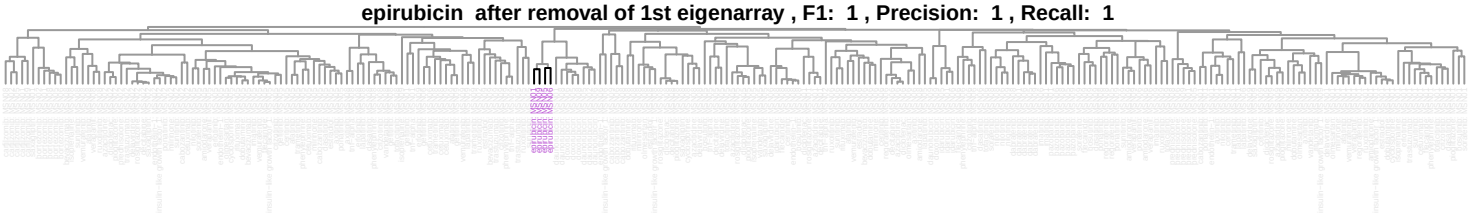

epirubicin in decomposed data (F1 score weight: 0.95 , F1: 1, Precision: 1, Recall: 1, mediane cosine similarity: 1, top 266 eigenarrays)

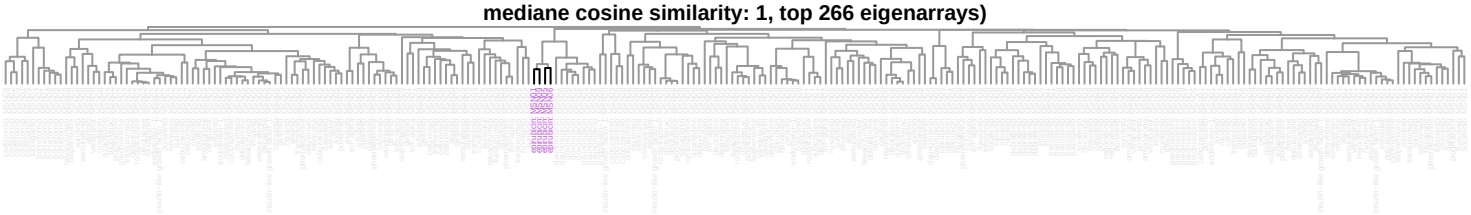

idarubicin after removal of 1st eigenarray , F1: 0.86 , Precision: 1 , Recall: 0.75

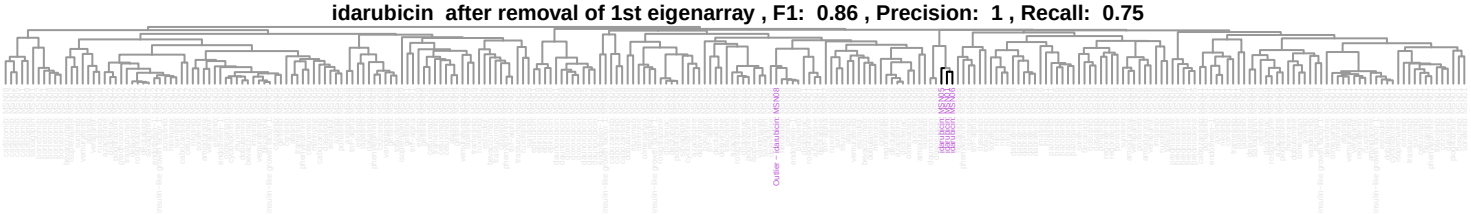

idarubicin in decomposed data (F1 score weight: 0 , F1: 0.86, Precision: 1, Recall: 0.75, mediane cosine similarity: 1, top 266 eigenarrays)

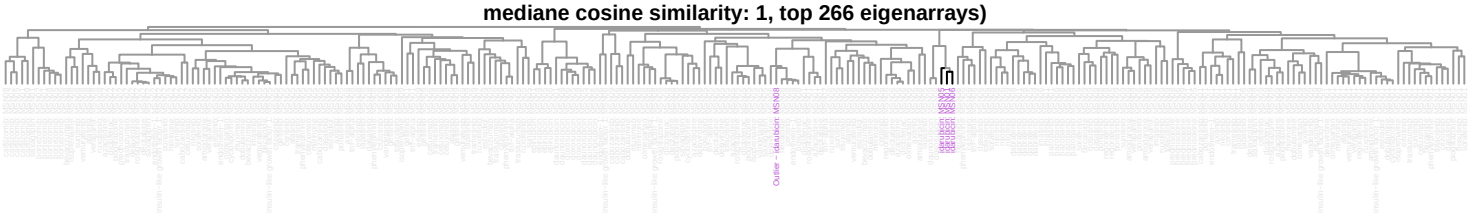

amiodarone after removal of 1st eigenarray , F1: 0.36 , Precision: 0.33 , Recall: 0.4

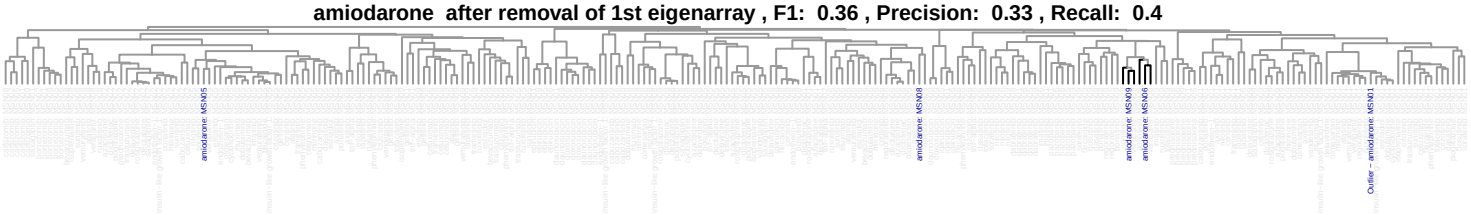

amiodarone in decomposed data (F1 score weight: 0.5 , F1: 0.67, Precision: 0.57, Recall: 0.8, mediane cosine similarity: 0.87, top 161 eigenarrays)

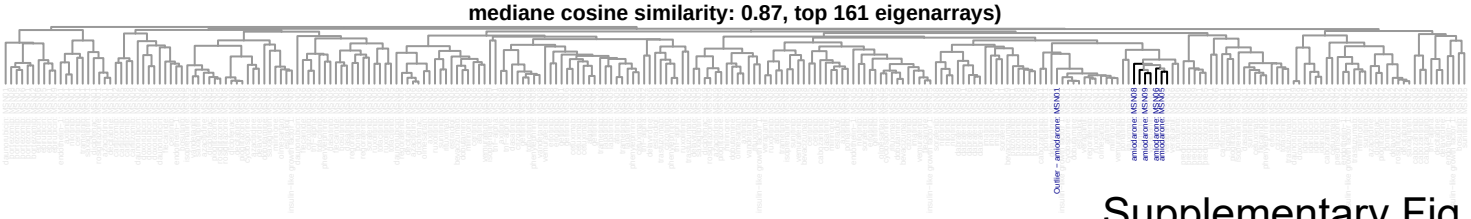

Supplementary Fig. 11

dobutamine after removal of 1st eigenarray , F1: 0.09 , Precision: 0.05 , Recall: 0.4

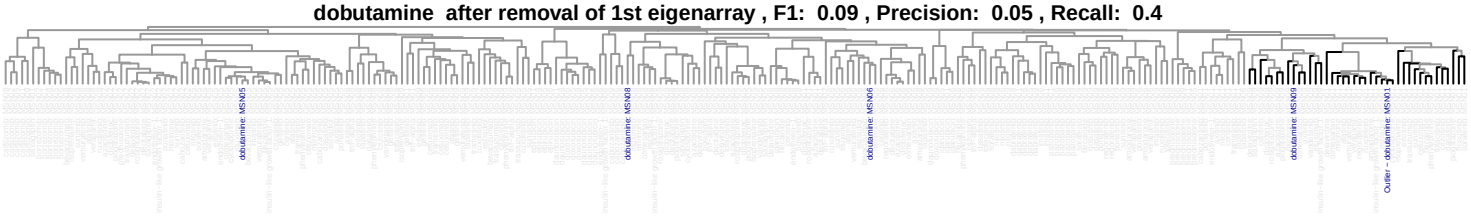

dobutamine in decomposed data (F1 score weight: 0.55 , F1: 0.8, Precision: 0.8, Recall: 0.8, mediane cosine similarity: 0.29, top 31 eigenarrays)

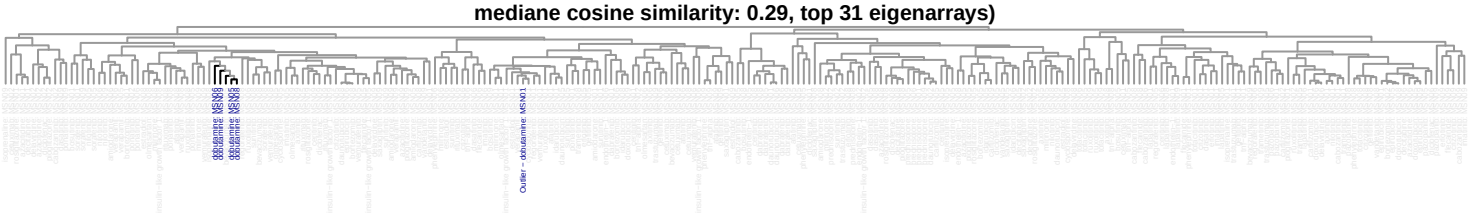

flecainide after removal of 1st eigenarray , F1: 0.09 , Precision: 0.05 , Recall: 0.4

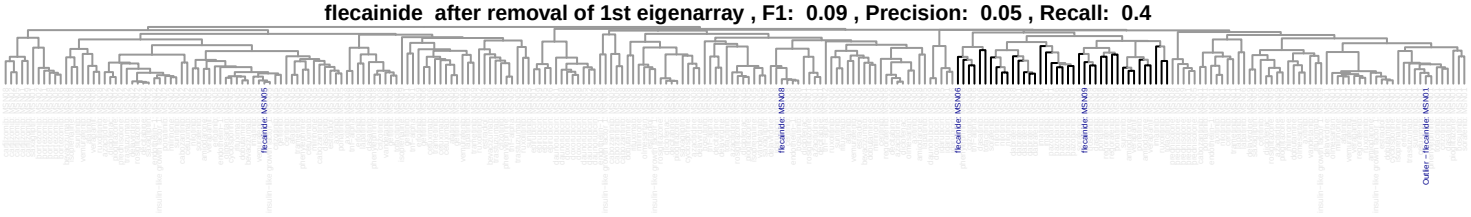

flecainide in decomposed data (F1 score weight: 0.55 , F1: 0.89, Precision: 1, Recall: 0.8, mediane cosine similarity: 0.21, top 24 eigenarrays)

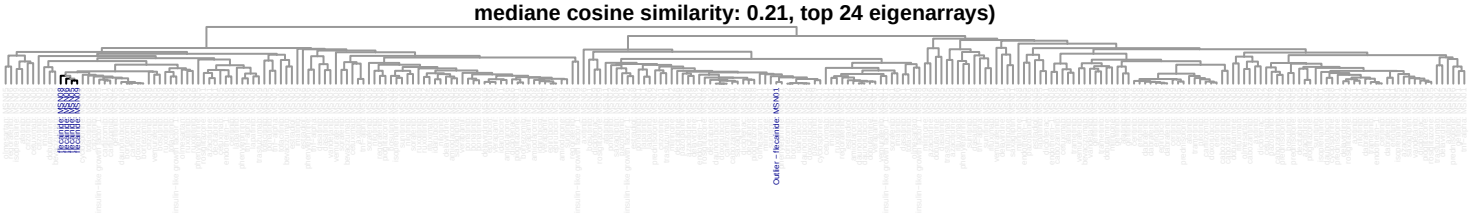

isoprenaline after removal of 1st eigenarray , F1: 0.04 , Precision: 0.02 , Recall: 0.5

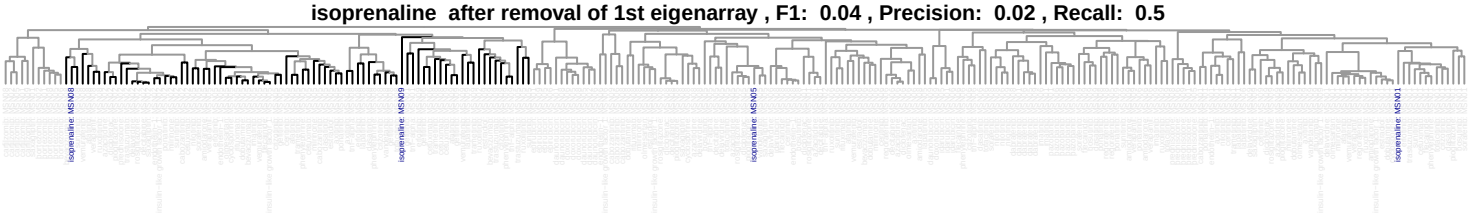

isoprenaline in decomposed data (F1 score weight: 0.95 , F1: 1, Precision: 1, Recall: 1, mediane cosine similarity: 0.5, top 34 eigenarrays)

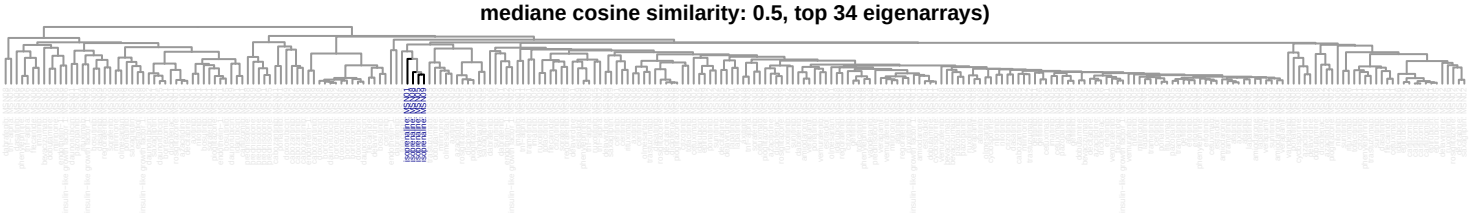

milrinone after removal of 1st eigenarray , F1: 0.09 , Precision: 0.05 , Recall: 0.33

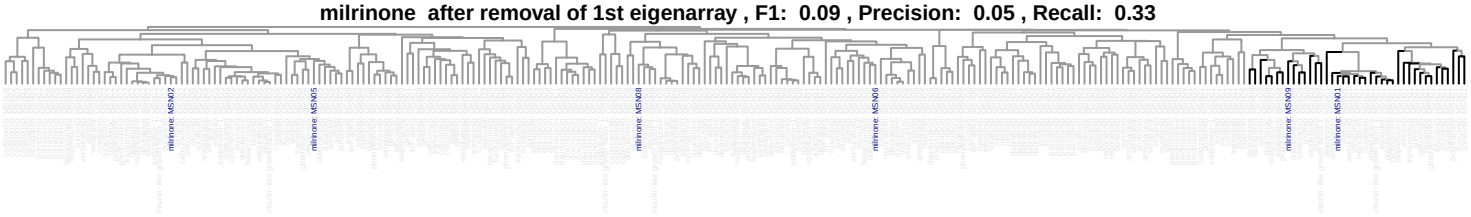

milrinone in decomposed data (F1 score weight: 0.95 , F1: 0.67, Precision: 1, Recall: 0.5, mediane cosine similarity: 0.12, top 14 eigenarrays)

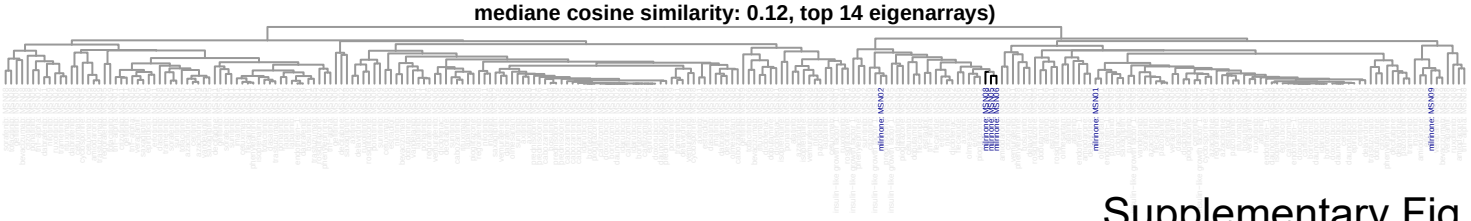

Supplementary Fig. 11

phenylephrine after removal of 1st eigenarray , F1: 0.1 , Precision: 0.06 , Recall: 0.4

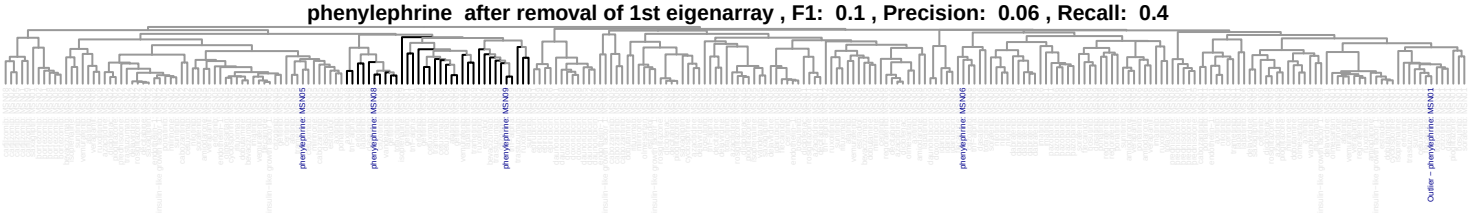

phenylephrine in decomposed data (F1 score weight: 0.55 , F1: 0.89, Precision: 1, Recall: 0.8, mediane cosine similarity: 0.14, top 13 eigenarrays)

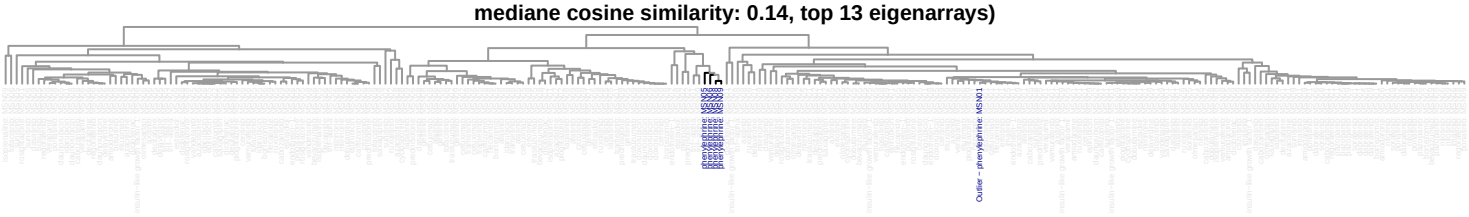

verapamil after removal of 1st eigenarray , F1: 0.36 , Precision: 0.33 , Recall: 0.4

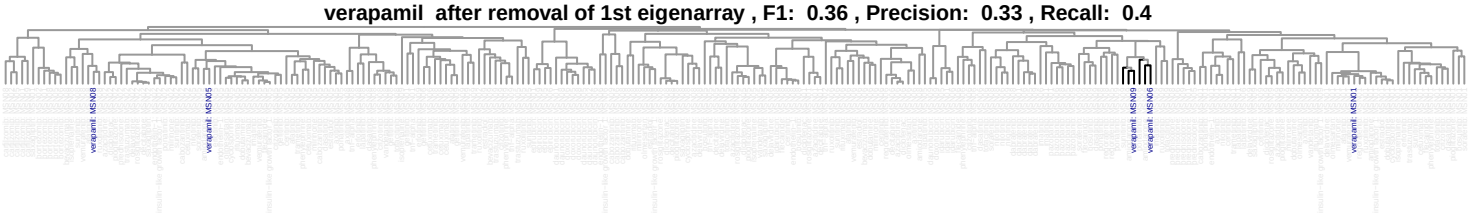

verapamil in decomposed data (F1 score weight: 0.95 , F1: 0.55, Precision: 0.5, Recall: 0.6, mediane cosine similarity: 0.83, top 91 eigenarrays)

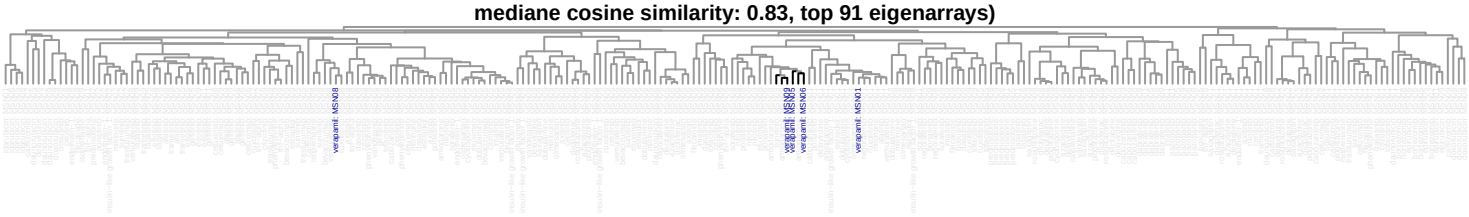

azacitidine after removal of 1st eigenarray , F1: 0.13 , Precision: 0.07 , Recall: 0.67

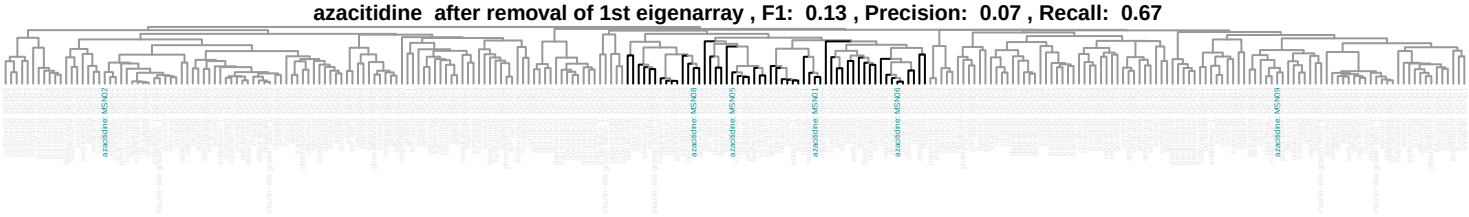

azacitidine in decomposed data (F1 score weight: 0.95 , F1: 0.8, Precision: 1, Recall: 0.67, mediane cosine similarity: 0.29, top 15 eigenarrays)

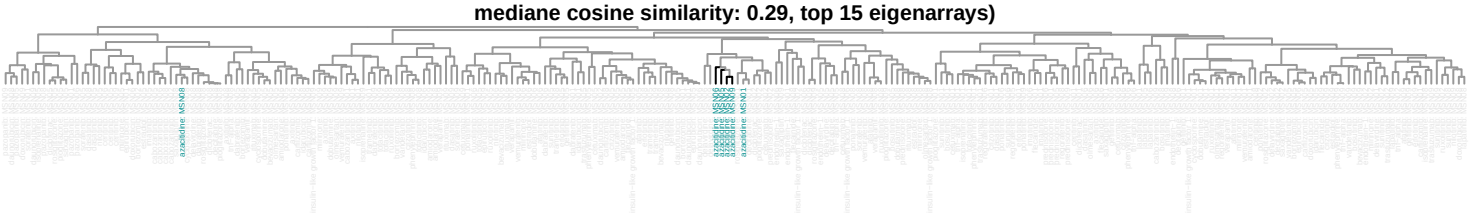

bortezomib after removal of 1st eigenarray , F1: 1 , Precision: 1 , Recall: 1

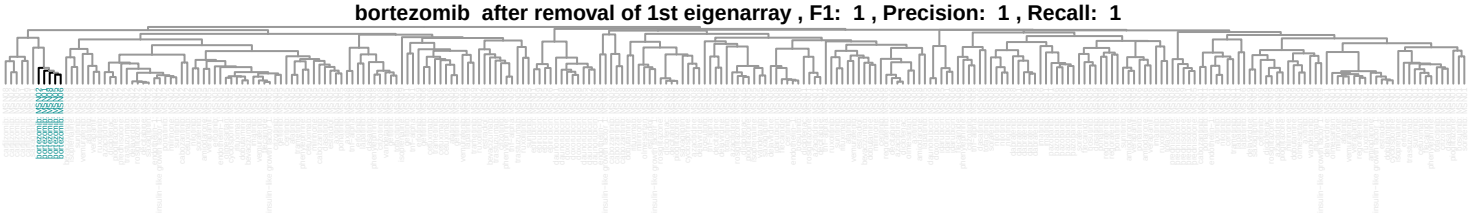

bortezomib in decomposed data (F1 score weight: 0.95 , F1: 1, Precision: 1, Recall: 1, mediane cosine similarity: 1, top 266 eigenarrays)

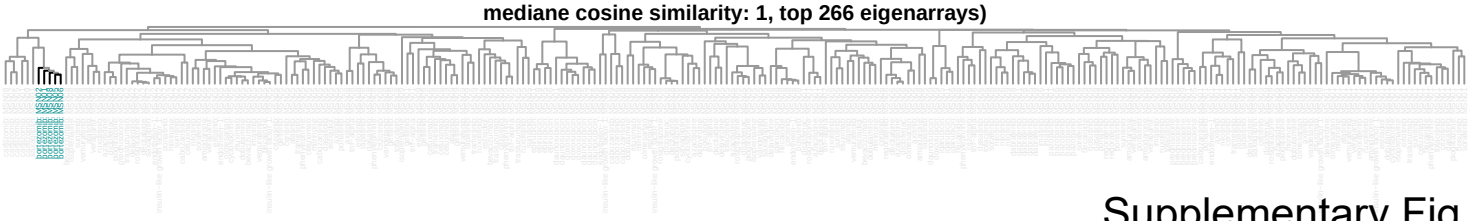

carfilzomib after removal of 1st eigenarray , F1: 1 , Precision: 1 , Recall: 1

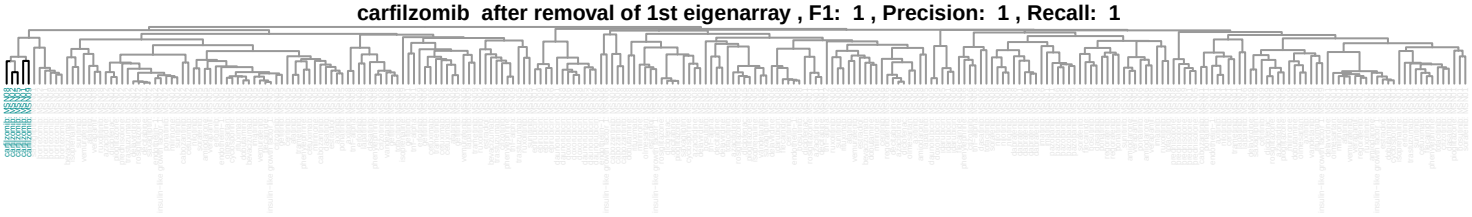

carfilzomib in decomposed data (F1 score weight: 0.95 , F1: 1, Precision: 1, Recall: 1, mediane cosine similarity: 1, top 266 eigenarrays)

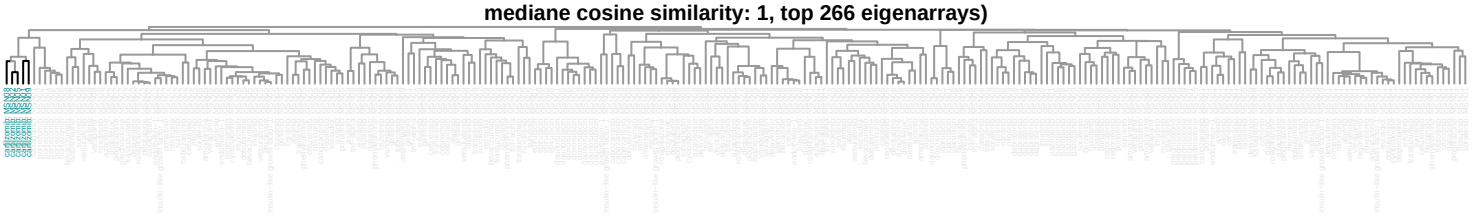

cyclosporine after removal of 1st eigenarray , F1: 0.02 , Precision: 0.01 , Recall: 0.67

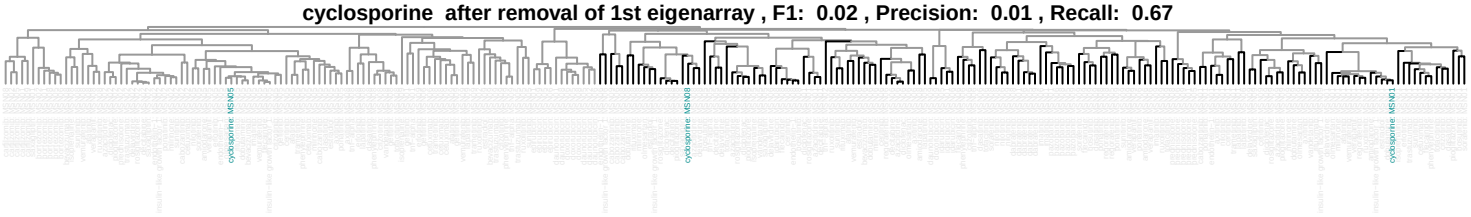

cyclosporine in decomposed data (F1 score weight: 0.95 , F1: 1, Precision: 1, Recall: 1, mediane cosine similarity: 0.22, top 34 eigenarrays)

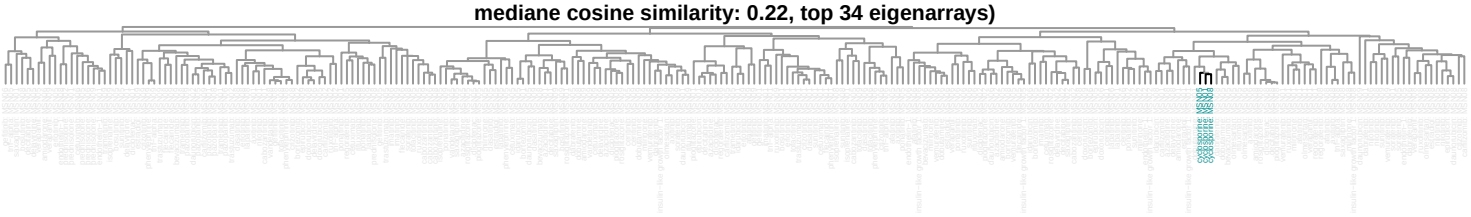

decitabine after removal of 1st eigenarray , F1: 0.13 , Precision: 0.07 , Recall: 0.8

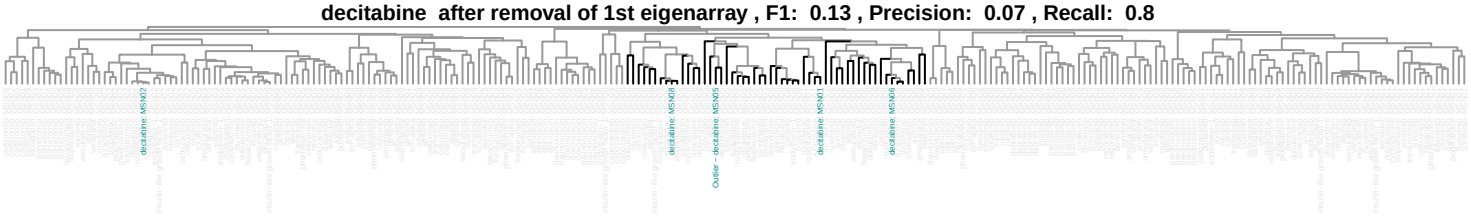

decitabine in decomposed data (F1 score weight: 0.65 , F1: 0.8, Precision: 0.8, Recall: 0.8, mediane cosine similarity: 0.09, top 12 eigenarrays)

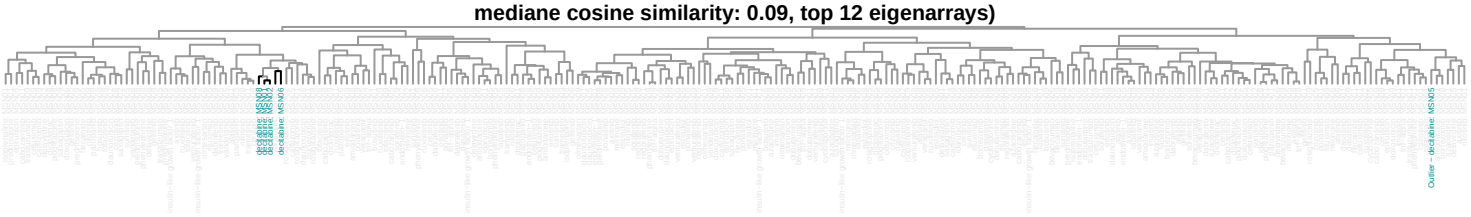

delavirdine after removal of 1st eigenarray , F1: 0.1 , Precision: 0.05 , Recall: 0.5

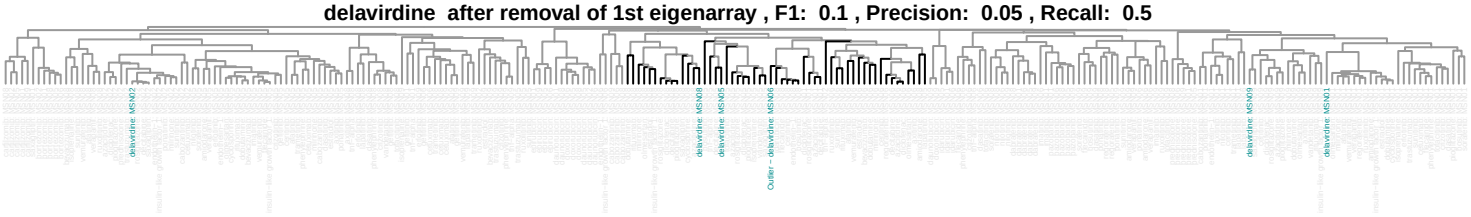

delavirdine in decomposed data (F1 score weight: 0.55 , F1: 0.91, Precision: 1, Recall: 0.83, mediane cosine similarity: 0.13, top 14 eigenarrays)

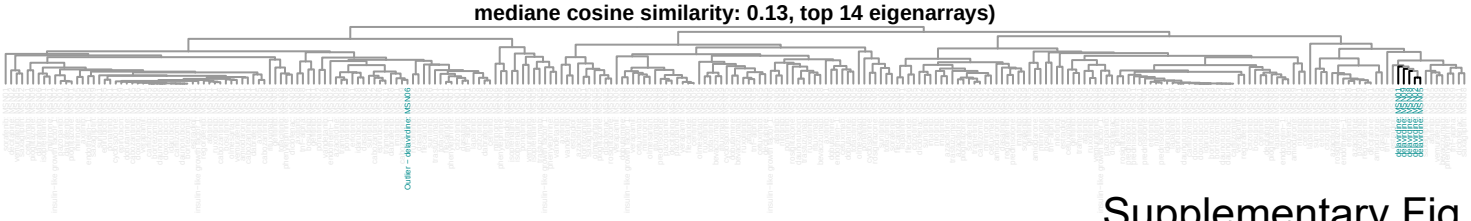

Supplementary Fig. 11

diclofenac after removal of 1st eigenarray , F1: 0.13 , Precision: 0.07 , Recall: 0.67

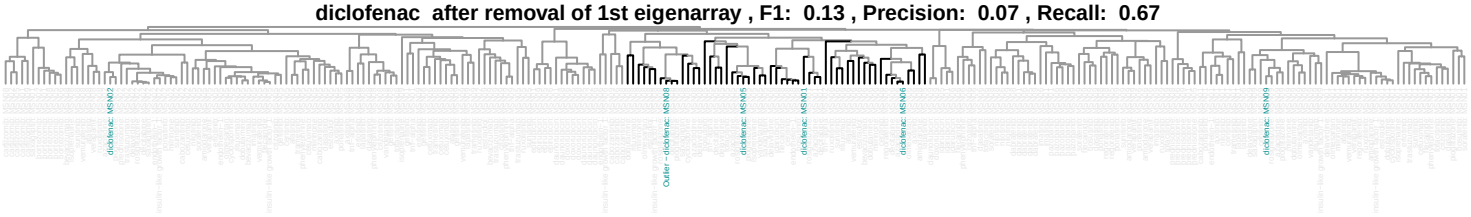

diclofenac in decomposed data (F1 score weight: 0.65 , F1: 0.73, Precision: 0.8, Recall: 0.67, mediane cosine similarity: 0.04, top 6 eigenarrays)

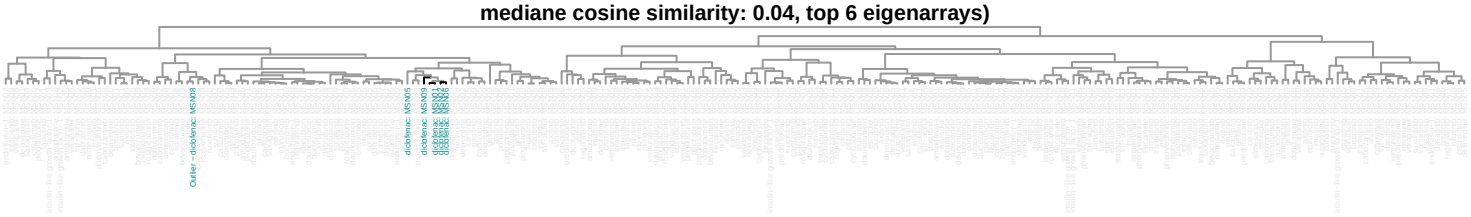

endothelin−1 after removal of 1st eigenarray , F1: 0.08 , Precision: 0.05 , Recall: 0.4

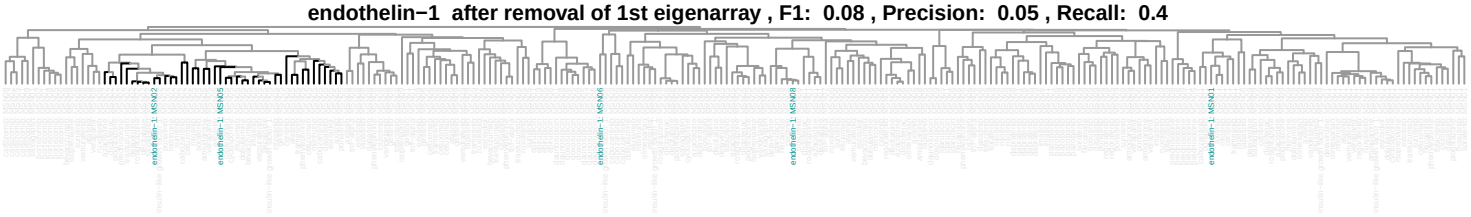

endothelin−1 in decomposed data (F1 score weight: 0.95 , F1: 0.75, Precision: 1, Recall: 0.6, mediane cosine similarity: 0.29, top 21 eigenarrays)

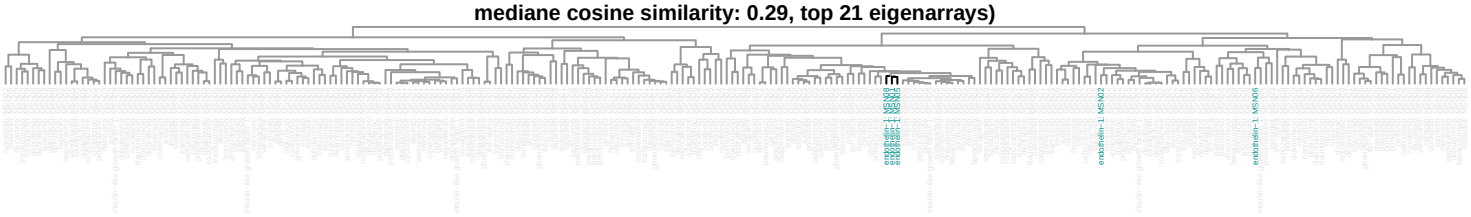

estradiol after removal of 1st eigenarray , F1: 0.07 , Precision: 0.04 , Recall: 0.4

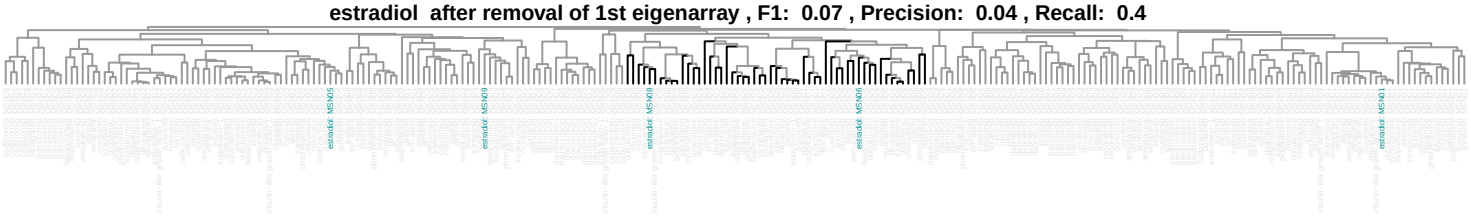

estradiol in decomposed data (F1 score weight: 0.95 , F1: 0.75, Precision: 1, Recall: 0.6, mediane cosine similarity: 0.3, top 34 eigenarrays)

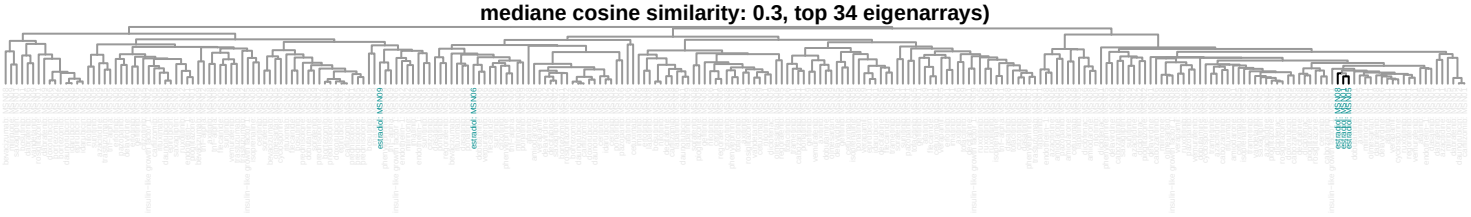

insulin−like growth factor 1 after removal of 1st eigenarray , F1: 0.09 , Precision: 0.05 , Recall: 0.33

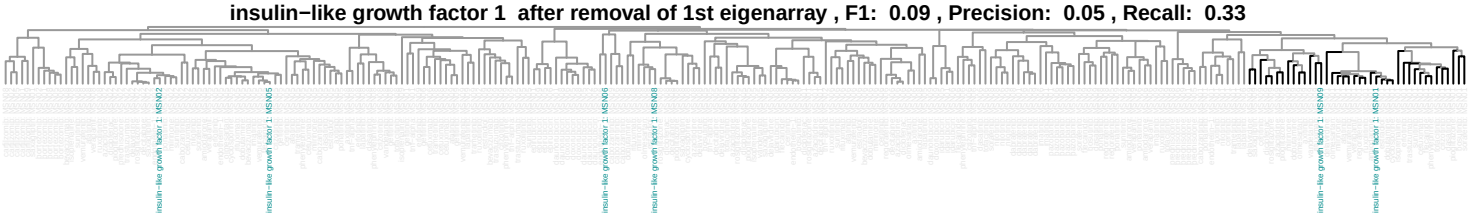

insulin−like growth factor 1 in decomposed data (F1 score weight: 0.95 , F1: 0.67, Precision: 1, Recall: 0.5, mediane cosine similarity: 0.5, top 63 eigenarrays)

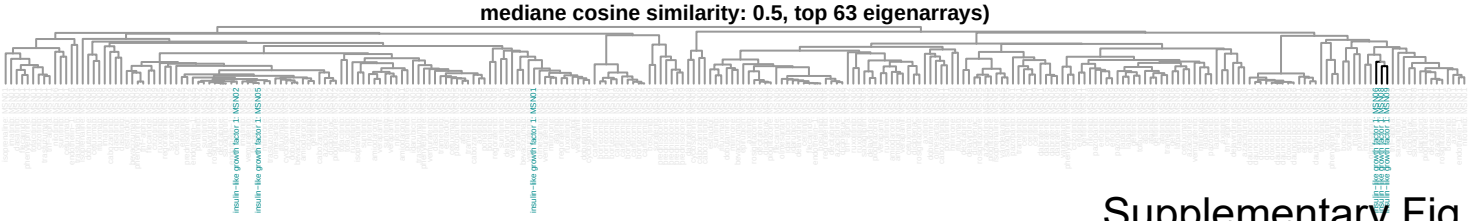

Supplementary Fig. 11

olmesartan after removal of 1st eigenarray , F1: 0.09 , Precision: 0.05 , Recall: 0.4

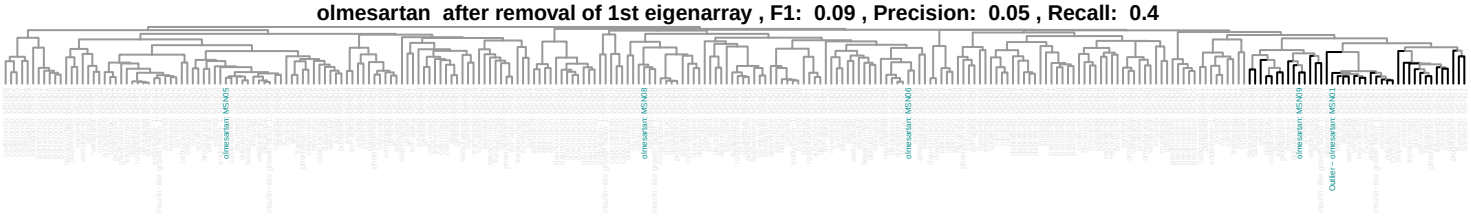

olmesartan in decomposed data (F1 score weight: 0.55 , F1: 0.89, Precision: 1, Recall: 0.8, mediane cosine similarity: 0.15, top 17 eigenarrays)

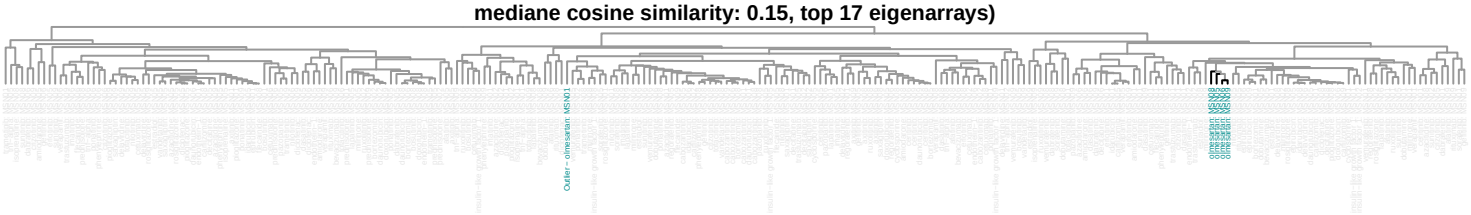

pioglitazone after removal of 1st eigenarray , F1: 0.09 , Precision: 0.05 , Recall: 0.4

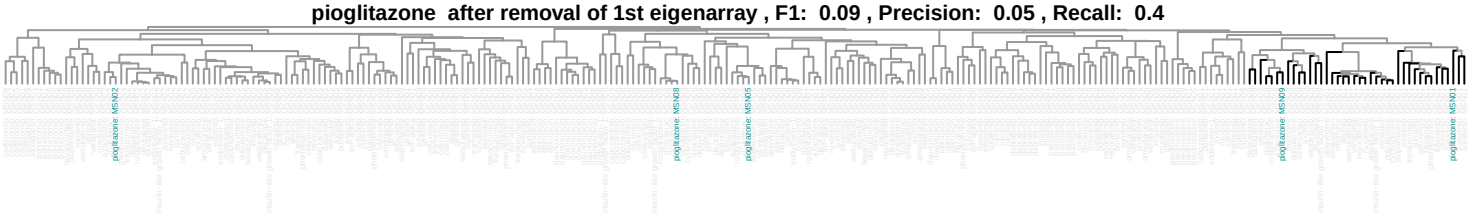

pioglitazone in decomposed data (F1 score weight: 0.95 , F1: 0.75, Precision: 1, Recall: 0.6, mediane cosine similarity: 0.06, top 8 eigenarrays)

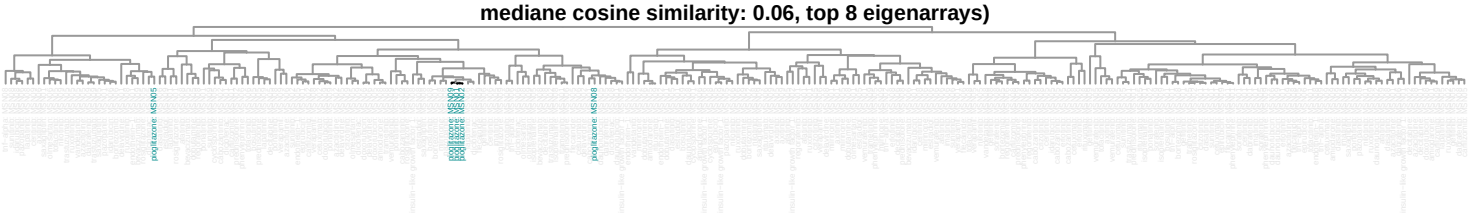

prednisolone after removal of 1st eigenarray , F1: 0.91 , Precision: 1 , Recall: 0.83

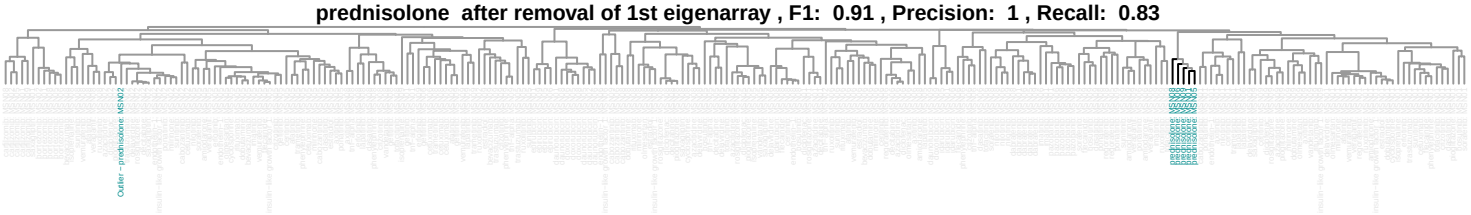

prednisolone in decomposed data (F1 score weight: 0 , F1: 0.91, Precision: 1, Recall: 0.83, mediane cosine similarity: 1, top 266 eigenarrays)

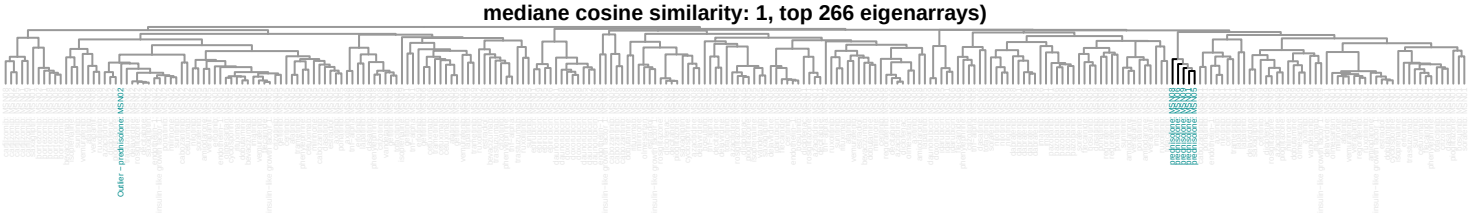

rosiglitazone after removal of 1st eigenarray , F1: 0.1 , Precision: 0.05 , Recall: 0.6

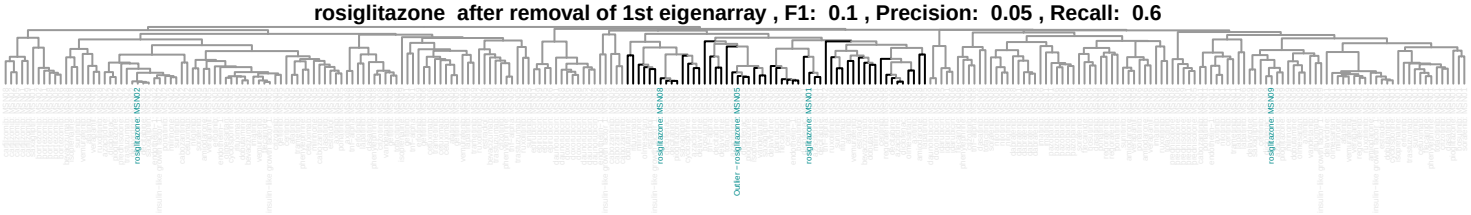

rosiglitazone in decomposed data (F1 score weight: 0.6 , F1: 0.8, Precision: 0.8, Recall: 0.8, mediane cosine similarity: 0.16, top 17 eigenarrays)

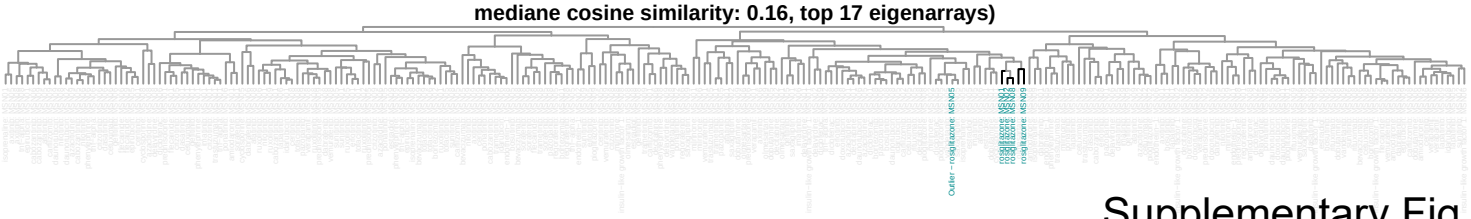

Supplementary Fig. 11

saxagliptin after removal of 1st eigenarray , F1: 0.07 , Precision: 0.04 , Recall: 0.4

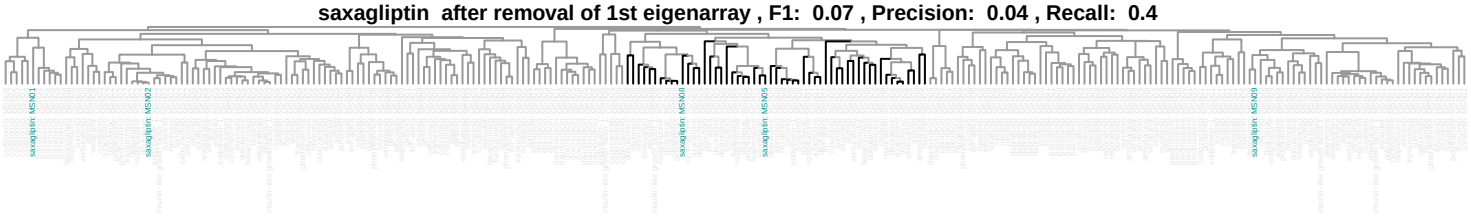

saxagliptin in decomposed data (F1 score weight: 0.95 , F1: 0.75, Precision: 1, Recall: 0.6, mediane cosine similarity: 0.07, top 5 eigenarrays)

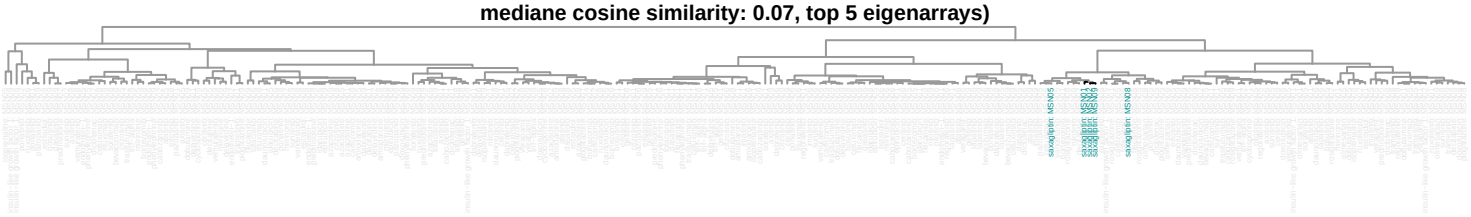

tnf−alpha after removal of 1st eigenarray , F1: 0.15 , Precision: 0.09 , Recall: 0.5

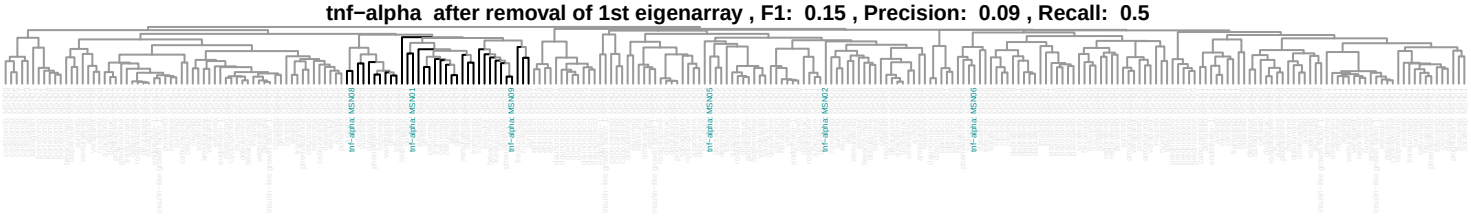

tnf−alpha in decomposed data (F1 score weight: 0.95 , F1: 0.67, Precision: 1, Recall: 0.5, mediane cosine similarity: 0.32, top 17 eigenarrays)

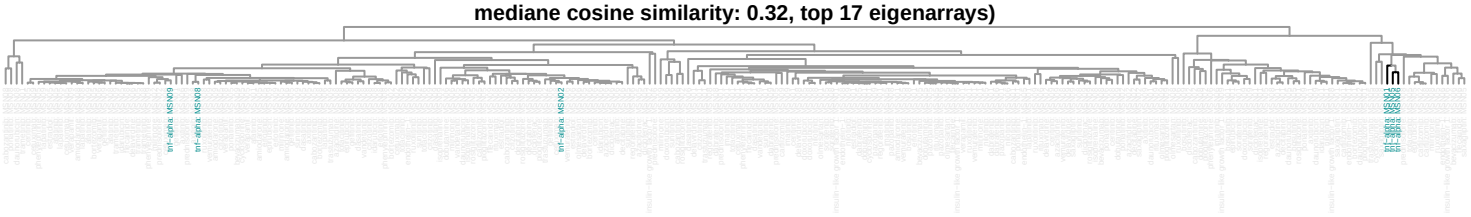

Supplementary Fig. 11

Supplementary Figure 11. Clustering results for each drug after removal of the first eigenarray and in the final drug-selective subspaces. Clusters with the highest F1 scores are labeled black. Small molecule kinase inhibitors, monoclonal antibodies, anthracyclines, cardiac acting and non-cardiac acting drugs are labeled orange, red, purple, blue and gray-blue. The cluster dendrogram shown in Suppl. Figure 10D is part of this figure set as well.

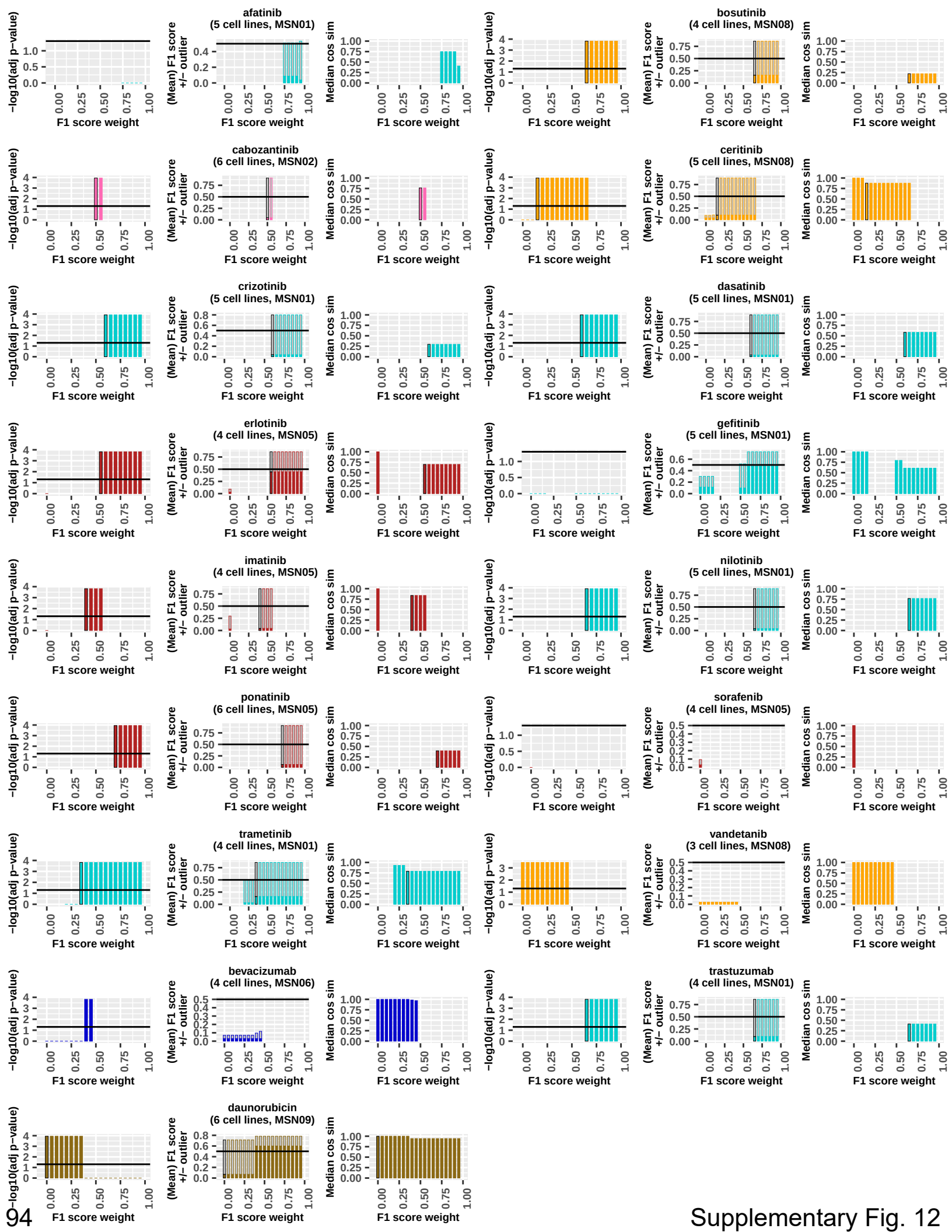

Supplementary Fig. 12

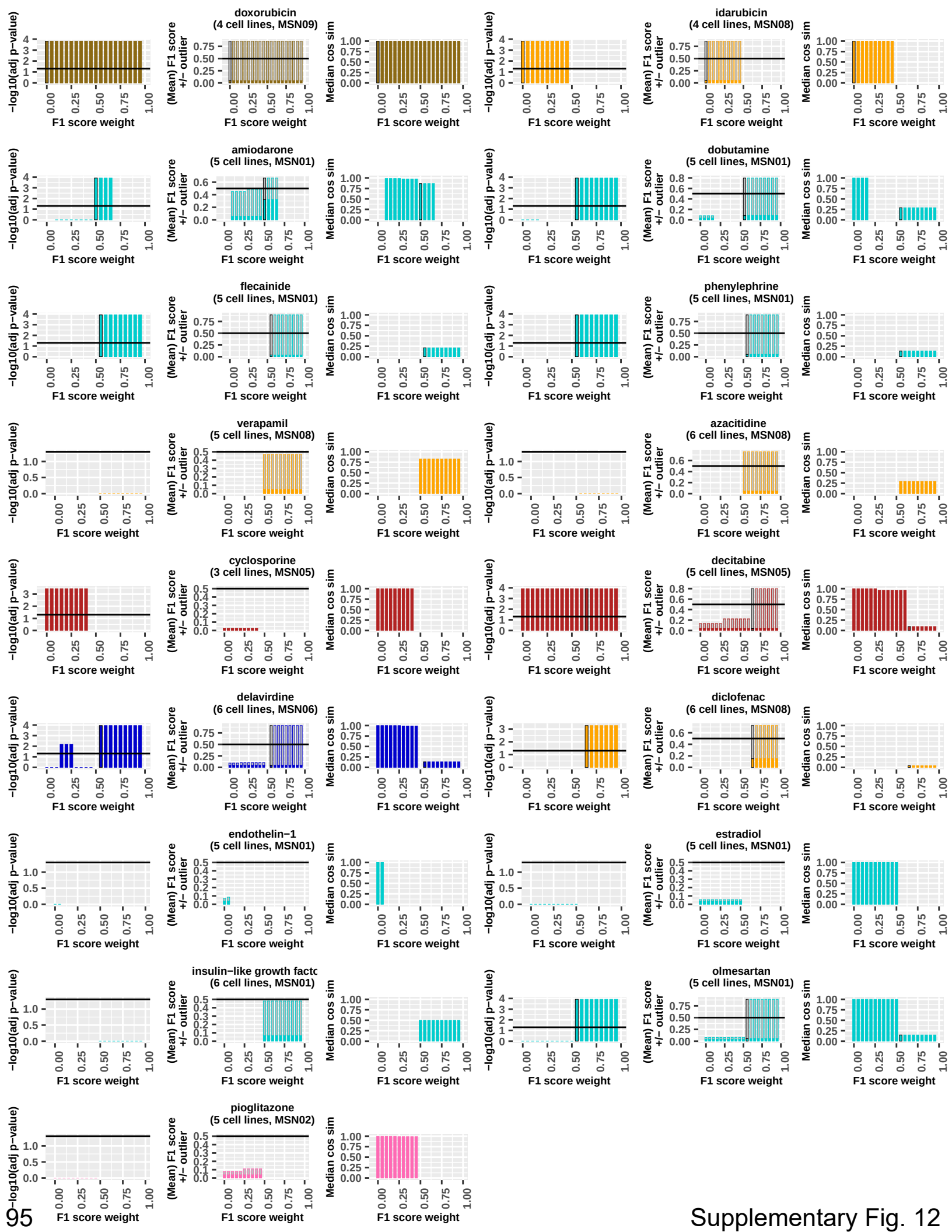

Supplementary Fig. 12

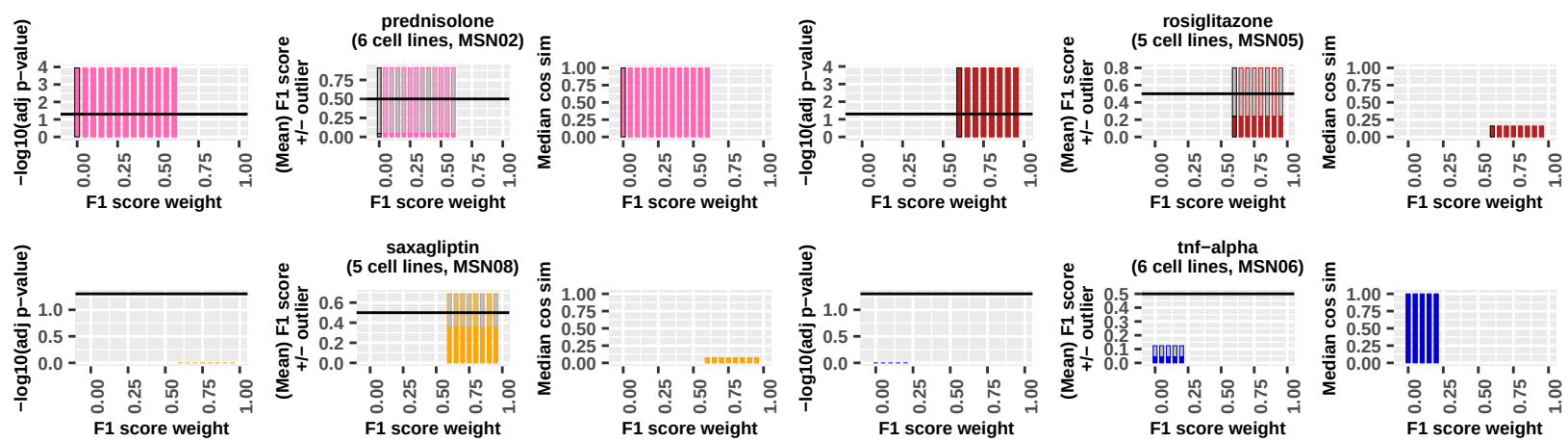

Supplementary Fig. 12

Supplementary Figure 12. Identification of outlier responses. For each drug, we screened all 20 potential drug-selective subspaces (that are defined by different F1 score weights) for subspaces where one cell line/drug combination shows a different transcriptomic response to the drug of interest than all other cell line/drug combinations. As shown for an example in Suppl. Figure 10D, we calculated cell line/drug combination-specific F1 scores, using the same approach described above, except that the cell line/drug combination of interest has to be part of the corresponding cluster. Dixon's Q test of cell line/drug combination-specific F1 scores was used to identify outliers (adj. p-value = 0.05). Identified outliers were only accepted, if the mean F1 score of all non-outlier cell line/drug combinations was larger than 0.5 (empty bars in middle figure). We selected that subspace with the most significant adjusted p-value as the final drug-selective subspace (black frame). Mean F1 scores of all non-outlier cell line/drug combinations and decreasing F1 score weight were used as first and second tiebreakers, respectively. If no outlier was identified, we selected that subspace with the highest selection score based on an F1 score weight of 0.95.

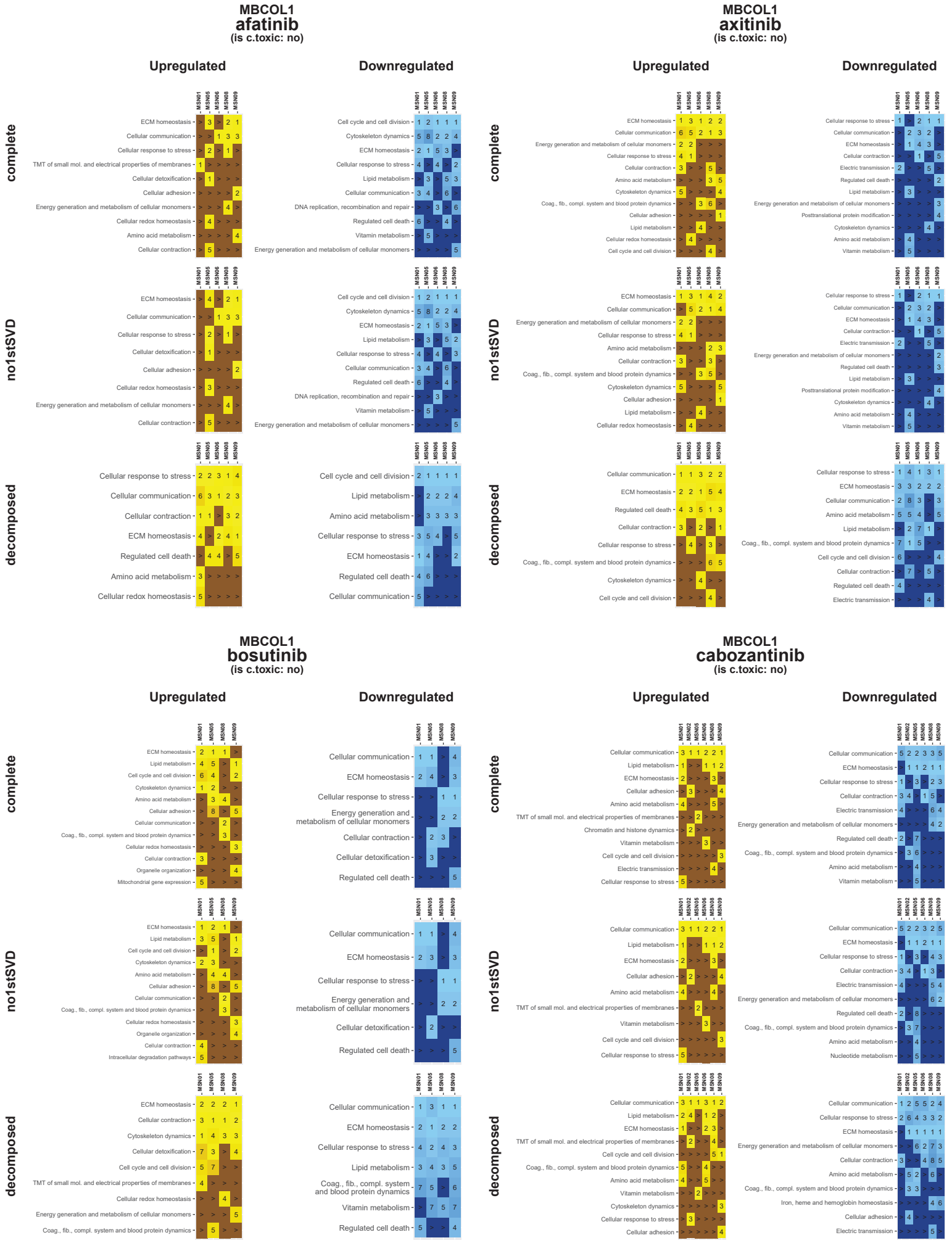

Supplementary Fig. 14B

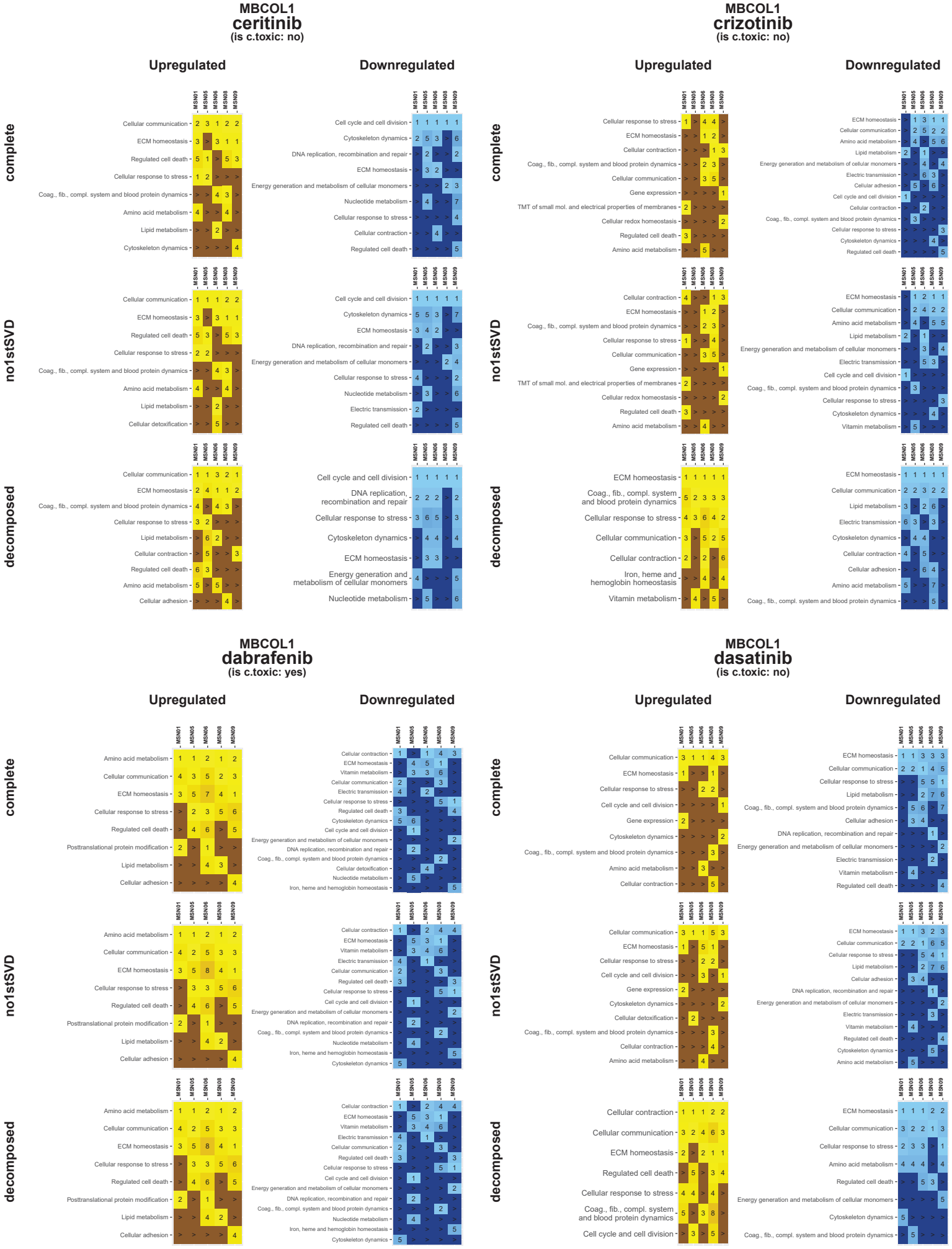

Supplementary Fig. 14B

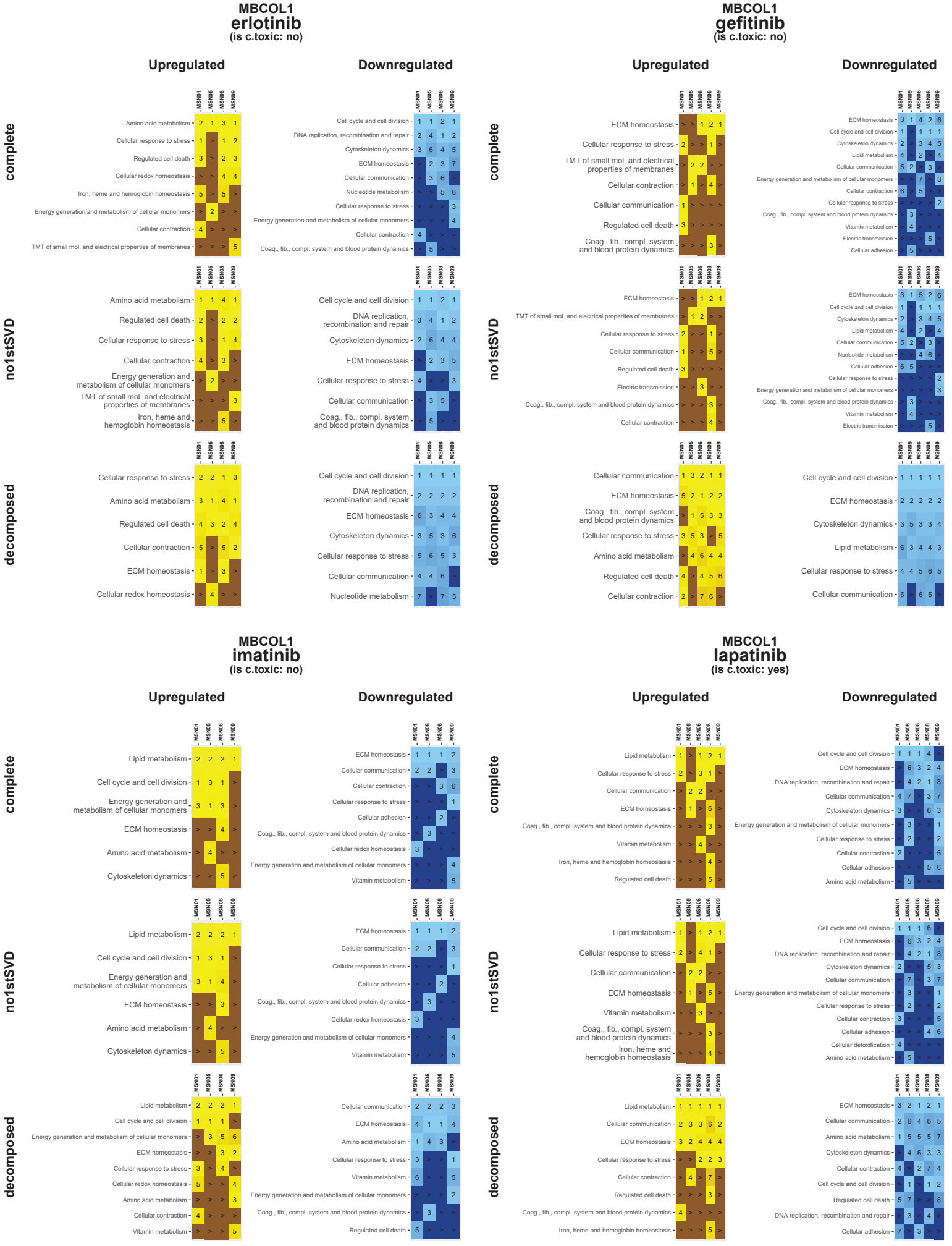

Supplementary Fig. 14B

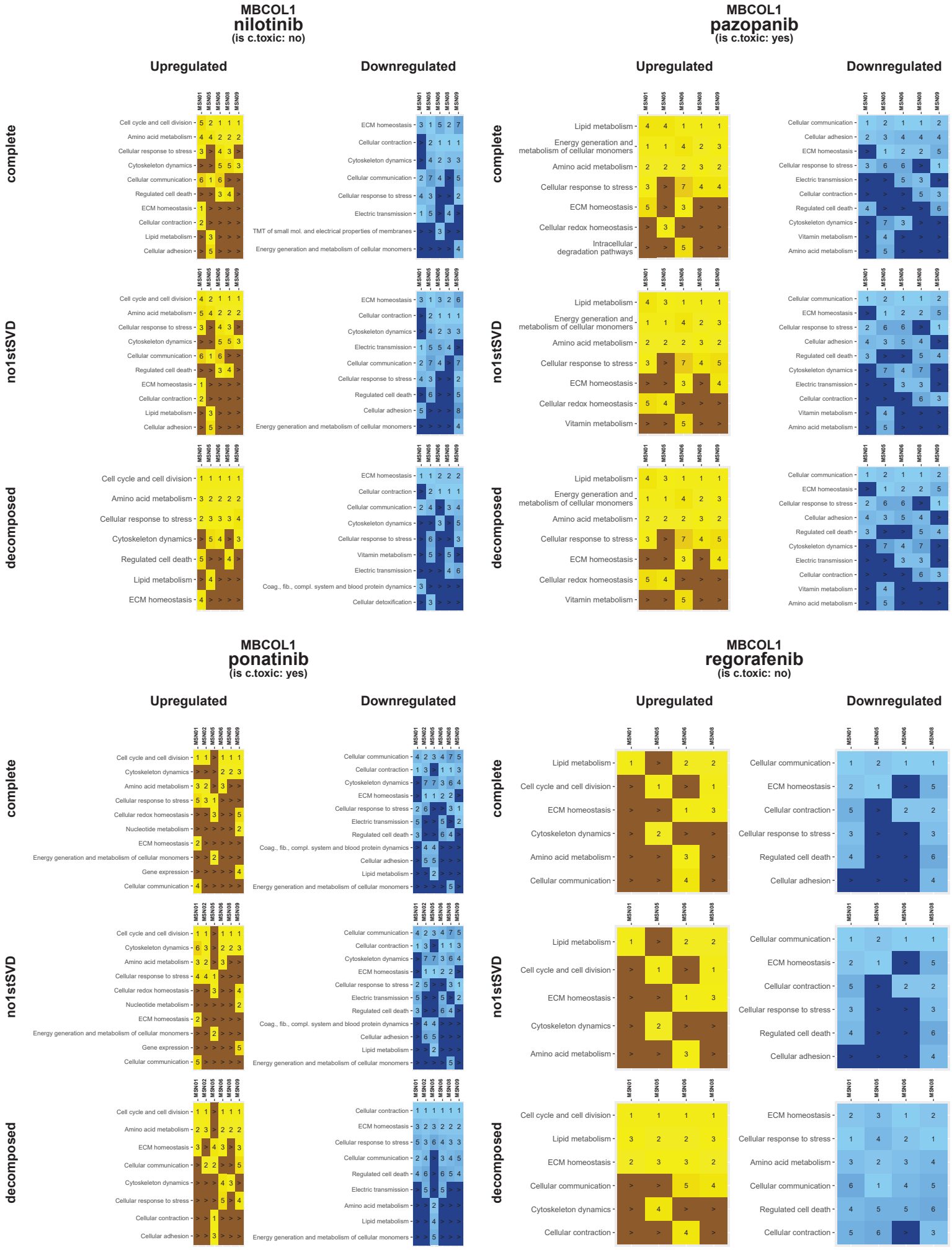

Supplementary Fig. 14B

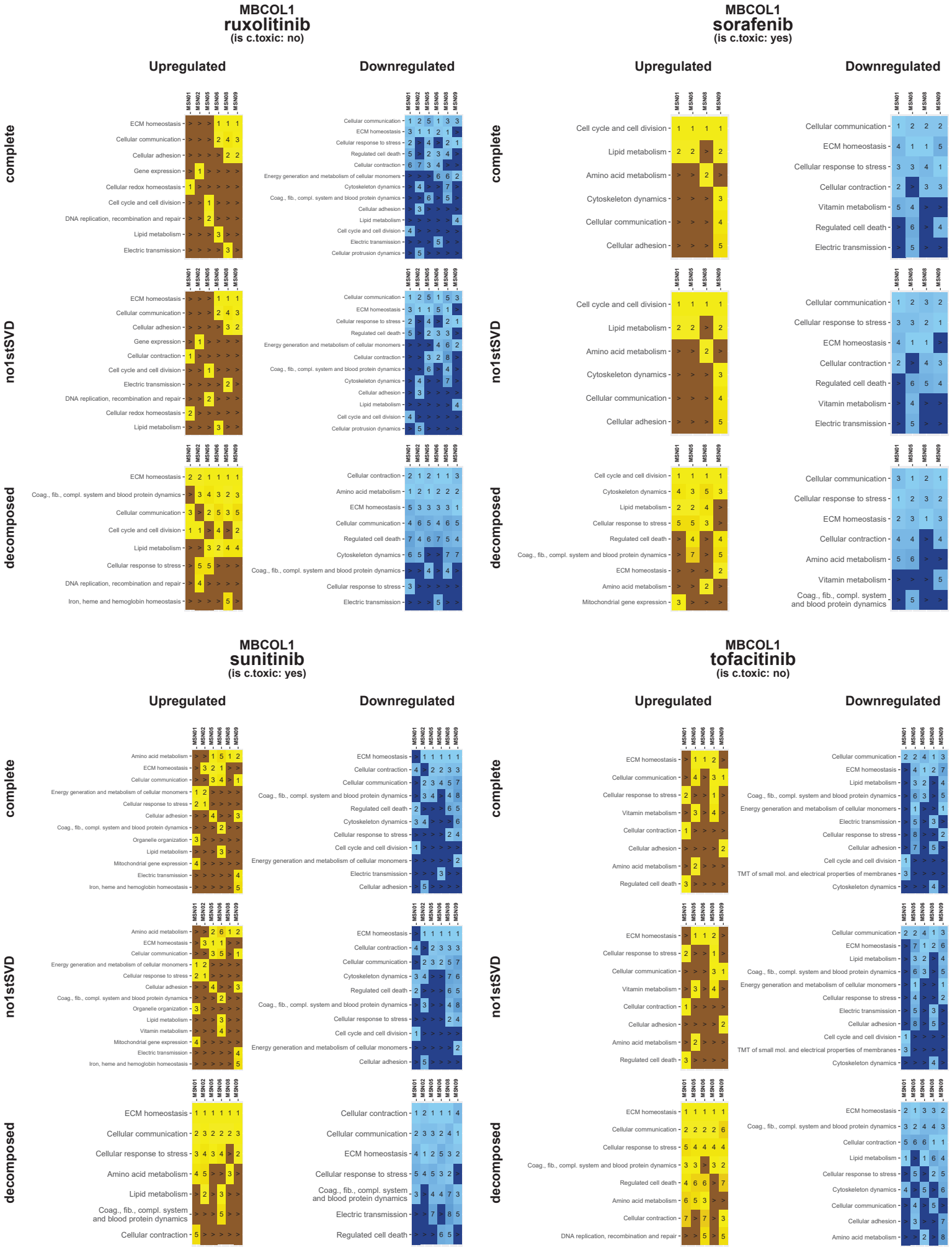

Supplementary Fig. 14B

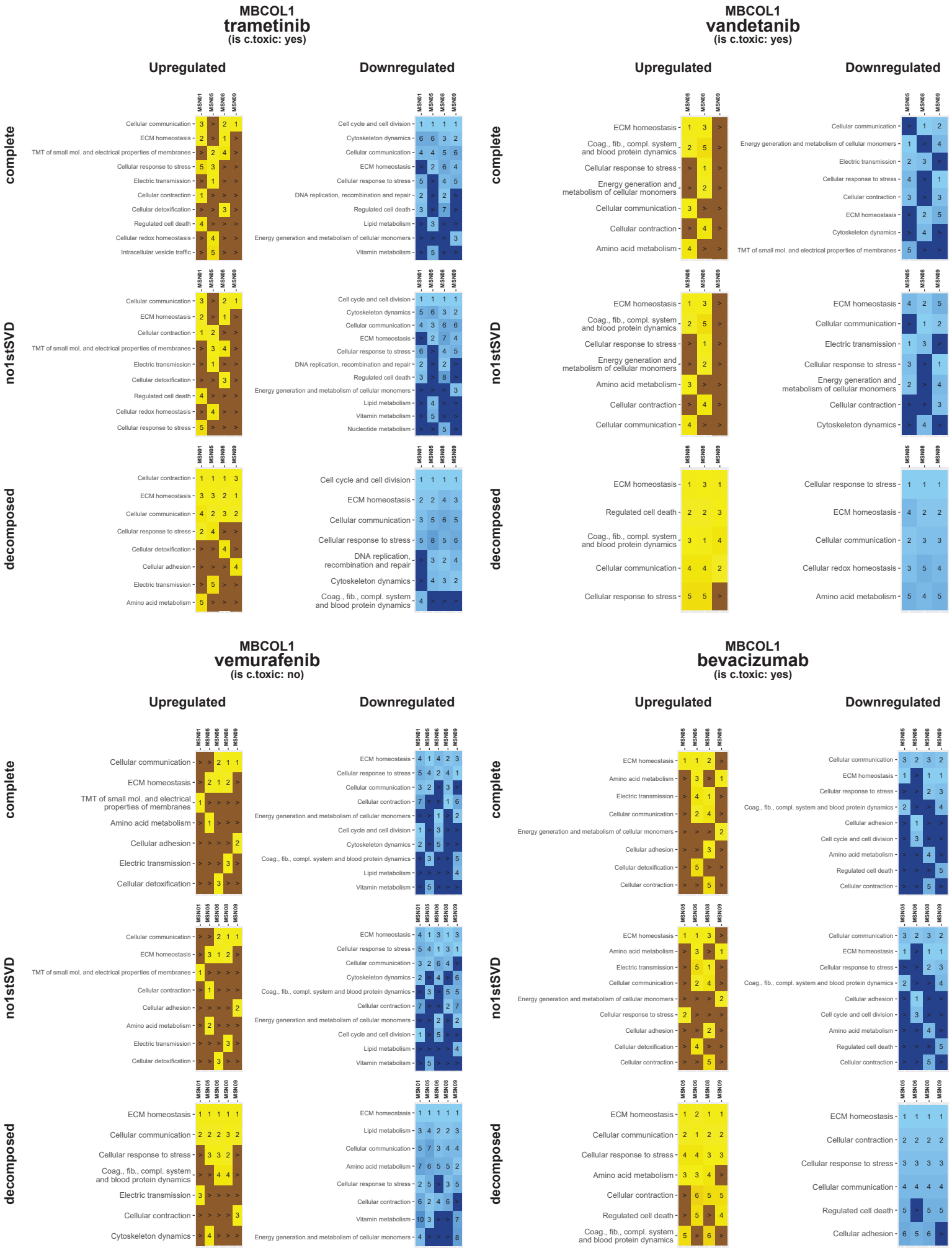

Supplementary Fig. 14B

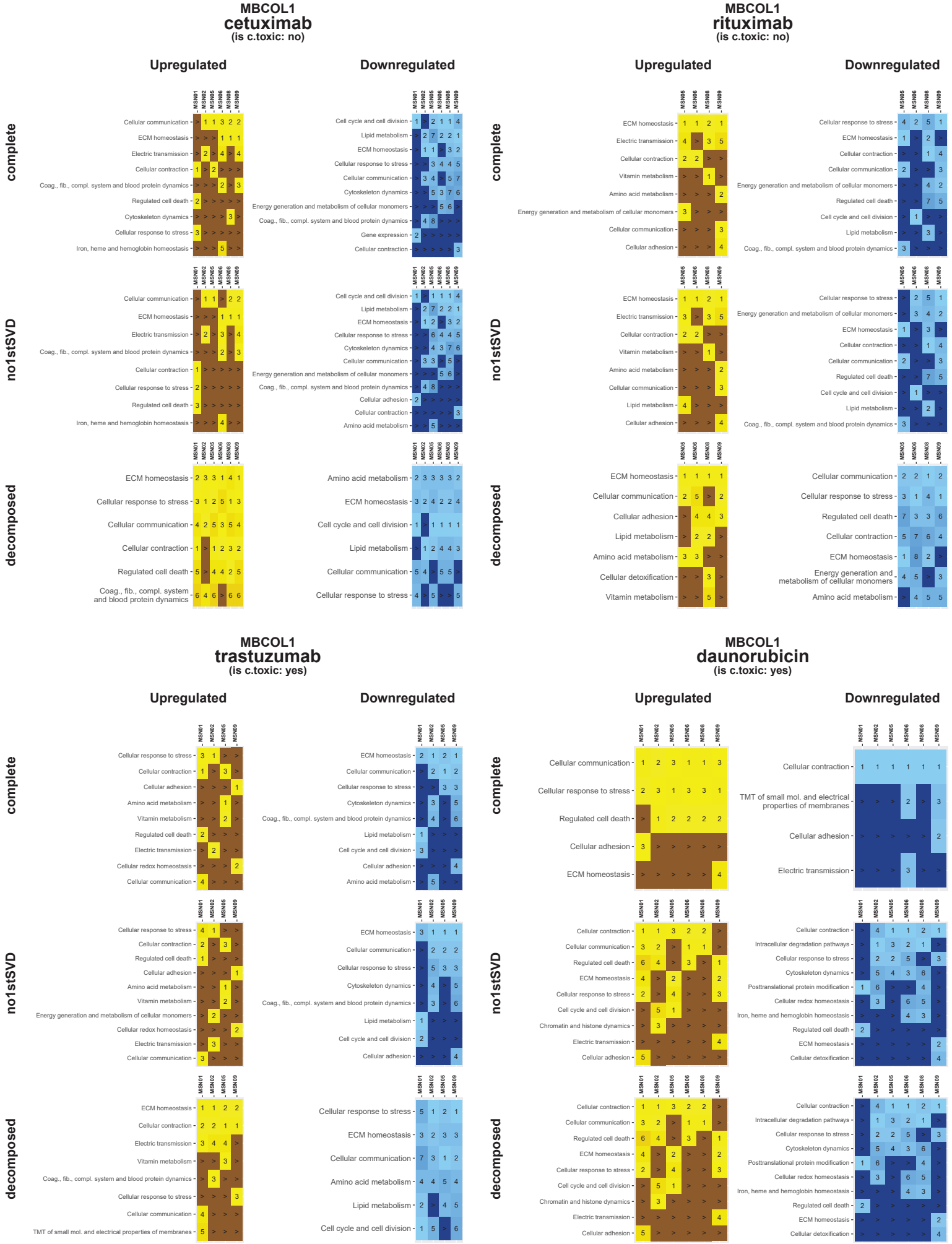

Supplementary Fig. 14B

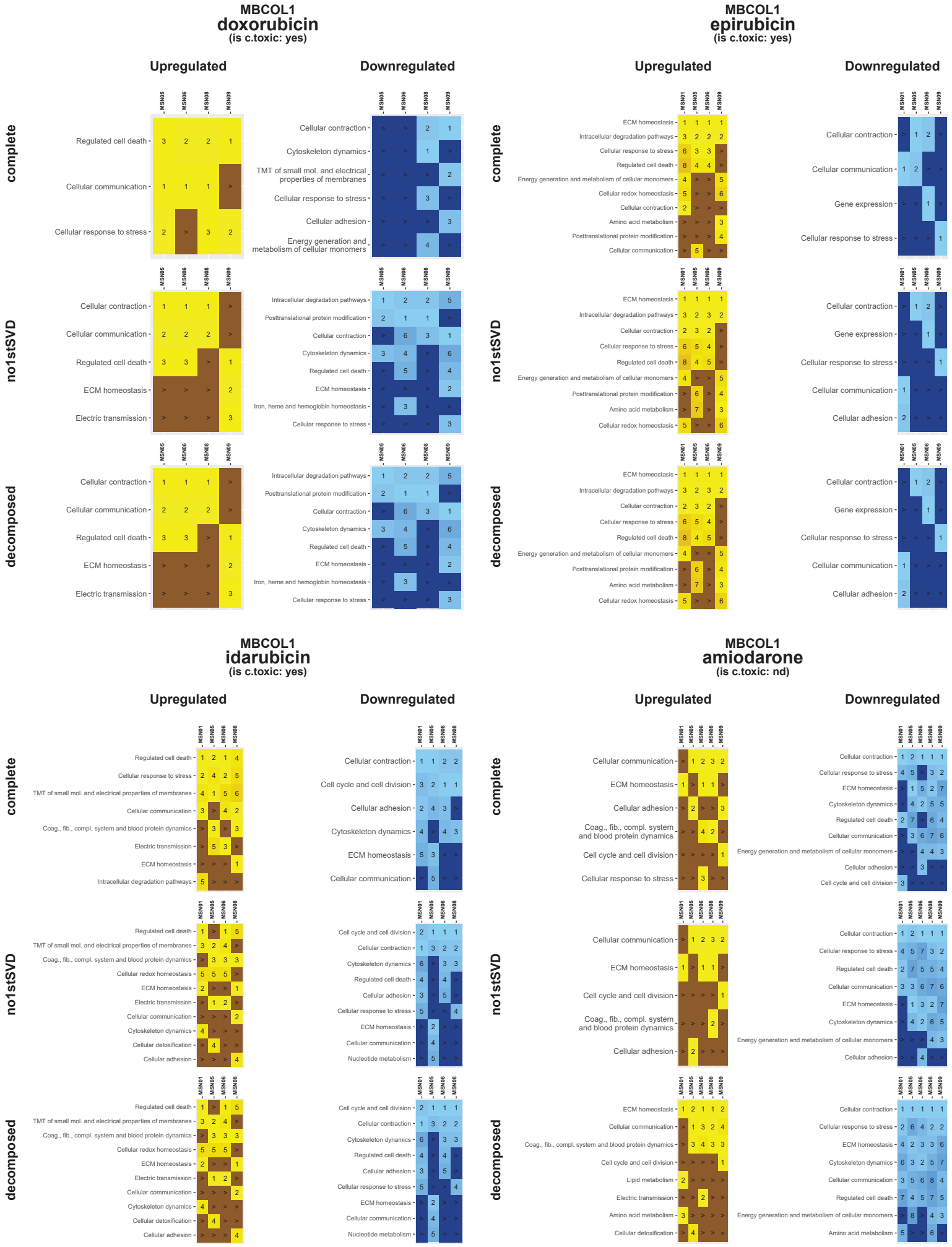

Supplementary Fig. 14B

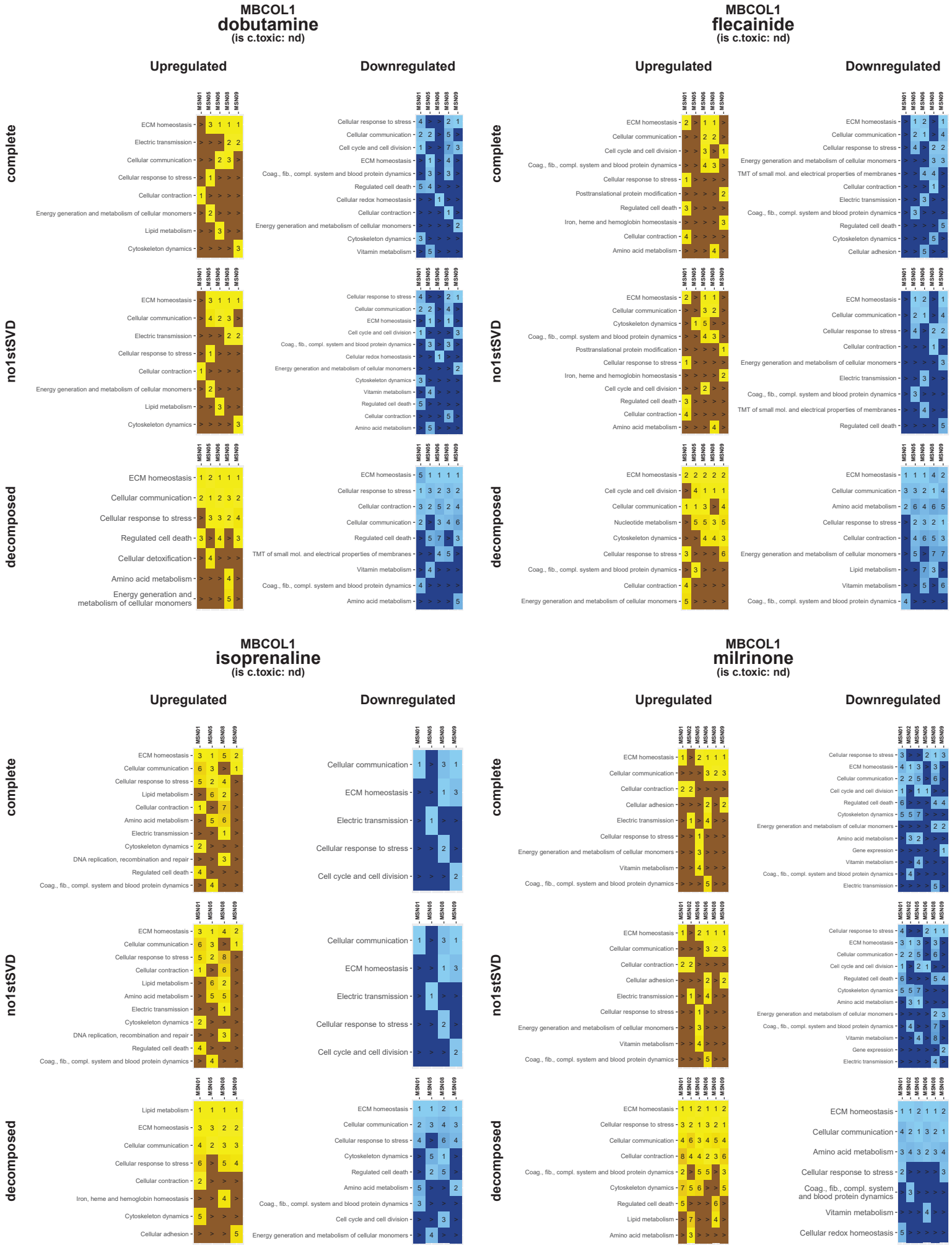

Supplementary Fig. 14B

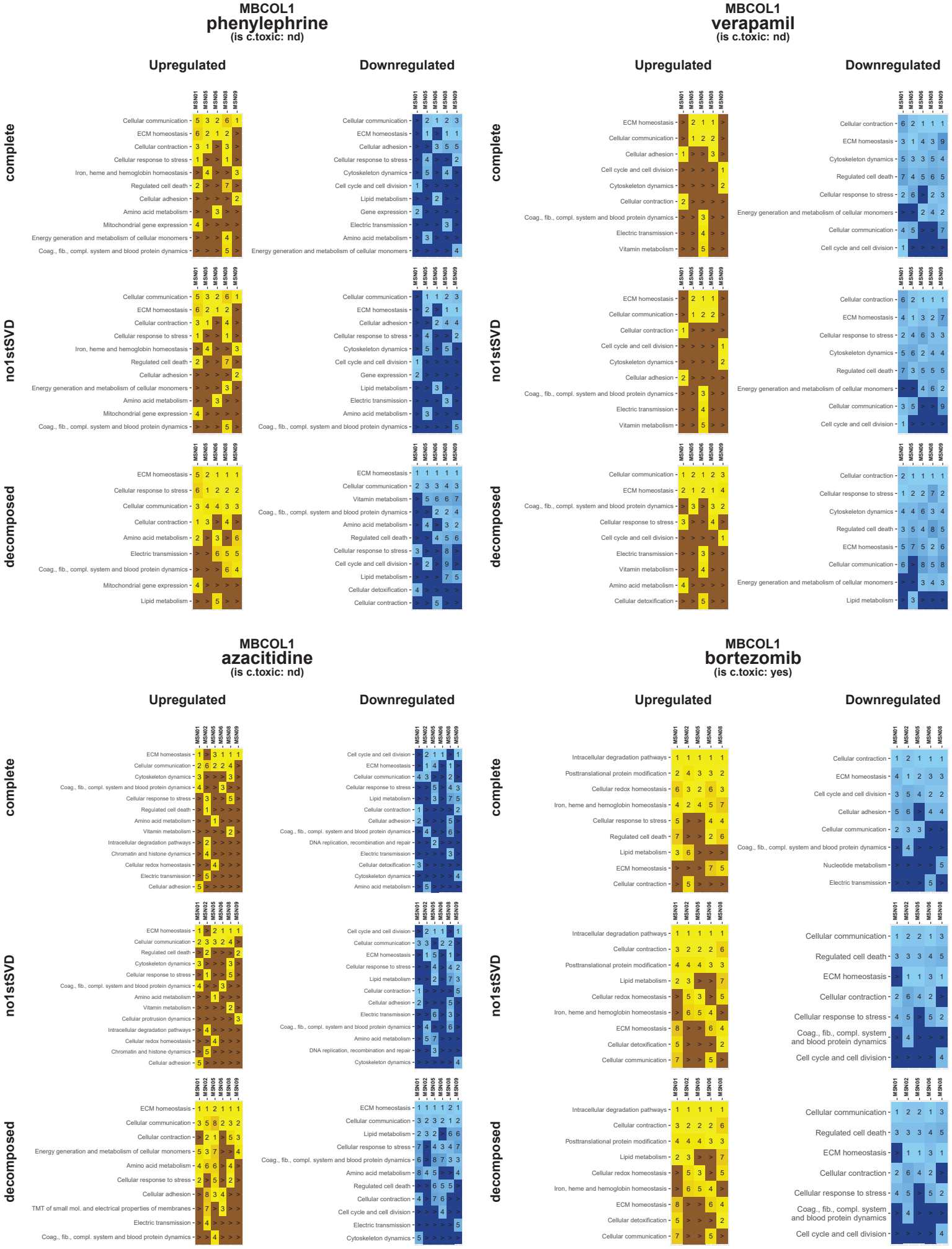

Supplementary Fig. 14B

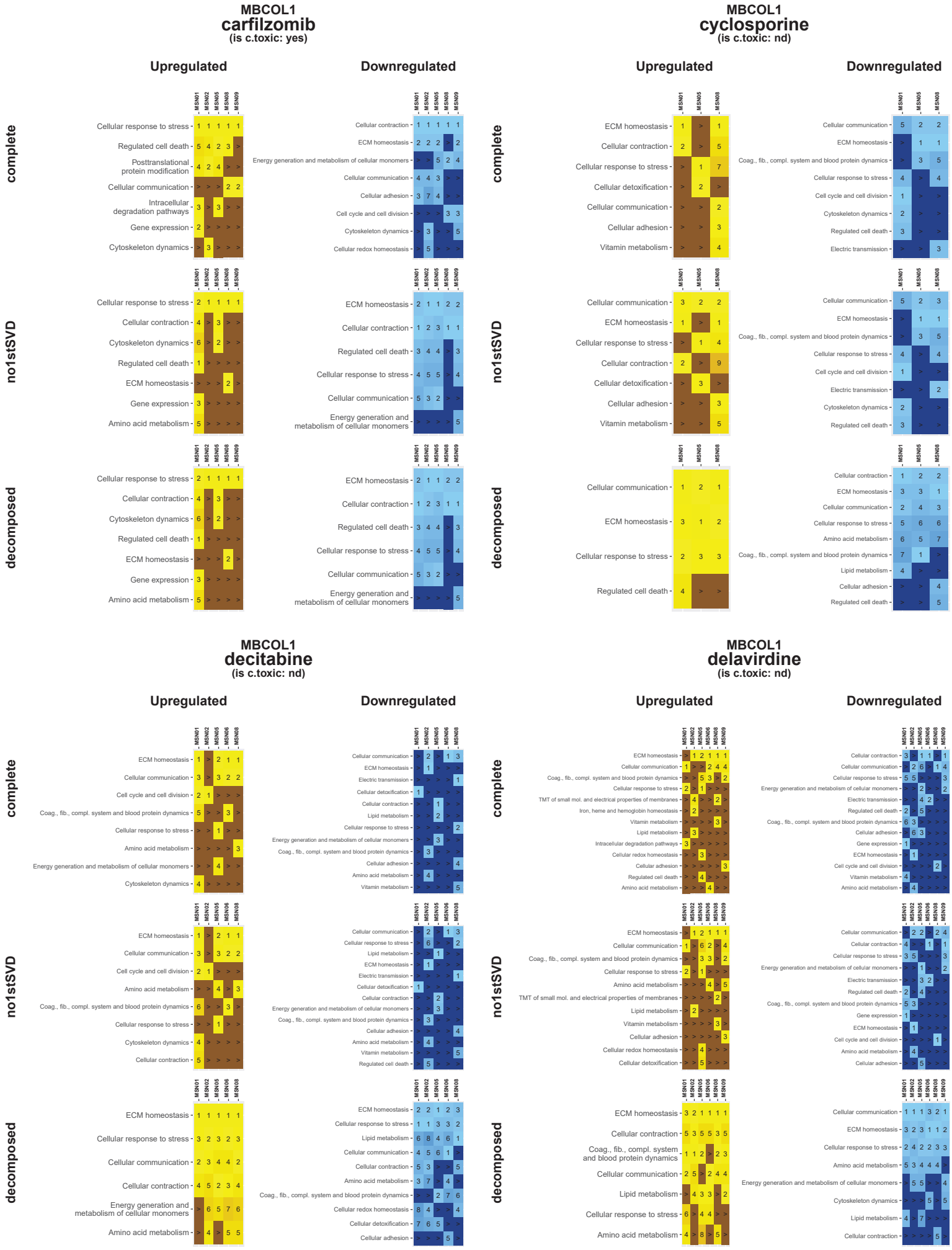

Supplementary Fig. 14B

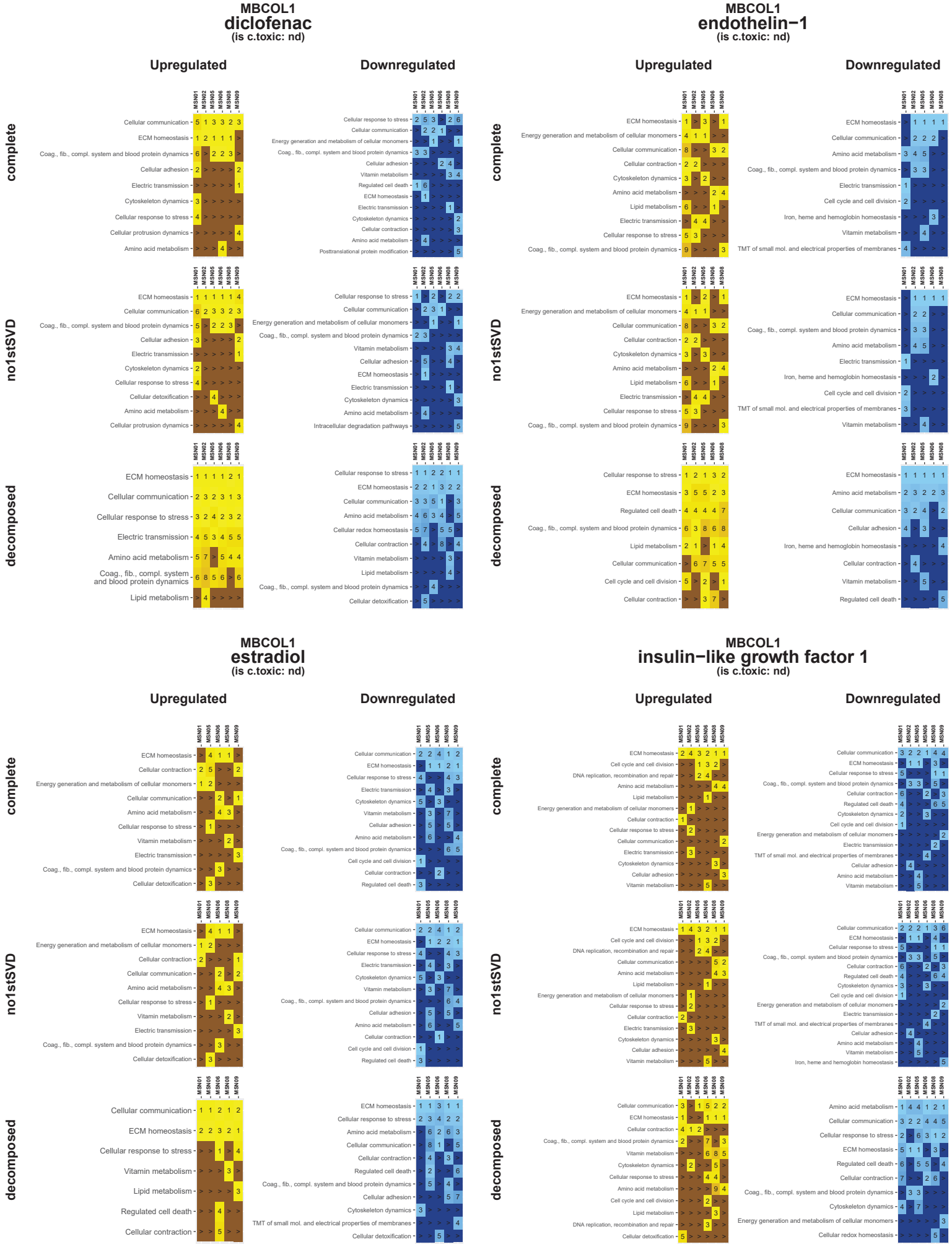

Supplementary Fig. 14B

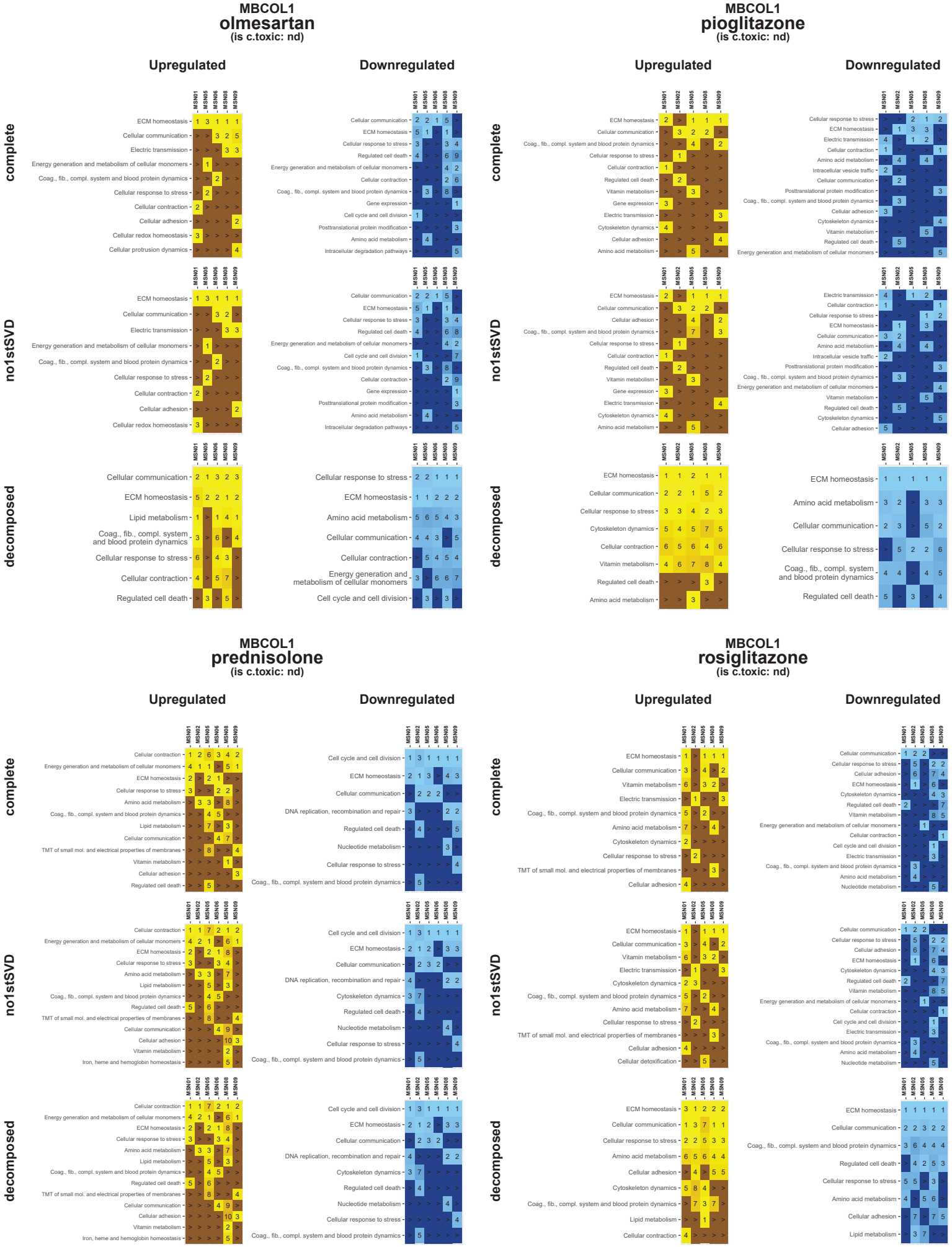

Supplementary Fig. 14B

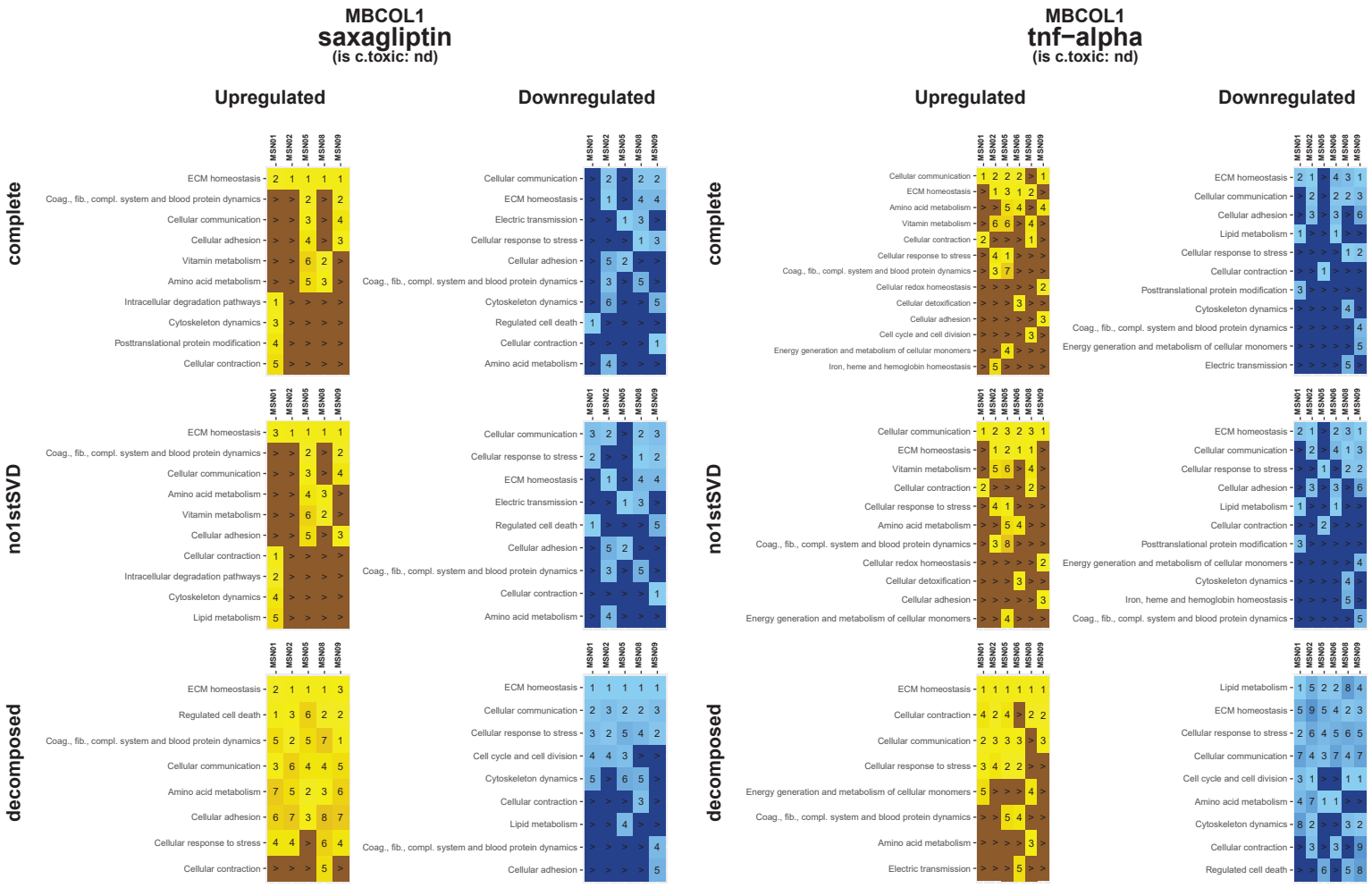

Supplementary Fig. 14B

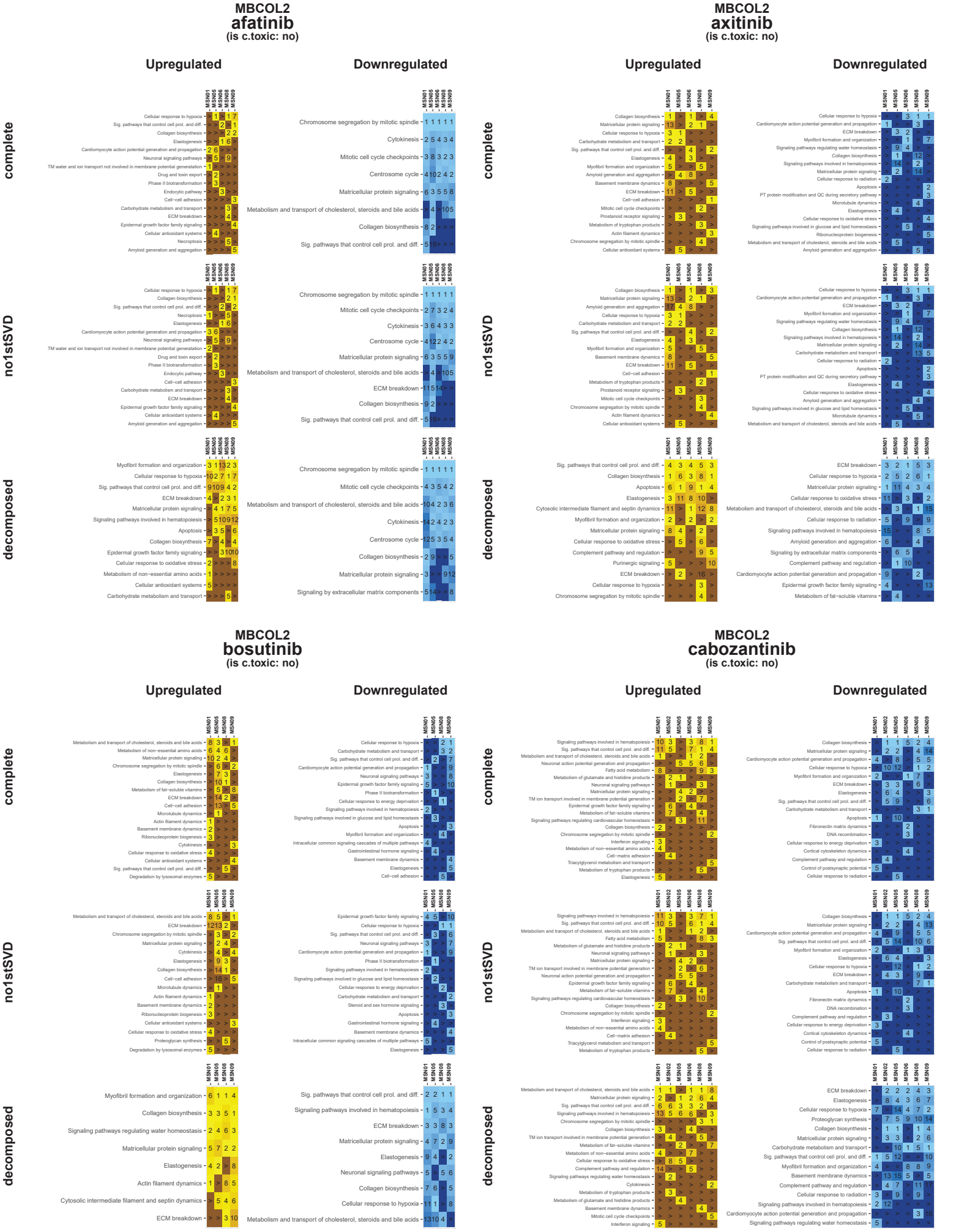

Supplementary Fig. 14C

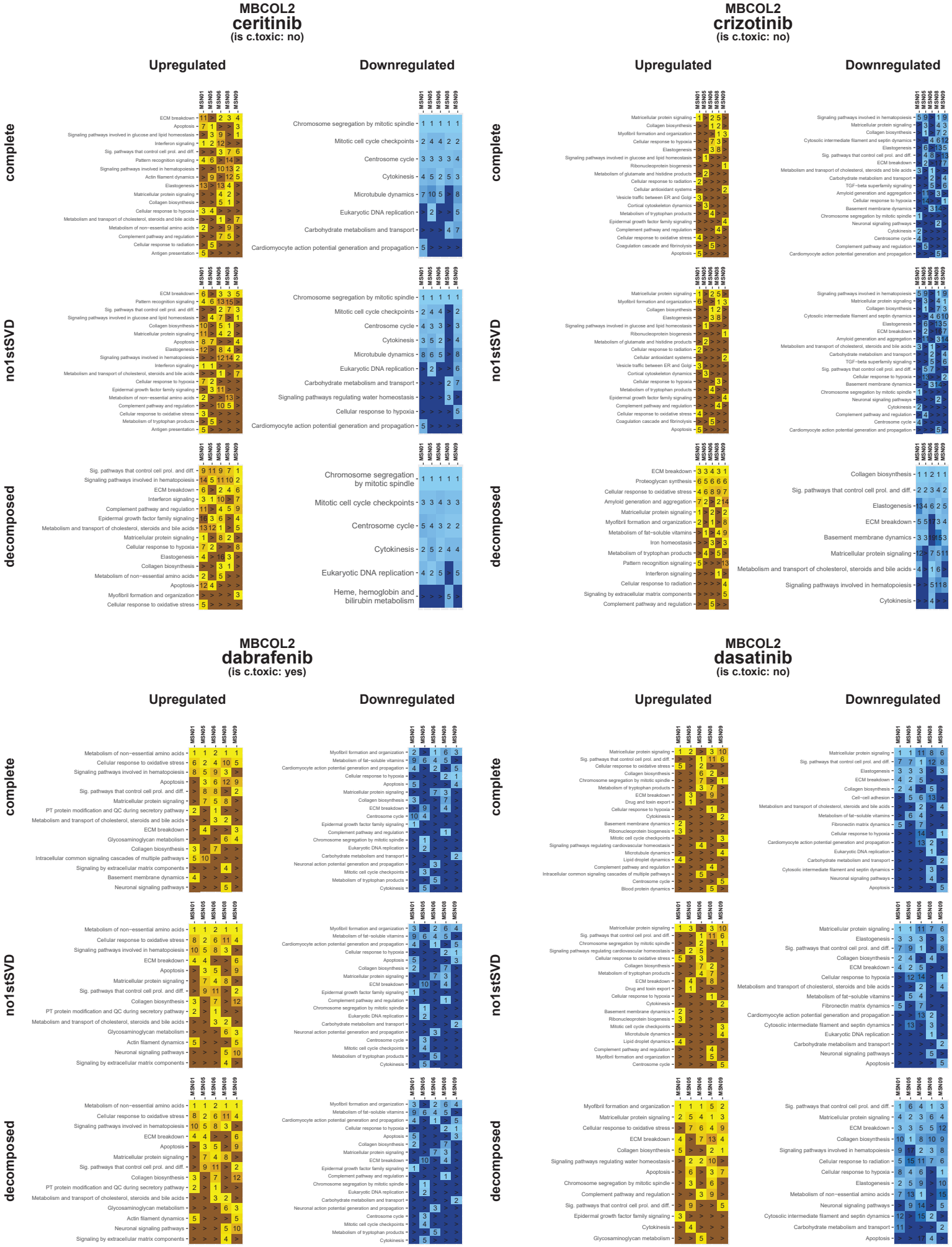

Supplementary Fig. 14C

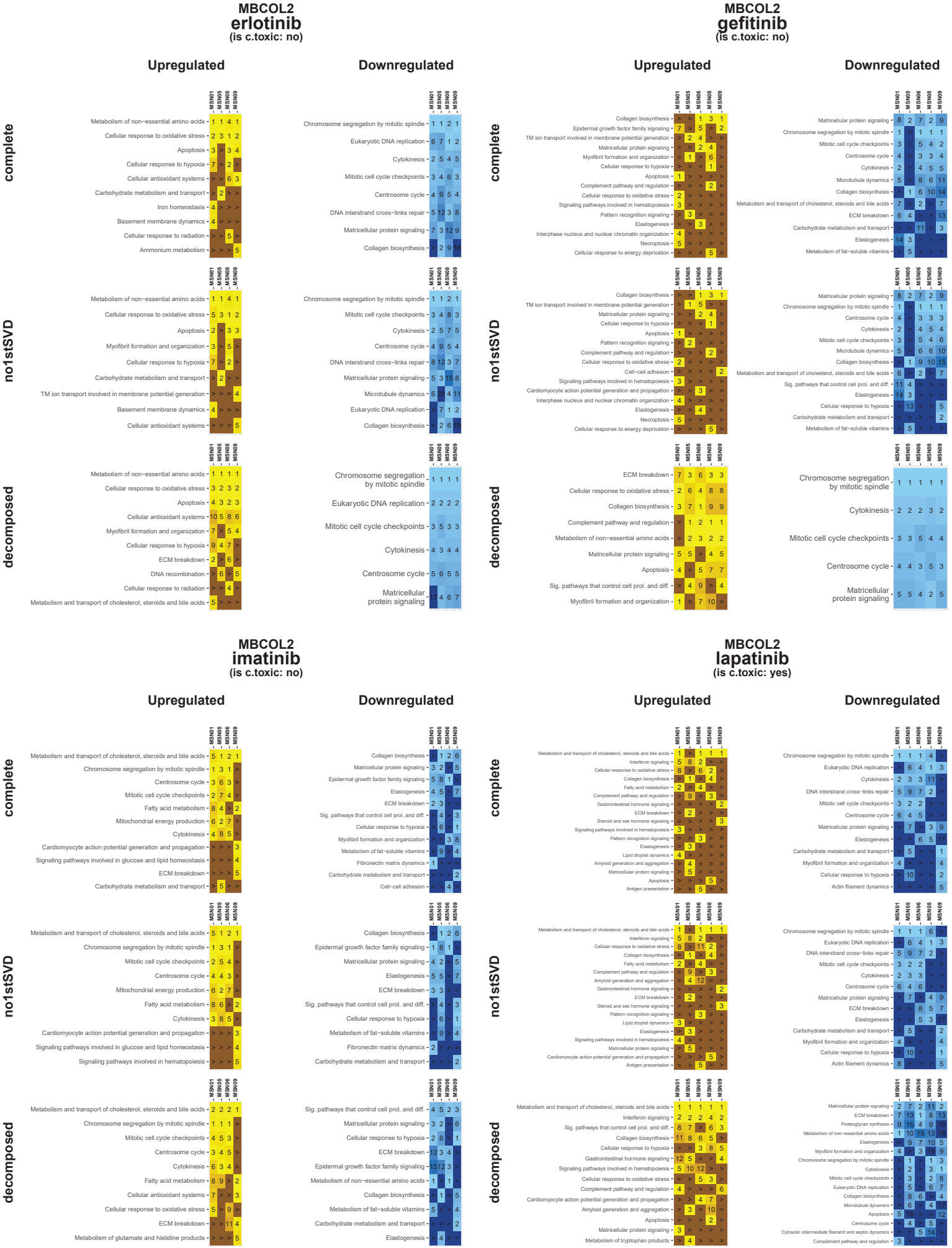

Supplementary Fig. 14C

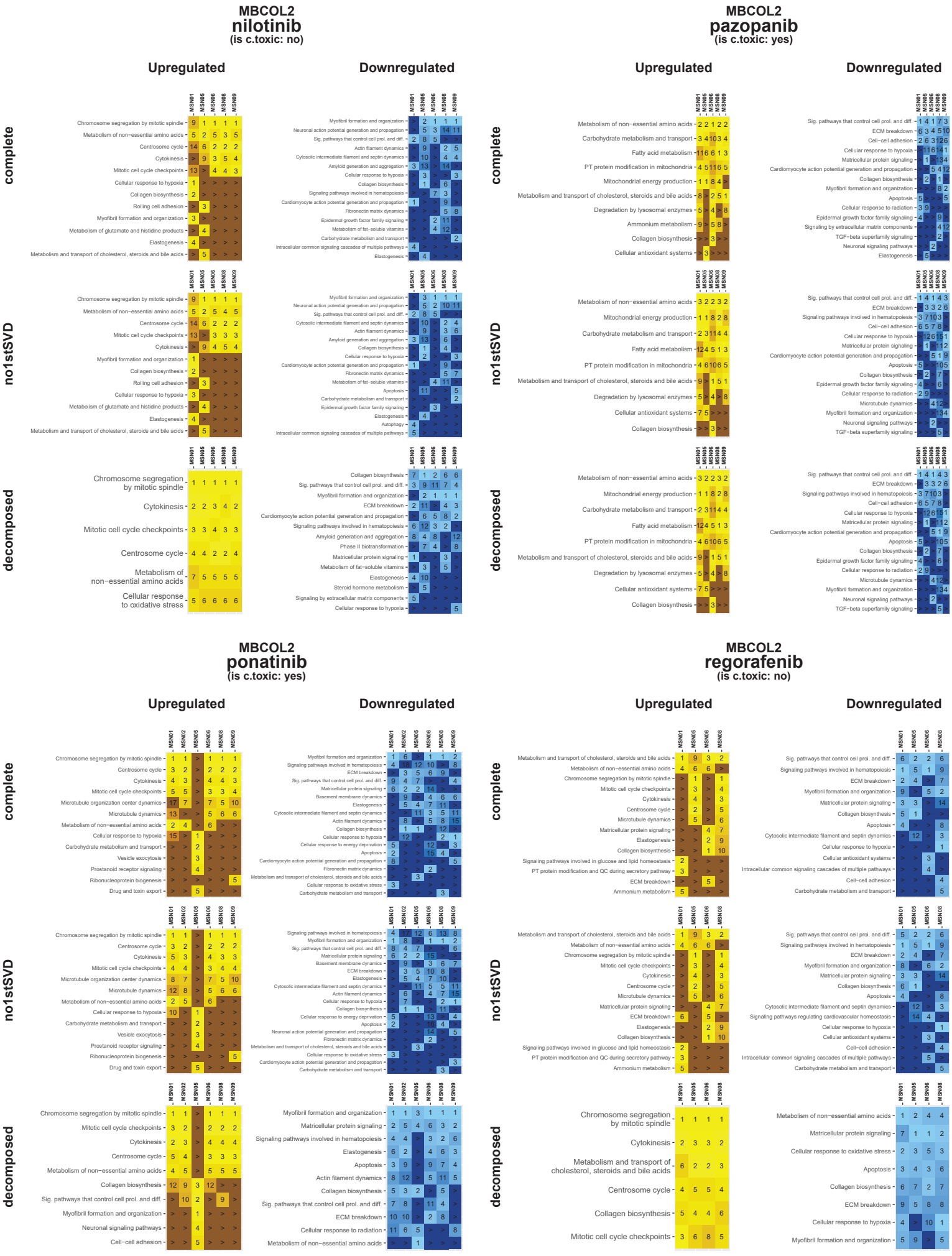

Supplementary Fig. 14C

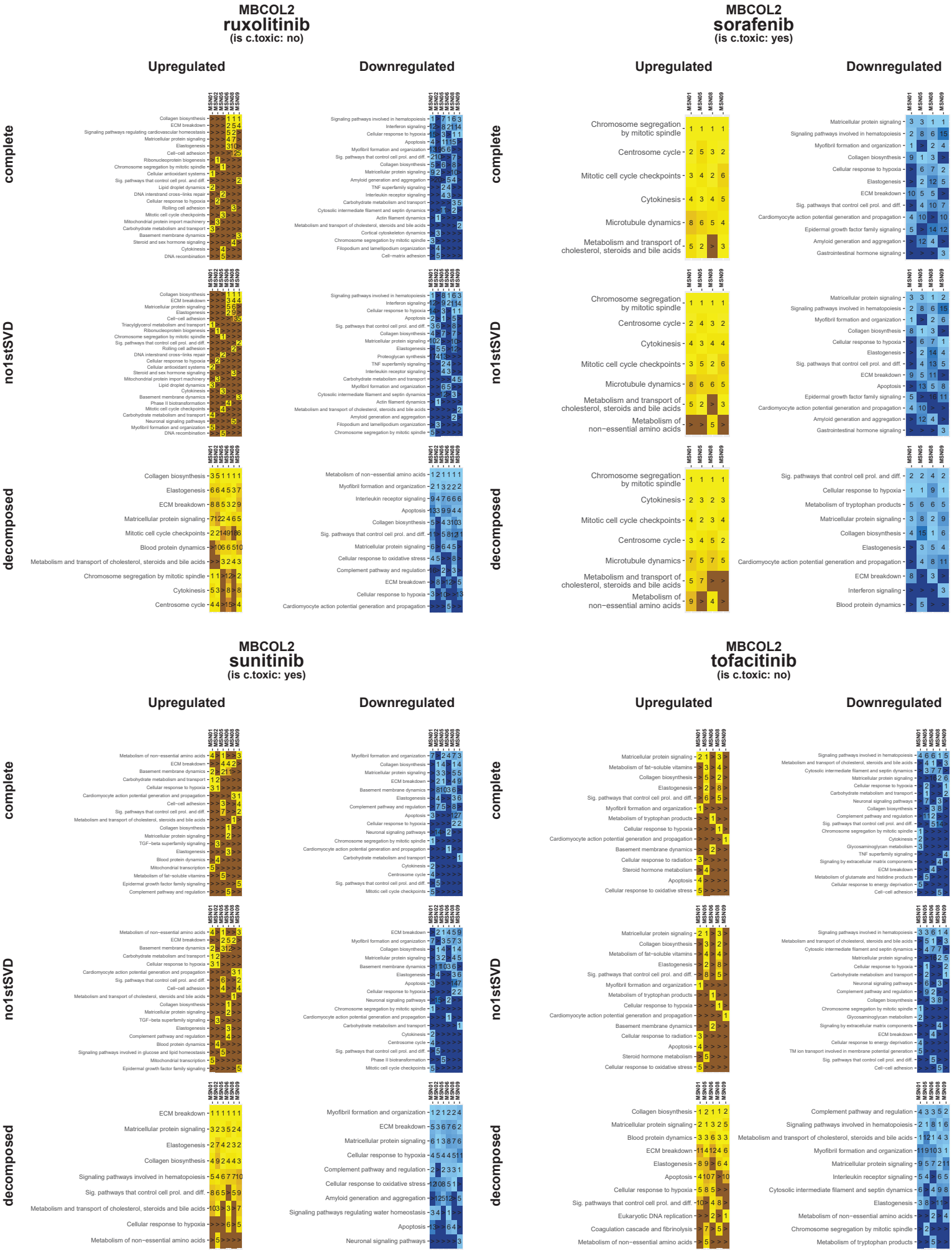

Supplementary Fig. 14C

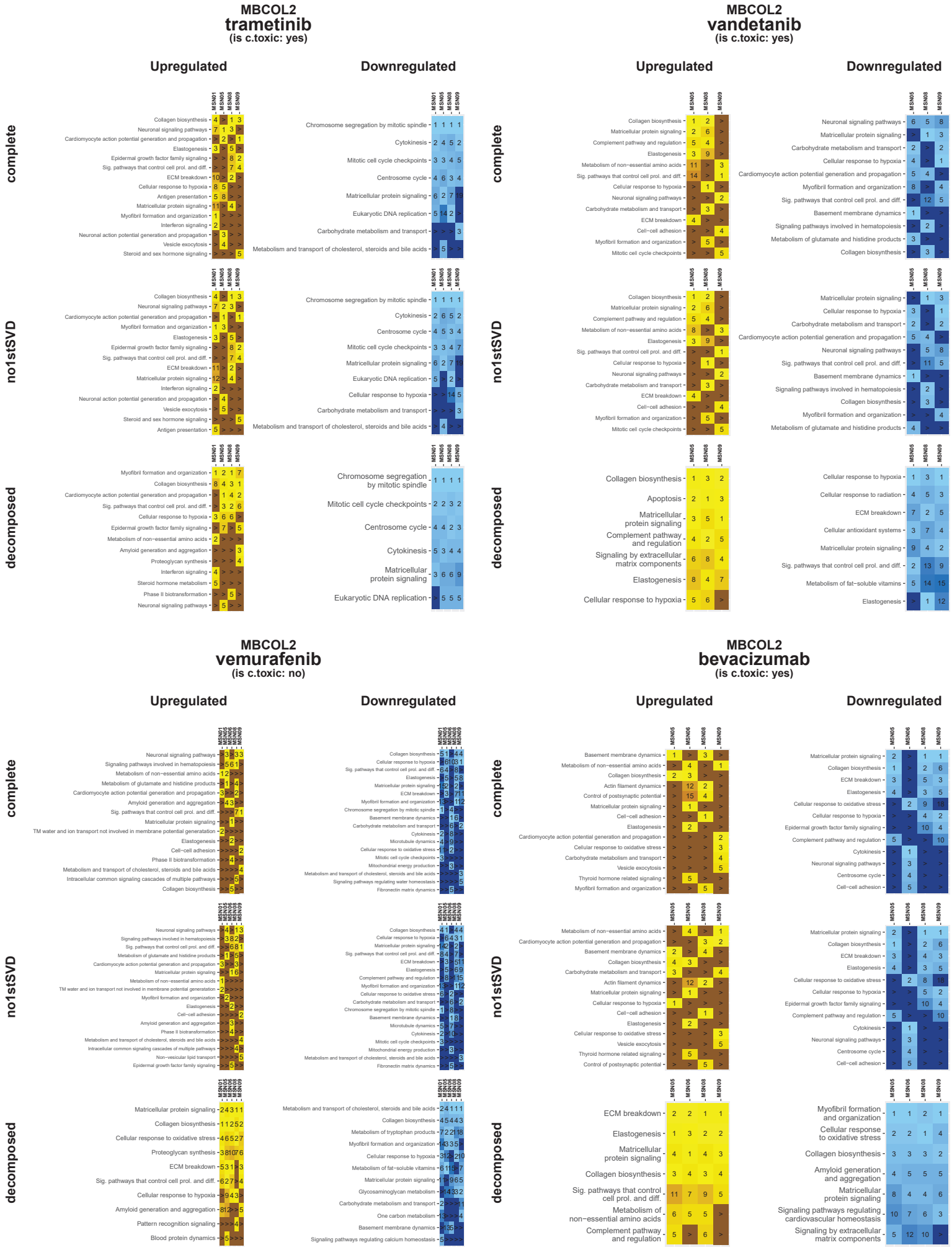

Supplementary Fig. 14C

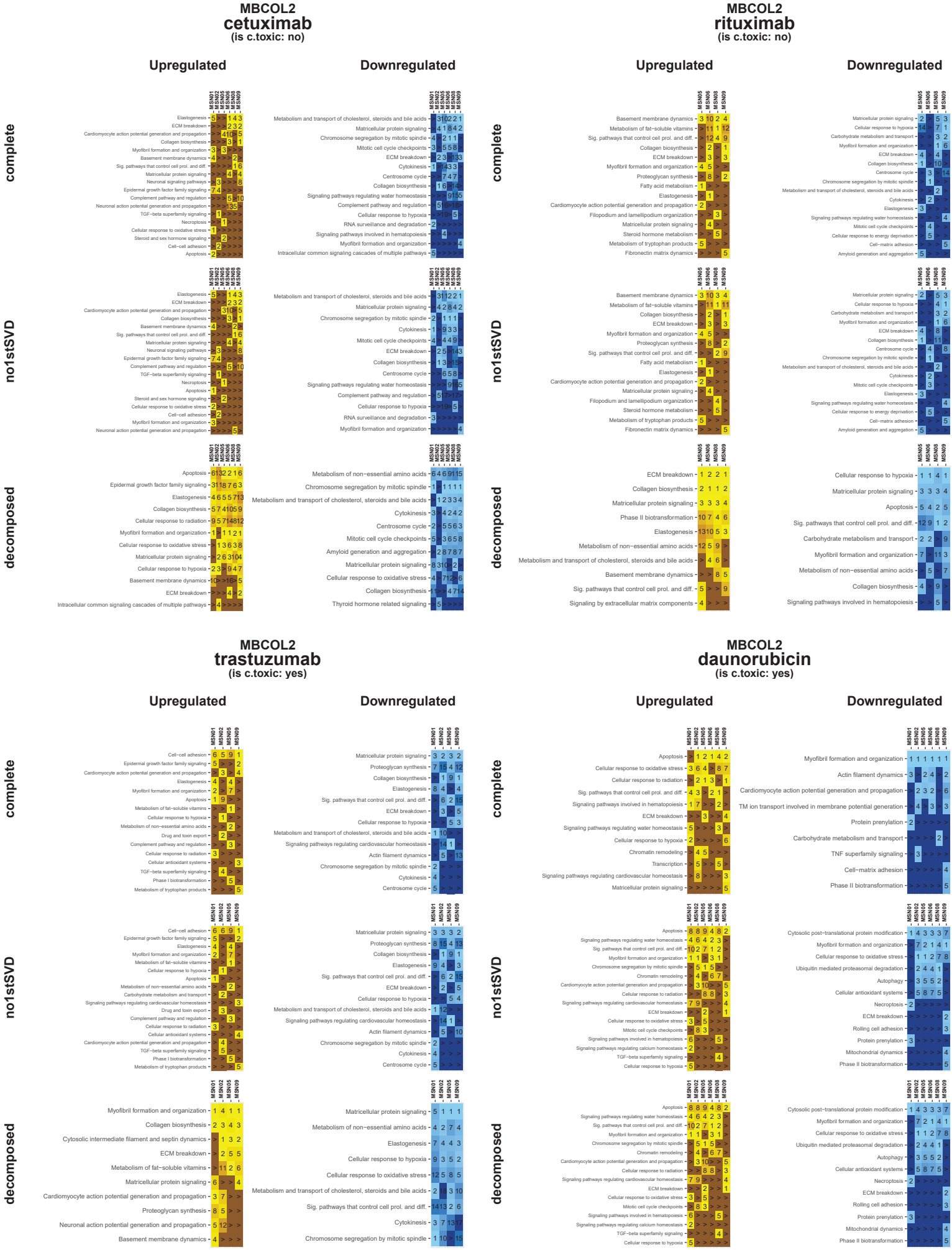

Supplementary Fig. 14C

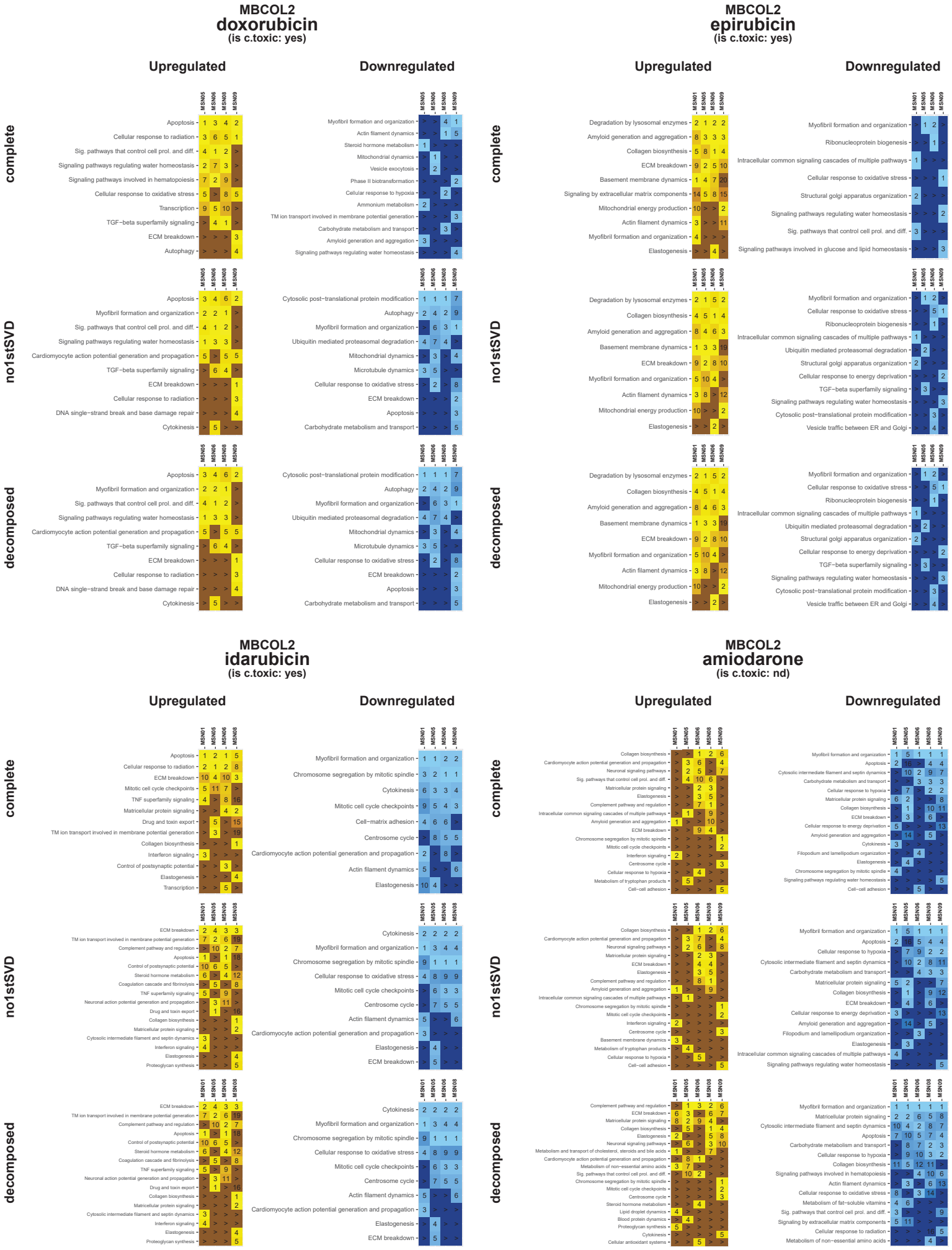

Supplementary Fig. 14C

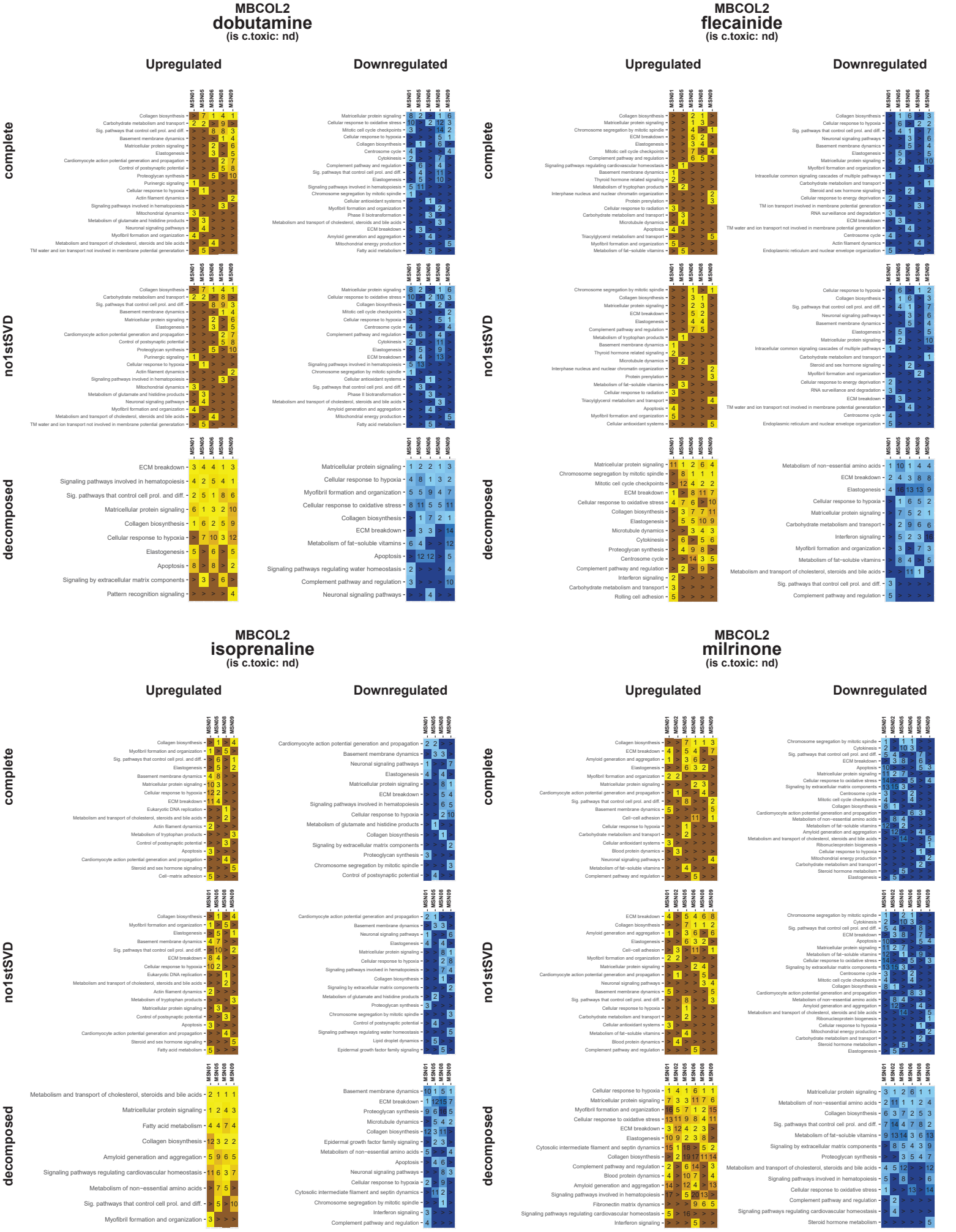

Supplementary Fig. 14C

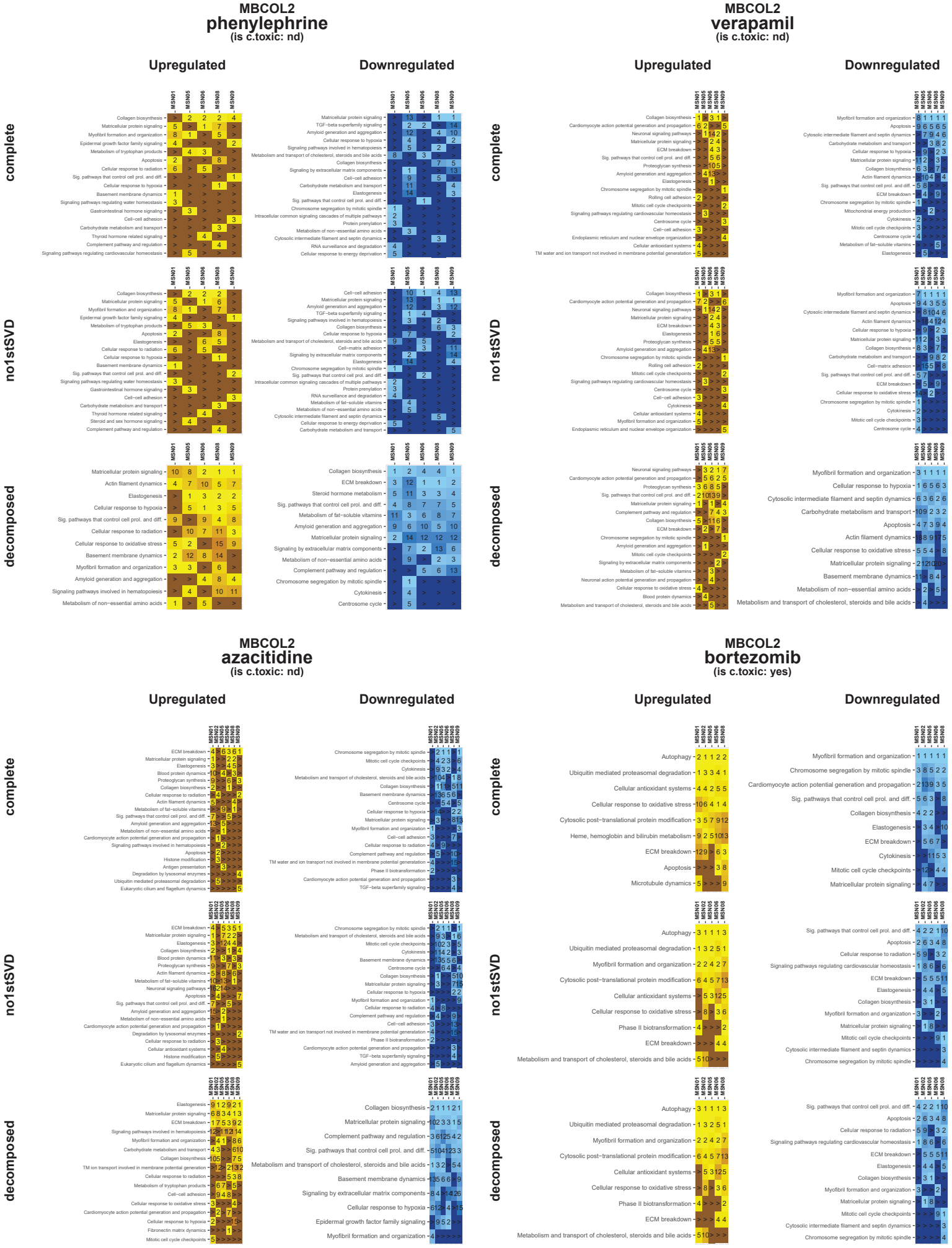

Supplementary Fig. 14C

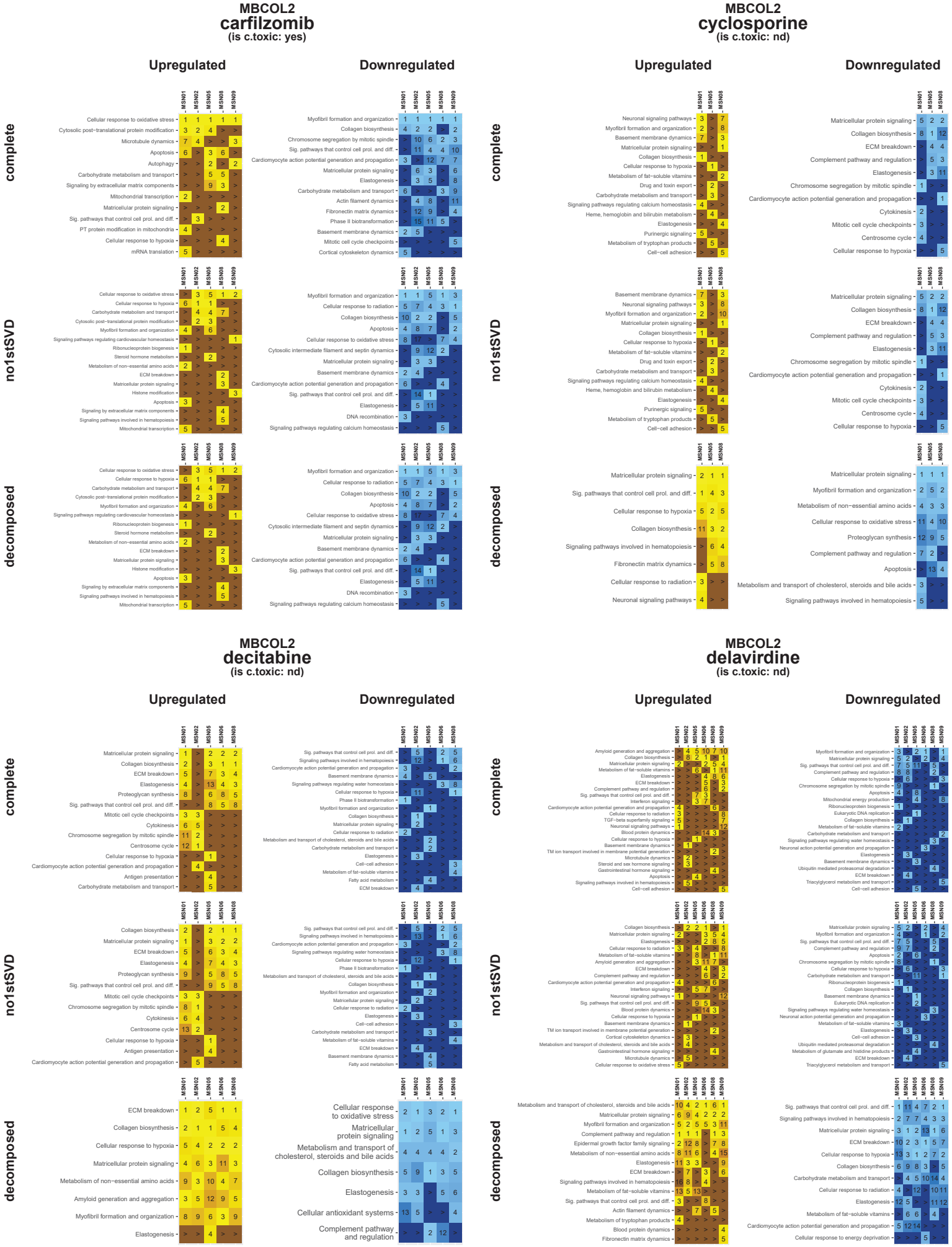

Supplementary Fig. 14C

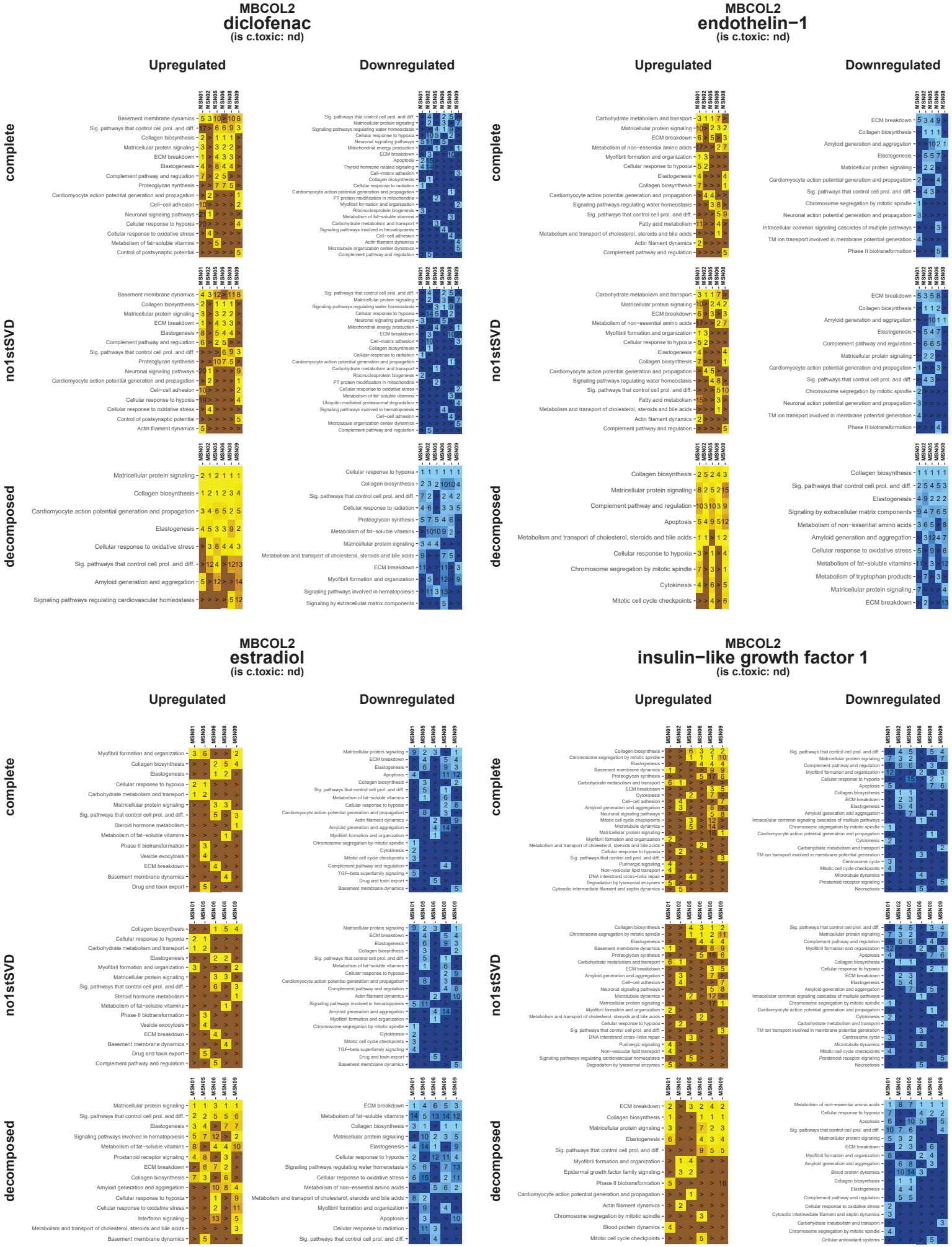

Supplementary Fig. 14C

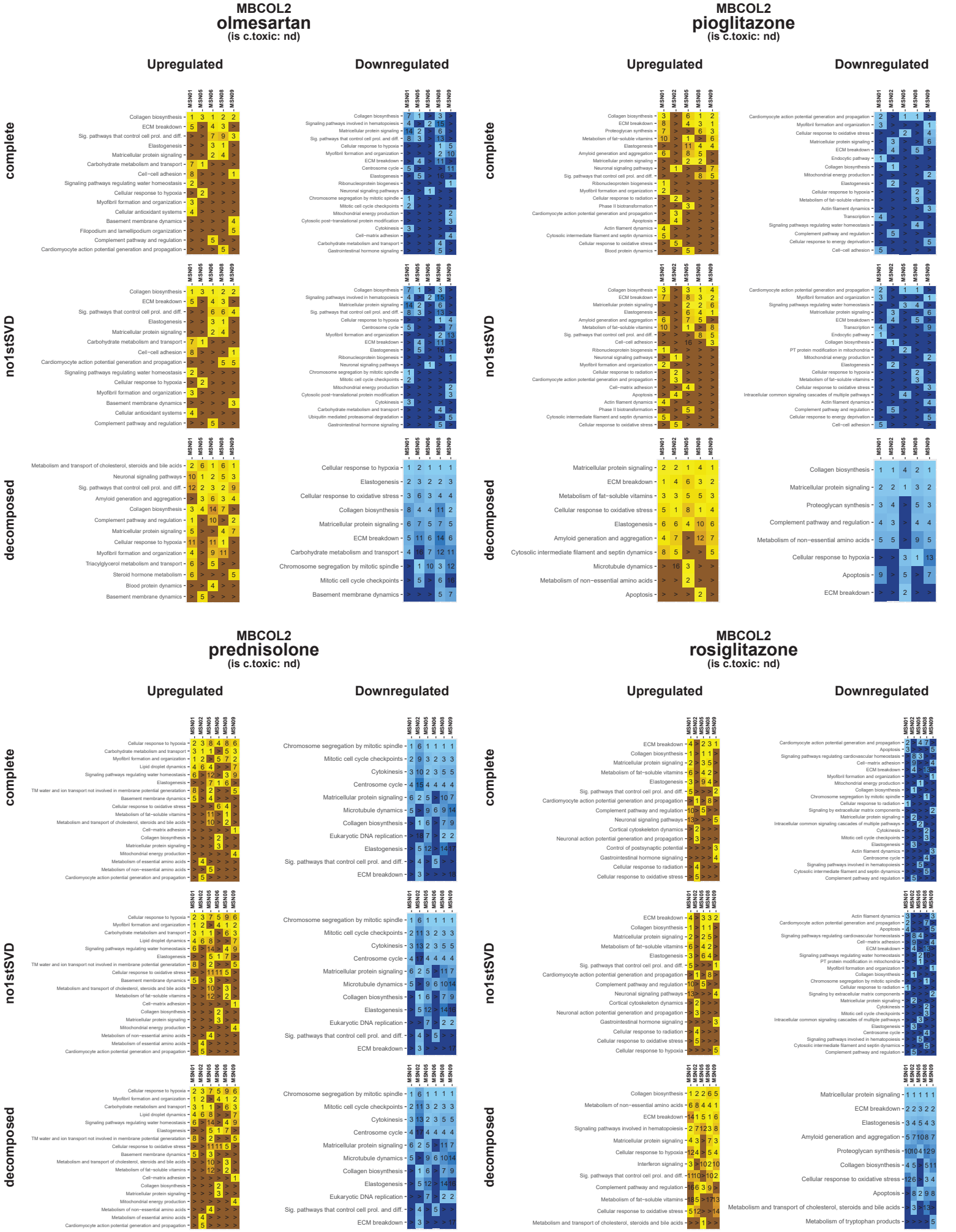

Supplementary Fig. 14C

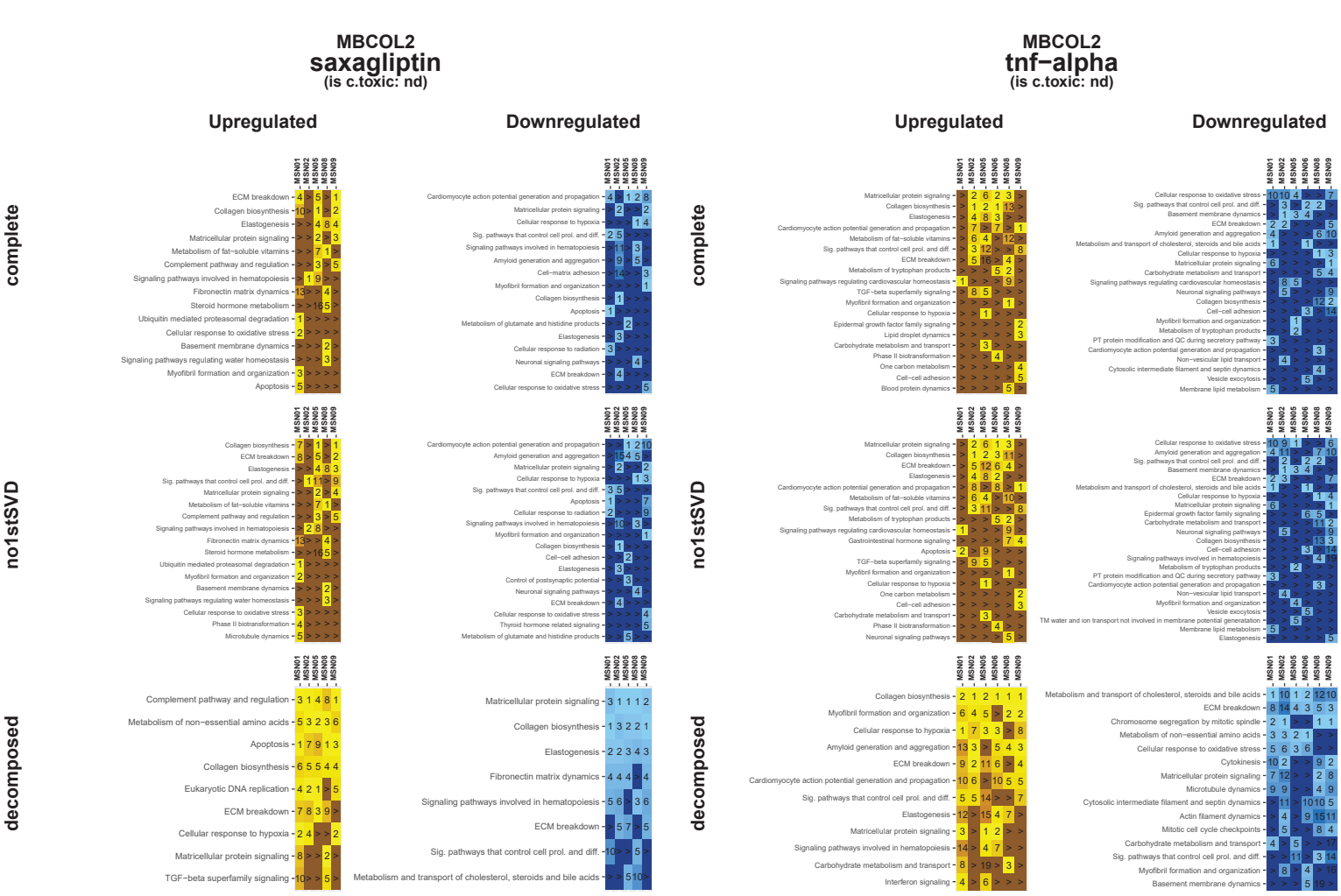

Supplementary Fig. 14C

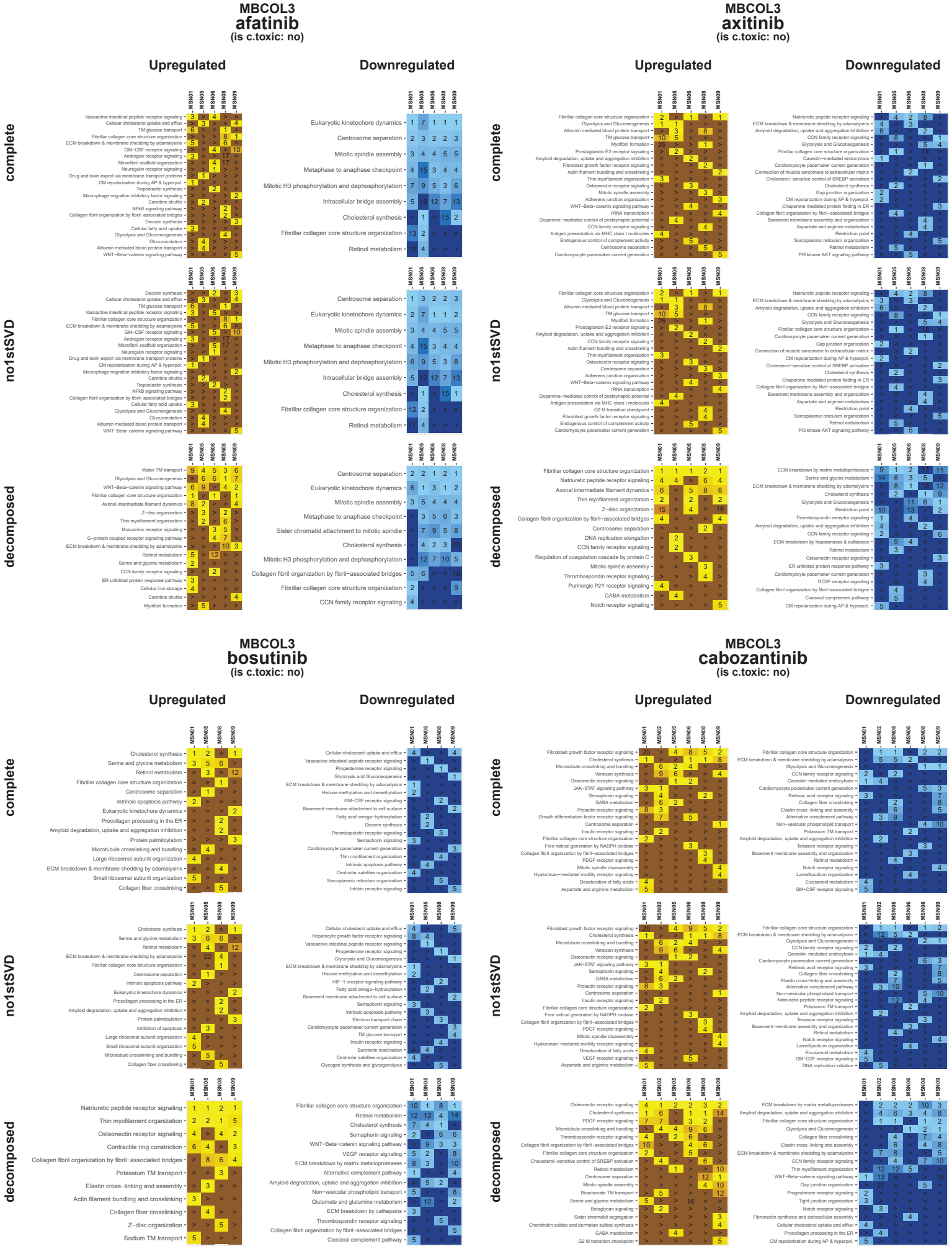

Supplementary Fig. 14D

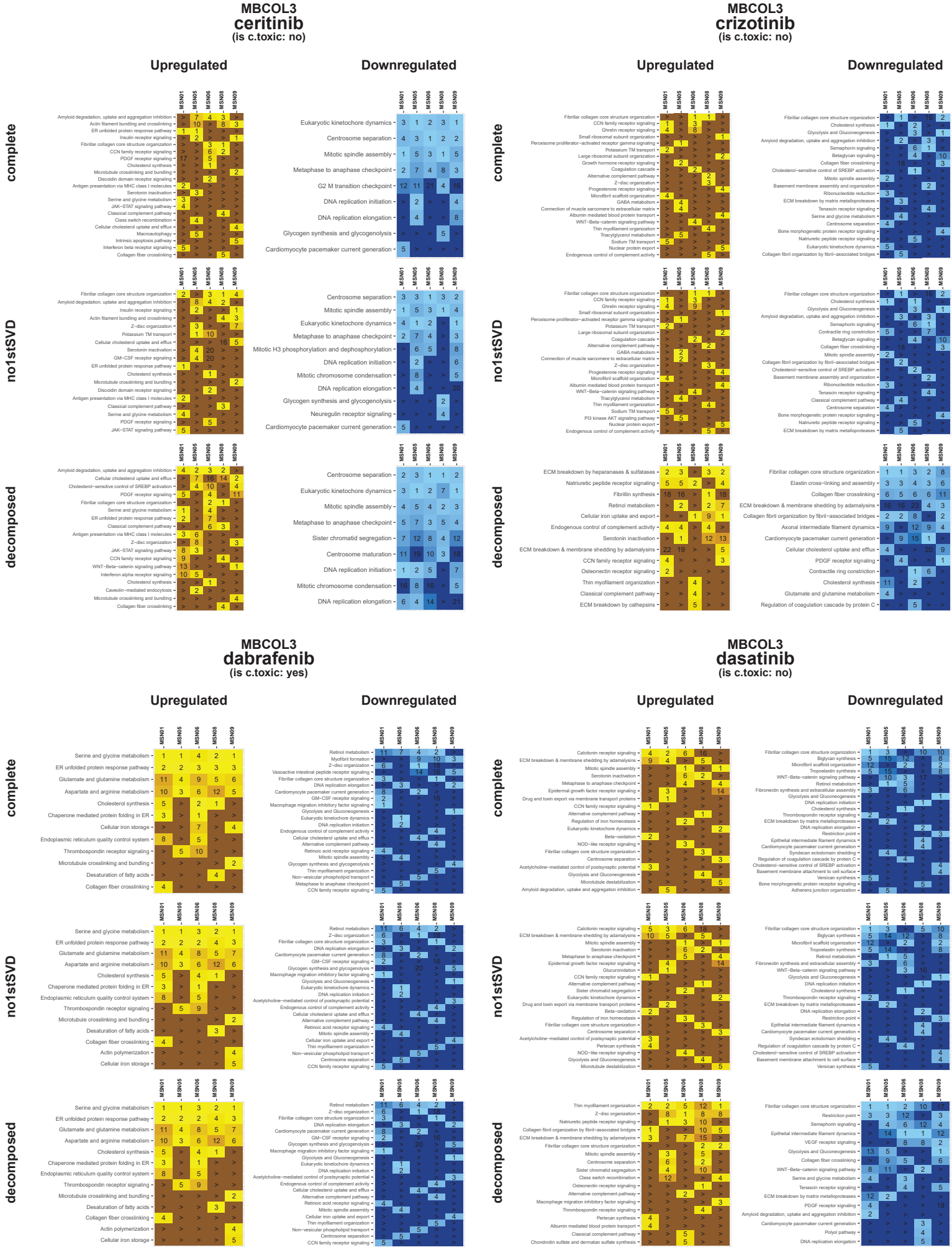

Supplementary Fig. 14D

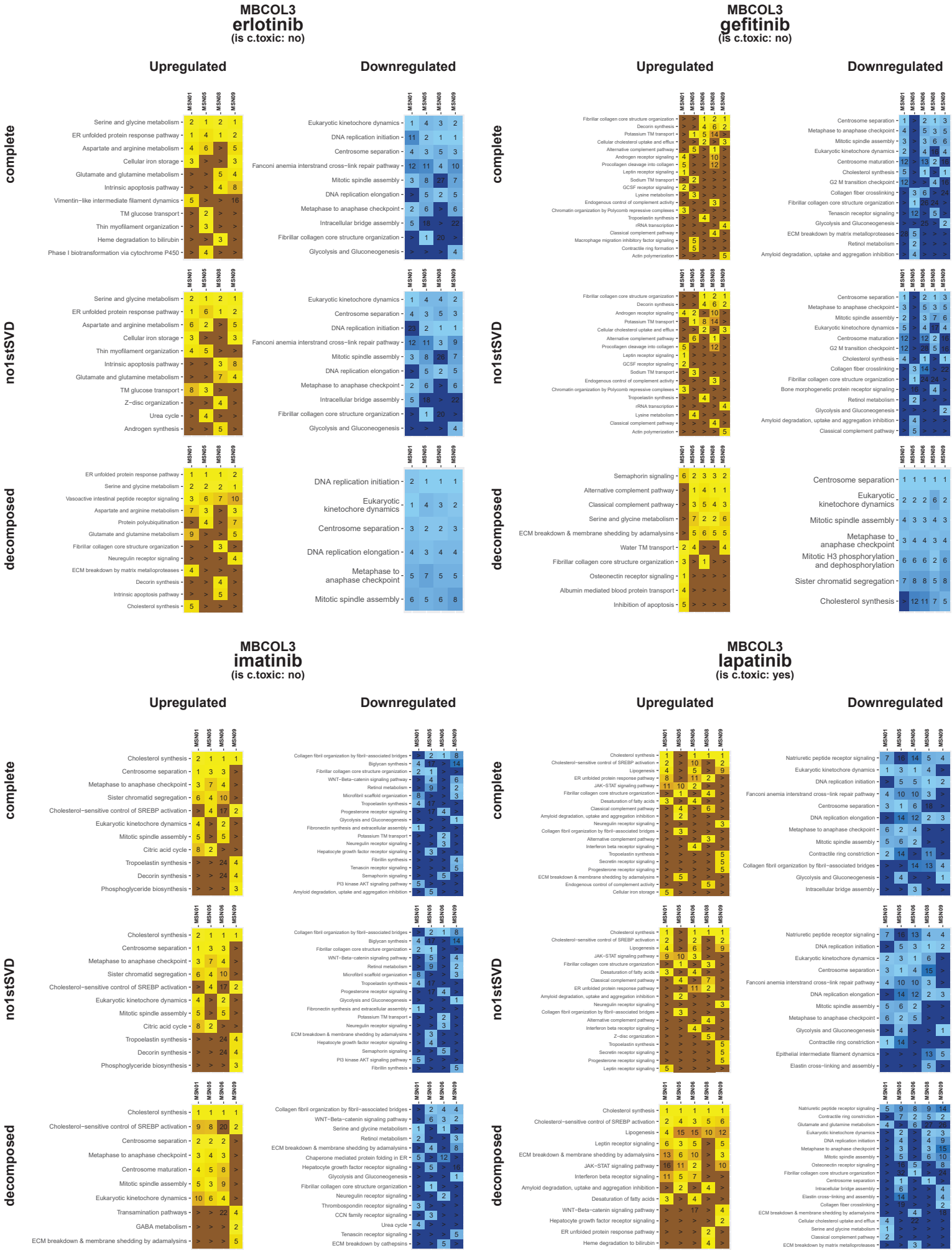

Supplementary Fig. 14D

MBCOL3
nilotinib
(is c.toxic: no)

MBCOL3
pazopanib
(is c.toxic: yes)

MBCOL3
ponatinib
(is c.toxic: yes)

MBCOL3
regorafenib
(is c.toxic: no)

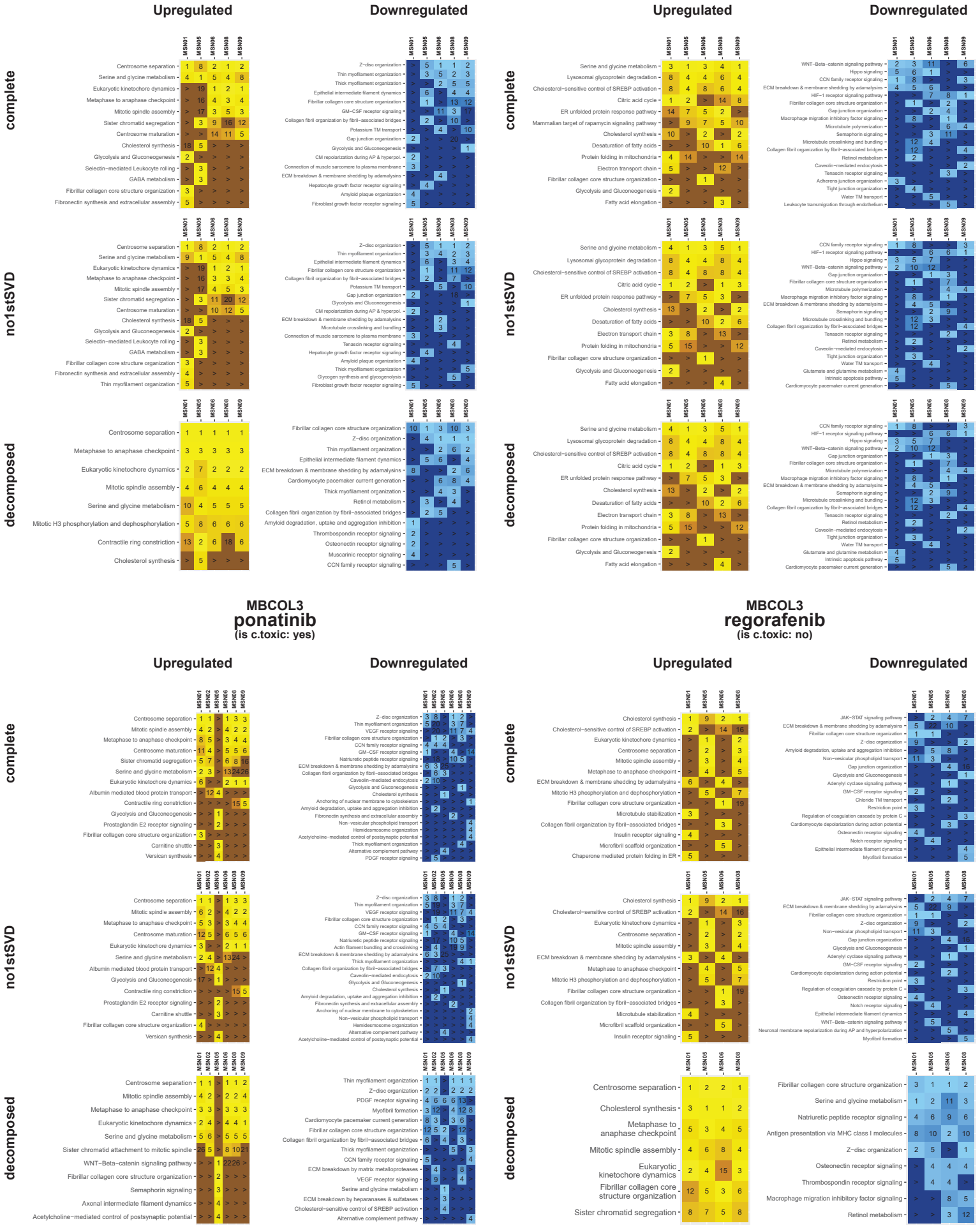

Supplementary Fig. 14D

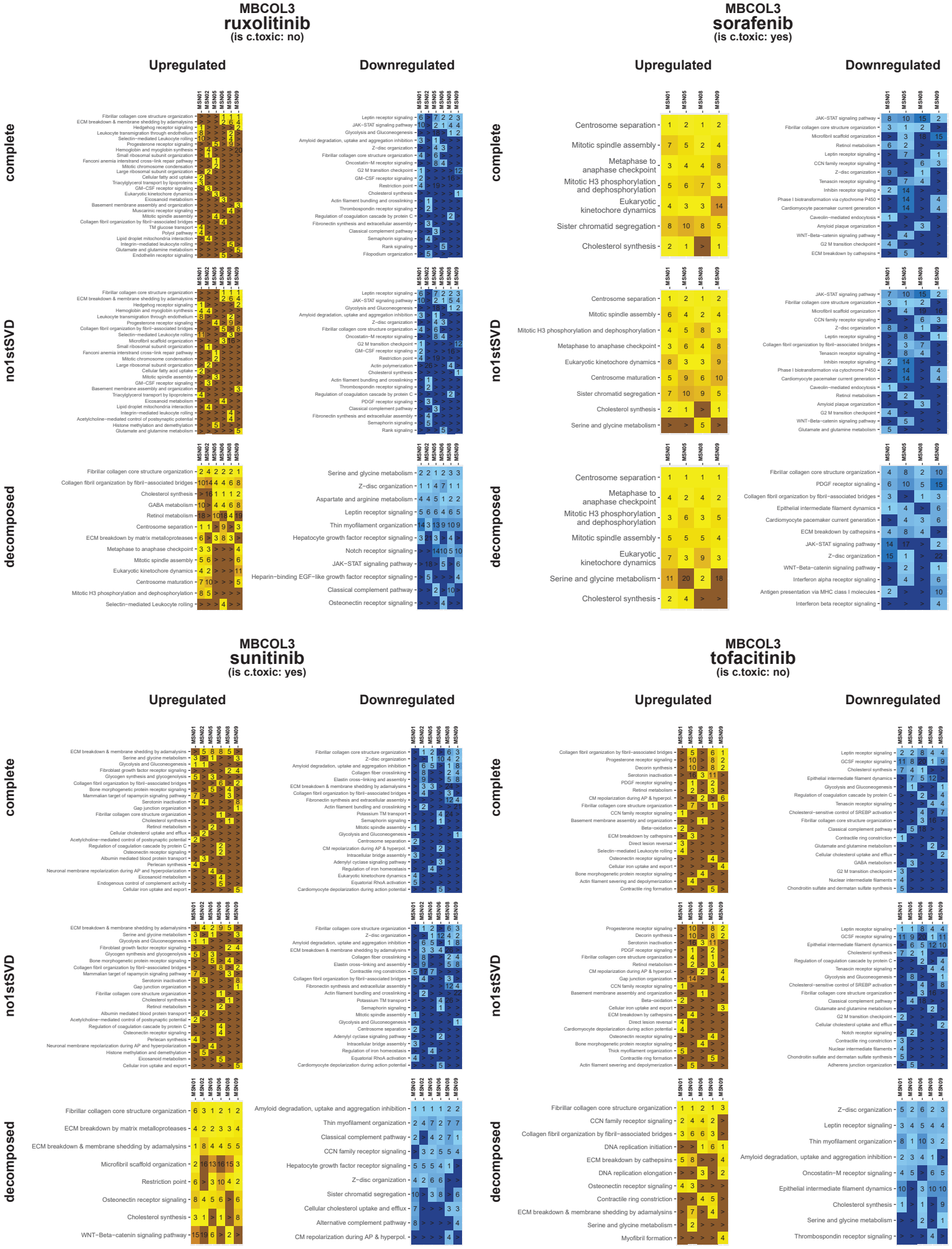

Supplementary Fig. 14D

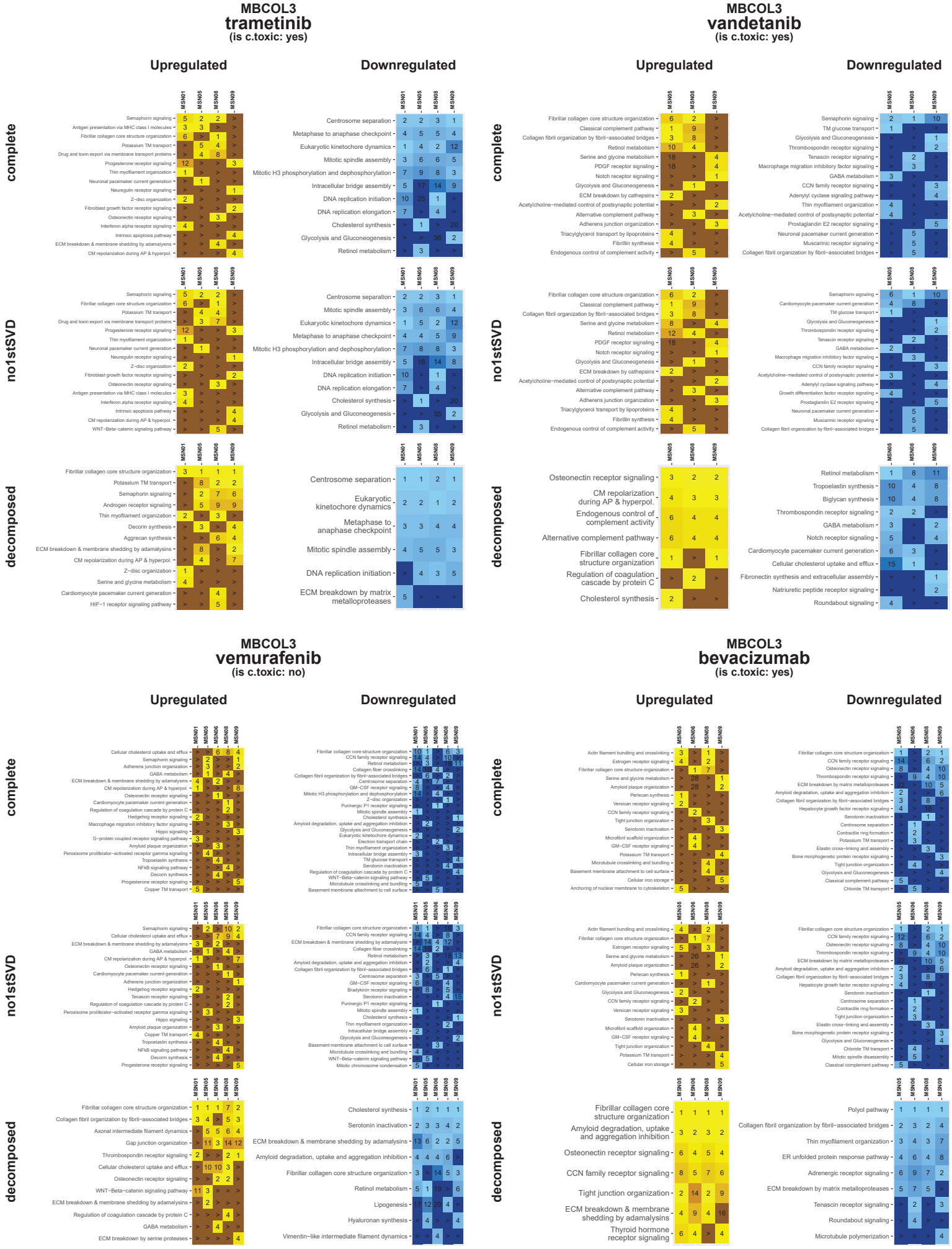

Supplementary Fig. 14D

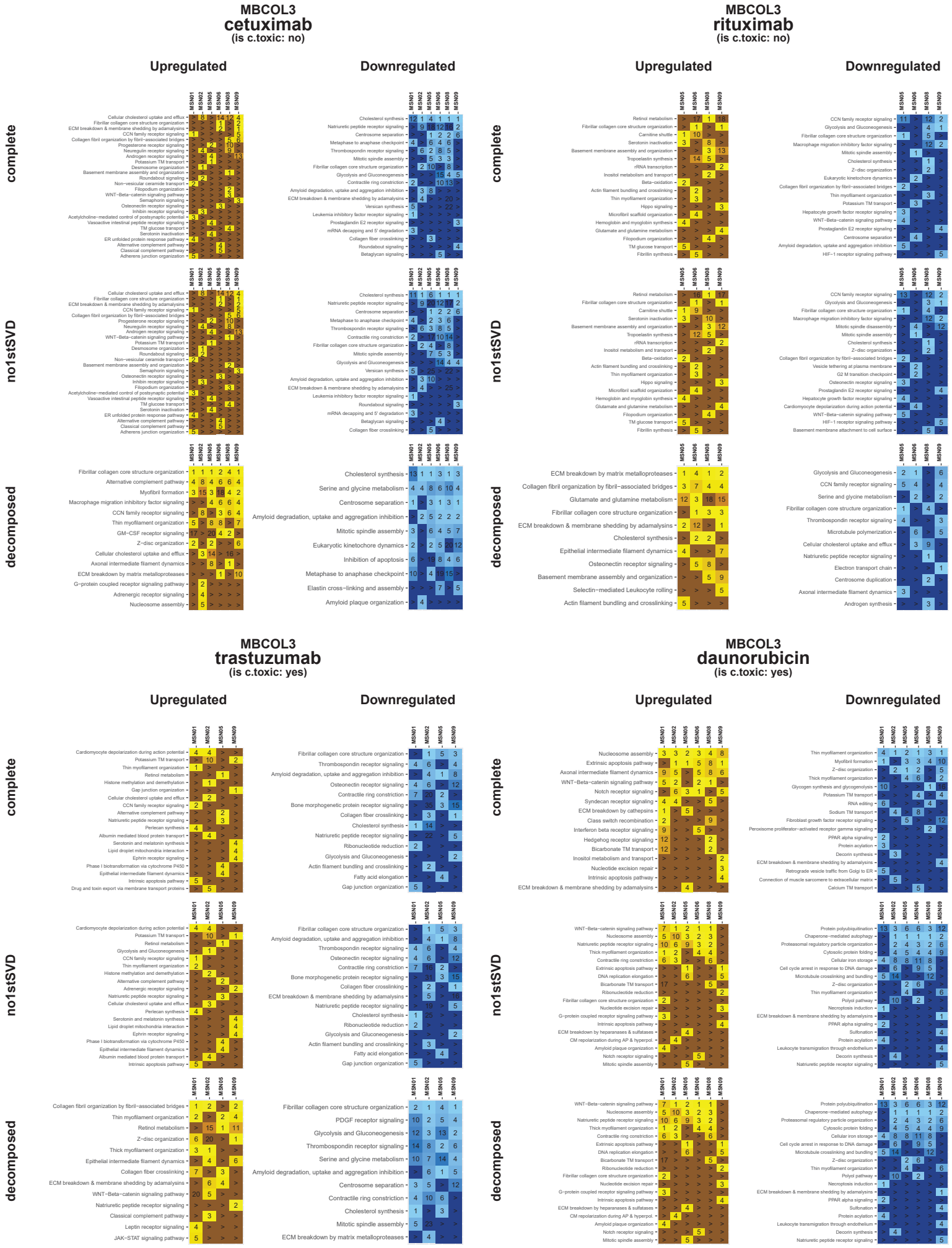

Supplementary Fig. 14D

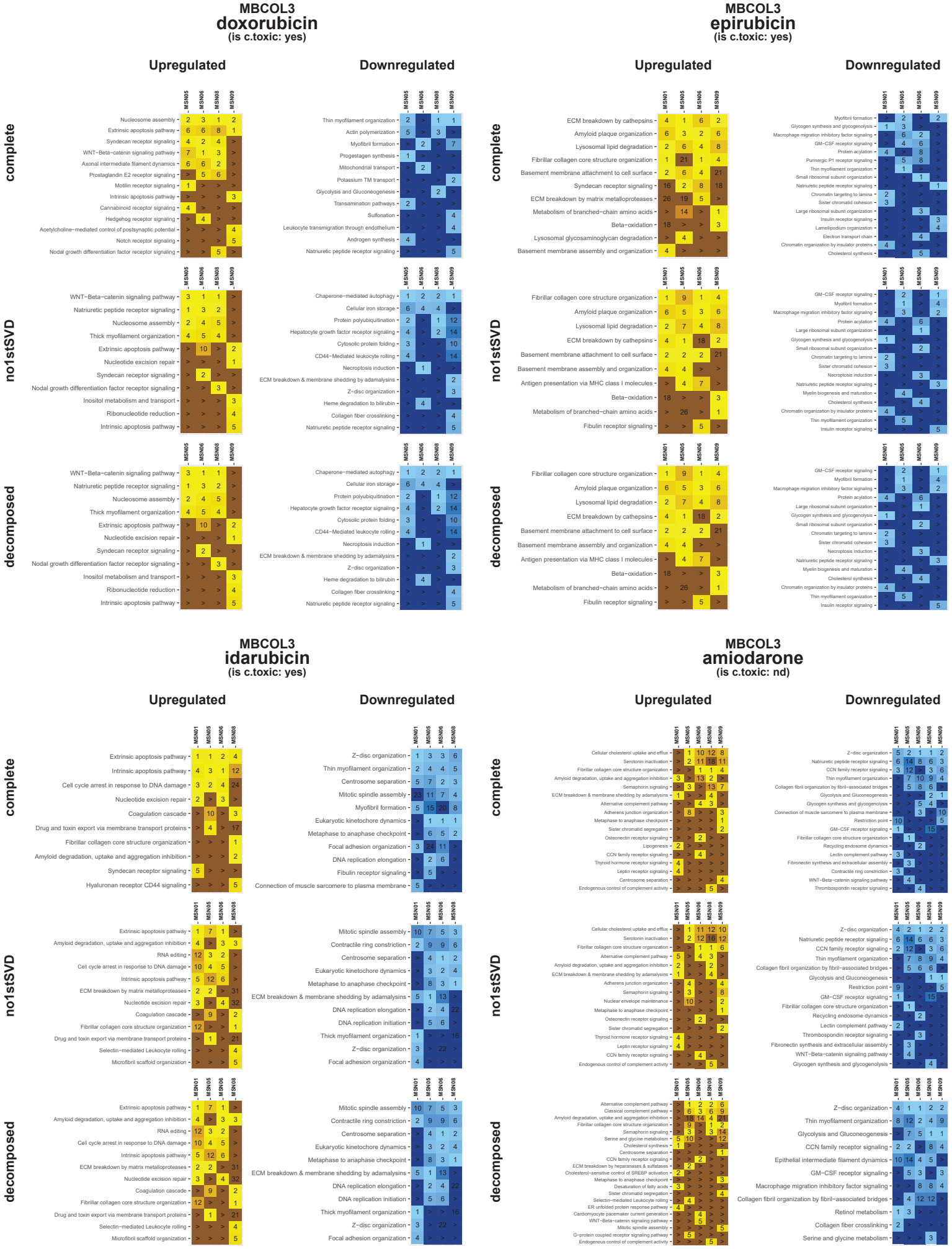

Supplementary Fig. 14D

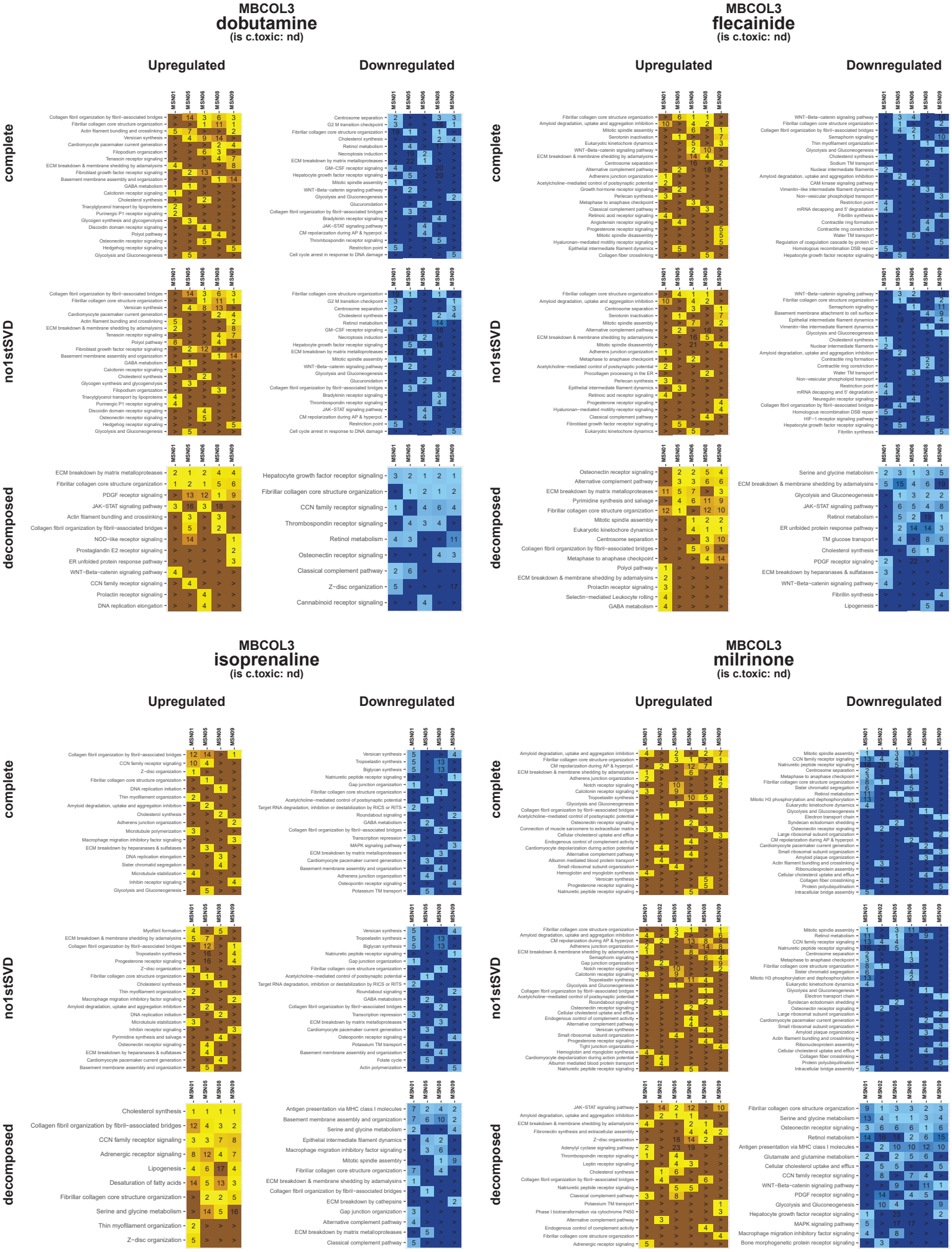

Supplementary Fig. 14D

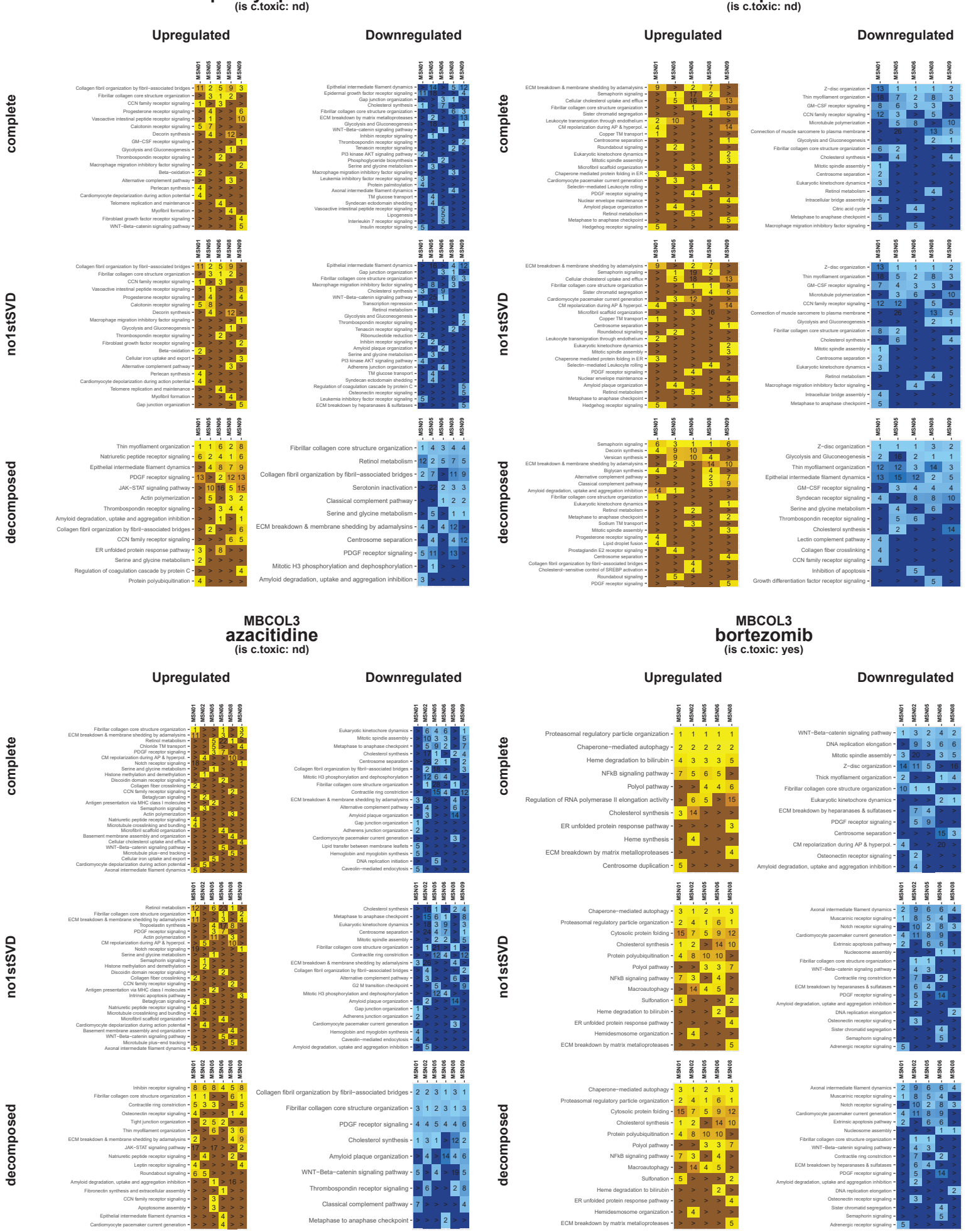

Supplementary Fig. 14D

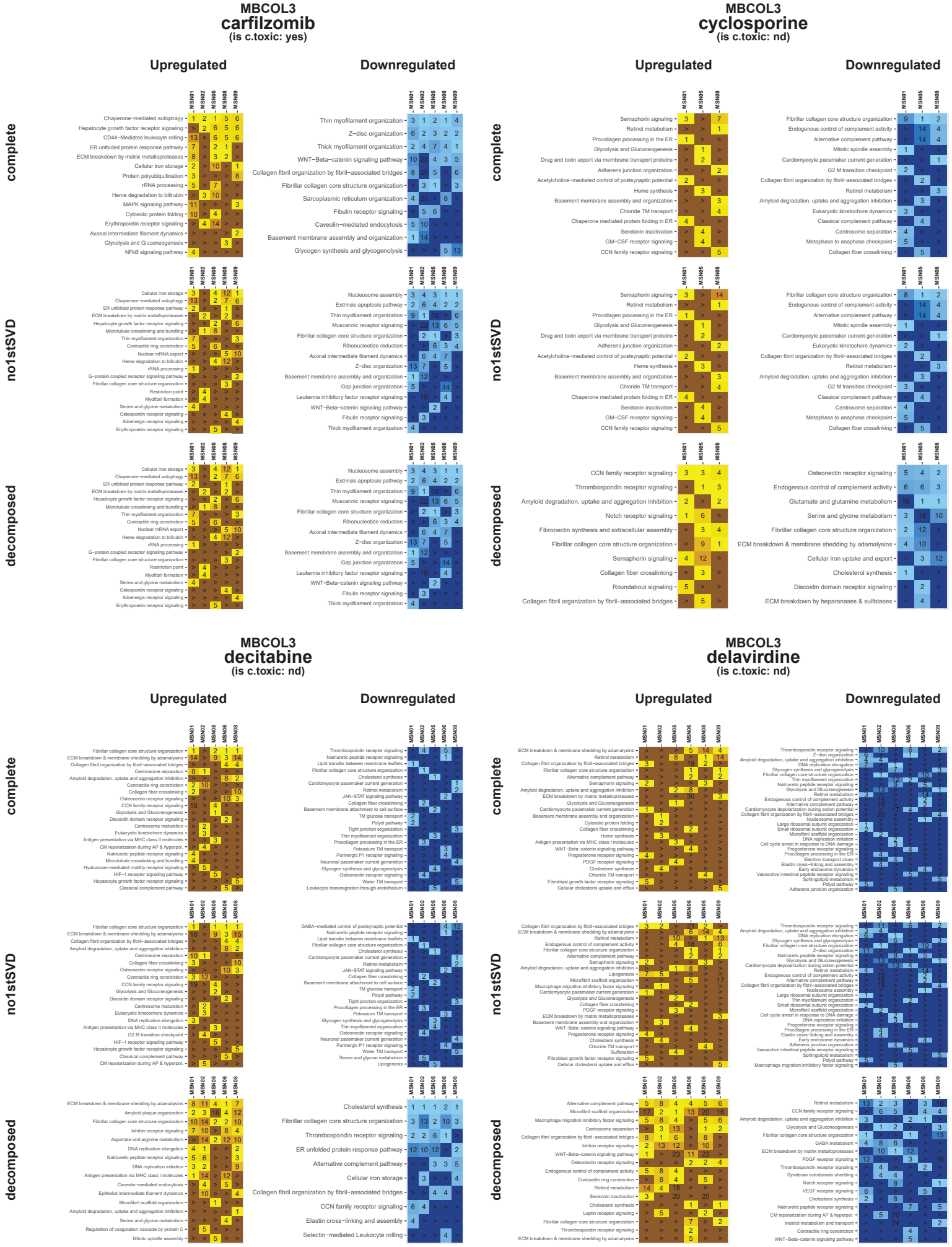

Supplementary Fig. 14D

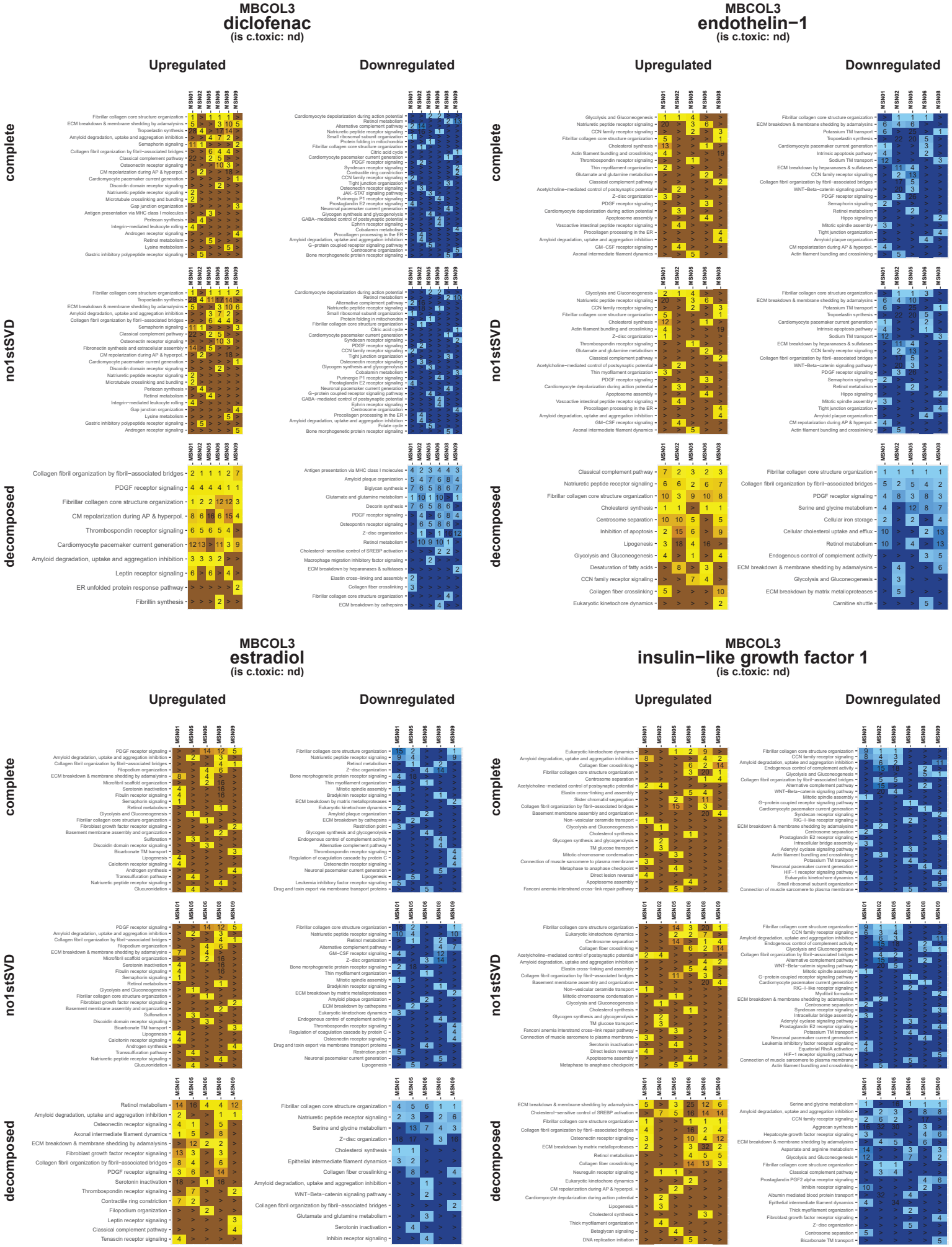

Supplementary Fig. 14D

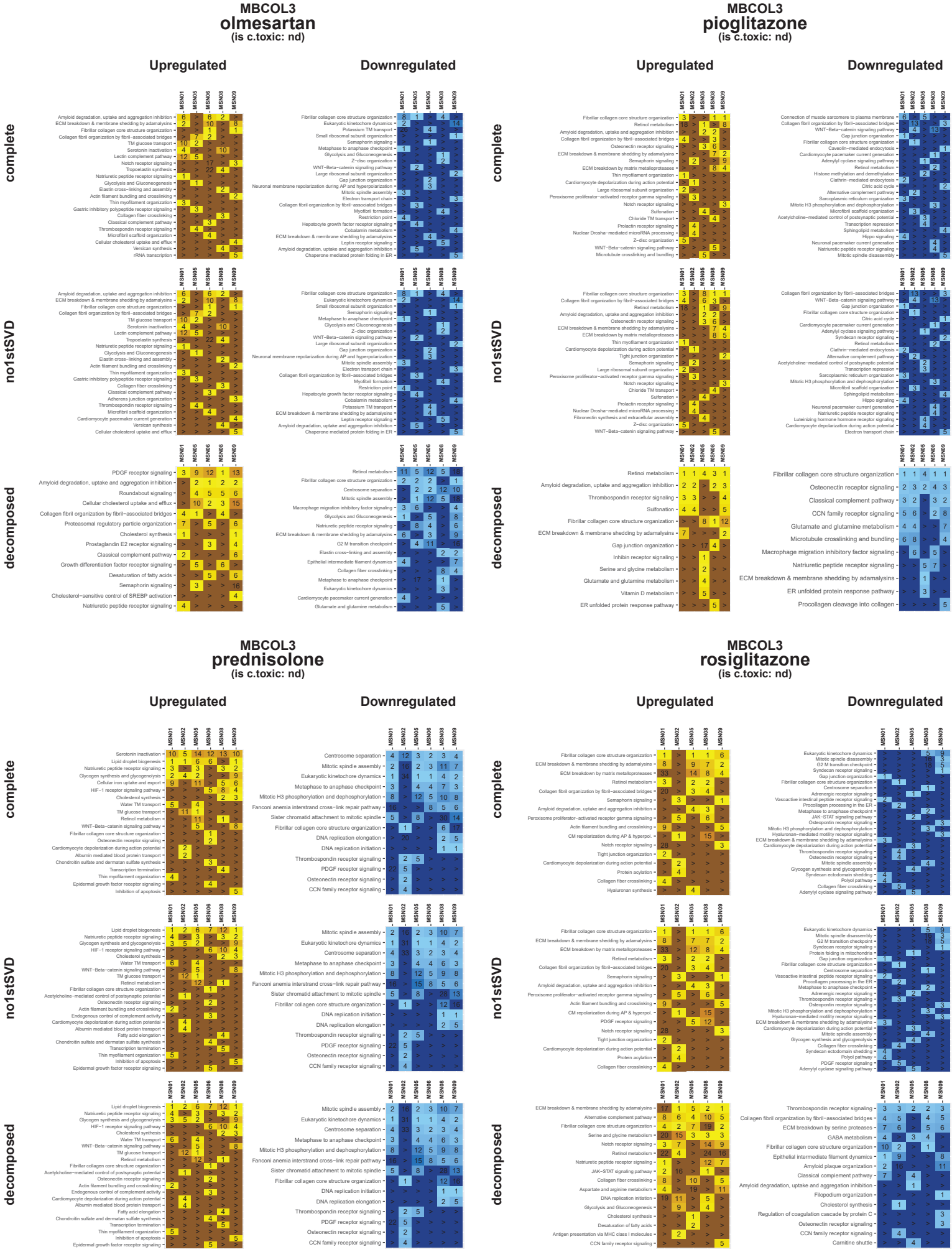

Supplementary Fig. 14D

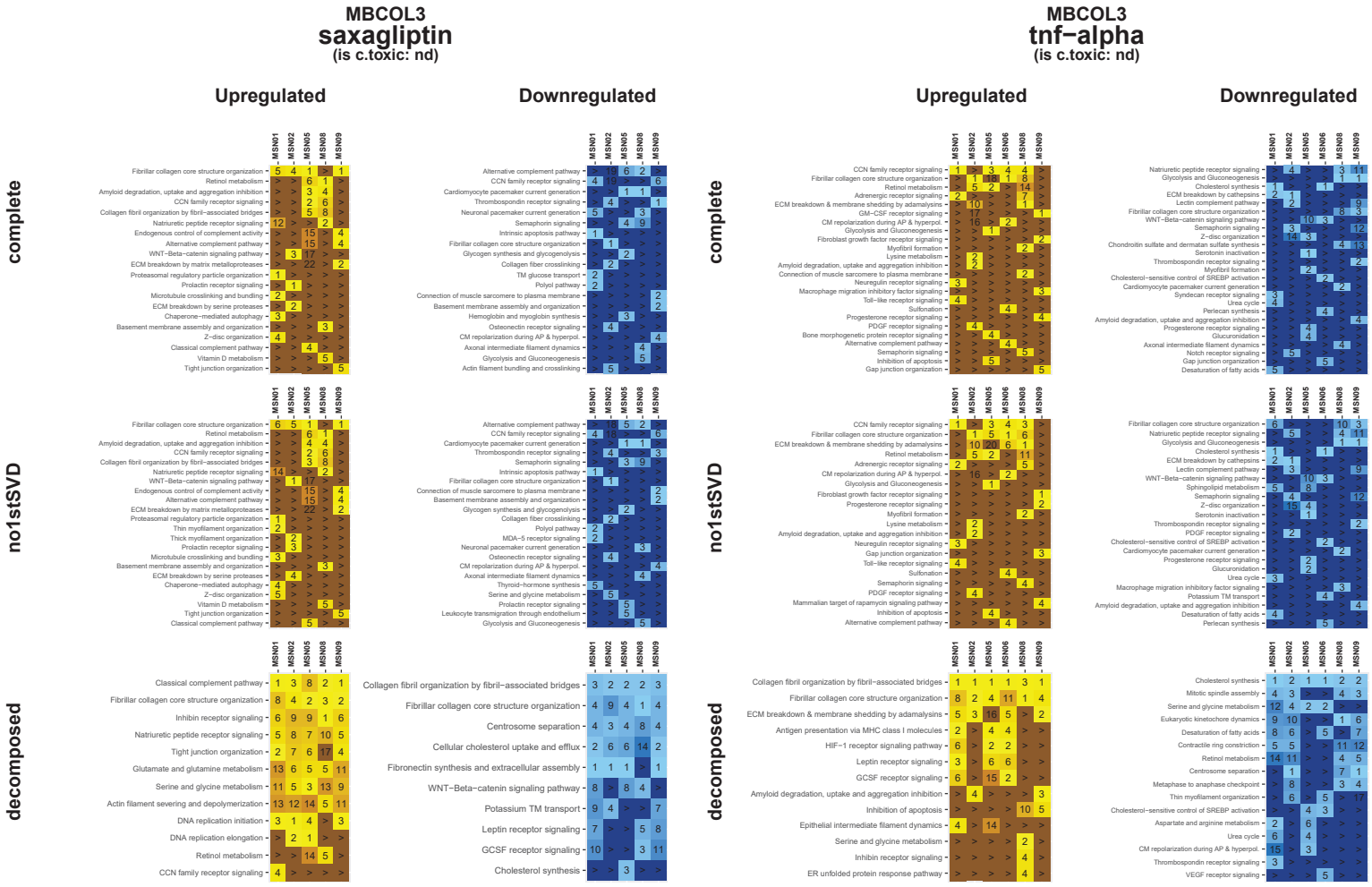

Supplementary Fig. 14D

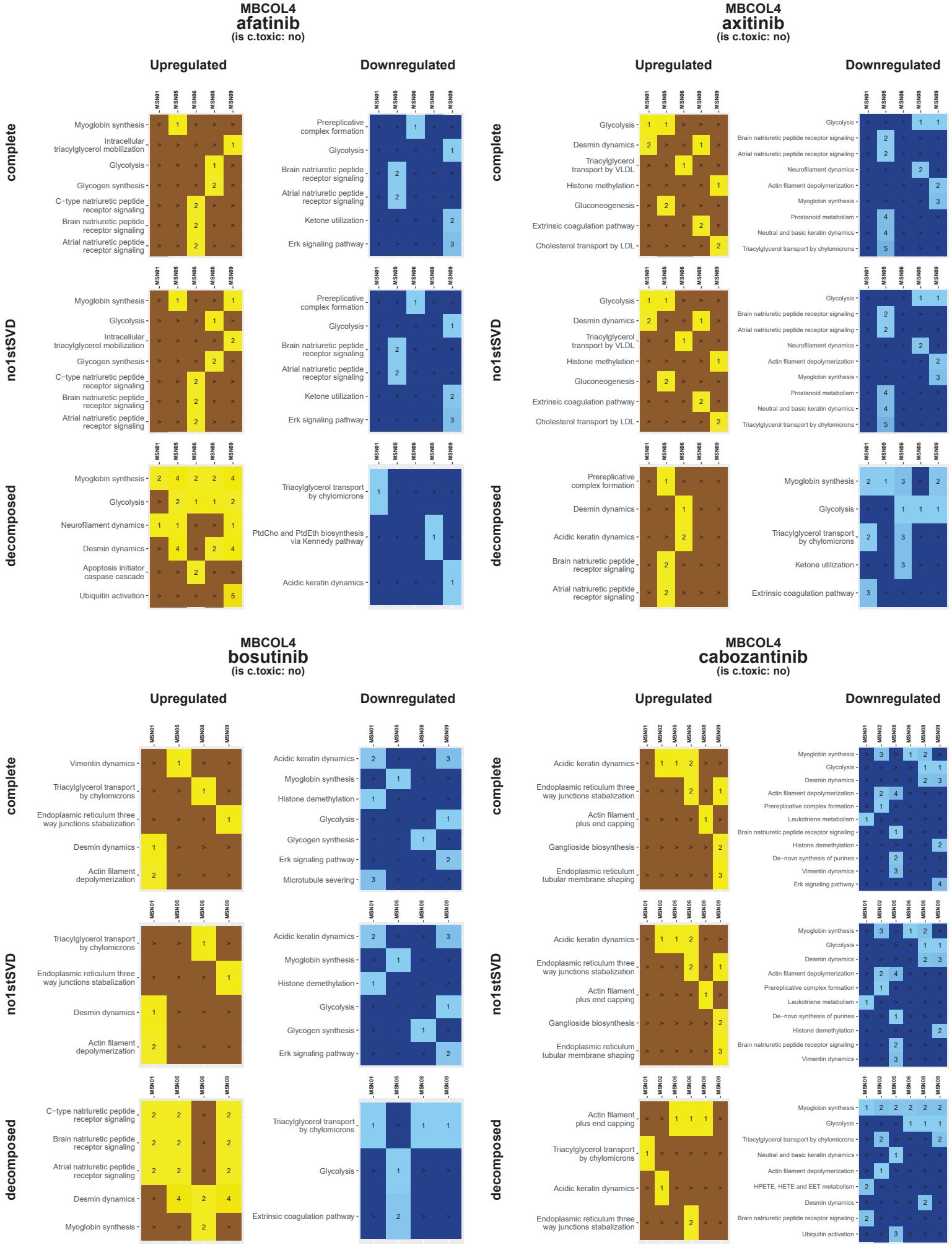

Supplementary Fig. 14E

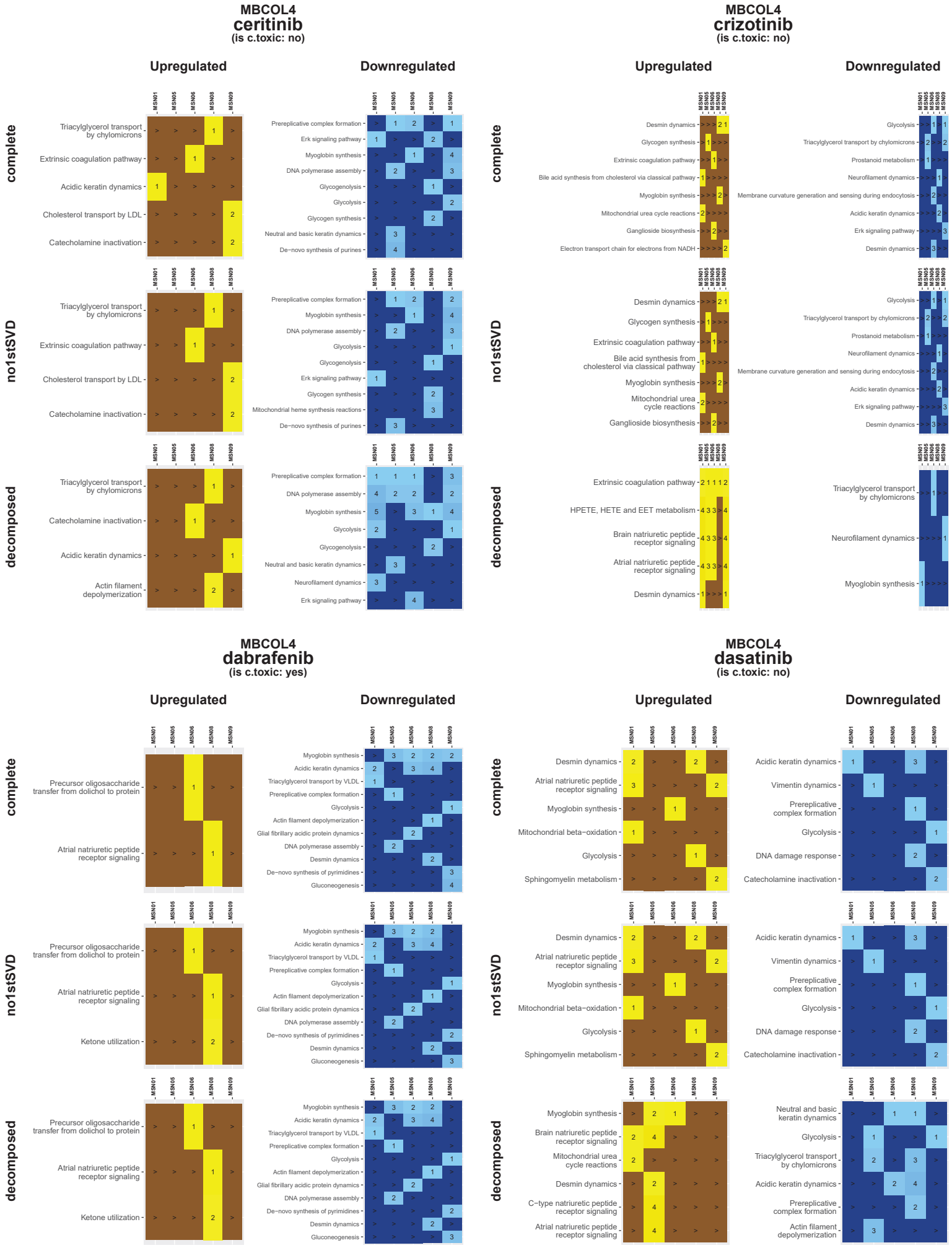

Supplementary Fig. 14E

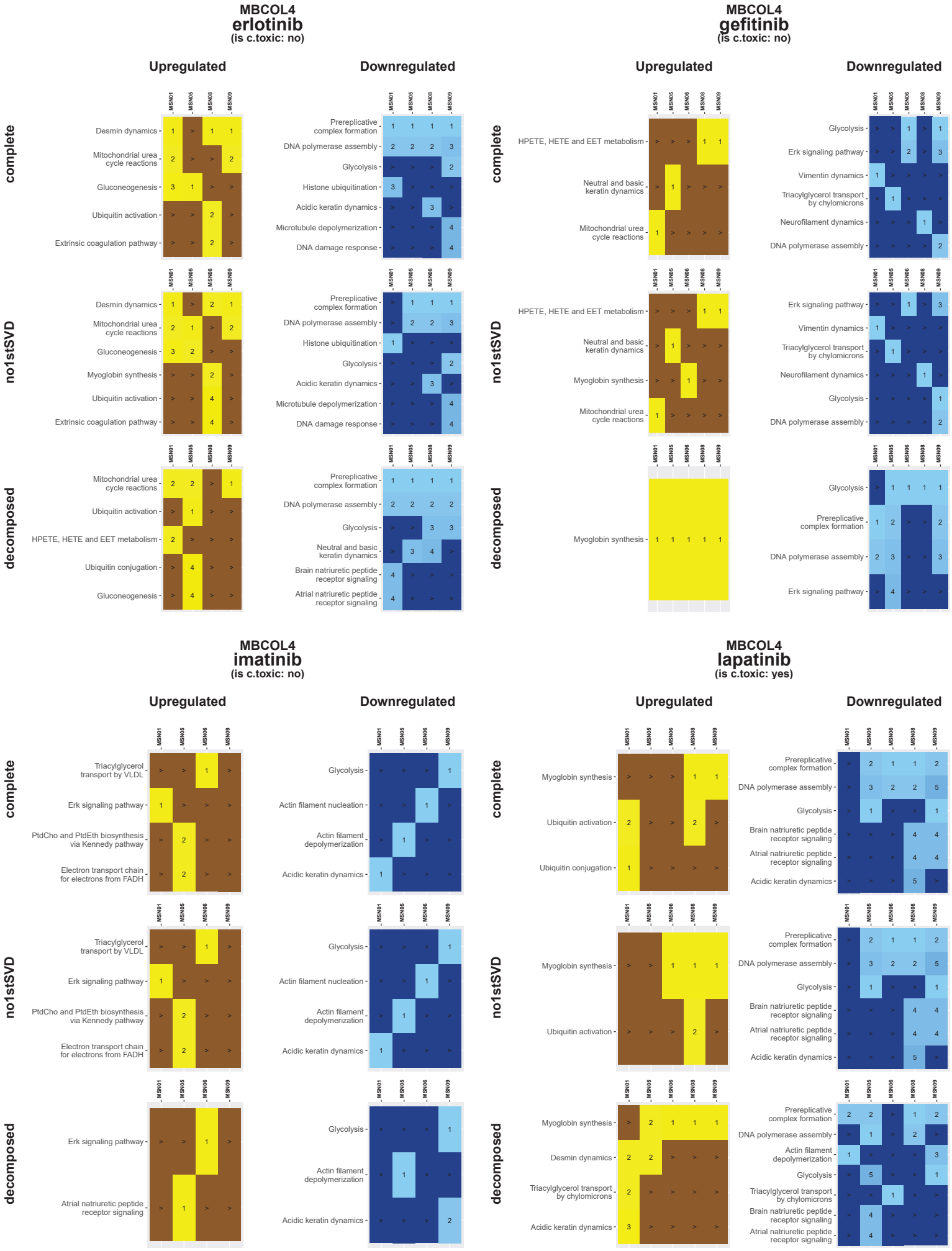

Supplementary Fig. 14E

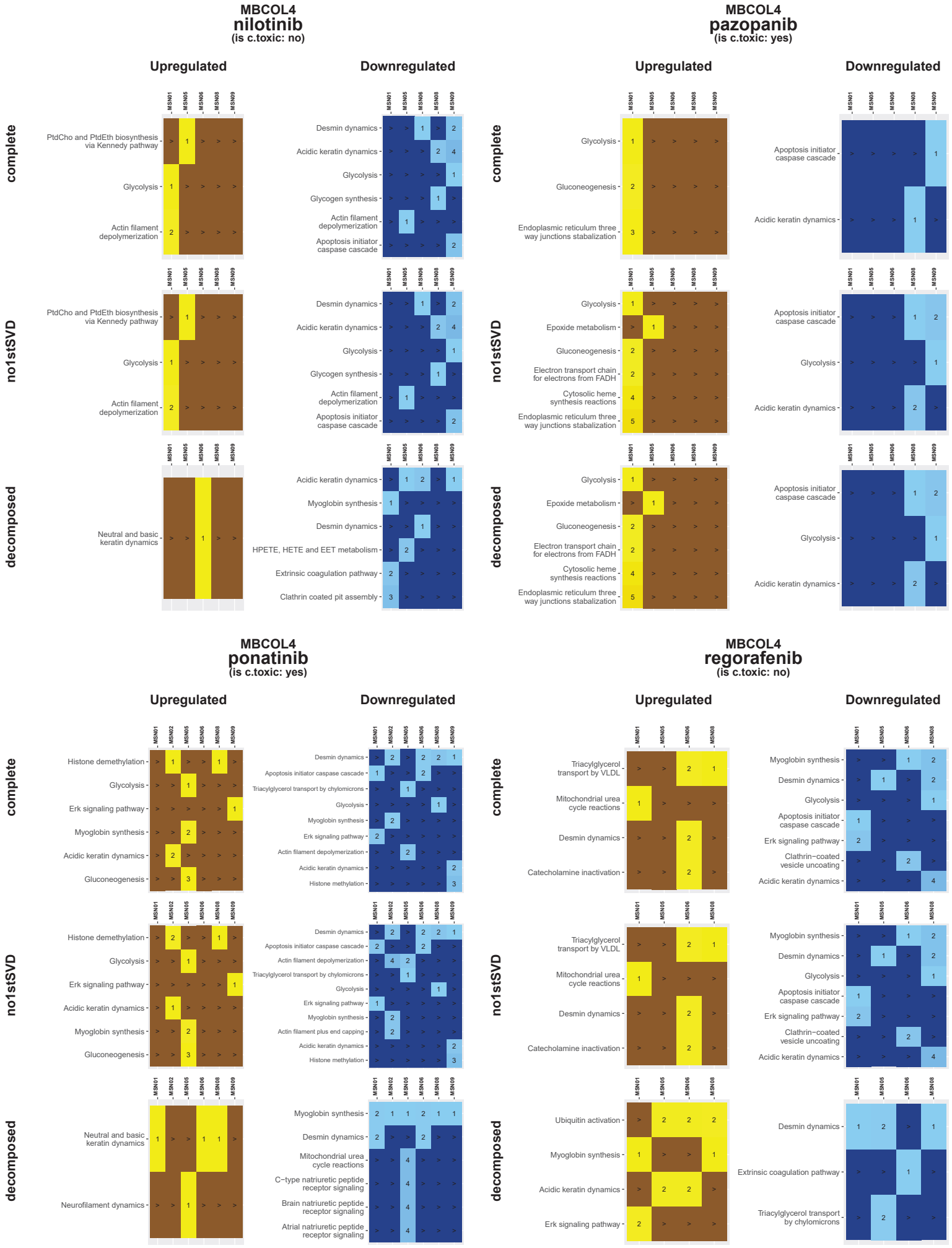

Supplementary Fig. 14E

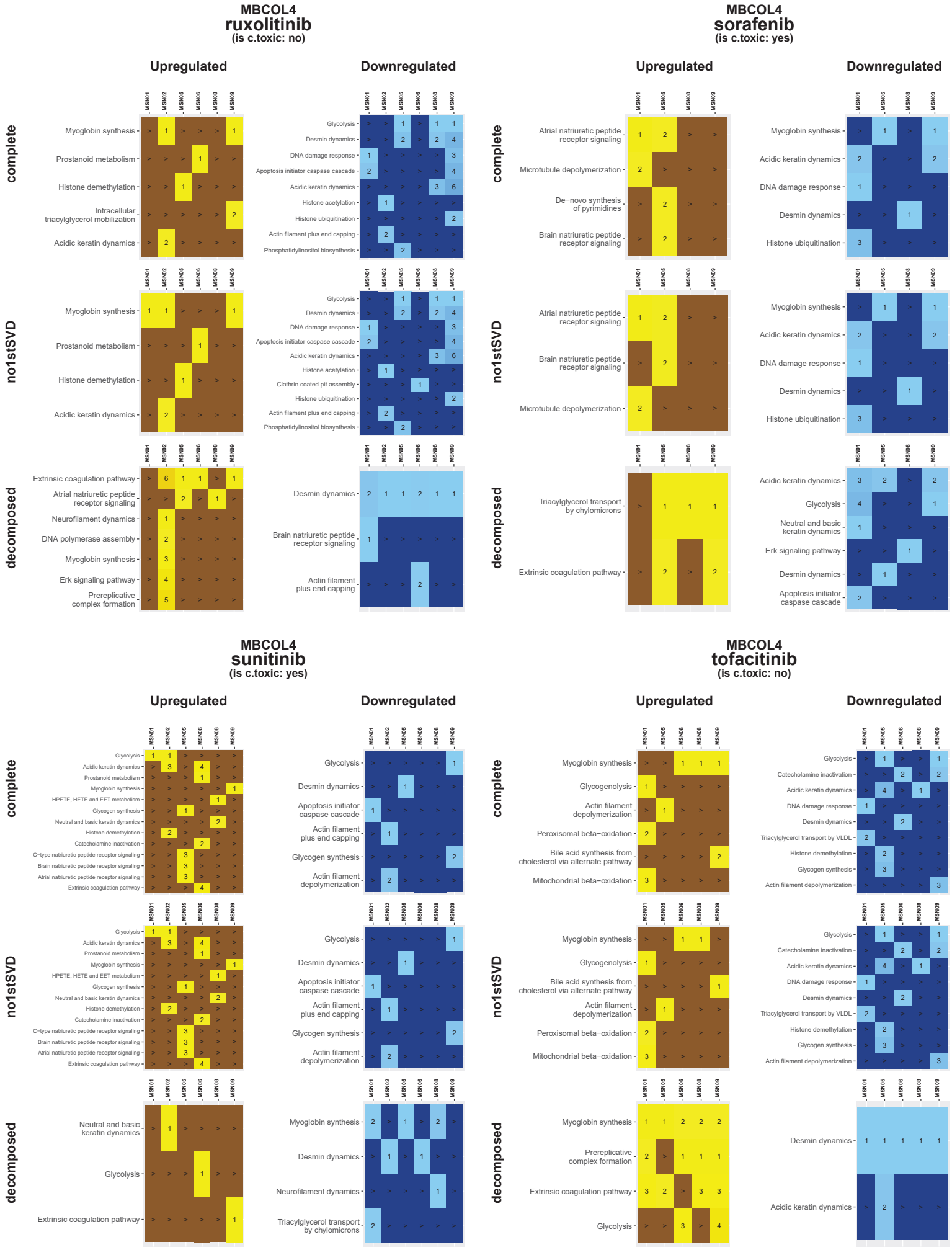

Supplementary Fig. 14E

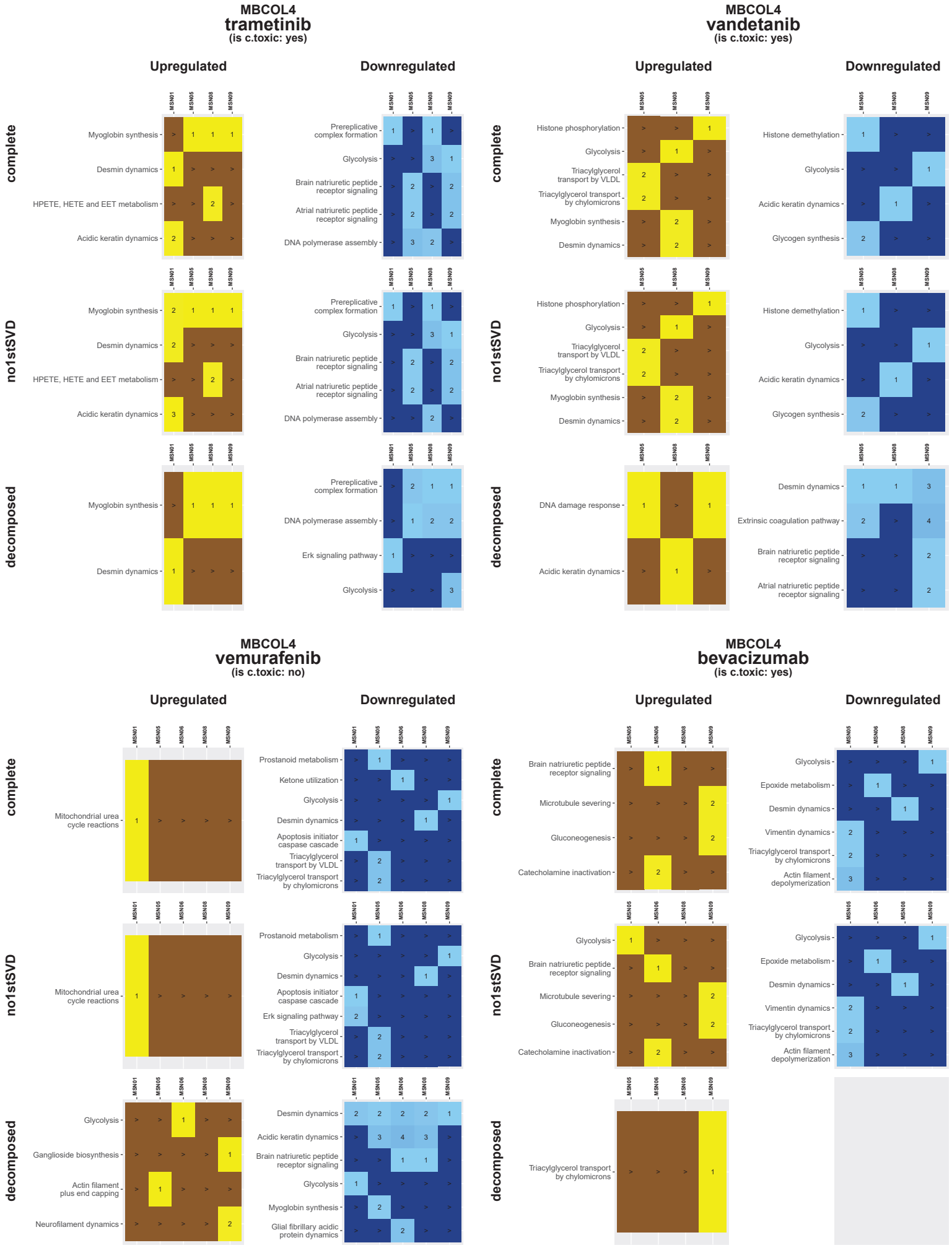

Supplementary Fig. 14E

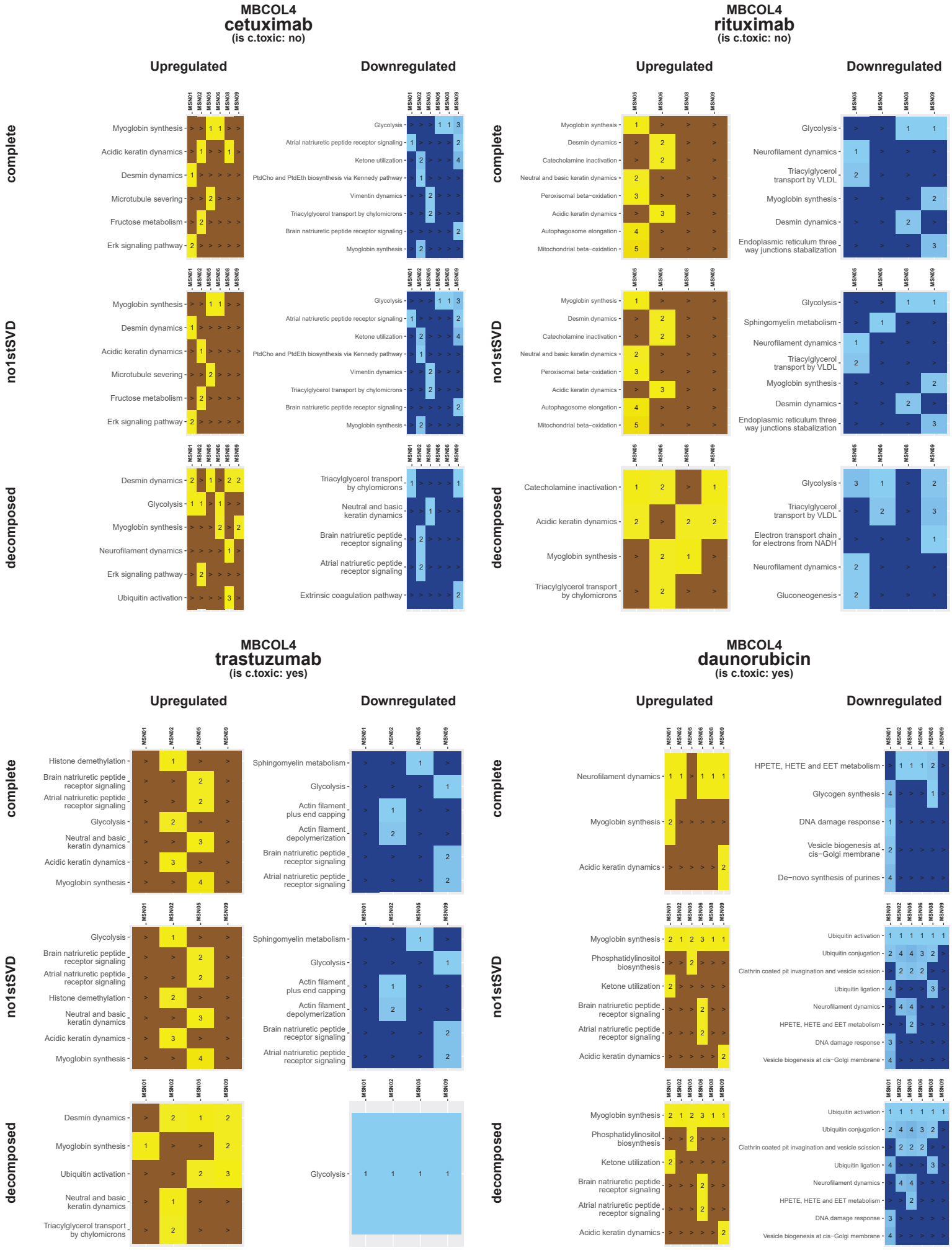

Supplementary Fig. 14E

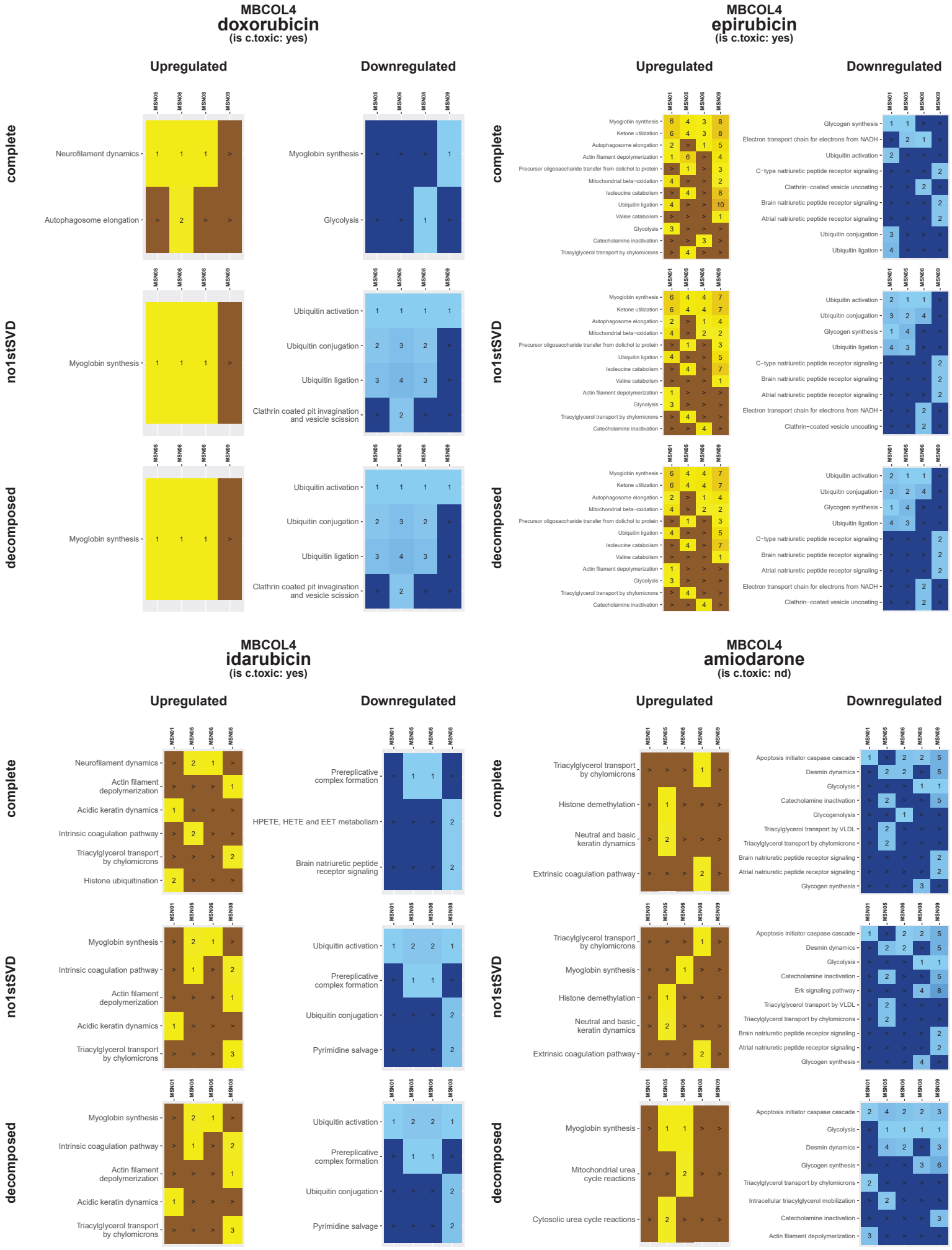

Supplementary Fig. 14E

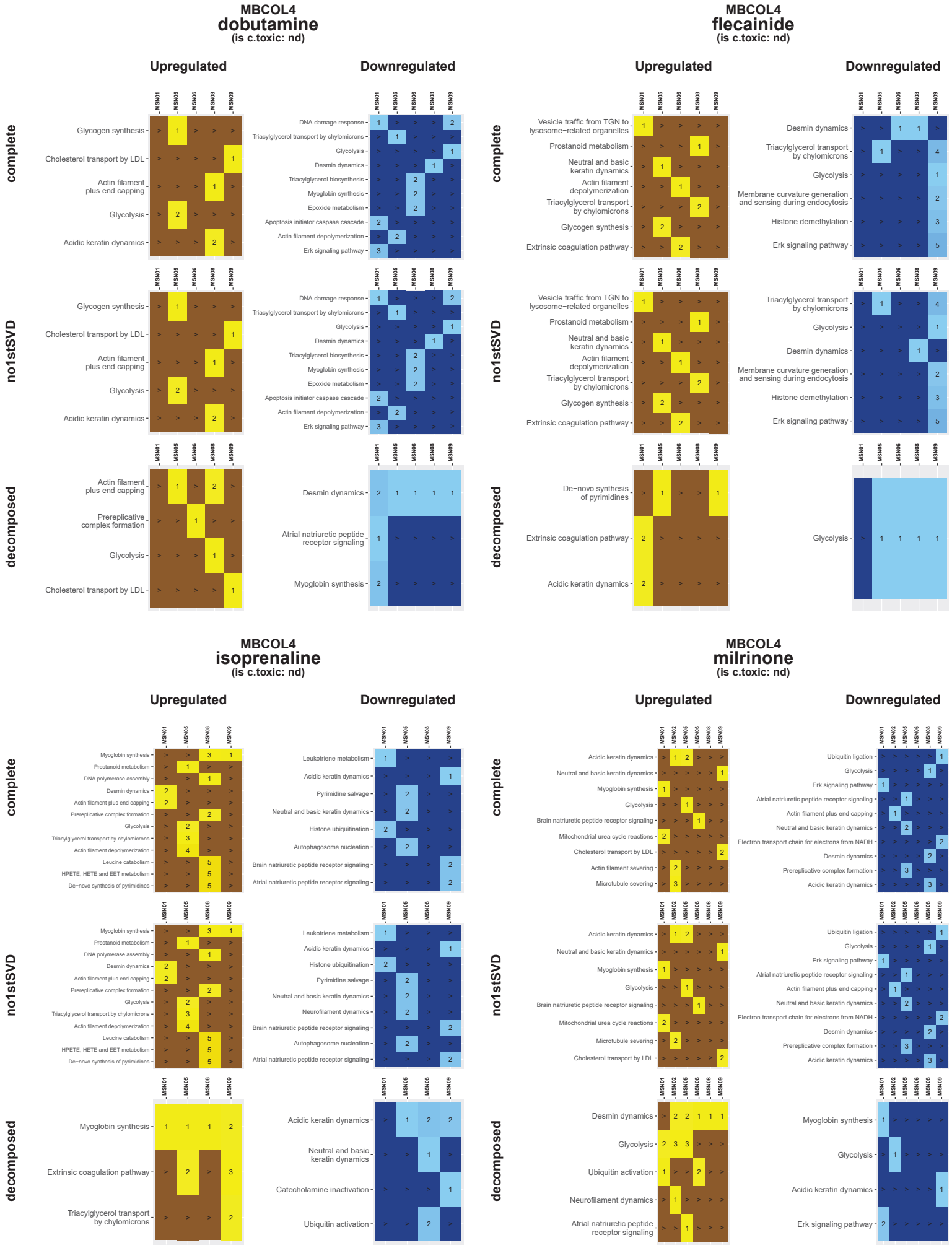

Supplementary Fig. 14E

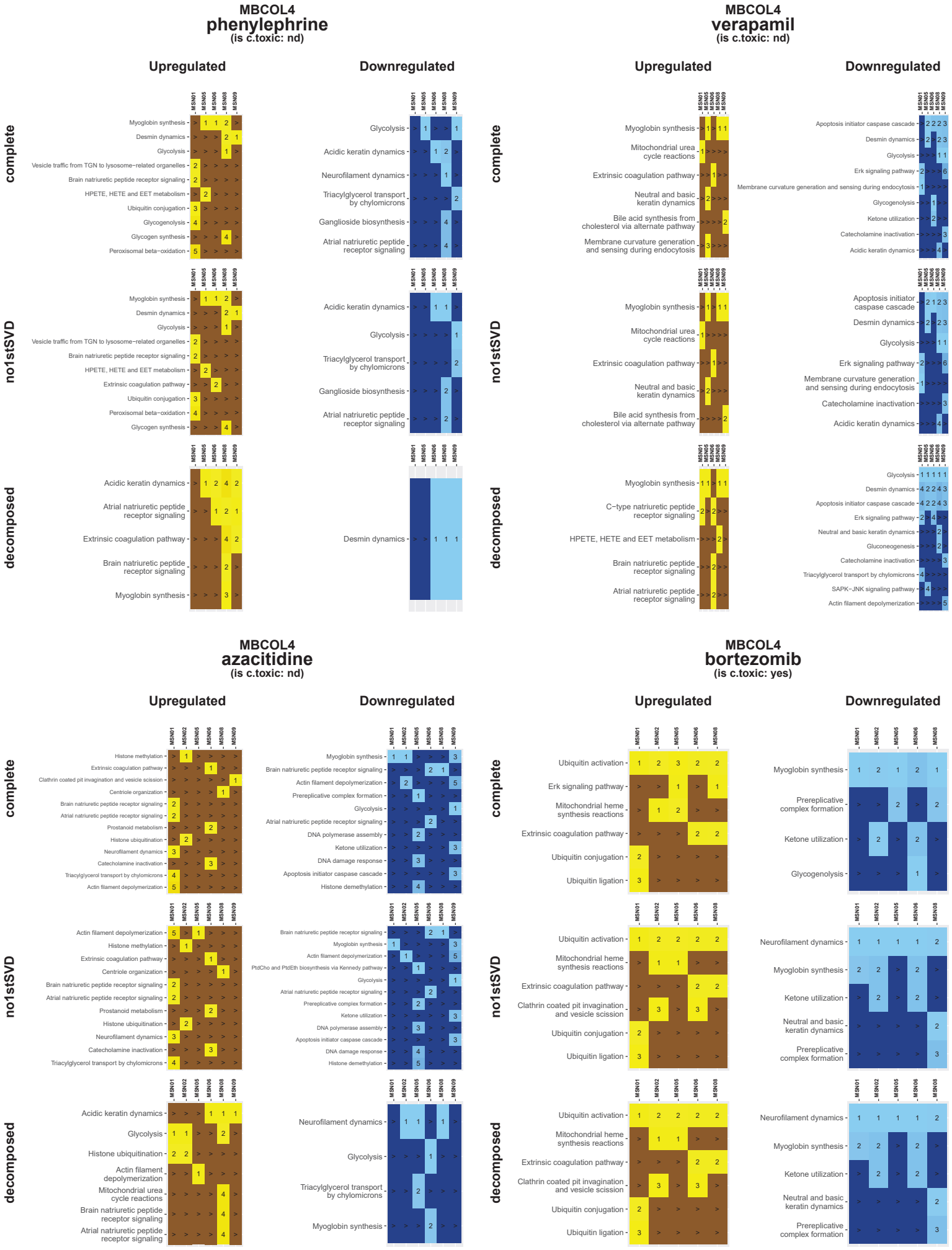

Supplementary Fig. 14E

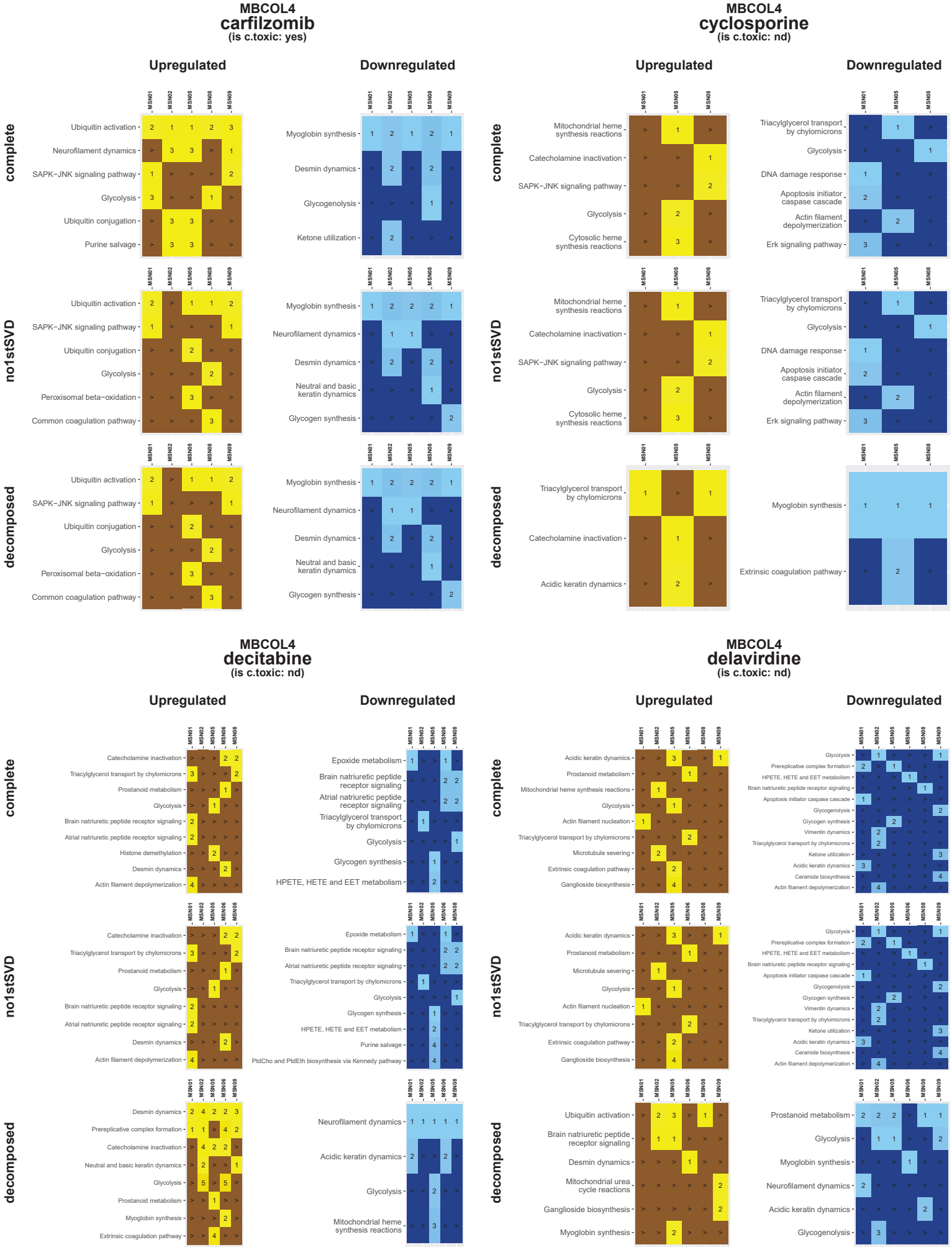

Supplementary Fig. 14E

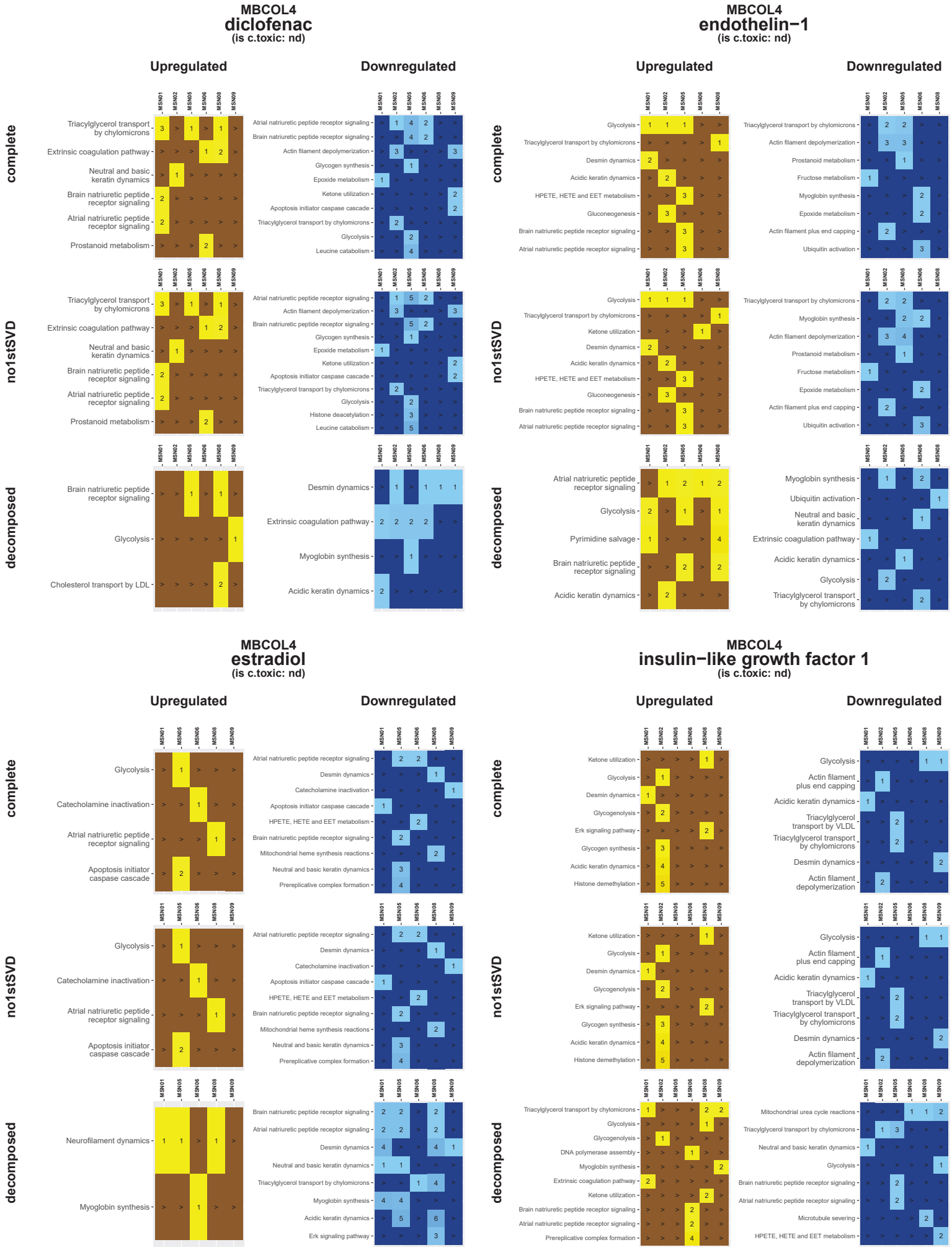

Supplementary Fig. 14E

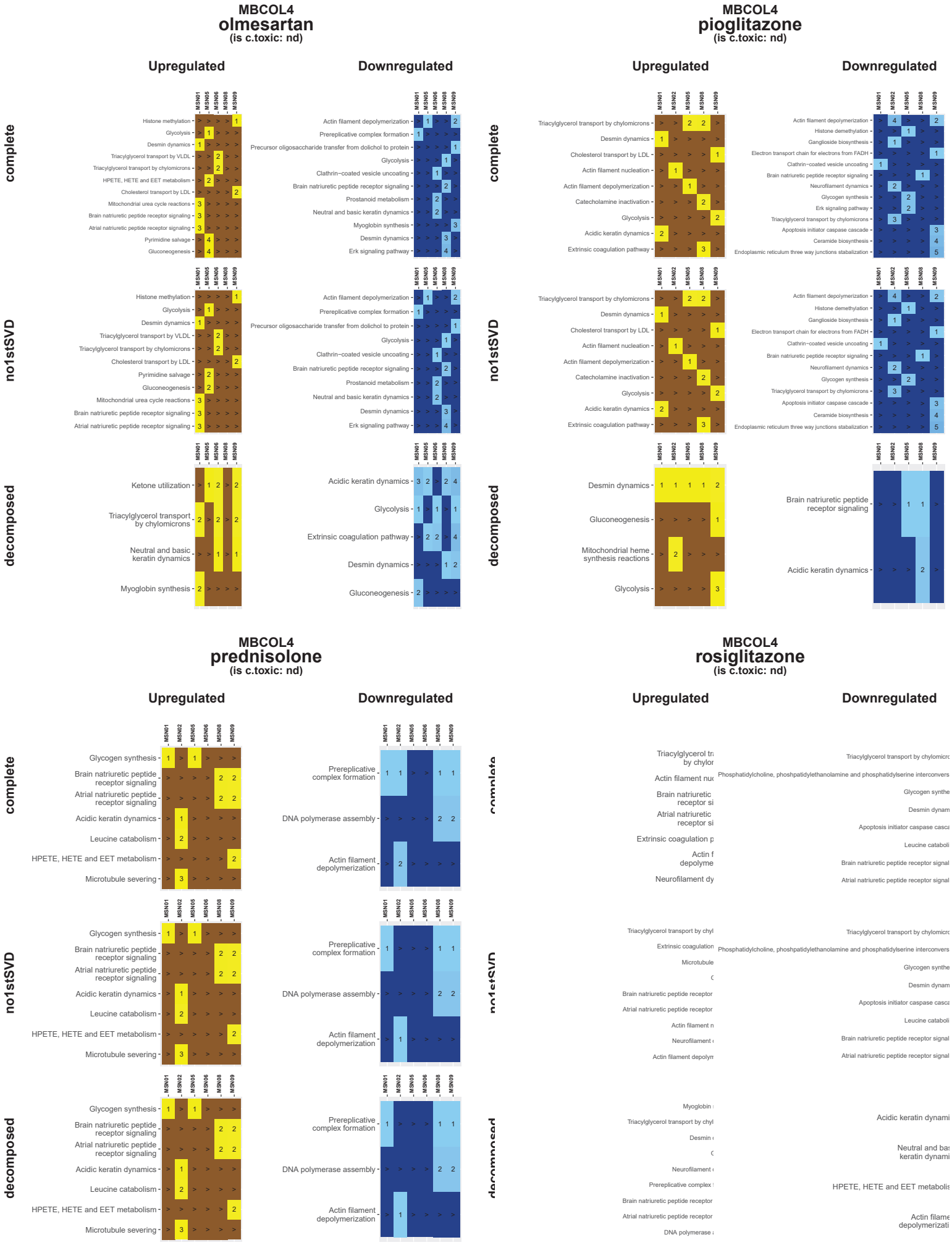

Supplementary Fig. 14E

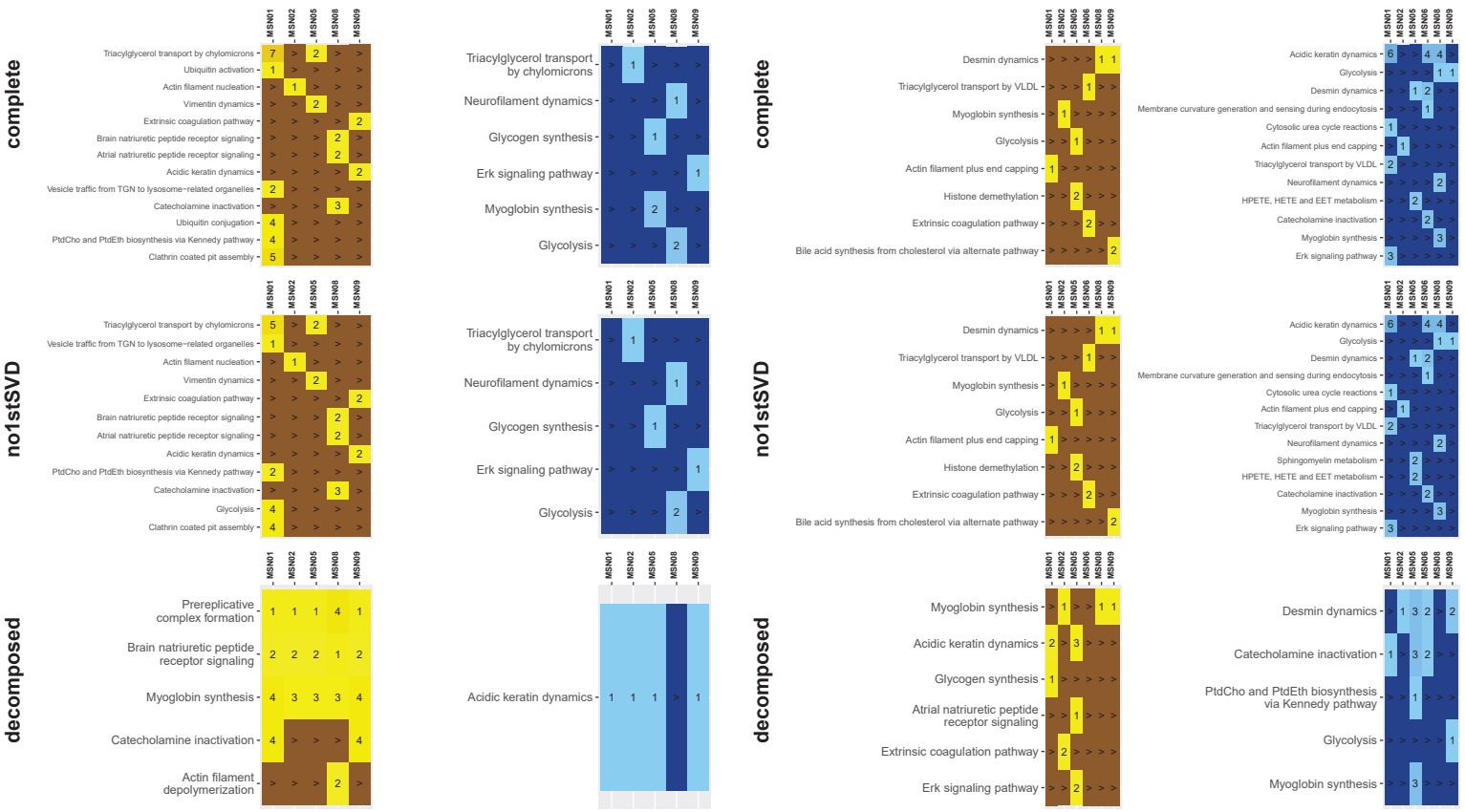

Supplementary Fig. 14E

Supplementary Figure 14. Top Subcellular Processes predicted from complete gene expression profiles, after removal of first eigenarray and from drug-selective gene expression profiles. **(A)** Complete, decomposed gene expression profiles and gene expression profiles after removal of the first eigenarray were subjected to pathway enrichment analysis using the Molecular Biology of the Cell Ontology and Fisher's Exact Test to identify up- and downregulated subcellular processes (SCPs). Significant up- or downregulated **(B)** level-1, **(C)** -2, **(D)** -3 and **(E)** -4 SCPs (p-value<=0.05) were separately ranked by significance for each cell line/drug combination. SCPs predicted for each drug are shown if they are among the top five ranked SCPs for at least one cell line. Numbers indicate ranks, '>' indicates that an SCP was not predicted or predicted with a rank above 99. Cell lines with identified outlier responses to treatment with a drug of interest are colored purple.

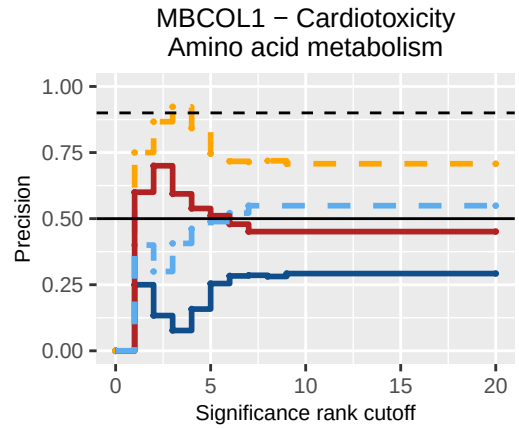
MBCOL1 − Cardiotoxicity
Amino acid metabolism
Precision
Significance rank cutoff

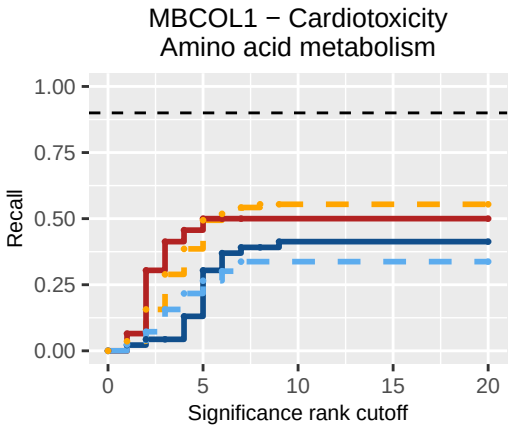
MBCOL1 − Cardiotoxicity
Amino acid metabolism
Recall
Significance rank cutoff

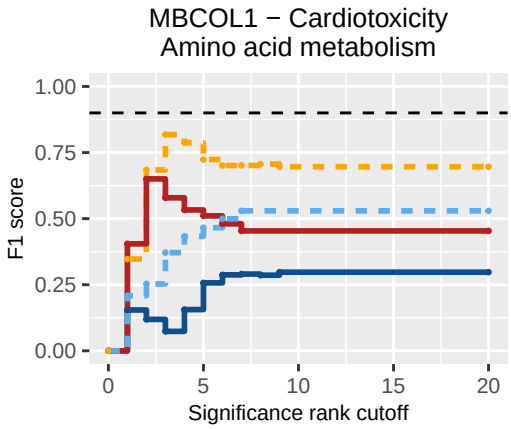
MBCOL1 − Cardiotoxicity
Amino acid metabolism
F1 score
Significance rank cutoff

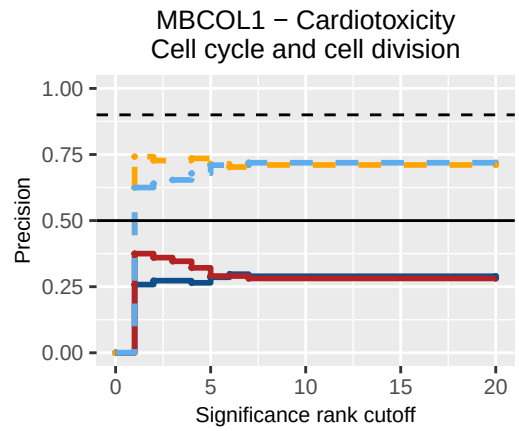
MBCOL1 − Cardiotoxicity
Cell cycle and cell division
Precision
Significance rank cutoff

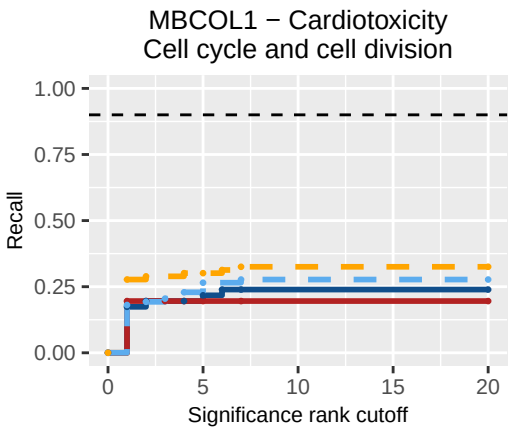
MBCOL1 − Cardiotoxicity
Cell cycle and cell division
Recall
Significance rank cutoff

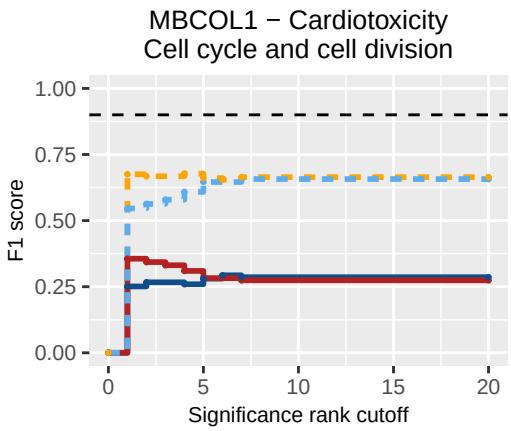
MBCOL1 − Cardiotoxicity
Cell cycle and cell division
F1 score
Significance rank cutoff

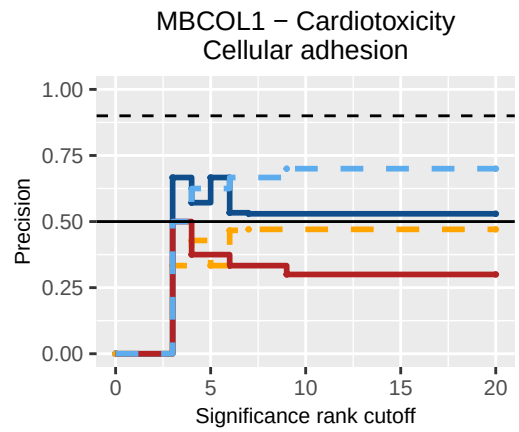
MBCOL1 − Cardiotoxicity
Cellular adhesion
Precision
Significance rank cutoff

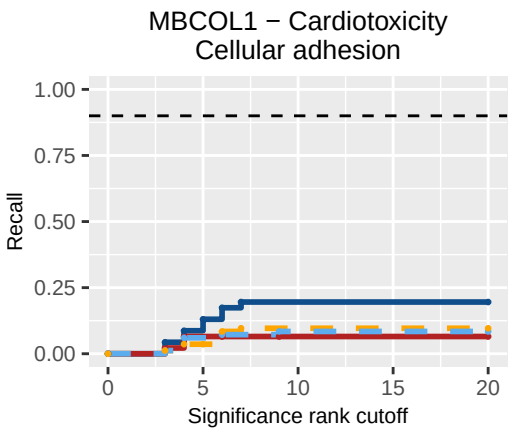
MBCOL1 − Cardiotoxicity
Cellular adhesion
Recall
Significance rank cutoff

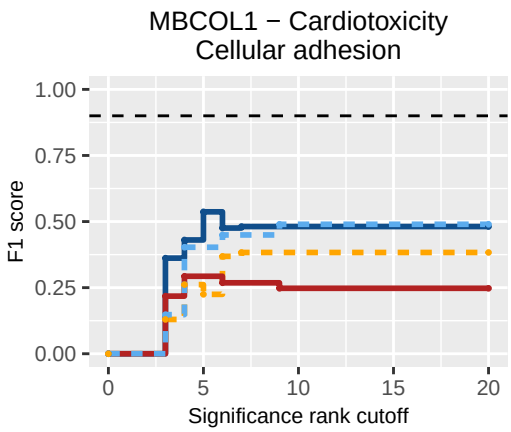
MBCOL1 − Cardiotoxicity
Cellular adhesion
F1 score
Significance rank cutoff

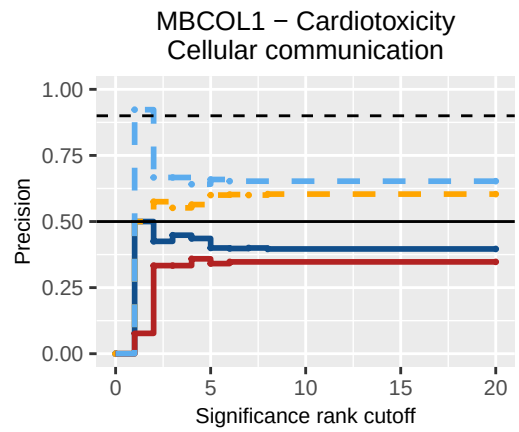
MBCOL1 − Cardiotoxicity
Cellular communication
Precision
Significance rank cutoff

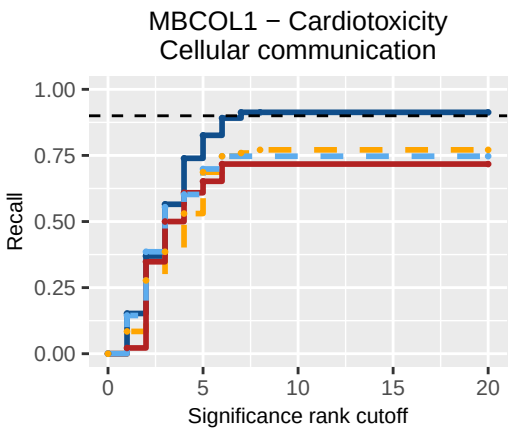
MBCOL1 − Cardiotoxicity
Cellular communication
Recall
Significance rank cutoff

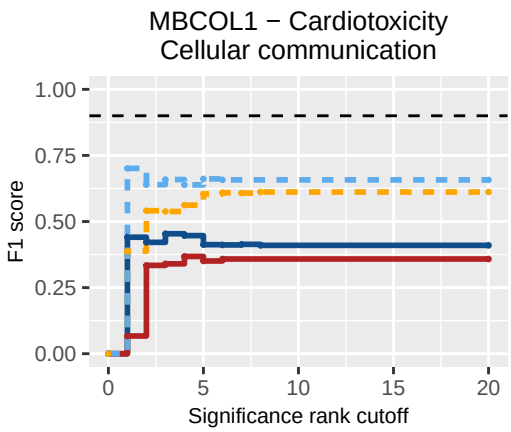
MBCOL1 − Cardiotoxicity
Cellular communication
F1 score
Significance rank cutoff

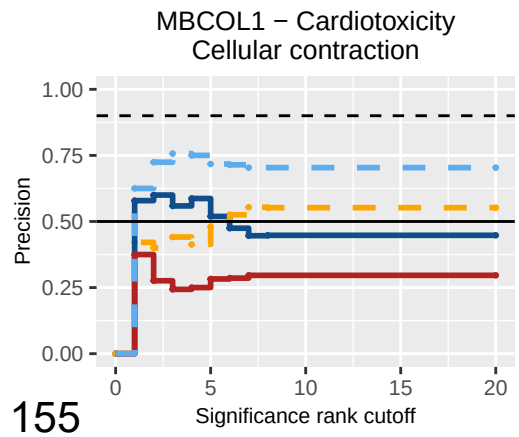
MBCOL1 − Cardiotoxicity
Cellular contraction
Precision
Significance rank cutoff

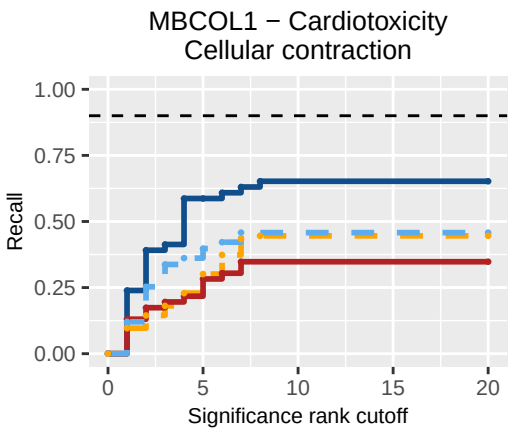
MBCOL1 − Cardiotoxicity
Cellular contraction
Recall
Significance rank cutoff

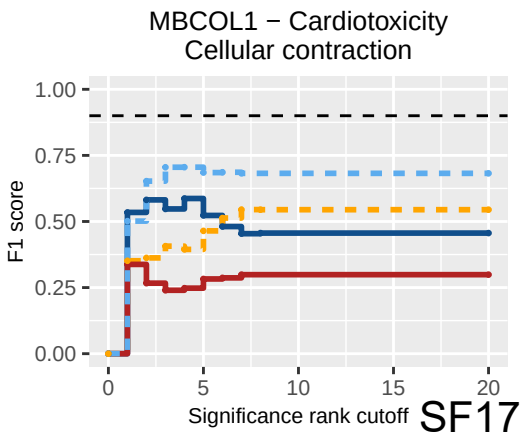
MBCOL1 − Cardiotoxicity
Cellular contraction
F1 score
Significance rank cutoff

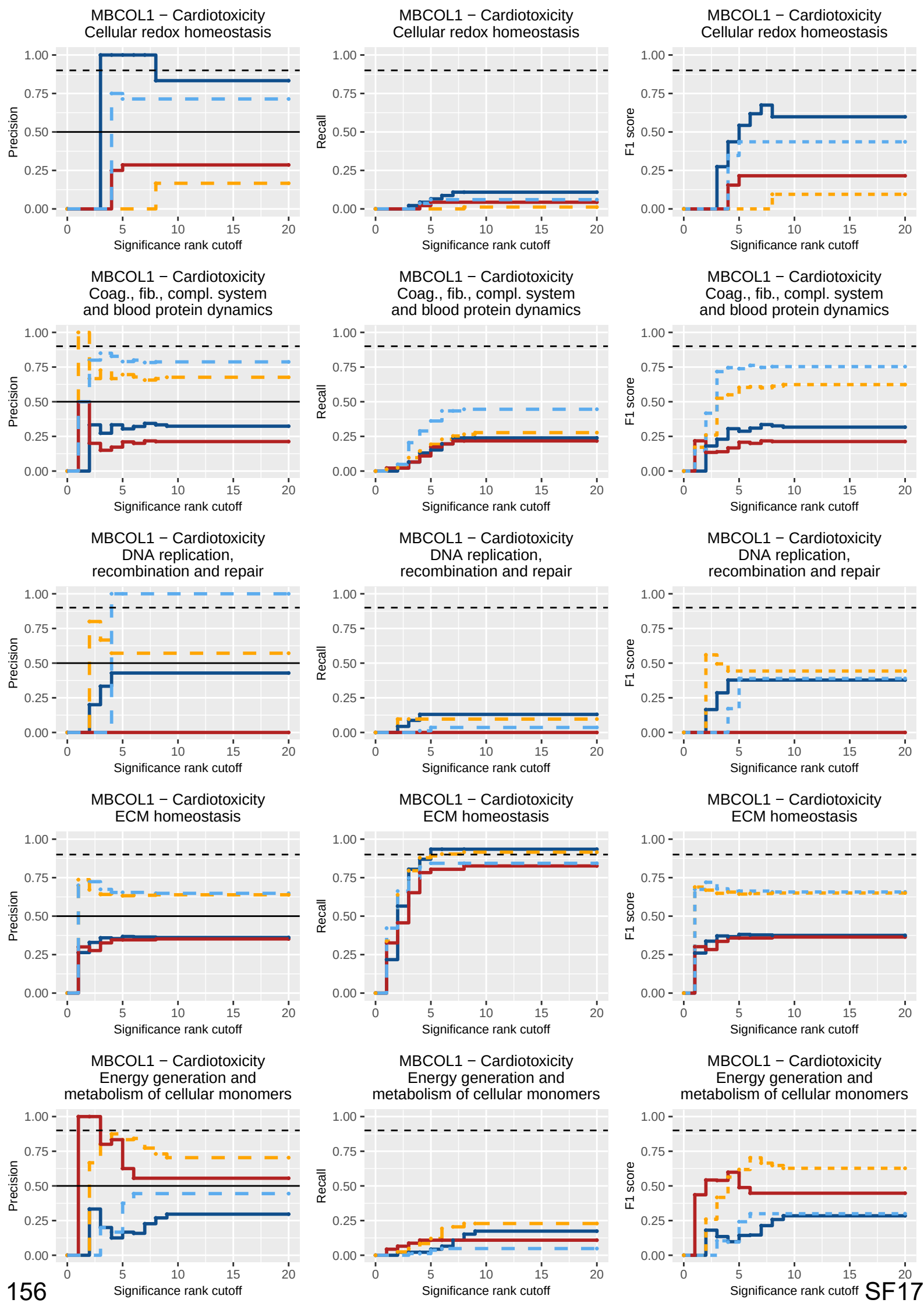
MBCOL1 − Cardiotoxicity
Cellular redox homeostasis
MBCOL1 − Cardiotoxicity
Cellular redox homeostasis
MBCOL1 − Cardiotoxicity
Cellular redox homeostasis
MBCOL1 − Cardiotoxicity
Coag., fib., compl. system
and blood protein dynamics
MBCOL1 − Cardiotoxicity
Coag., fib., compl. system
and blood protein dynamics
MBCOL1 − Cardiotoxicity
Coag., fib., compl. system
and blood protein dynamics
MBCOL1 − Cardiotoxicity
DNA replication,
recombination and repair
MBCOL1 − Cardiotoxicity
DNA replication,
recombination and repair
MBCOL1 − Cardiotoxicity
DNA replication,
recombination and repair
MBCOL1 − Cardiotoxicity
ECM homeostasis
MBCOL1 − Cardiotoxicity
ECM homeostasis
MBCOL1 − Cardiotoxicity
ECM homeostasis
MBCOL1 − Cardiotoxicity
Energy generation and
metabolism of cellular monomers
MBCOL1 − Cardiotoxicity
Energy generation and
metabolism of cellular monomers
MBCOL1 − Cardiotoxicity
Energy generation and
metabolism of cellular monomers
Precision
Recall
F1 score
1.00
0.75
0.50
0.25
0.00
0
5
10
15
20
Significance rank cutoff

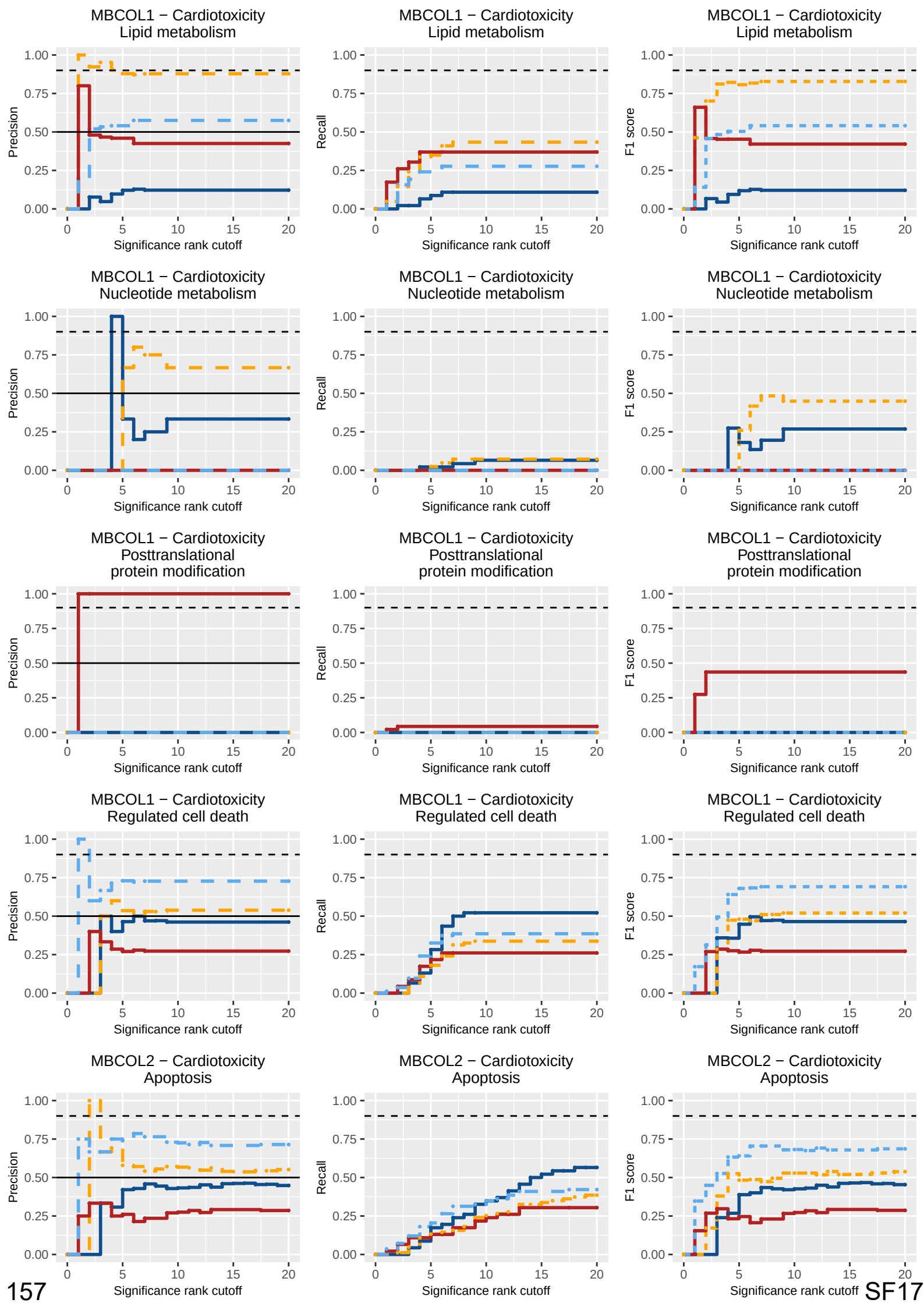
MBCOL1 − Cardiotoxicity
Lipid metabolism
Precision
Recall
F1 score
Significance rank cutoff
MBCOL1 − Cardiotoxicity
Nucleotide metabolism
MBCOL1 − Cardiotoxicity
Posttranslational
protein modification
MBCOL1 − Cardiotoxicity
Regulated cell death
MBCOL2 − Cardiotoxicity
Apoptosis

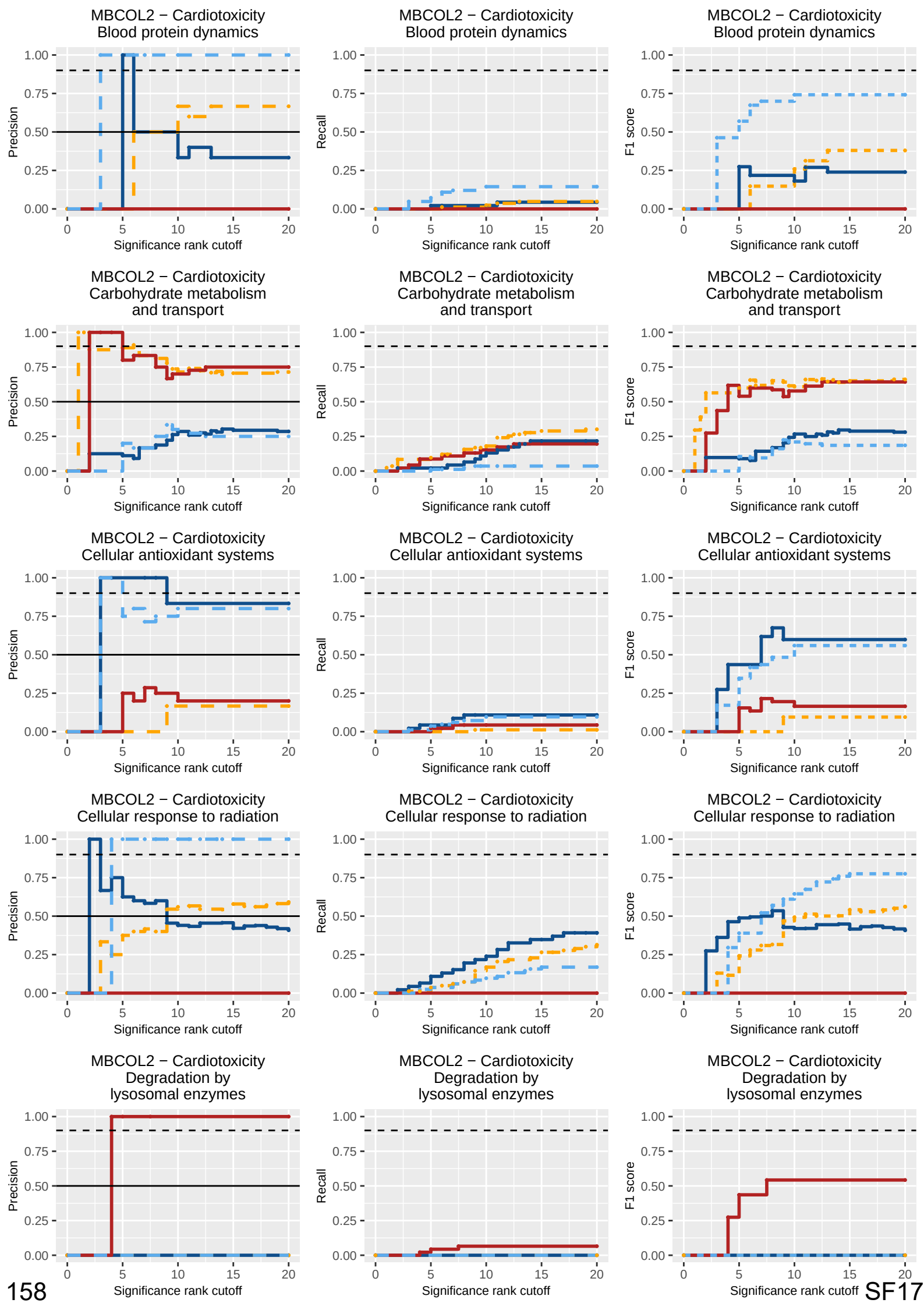
MBCOL2 − Cardiotoxicity
Blood protein dynamics
MBCOL2 − Cardiotoxicity
Blood protein dynamics
MBCOL2 − Cardiotoxicity
Blood protein dynamics
MBCOL2 − Cardiotoxicity
Carbohydrate metabolism and transport
MBCOL2 − Cardiotoxicity
Carbohydrate metabolism and transport
MBCOL2 − Cardiotoxicity
Carbohydrate metabolism and transport
MBCOL2 − Cardiotoxicity
Cellular antioxidant systems
MBCOL2 − Cardiotoxicity
Cellular antioxidant systems
MBCOL2 − Cardiotoxicity
Cellular antioxidant systems
MBCOL2 − Cardiotoxicity
Cellular response to radiation
MBCOL2 − Cardiotoxicity
Cellular response to radiation
MBCOL2 − Cardiotoxicity
Cellular response to radiation
MBCOL2 − Cardiotoxicity
Degradation by lysosomal enzymes
MBCOL2 − Cardiotoxicity
Degradation by lysosomal enzymes
MBCOL2 − Cardiotoxicity
Degradation by lysosomal enzymes
Precision
Recall
F1 score
1.00
0.75
0.50
0.25
0.00
0
5
10
15
20
Significance rank cutoff

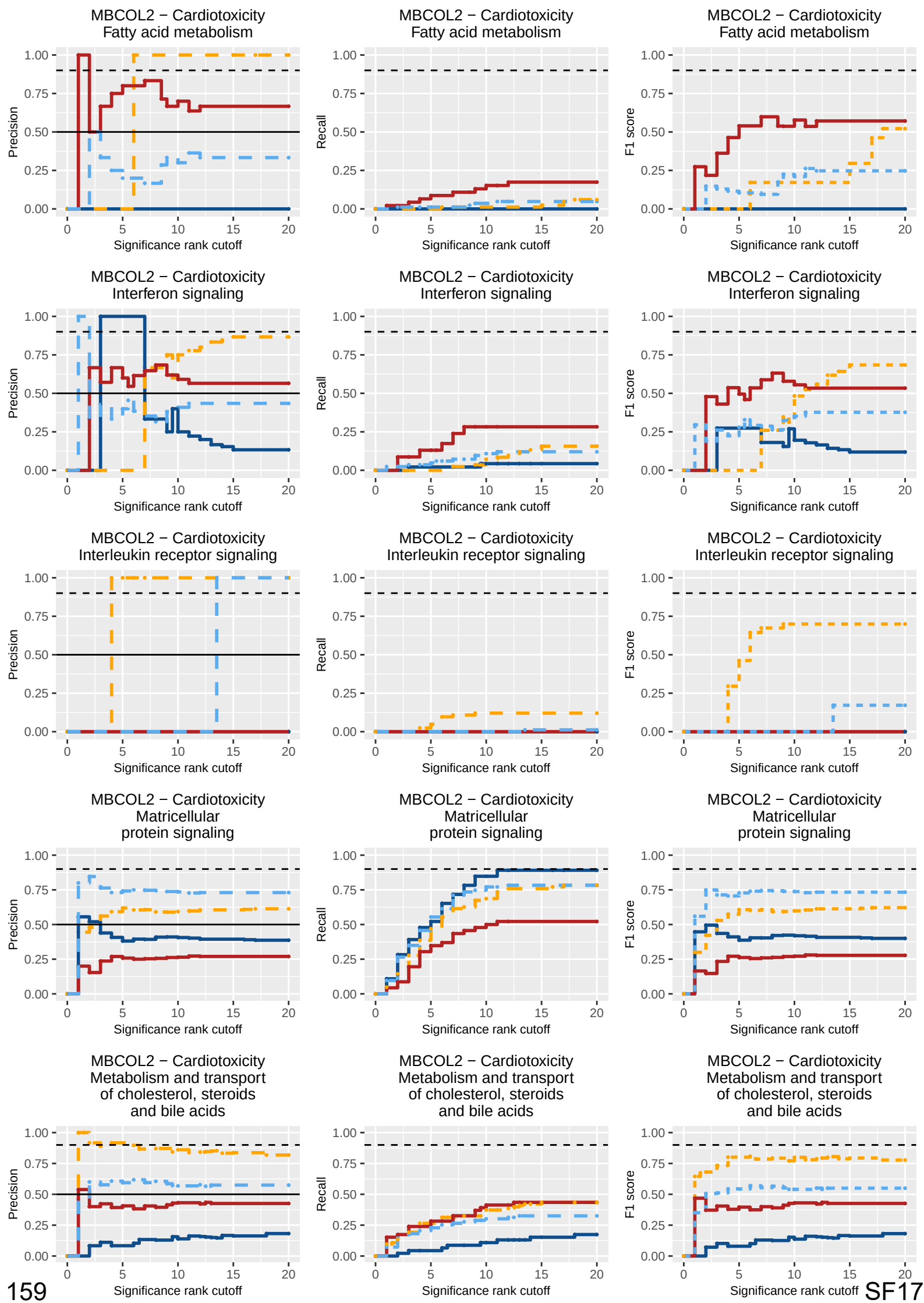
MBCOL2 − Cardiotoxicity
Fatty acid metabolism
Precision
Recall
F1 score
Significance rank cutoff
MBCOL2 − Cardiotoxicity
Interferon signaling
MBCOL2 − Cardiotoxicity
Interleukin receptor signaling
MBCOL2 − Cardiotoxicity
Matricellular
protein signaling
MBCOL2 − Cardiotoxicity
Metabolism and transport
of cholesterol, steroids
and bile acids

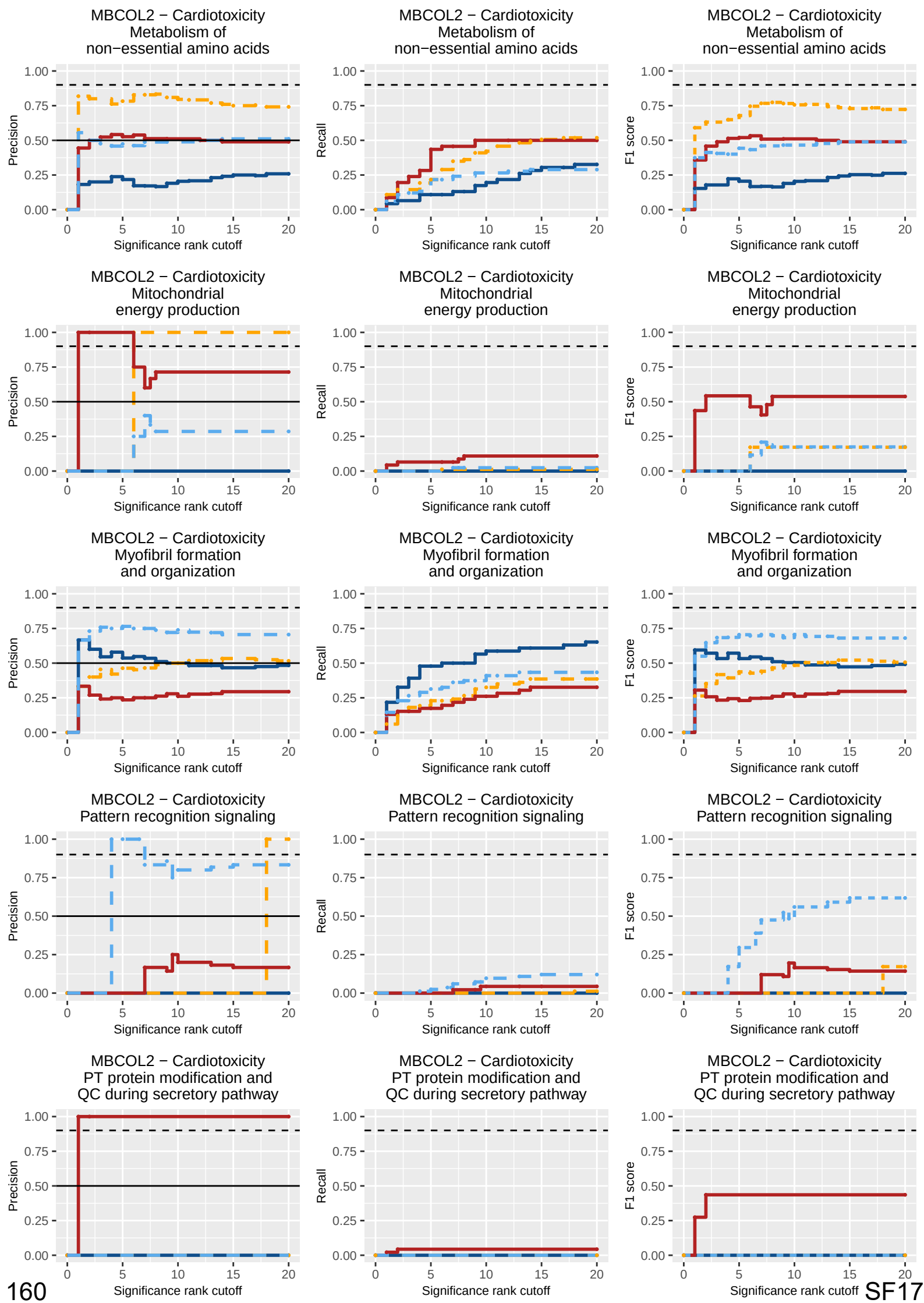
MBCOL2 − Cardiotoxicity
Metabolism of
non−essential amino acids
MBCOL2 − Cardiotoxicity
Mitochondrial
energy production
MBCOL2 − Cardiotoxicity
Myofibril formation
and organization
MBCOL2 − Cardiotoxicity
Pattern recognition signaling
MBCOL2 − Cardiotoxicity
PT protein modification and
QC during secretory pathway
Precision
Recall
F1 score
Significance rank cutoff
0.00
0.25
0.50
0.75
1.00
0
5
10
15
20

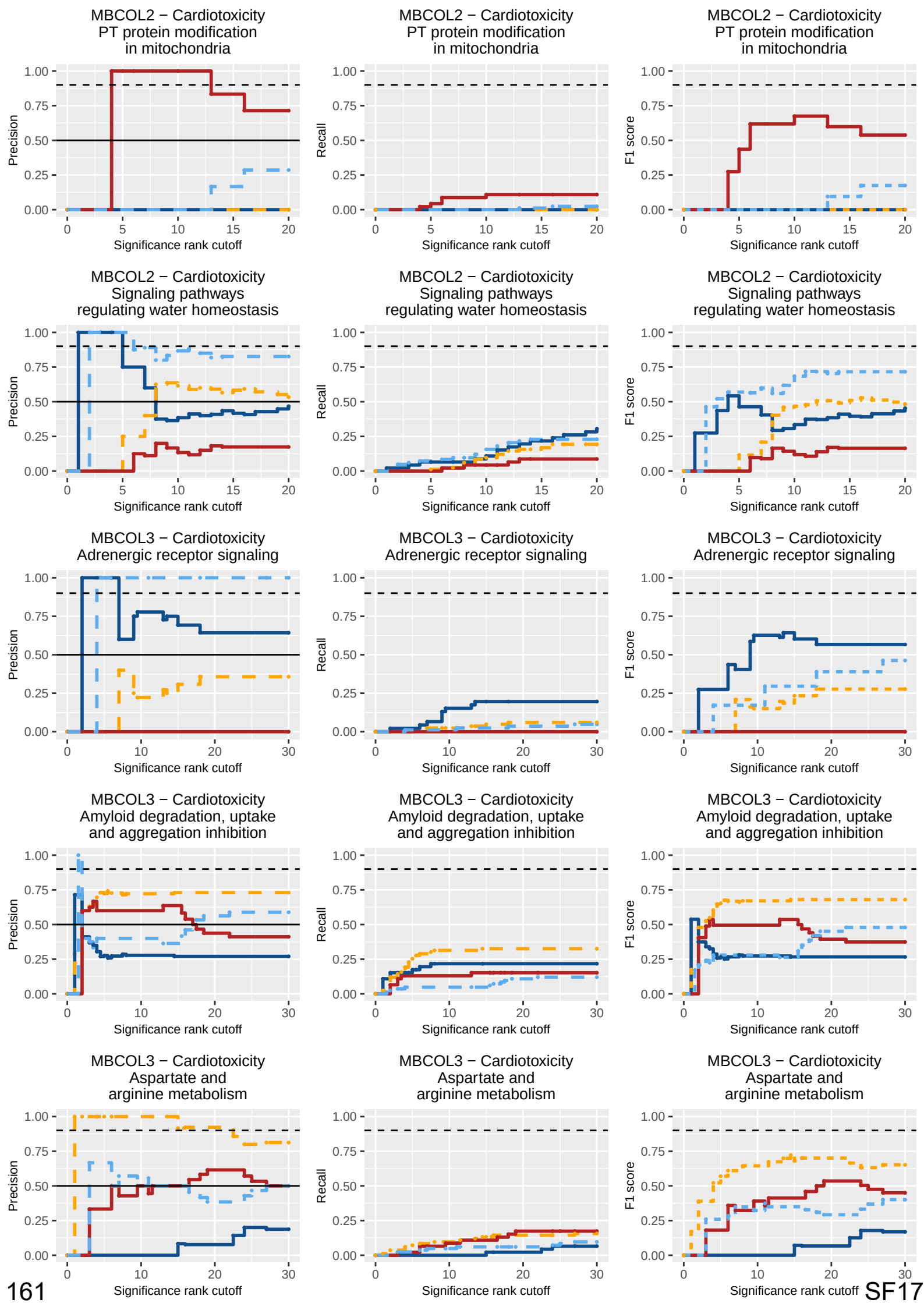
MBCOL2 − Cardiotoxicity
PT protein modification
in mitochondria
MBCOL2 − Cardiotoxicity
PT protein modification
in mitochondria
MBCOL2 − Cardiotoxicity
PT protein modification
in mitochondria
MBCOL2 − Cardiotoxicity
Signaling pathways
regulating water homeostasis
MBCOL2 − Cardiotoxicity
Signaling pathways
regulating water homeostasis
MBCOL2 − Cardiotoxicity
Signaling pathways
regulating water homeostasis
MBCOL3 − Cardiotoxicity
Adrenergic receptor signaling
MBCOL3 − Cardiotoxicity
Adrenergic receptor signaling
MBCOL3 − Cardiotoxicity
Adrenergic receptor signaling
MBCOL3 − Cardiotoxicity
Amyloid degradation, uptake
and aggregation inhibition
MBCOL3 − Cardiotoxicity
Amyloid degradation, uptake
and aggregation inhibition
MBCOL3 − Cardiotoxicity
Amyloid degradation, uptake
and aggregation inhibition
MBCOL3 − Cardiotoxicity
Aspartate and
arginine metabolism
MBCOL3 − Cardiotoxicity
Aspartate and
arginine metabolism
MBCOL3 − Cardiotoxicity
Aspartate and
arginine metabolism
Precision
Recall
F1 score
Significance rank cutoff

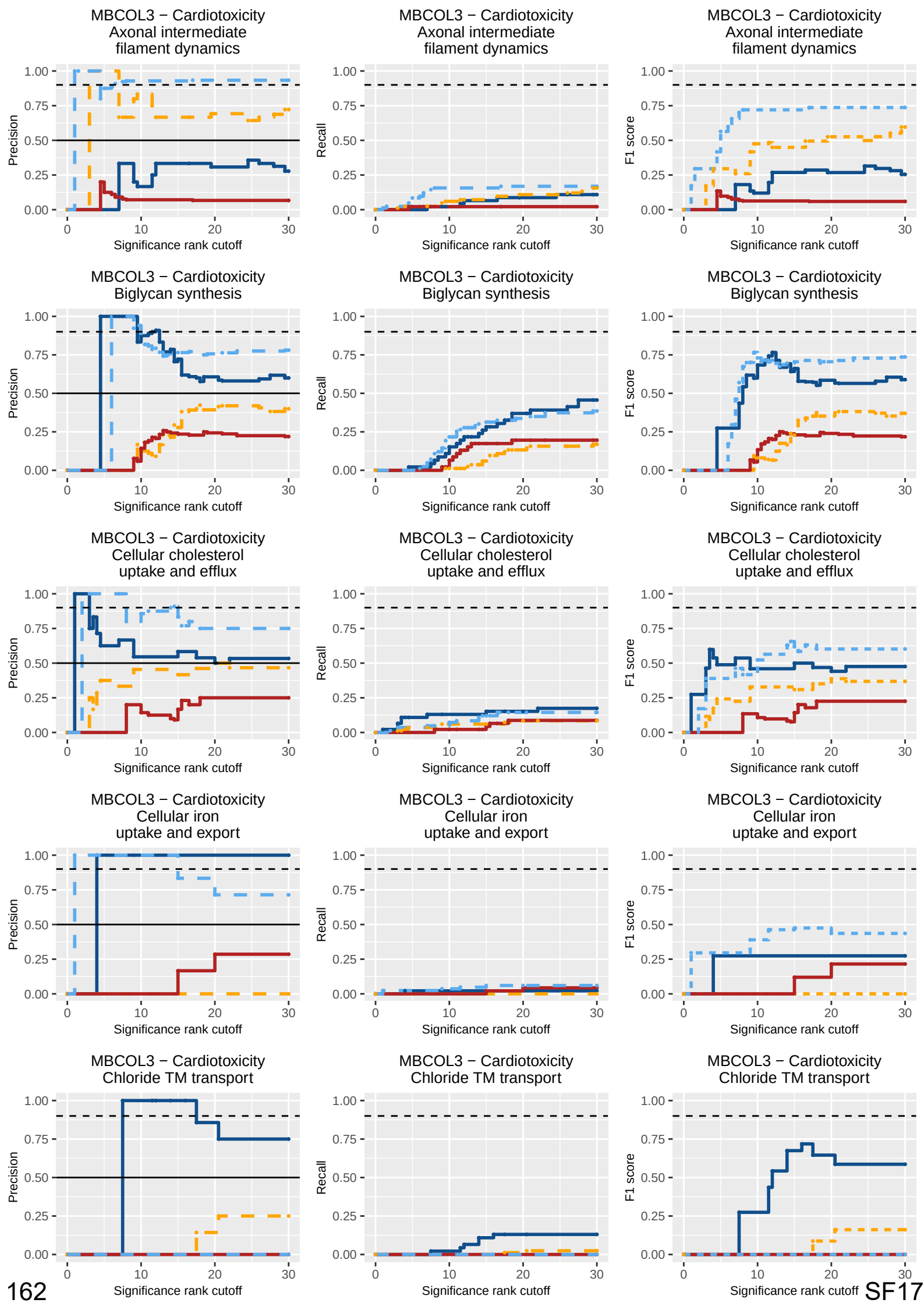
MBCOL3 − Cardiotoxicity
Axonal intermediate filament dynamics
MBCOL3 − Cardiotoxicity
Biglycan synthesis
MBCOL3 − Cardiotoxicity
Cellular cholesterol uptake and efflux
MBCOL3 − Cardiotoxicity
Cellular iron uptake and export
MBCOL3 − Cardiotoxicity
Chloride TM transport
Precision
Recall
F1 score
Significance rank cutoff
0.00
0.25
0.50
0.75
1.00
0
10
20
30

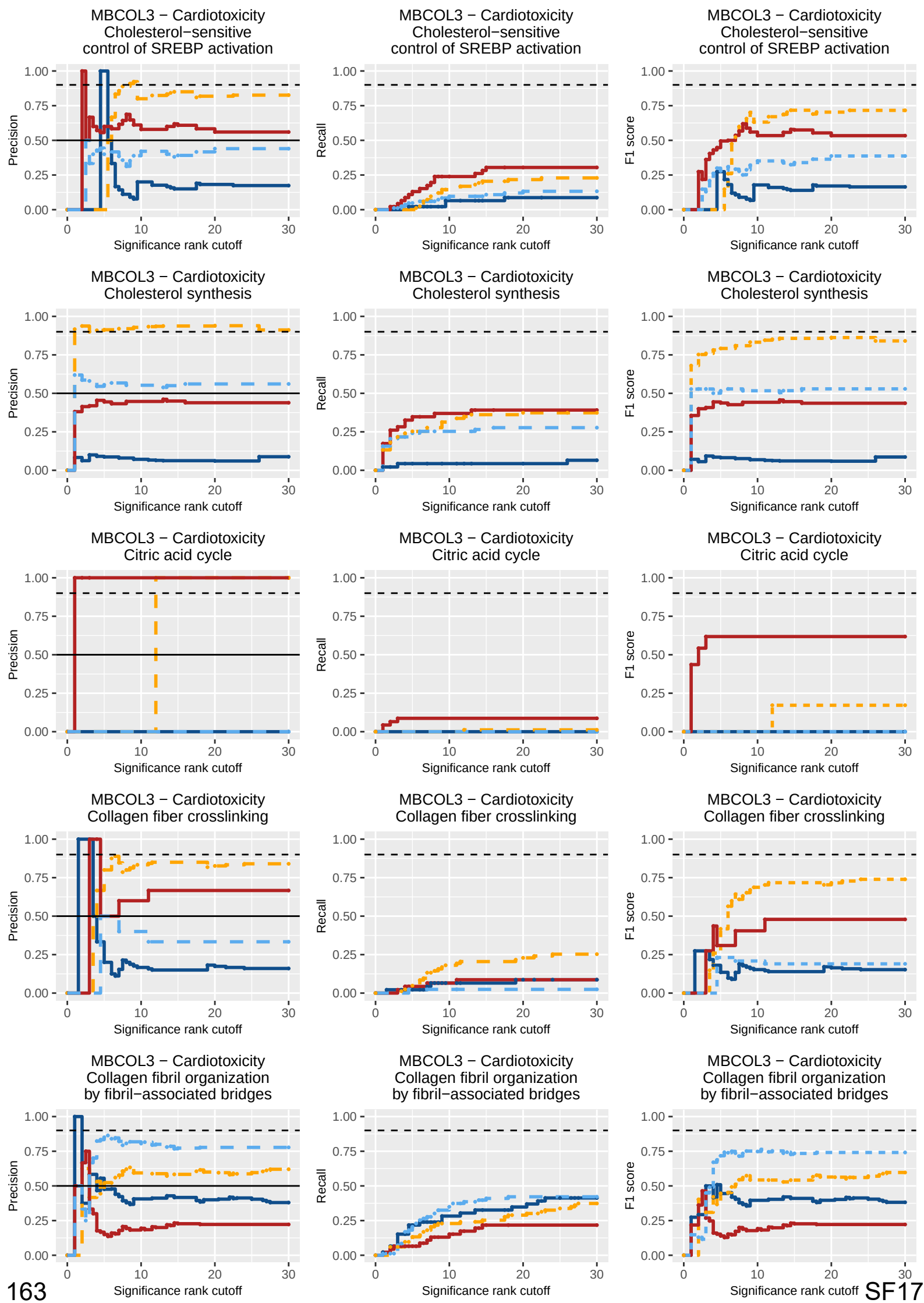
MBCOL3 − Cardiotoxicity
Cholesterol−sensitive
control of SREBP activation
MBCOL3 − Cardiotoxicity
Cholesterol synthesis
MBCOL3 − Cardiotoxicity
Citric acid cycle
MBCOL3 − Cardiotoxicity
Collagen fiber crosslinking
MBCOL3 − Cardiotoxicity
Collagen fibril organization
by fibril−associated bridges
Precision
Recall
F1 score
Significance rank cutoff
0.00
0.25
0.50
0.75
1.00
0
10
20
30

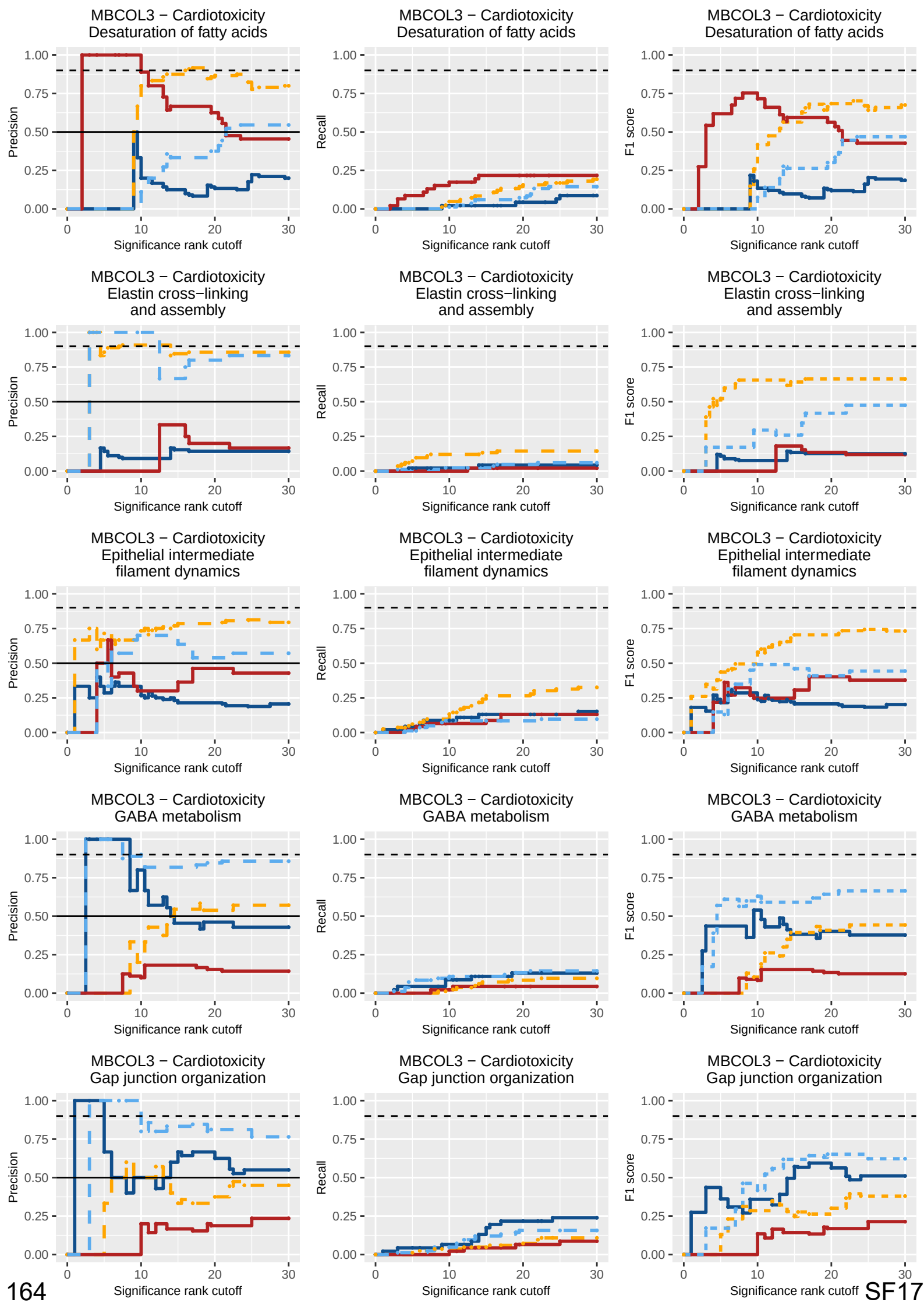
MBCOL3 − Cardiotoxicity
Desaturation of fatty acids
Precision
Recall
F1 score
Significance rank cutoff
MBCOL3 − Cardiotoxicity
Elastin cross−linking
and assembly
MBCOL3 − Cardiotoxicity
Epithelial intermediate
filament dynamics
MBCOL3 − Cardiotoxicity
GABA metabolism
MBCOL3 − Cardiotoxicity
Gap junction organization

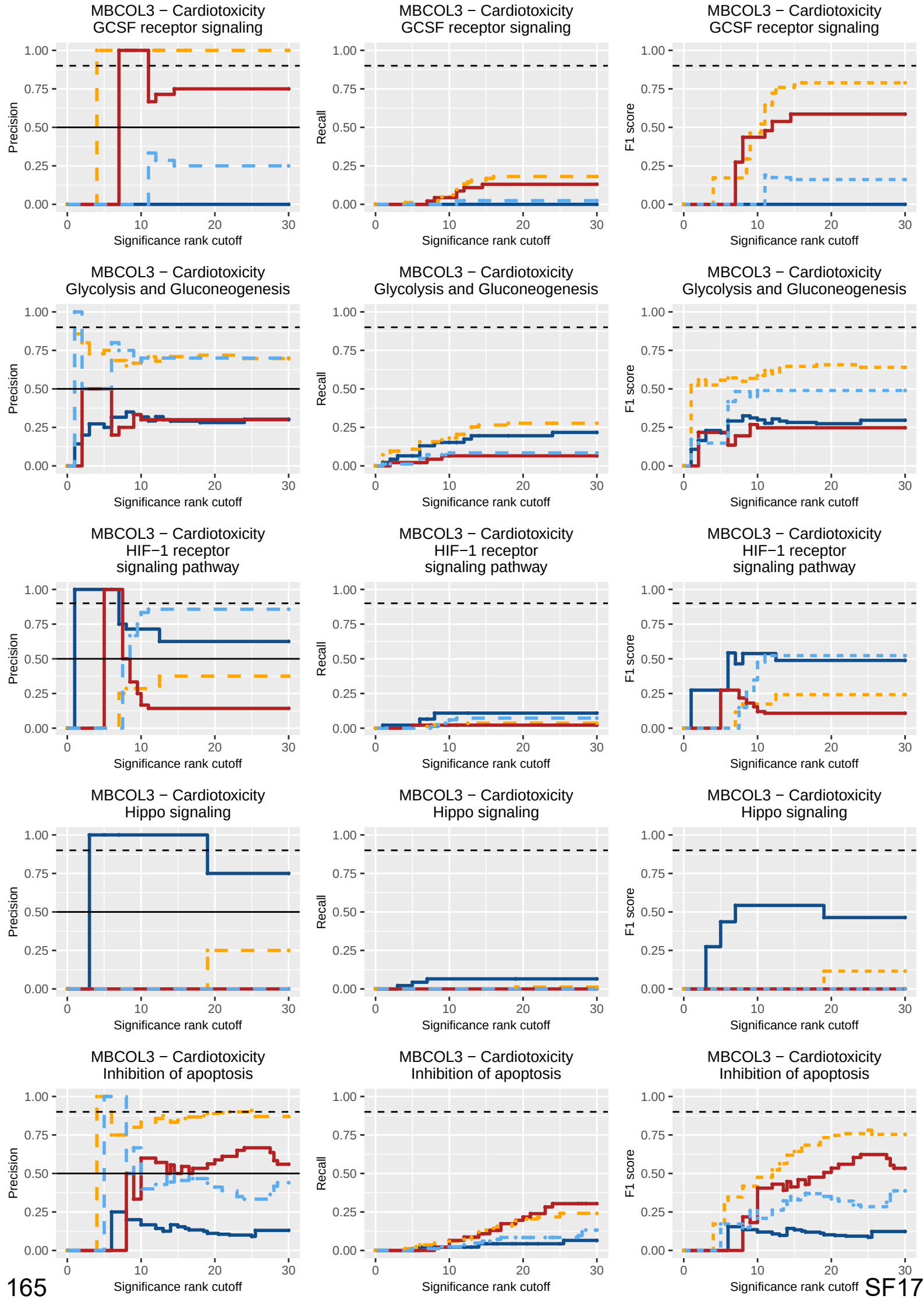
MBCOL3 − Cardiotoxicity
GCSF receptor signaling
MBCOL3 − Cardiotoxicity
GCSF receptor signaling
MBCOL3 − Cardiotoxicity
GCSF receptor signaling
MBCOL3 − Cardiotoxicity
Glycolysis and Gluconeogenesis
MBCOL3 − Cardiotoxicity
Glycolysis and Gluconeogenesis
MBCOL3 − Cardiotoxicity
Glycolysis and Gluconeogenesis
MBCOL3 − Cardiotoxicity
HIF−1 receptor
signaling pathway
MBCOL3 − Cardiotoxicity
HIF−1 receptor
signaling pathway
MBCOL3 − Cardiotoxicity
HIF−1 receptor
signaling pathway
MBCOL3 − Cardiotoxicity
Hippo signaling
MBCOL3 − Cardiotoxicity
Hippo signaling
MBCOL3 − Cardiotoxicity
Hippo signaling
MBCOL3 − Cardiotoxicity
Inhibition of apoptosis
MBCOL3 − Cardiotoxicity
Inhibition of apoptosis
MBCOL3 − Cardiotoxicity
Inhibition of apoptosis
Precision
Recall
F1 score
Significance rank cutoff
0.00
0.25
0.50
0.75
1.00
0
10
20
30

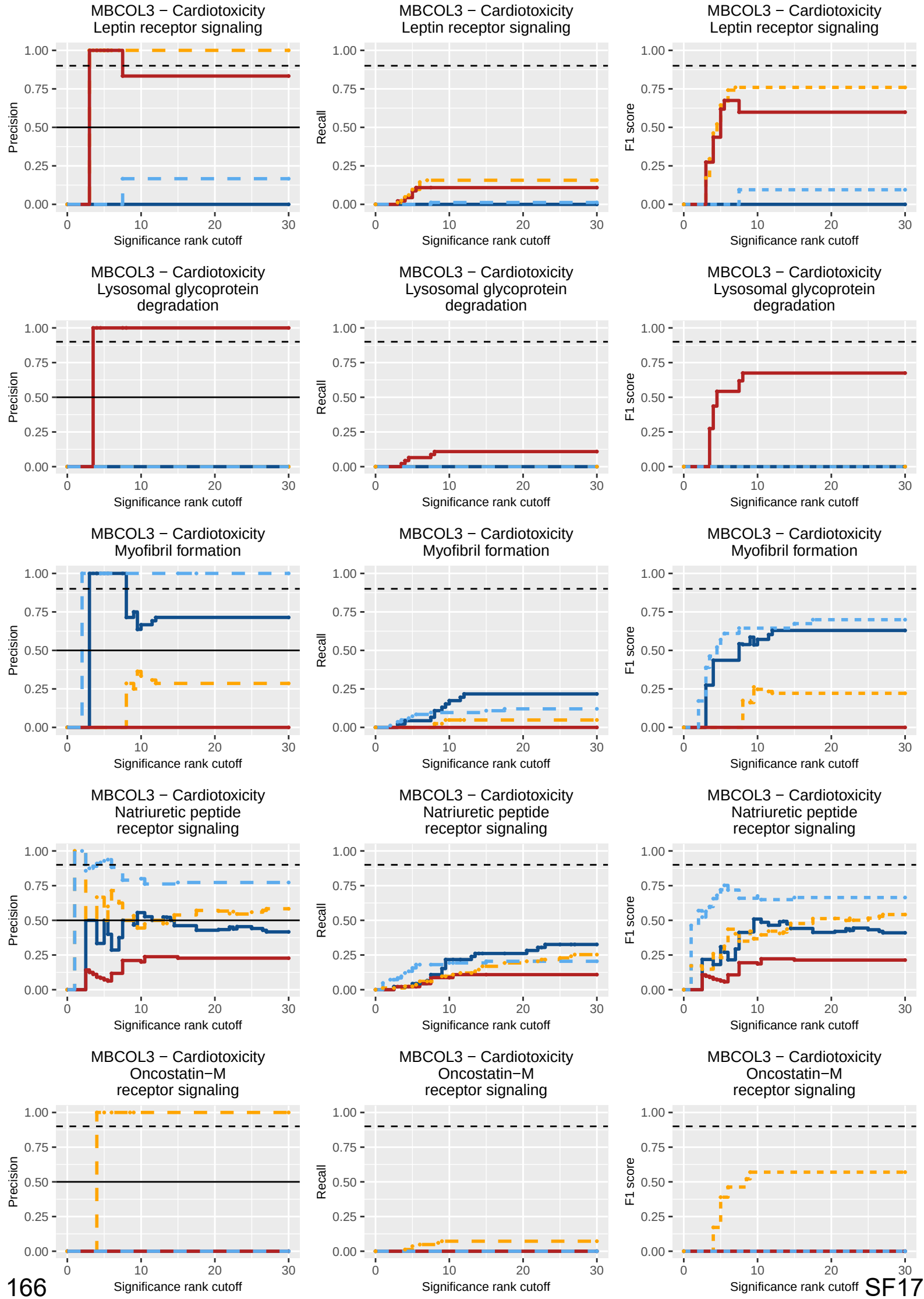
MBCOL3 − Cardiotoxicity
Leptin receptor signaling
Precision
Recall
F1 score
Significance rank cutoff
MBCOL3 − Cardiotoxicity
Lysosomal glycoprotein degradation
MBCOL3 − Cardiotoxicity
Myofibril formation
MBCOL3 − Cardiotoxicity
Natriuretic peptide receptor signaling
MBCOL3 − Cardiotoxicity
Oncostatin−M receptor signaling
0.00
0.25
0.50
0.75
1.00
0
10
20
30

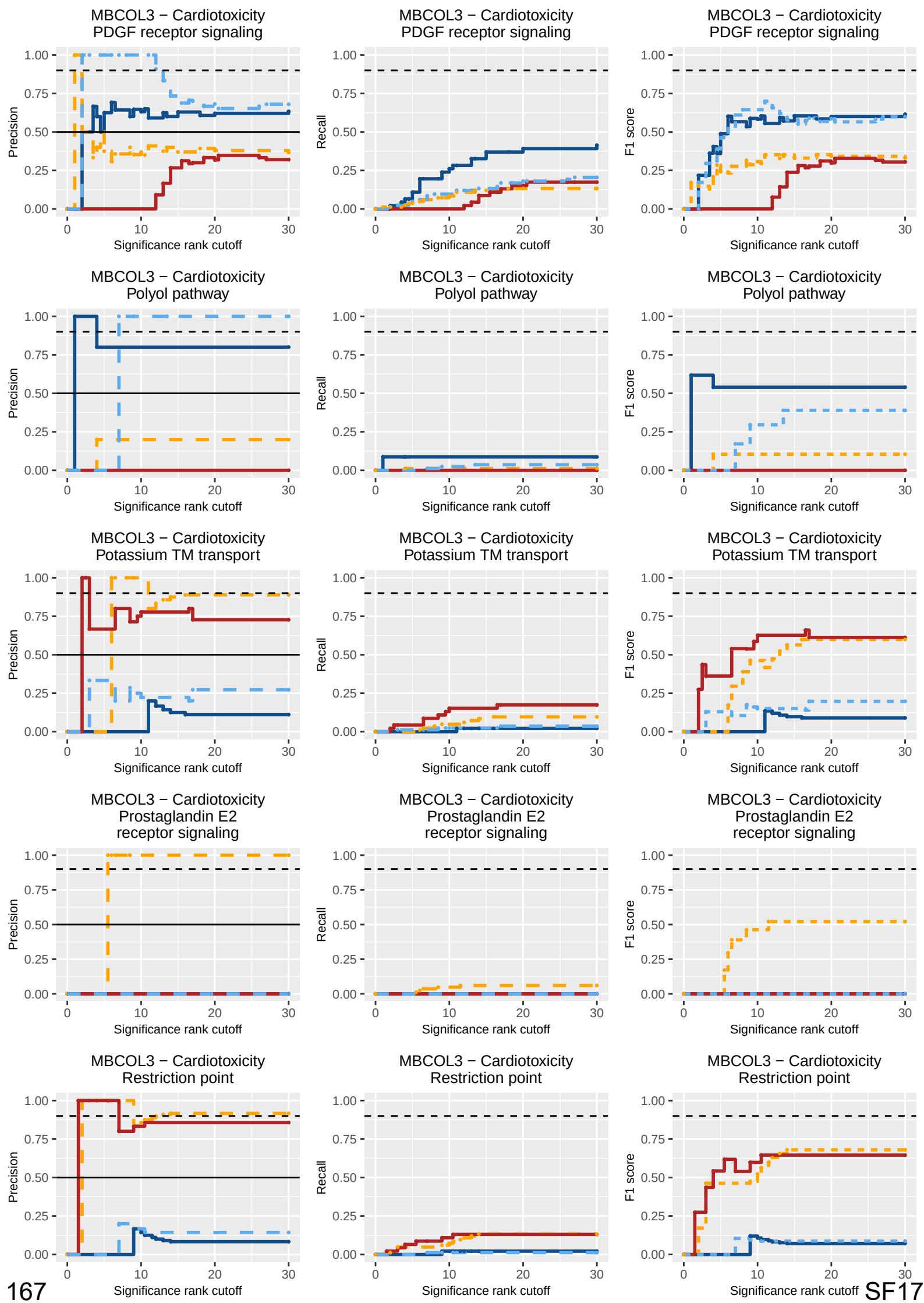
MBCOL3 − Cardiotoxicity
PDGF receptor signaling
Precision
Recall
F1 score
Significance rank cutoff
MBCOL3 − Cardiotoxicity
Polyol pathway
MBCOL3 − Cardiotoxicity
Potassium TM transport
MBCOL3 − Cardiotoxicity
Prostaglandin E2
receptor signaling
MBCOL3 − Cardiotoxicity
Restriction point
0.00
0.25
0.50
0.75
1.00
0
10
20
30

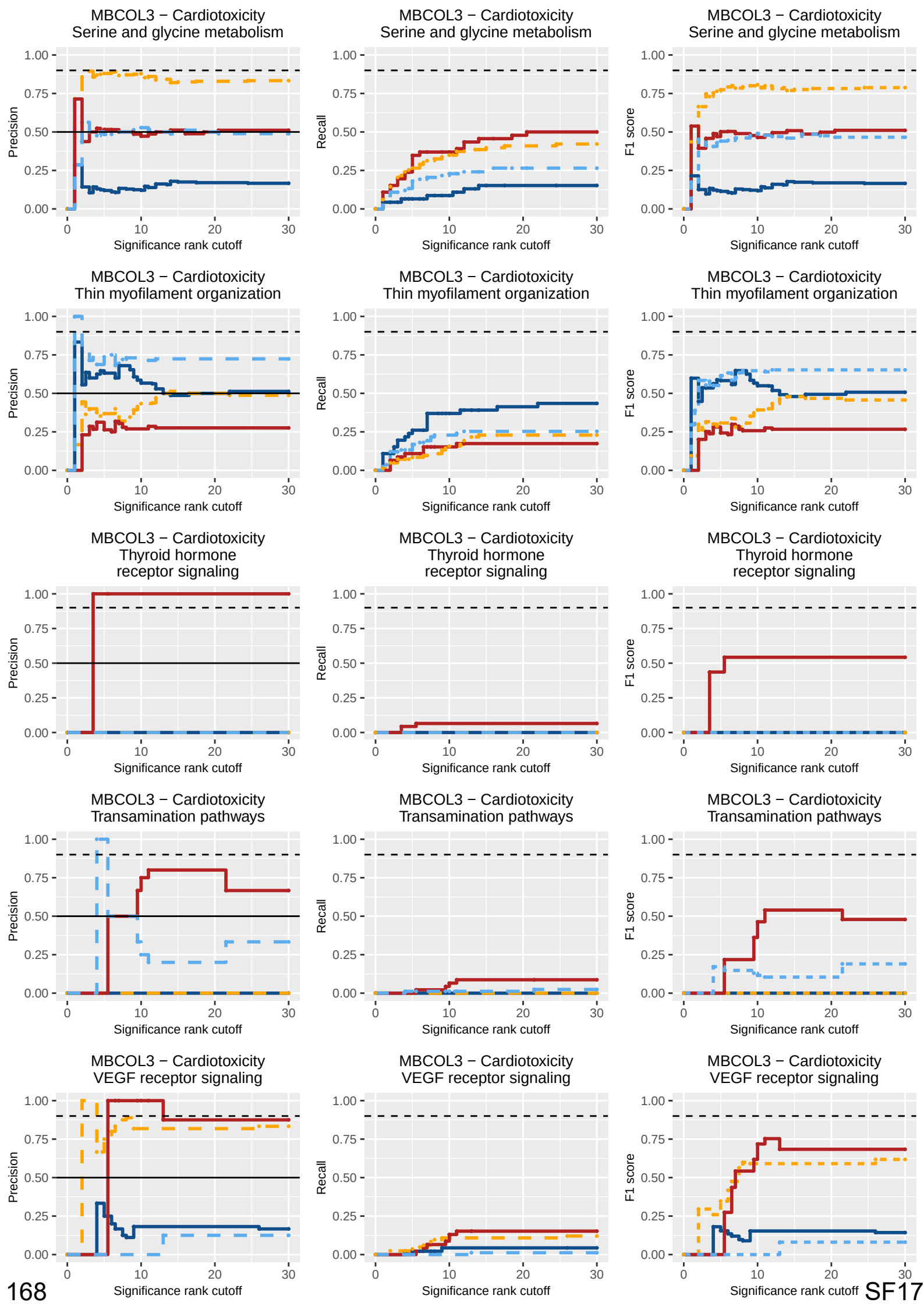
MBCOL3 − Cardiotoxicity
Serine and glycine metabolism
MBCOL3 − Cardiotoxicity
Thin myofilament organization
MBCOL3 − Cardiotoxicity
Thyroid hormone receptor signaling
MBCOL3 − Cardiotoxicity
Transamination pathways
MBCOL3 − Cardiotoxicity
VEGF receptor signaling
Precision
Recall
F1 score
Significance rank cutoff
0.00
0.25
0.50
0.75
1.00
0
10
20
30

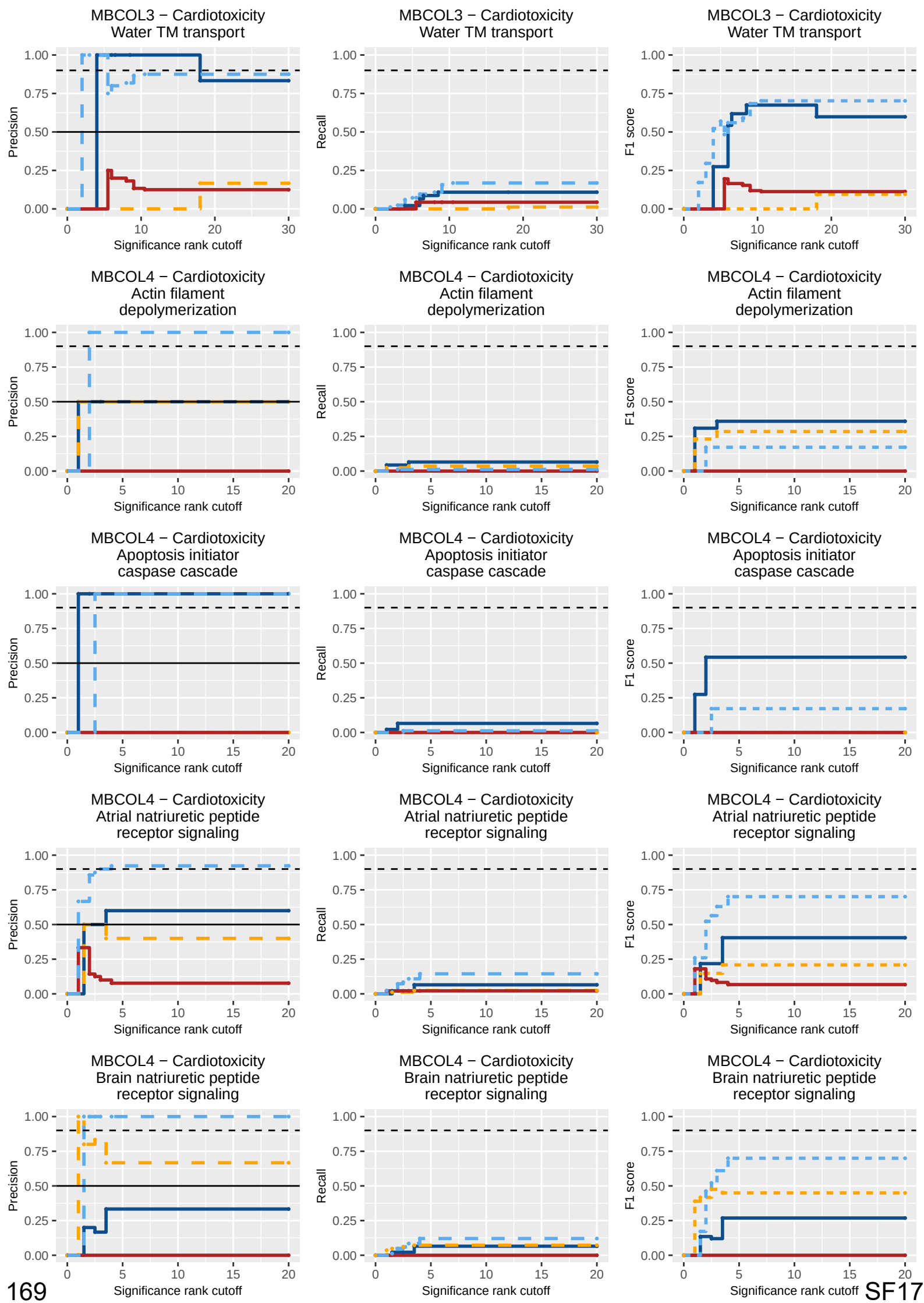
MBCOL3 − Cardiotoxicity
Water TM transport
MBCOL3 − Cardiotoxicity
Water TM transport
MBCOL3 − Cardiotoxicity
Water TM transport
MBCOL4 − Cardiotoxicity
Actin filament
depolymerization
MBCOL4 − Cardiotoxicity
Actin filament
depolymerization
MBCOL4 − Cardiotoxicity
Actin filament
depolymerization
MBCOL4 − Cardiotoxicity
Apoptosis initiator
caspase cascade
MBCOL4 − Cardiotoxicity
Apoptosis initiator
caspase cascade
MBCOL4 − Cardiotoxicity
Apoptosis initiator
caspase cascade
MBCOL4 − Cardiotoxicity
Atrial natriuretic peptide
receptor signaling
MBCOL4 − Cardiotoxicity
Atrial natriuretic peptide
receptor signaling
MBCOL4 − Cardiotoxicity
Atrial natriuretic peptide
receptor signaling
MBCOL4 − Cardiotoxicity
Brain natriuretic peptide
receptor signaling
MBCOL4 − Cardiotoxicity
Brain natriuretic peptide
receptor signaling
MBCOL4 − Cardiotoxicity
Brain natriuretic peptide
receptor signaling
Precision
Recall
F1 score
Significance rank cutoff
0.00
0.25
0.50
0.75
1.00
0
5
10
15
20
30

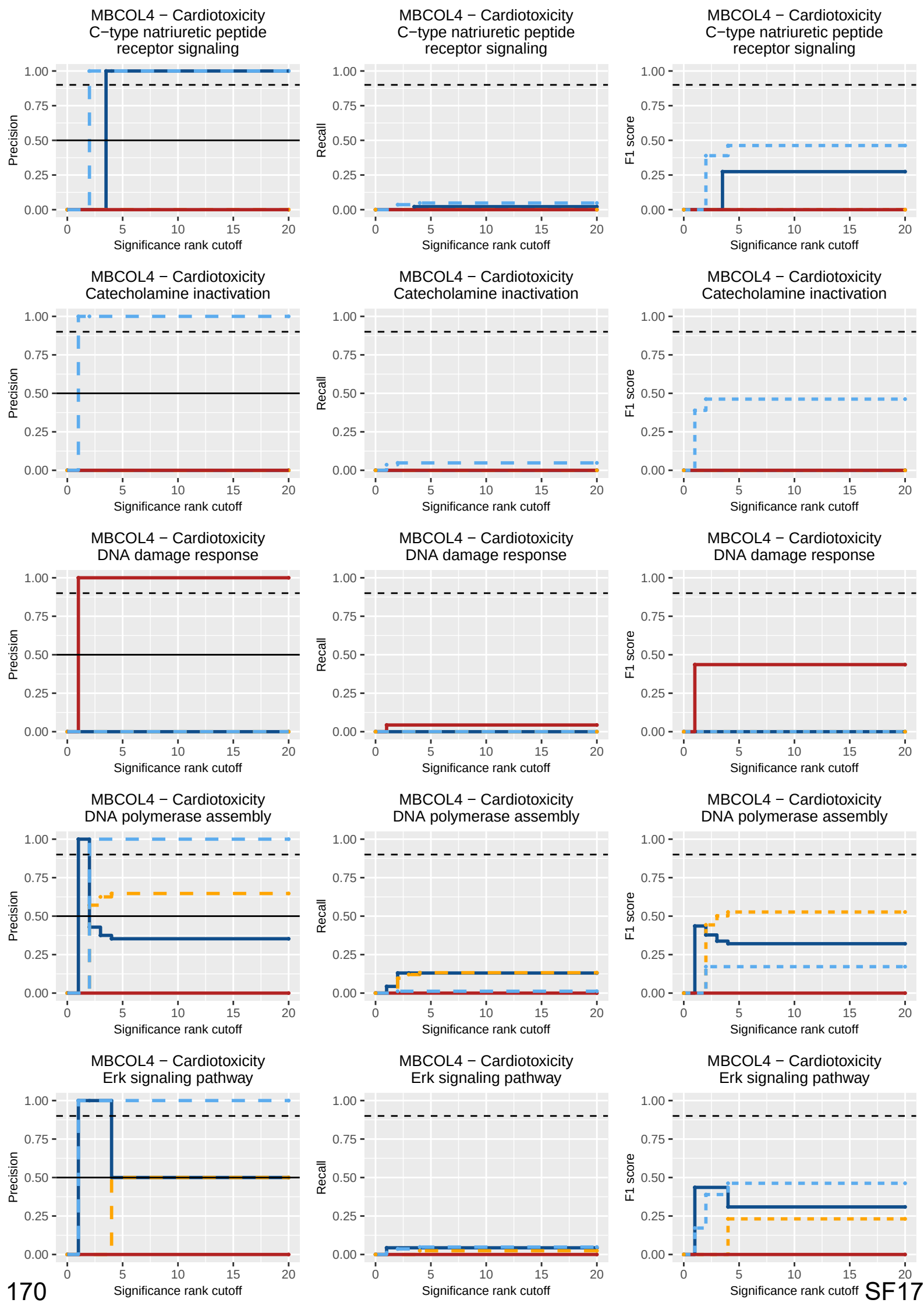
MBCOL4 − Cardiotoxicity
C−type natriuretic peptide receptor signaling
Precision
Recall
F1 score
Significance rank cutoff
MBCOL4 − Cardiotoxicity
Catecholamine inactivation
MBCOL4 − Cardiotoxicity
DNA damage response
MBCOL4 − Cardiotoxicity
DNA polymerase assembly
MBCOL4 − Cardiotoxicity
Erk signaling pathway

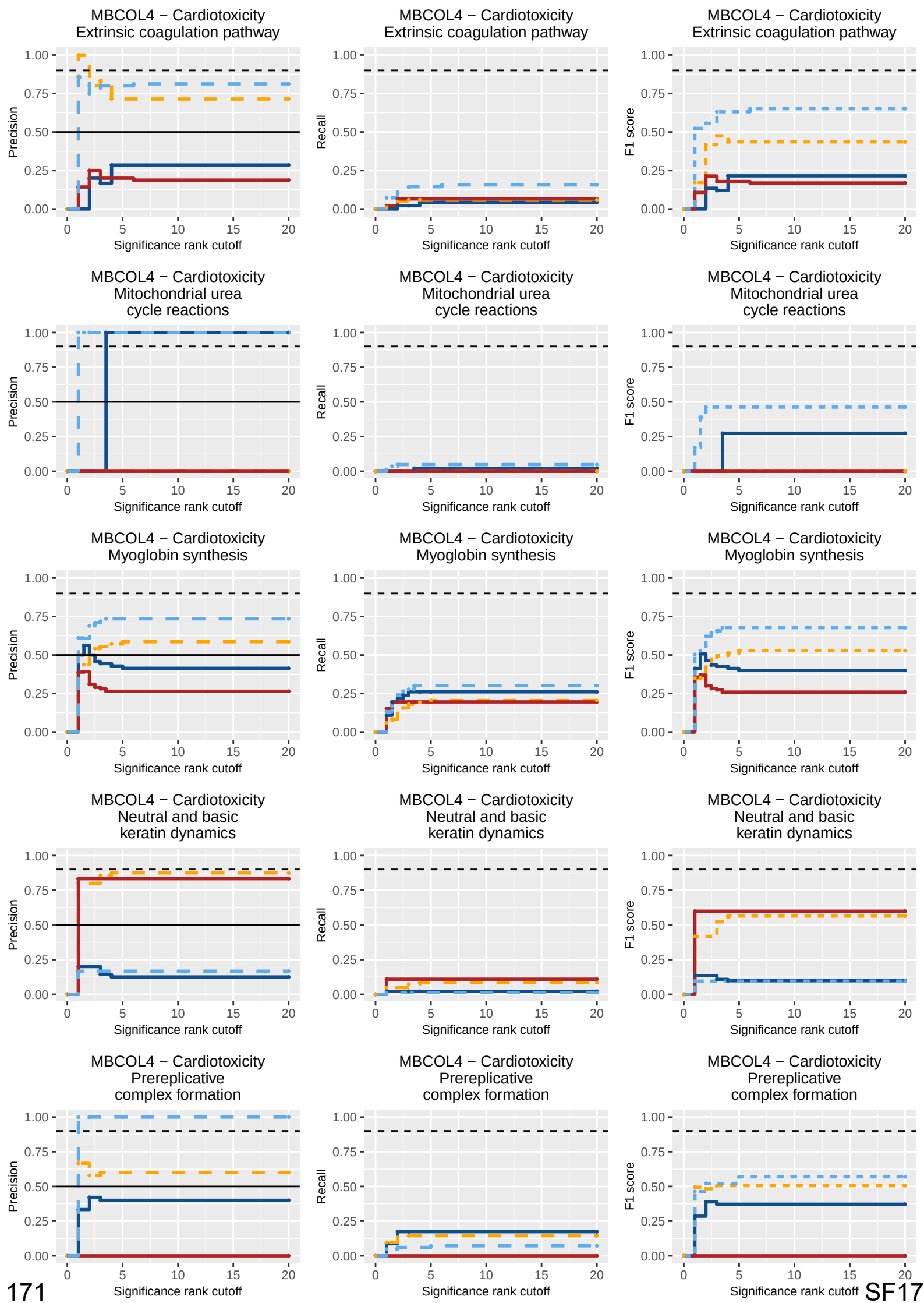
MBCOL4 − Cardiotoxicity
Extrinsic coagulation pathway
Precision
Recall
F1 score
Significance rank cutoff
MBCOL4 − Cardiotoxicity
Mitochondrial urea cycle reactions
MBCOL4 − Cardiotoxicity
Myoglobin synthesis
MBCOL4 − Cardiotoxicity
Neutral and basic keratin dynamics
MBCOL4 − Cardiotoxicity
Prereplicative complex formation

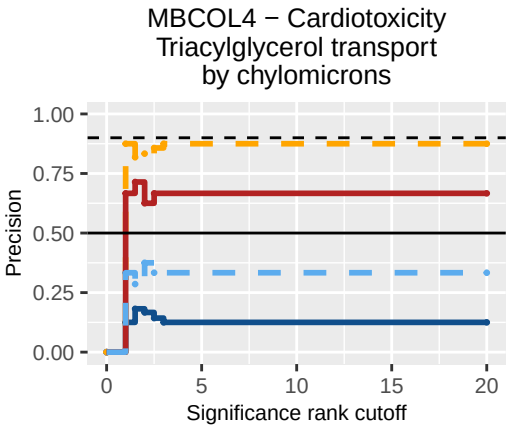
MBCOL4 − Cardiotoxicity
Triacylglycerol transport
by chylomicrons
Precision
1.00
0.75
0.50
0.25
0.00
0
5
10
15
20
Significance rank cutoff

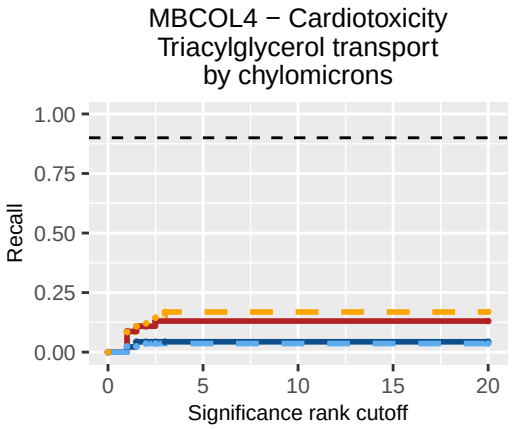
MBCOL4 − Cardiotoxicity
Triacylglycerol transport
by chylomicrons
Recall
1.00
0.75
0.50
0.25
0.00
0
5
10
15
20
Significance rank cutoff

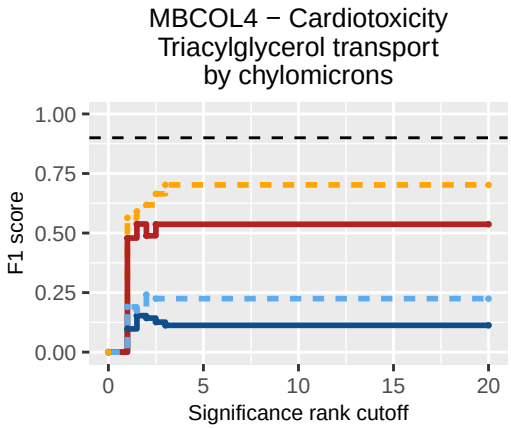
MBCOL4 − Cardiotoxicity
Triacylglycerol transport
by chylomicrons
F1 score
1.00
0.75
0.50
0.25
0.00
0
5
10
15
20
Significance rank cutoff

Supplementary Figure 17. F1 score and Area under the Curve statistics. At each significance rank cutoff we counted how many cardiotoxic or non-cardiotoxic TKIs up- or down-regulate a particular SCP with a significance rank below or equal to the current cutoff. Results were used to calculate precision, recall and F1 score (beta = 0.2) of each SCP at each rank to be either up- or downregulated by either the cardiotoxic or noncardiotoxic drugs. Shown are the results for the SCPs that our algorithm selected to be associated with a cardiotoxic or non-cardiotoxic response. See methods for description of the algorithm. Solid lines indicate results for the SCP, if up- (red) or downregulated (dark blue) by cardiotoxic TKIs, dashed lines indicate results for the SCP, if up- (light blue) or downregulated (orange) by non-cardiotoxic TKIs. Color combinations were selected to indicate if the higher (red, orange) or lower (dark blue, light blue) activity of an SCP favors a cardiotoxic response.

MBCOL1
dabrafenib
(is c.toxic: yes)

Upregulated

complete

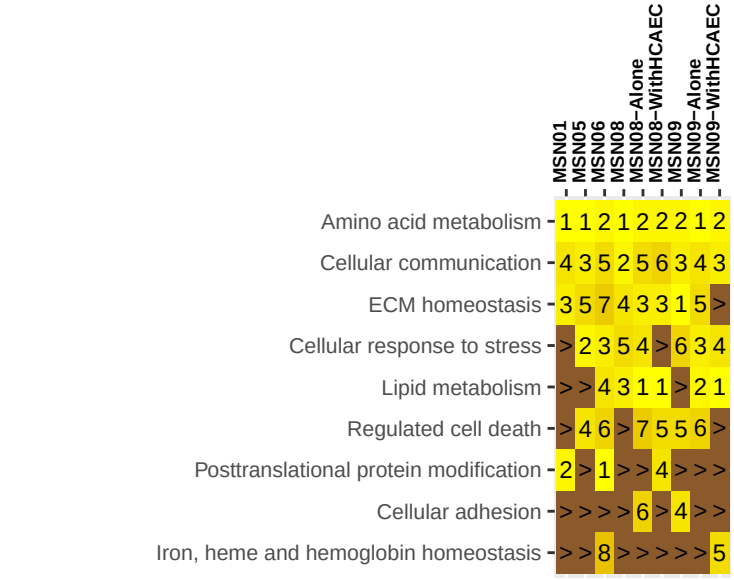

no1stSVD

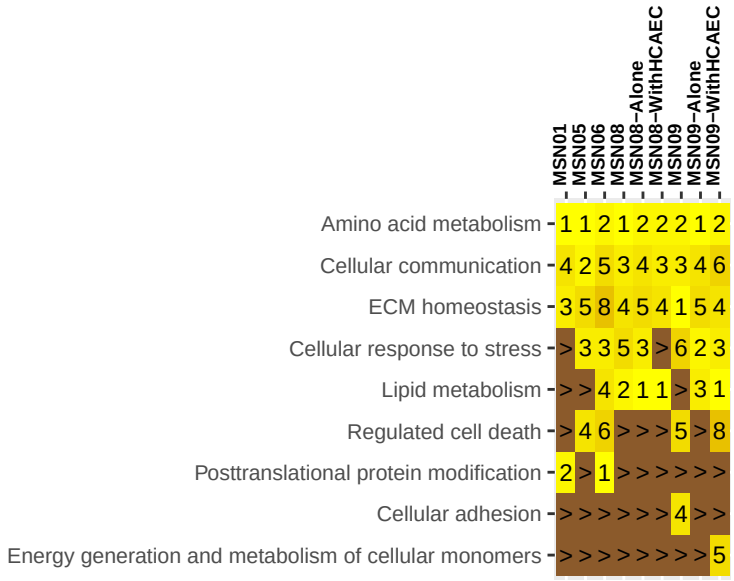

decomposed

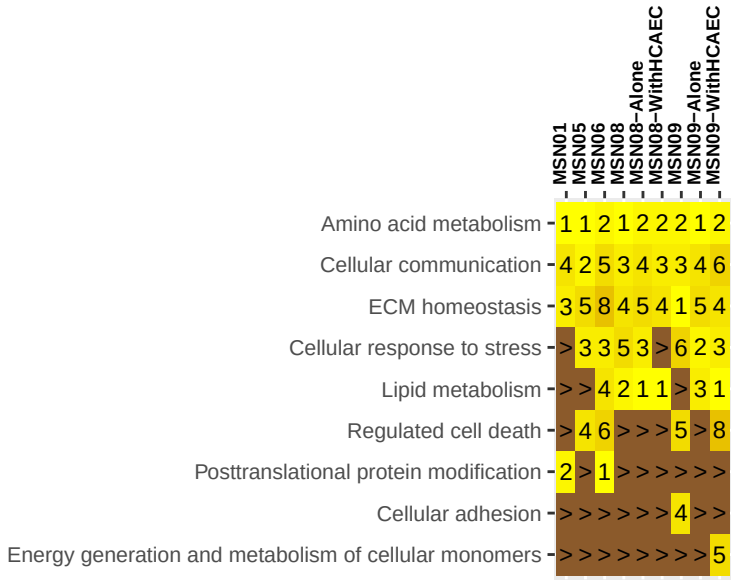

Downregulated

complete

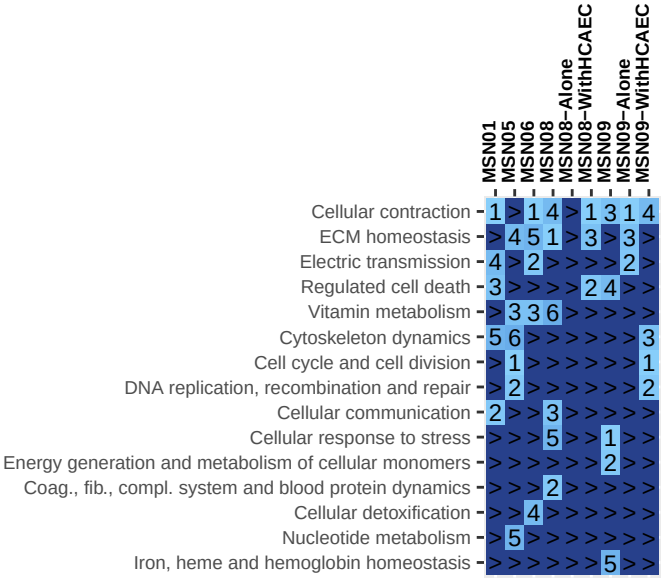

no1stSVD

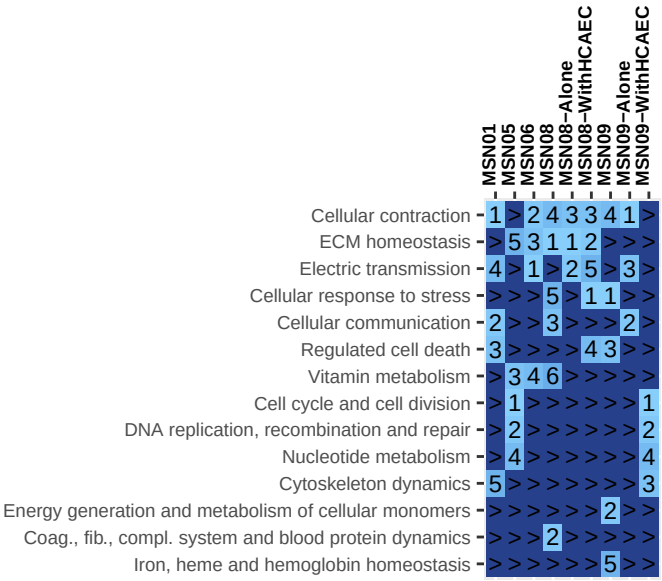

decomposed

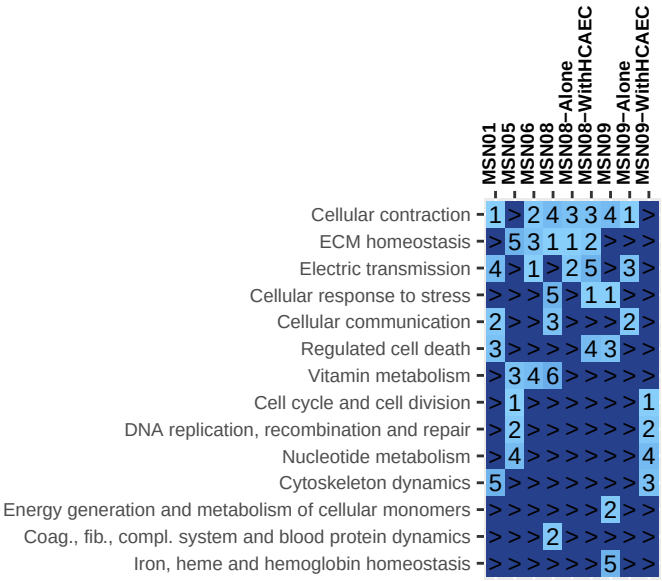

Supplementary Fig. 29A

MBCOL1
pazopanib
(is c.toxic: yes)

Upregulated

Downregulated

complete

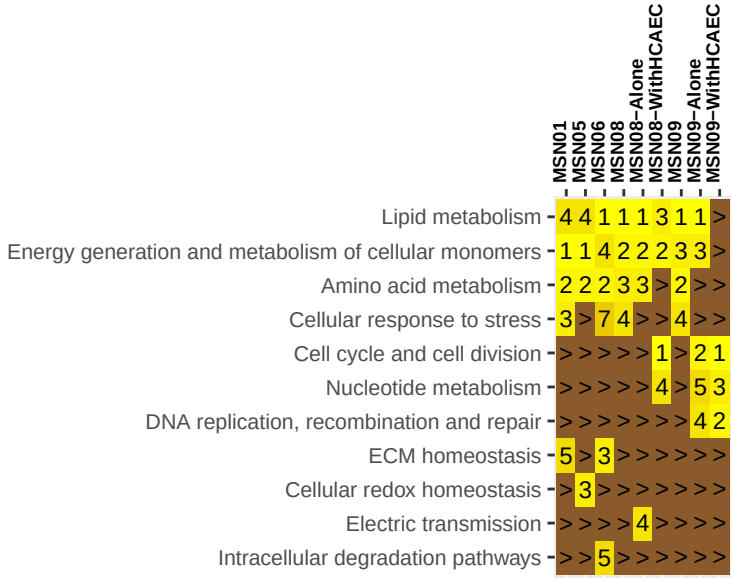

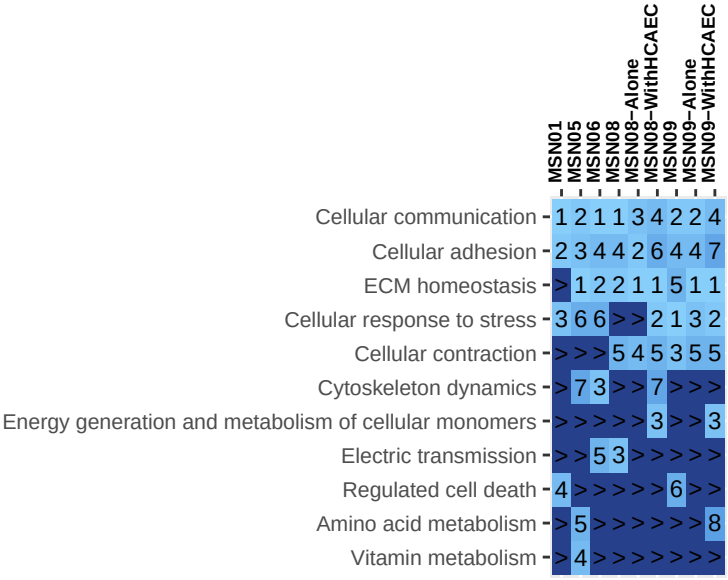

no1stSVD

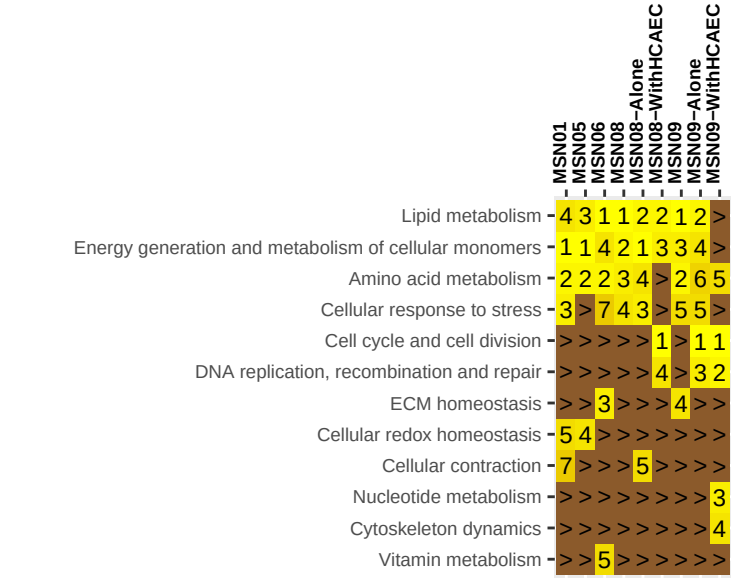

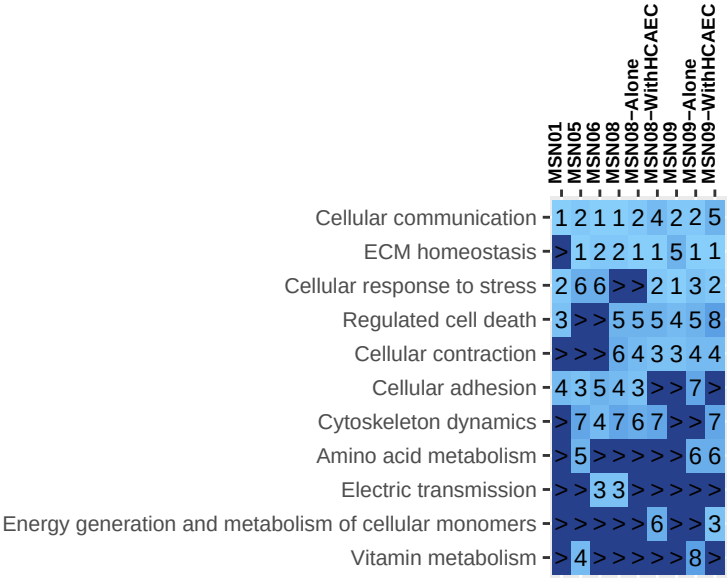

decomposed

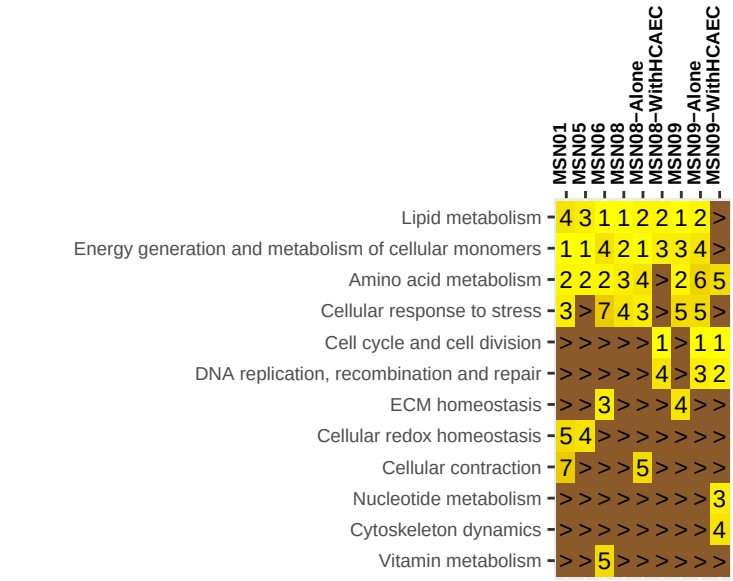

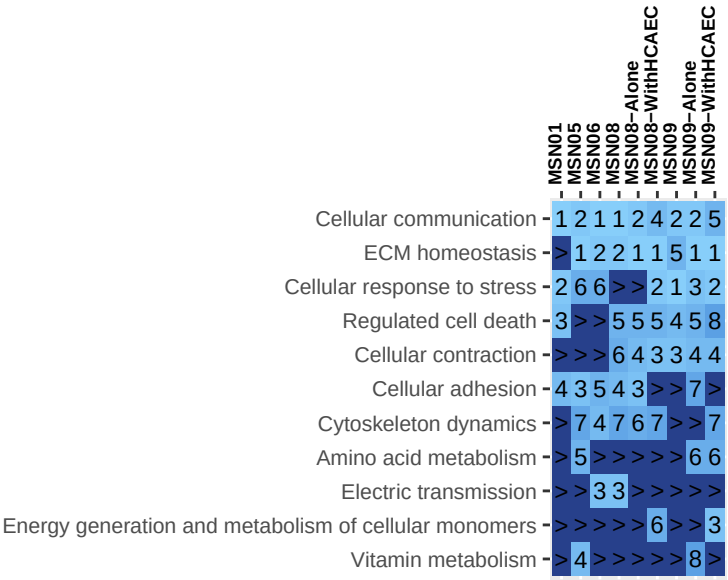

MBCOL2
dabrafenib
(is c.toxic: yes)

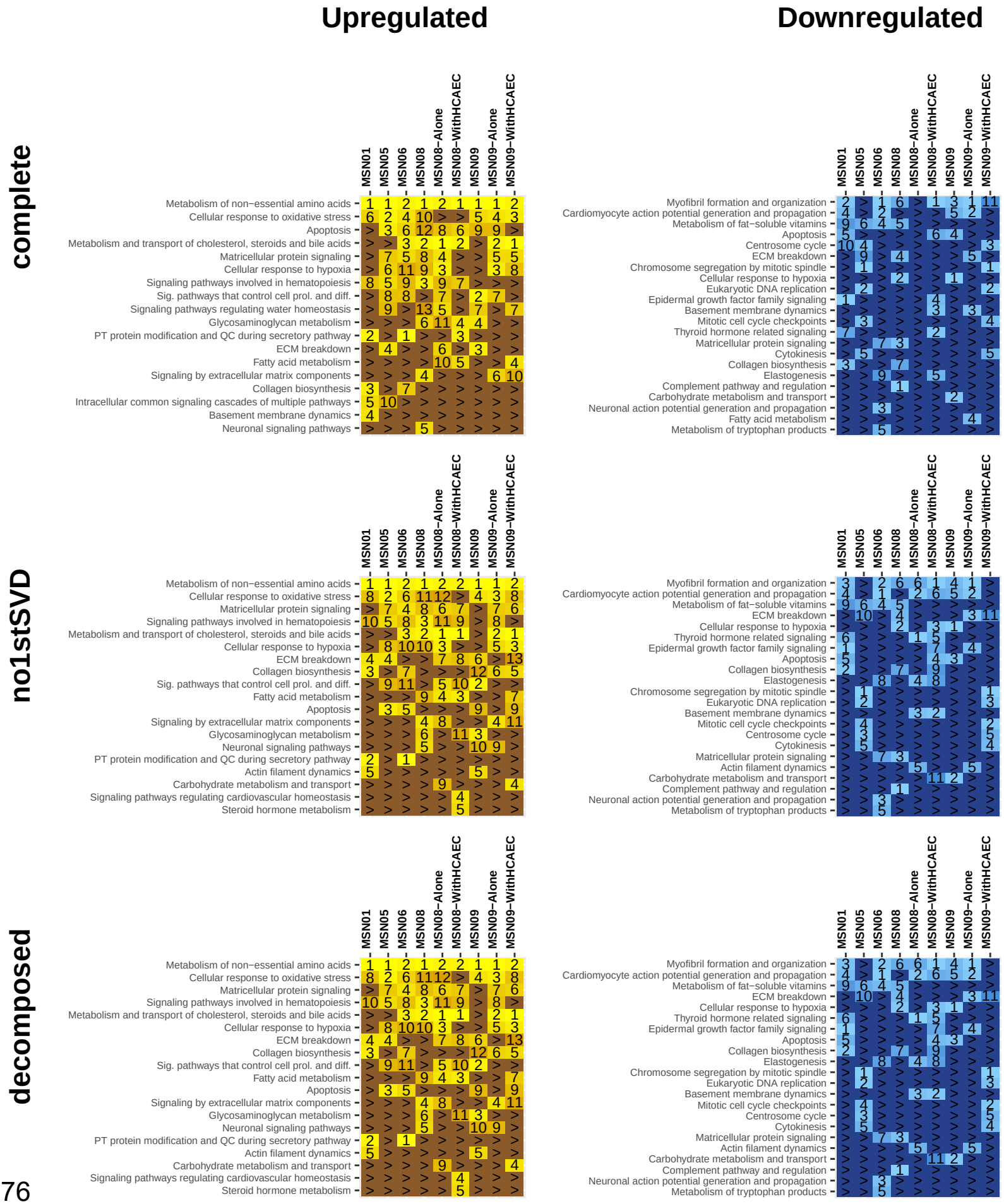

MBCOL2
pazopanib
(is c.toxic: yes)

Upregulated

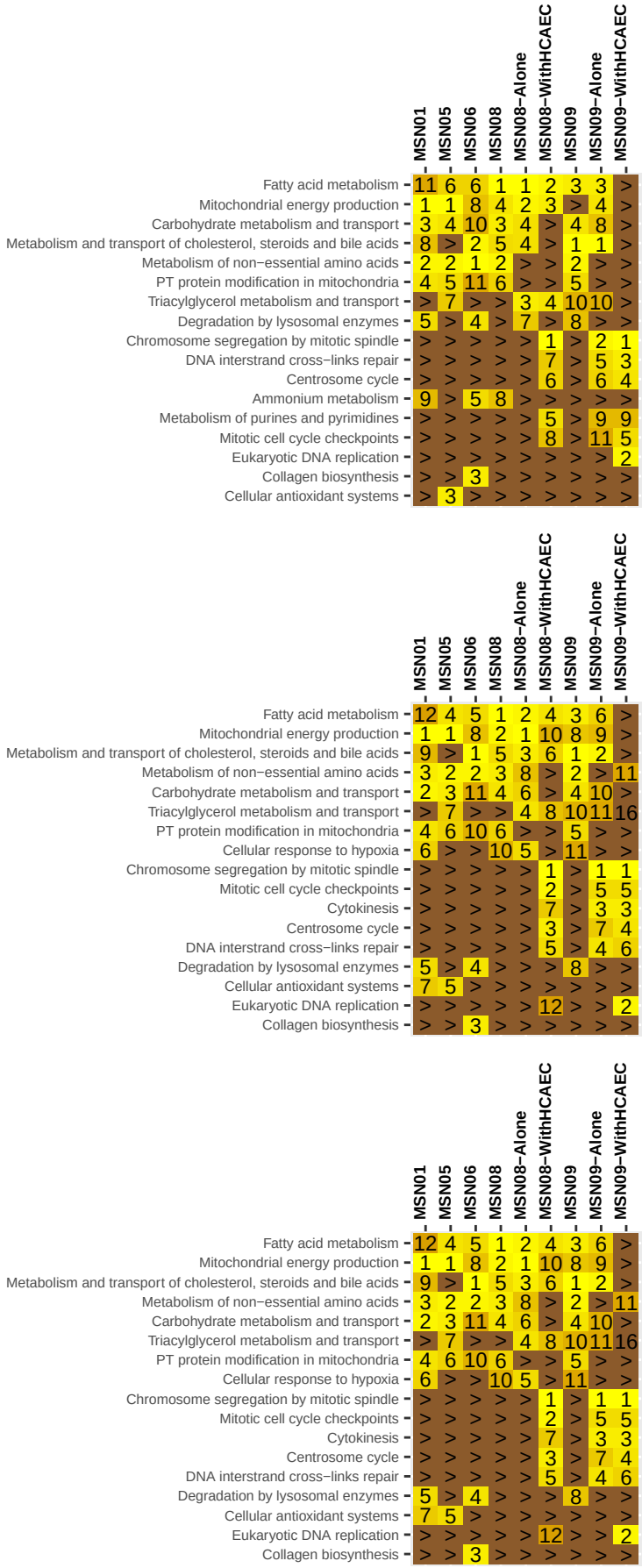

Downregulated

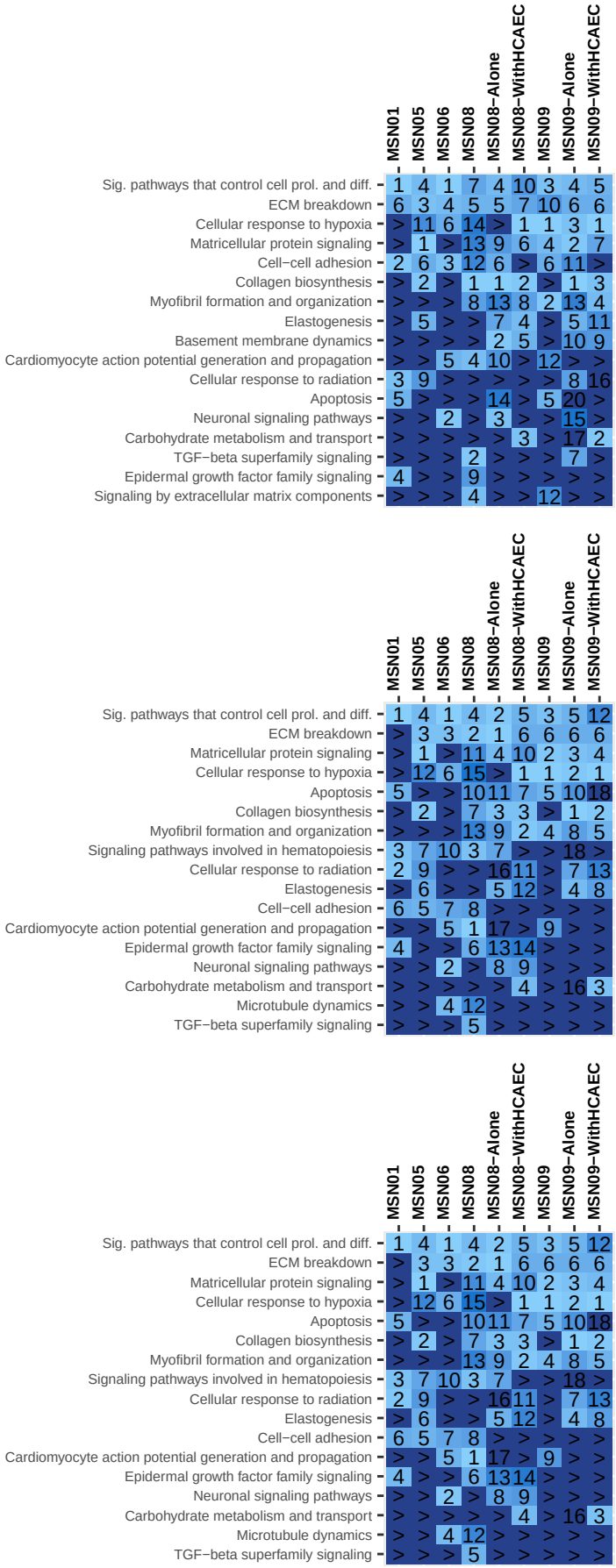

MBCOL3
dabrafenib
(is c.toxic: yes)

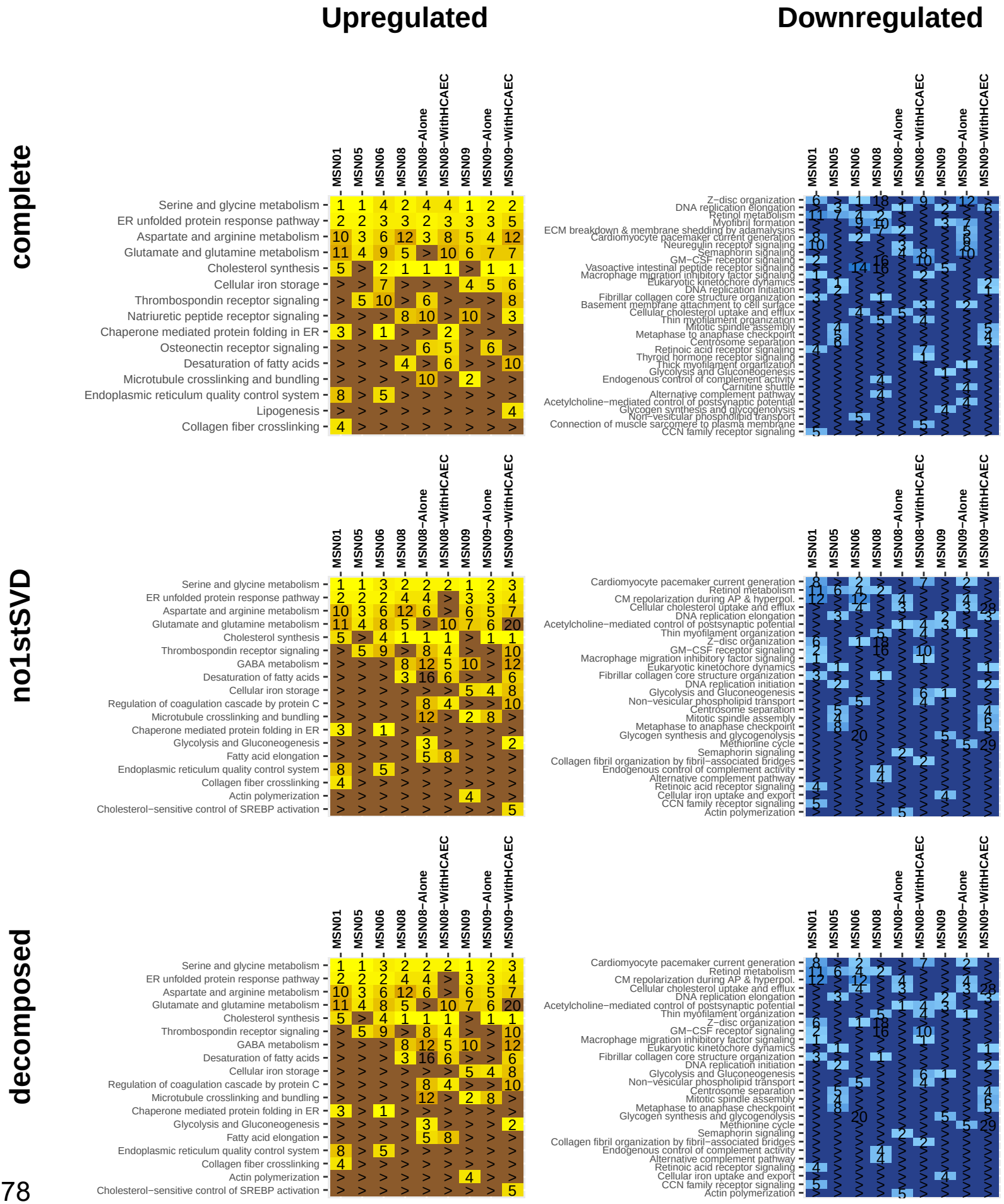

Supplementary Fig. 29C

MBCOL3
pazopanib
(is c.toxic: yes)

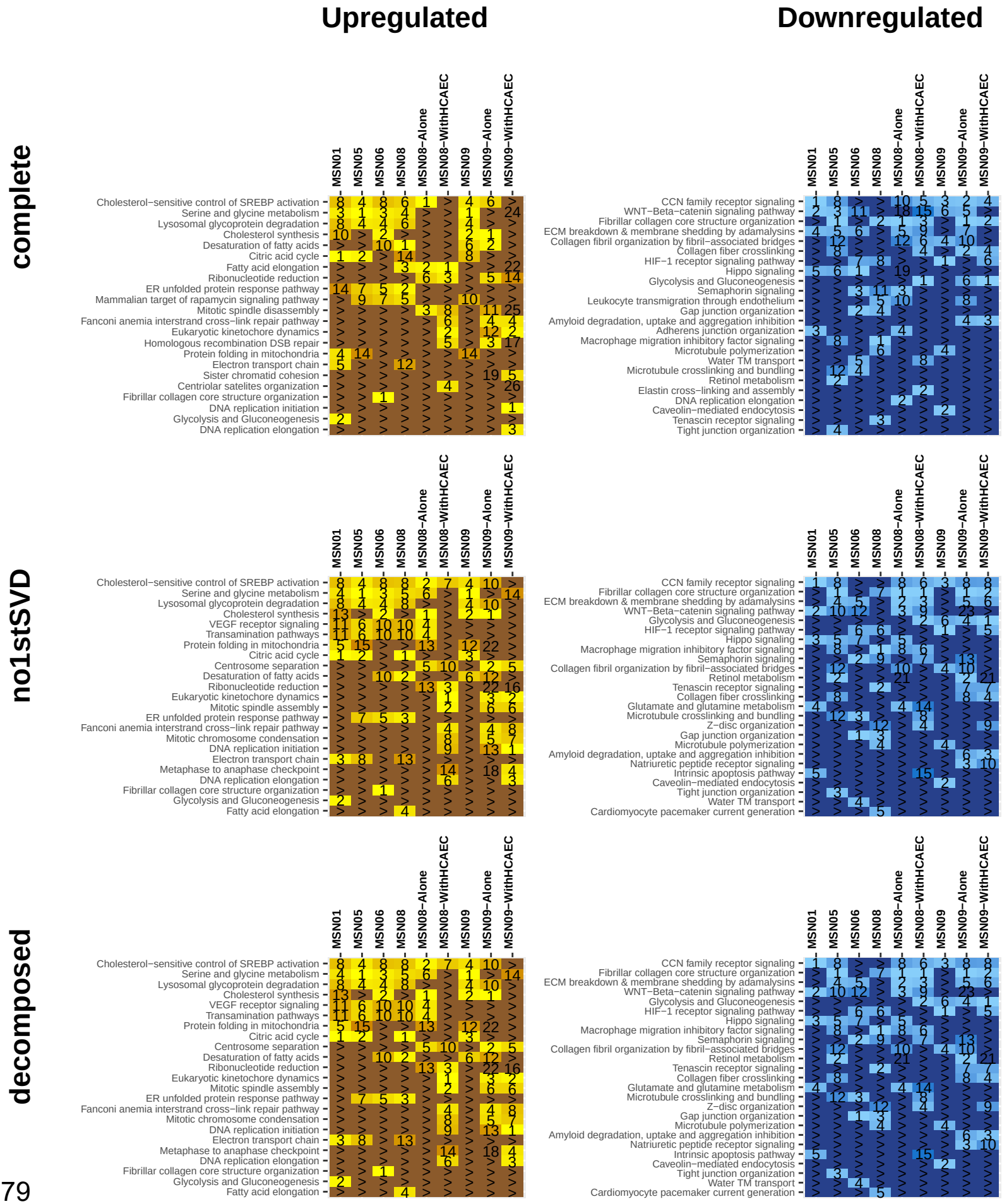

MBCOL4
dabrafenib
(is c.toxic: yes)

Upregulated

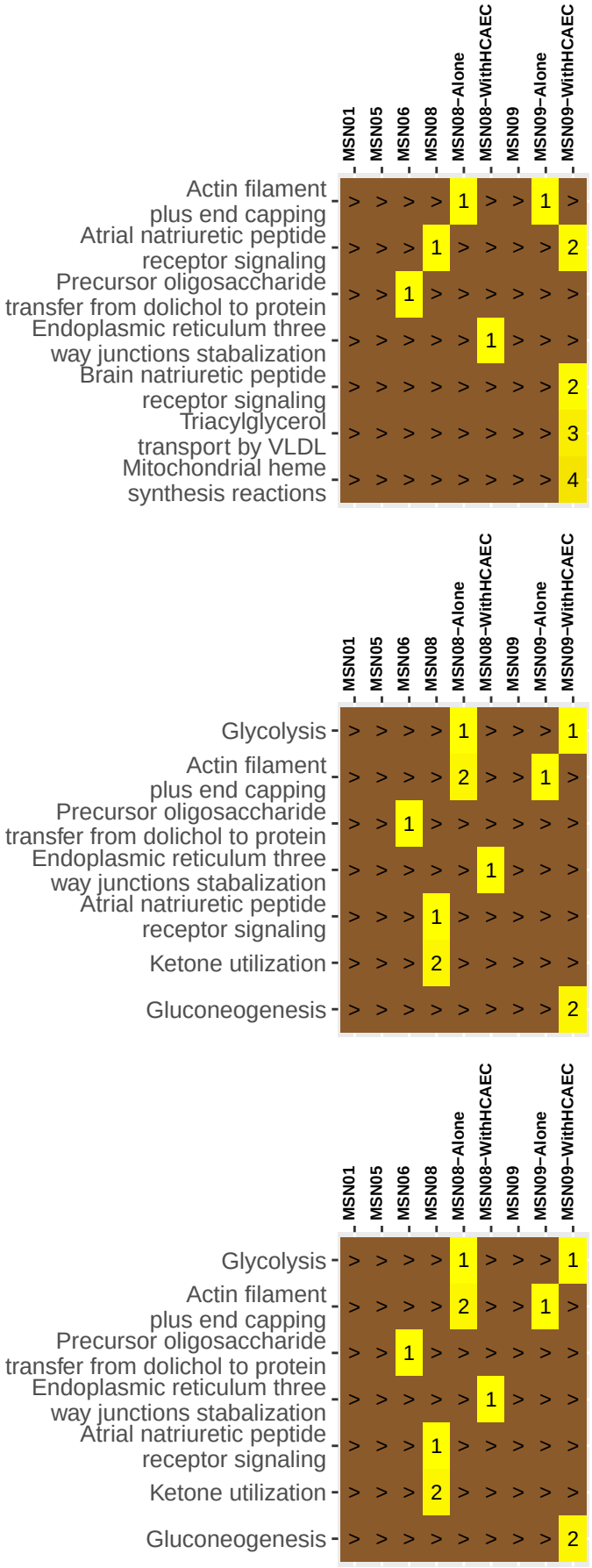

Downregulated

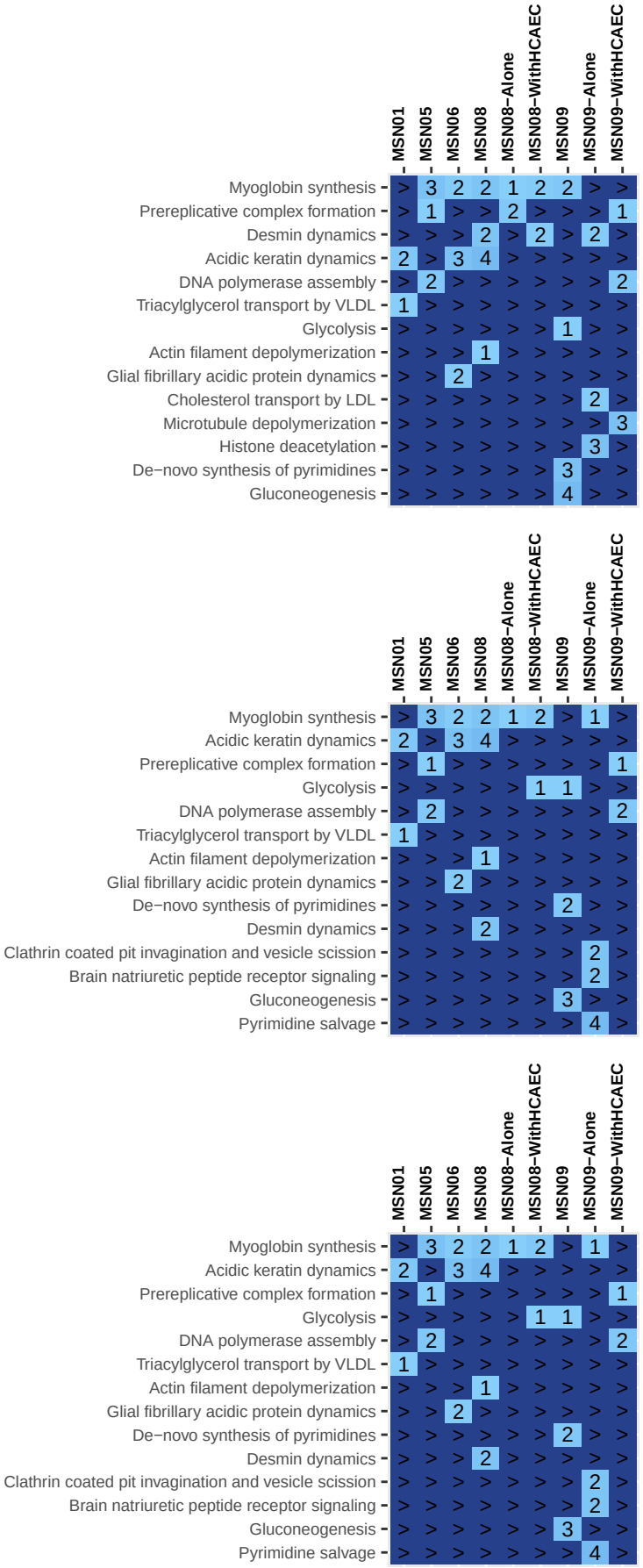

MBCOL4
pazopanib
(is c.toxic: yes)

Upregulated

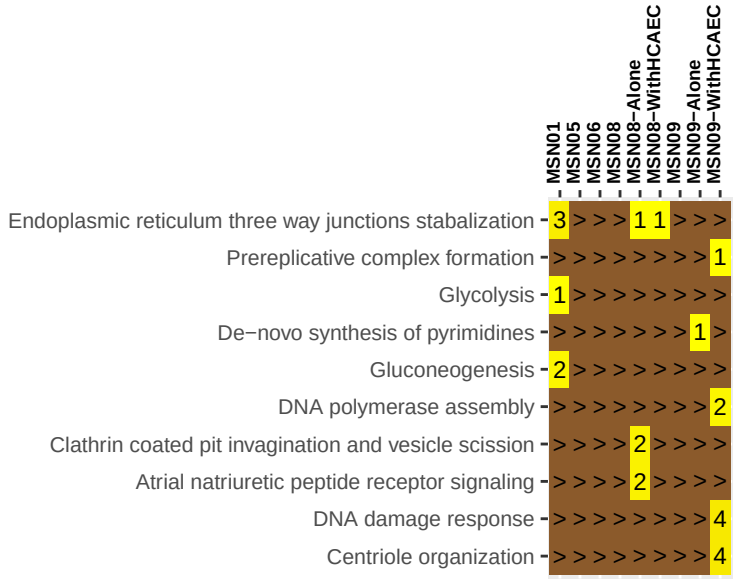

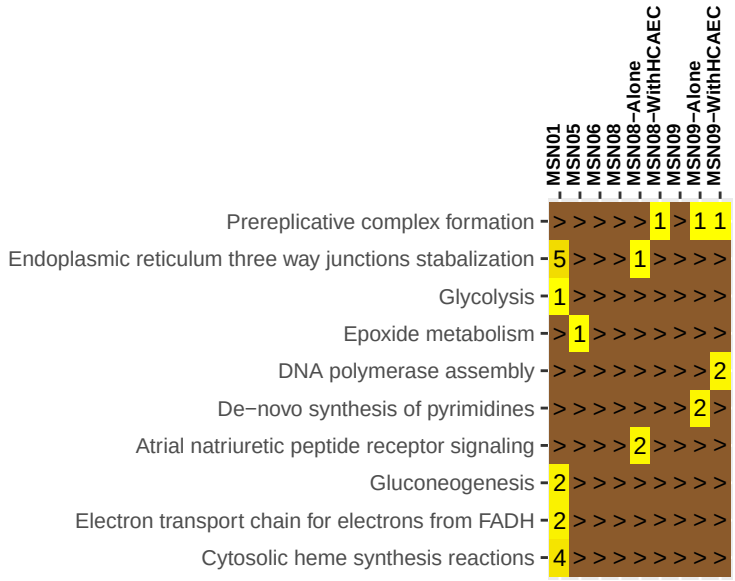

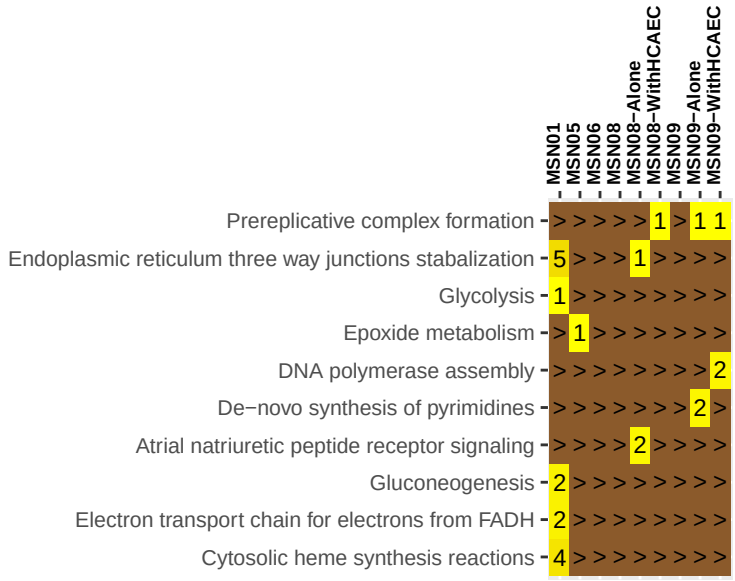

Downregulated

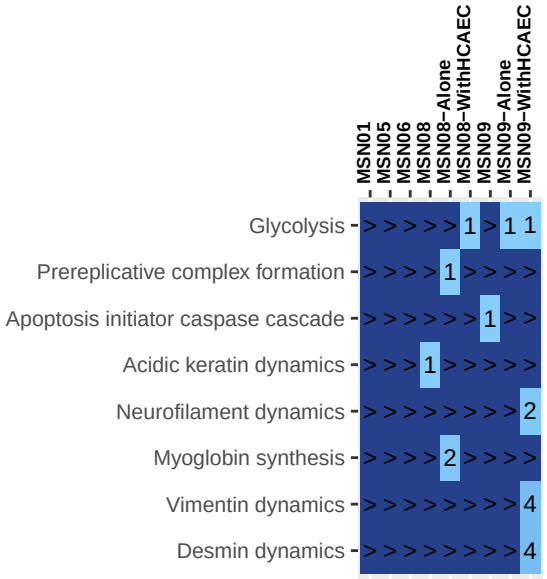

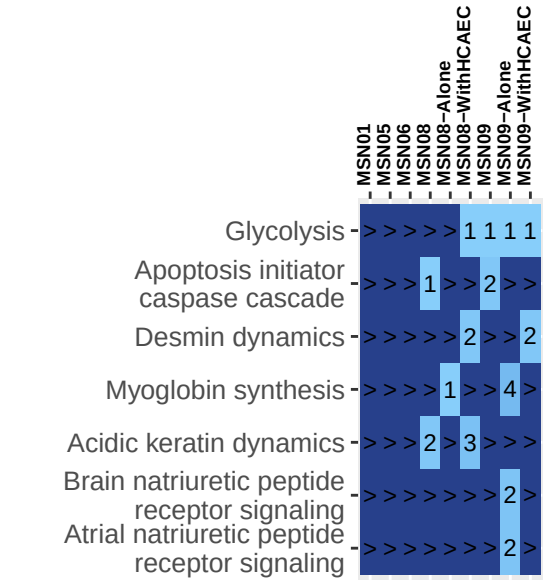

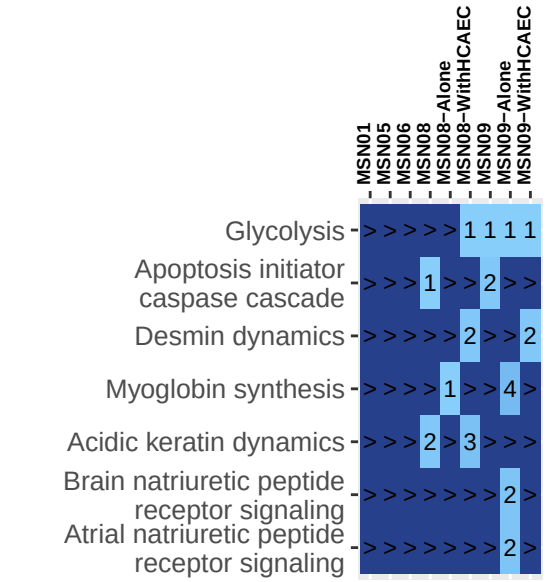

Supplementary Figure 29. Top Subcellular Processes predicted from complete gene expression profiles, after removal of first eigenarray and from drug-selective gene expression profiles of all dabrafenib or pazopanib-treated samples. **(A)** Complete, decomposed gene expression profiles and gene expression profiles after removal of the first eigenarray of the original and new dabrafenib or pazopanib treated samples were subjected to pathway enrichment analysis using the Molecular Biology of the Cell Ontology and Fisher's Exact Test to identify up- and downregulated subcellular processes (SCPs). Significant up- or downregulated **(B)** level-1, **(C)** -2, **(D)** -3 and **(E)** -4 SCPs (pvalue <= 0.05) were separately ranked by significance for each cell line/drug combination. SCPs predicted for each drug are shown if they are among the top five ranked SCPs for at least one cell line. Numbers indicate ranks, '>' indicates that an SCP was not predicted or predicted with a rank above 99. 'Alone' and 'With HCAEC' label additional datasets obtained without or with endothelial cell cocultures, respectively. Results for the original samples are also shown in Supplemental figure 14.

100 Herrmann, J. Adverse cardiac effects of cancer therapies: cardiotoxicity and arrhythmia. *Nat Rev Cardiol* **17**, 474-502 (2020). https://doi.org:10.1038/s41569-020-0348-1
101 Gammella, E., Maccarinelli, F., Buratti, P., Recalcati, S. & Cairo, G. The role of iron in anthracycline cardiotoxicity. *Front Pharmacol* **5**, 25 (2014). https://doi.org:10.3389/fphar.2014.00025
102 Cole, D. C. & Frishman, W. H. Cardiovascular Complications of Proteasome Inhibitors Used in Multiple Myeloma. *Cardiol Rev* **26**, 122-129 (2018). https://doi.org:10.1097/CRD.0000000000000183
103 Fabarius, A. *et al.* Centrosome aberrations after nilotinib and imatinib treatment in vitro are associated with mitotic spindle defects and genetic instability. *Br J Haematol* **138**, 369-373 (2007). https://doi.org:10.1111/j.1365-2141.2007.06678.x
104 Giehl, M. *et al.* Detection of centrosome aberrations in disease-unrelated cells from patients with tumor treated with tyrosine kinase inhibitors. *Eur J Haematol* **85**, 139-148 (2010). https://doi.org:10.1111/j.1600-0609.2010.01459.x
105 Sethunath, V. *et al.* Targeting the Mevalonate Pathway to Overcome Acquired Anti-HER2 Treatment Resistance in Breast Cancer. *Mol Cancer Res* **17**, 2318-2330 (2019). https://doi.org:10.1158/1541-7786.MCR-19-0756
106 Bienengraeber, M. *et al.* ABCC9 mutations identified in human dilated cardiomyopathy disrupt catalytic KATP channel gating. *Nat Genet* **36**, 382-387 (2004). https://doi.org:10.1038/ng1329
107 Dupont, E. *et al.* Altered connexin expression in human congestive heart failure. *J Mol Cell Cardiol* **33**, 359-371 (2001). https://doi.org:10.1006/jmcc.2000.1308
108 Perea-Gil, I. *et al.* Serine biosynthesis as a novel therapeutic target for dilated cardiomyopathy. *Eur Heart J* **43**, 3477-3489 (2022). https://doi.org:10.1093/eurheartj/ehac305
109 Gorabi, A. M. *et al.* Statins Attenuate Fibrotic Manifestations of Cardiac Tissue Damage. *Curr Mol Pharmacol* **14**, 782-797 (2021). https://doi.org:10.2174/1874467214666210210123206
110 Okuyama, H. *et al.* Statins stimulate atherosclerosis and heart failure: pharmacological mechanisms. *Expert Rev Clin Pharmacol* **8**, 189-199 (2015). https://doi.org:10.1586/17512433.2015.1011125
111 Rotariu, D. *et al.* Oxidative stress - Complex pathological issues concerning the hallmark of cardiovascular and metabolic disorders. *Biomed Pharmacother* **152**, 113238 (2022). https://doi.org:10.1016/j.biopha.2022.113238
112 Groenendyk, J., Sreenivasaiah, P. K., Kim, D. H., Agellon, L. B. & Michalak, M. Biology of endoplasmic reticulum stress in the heart. *Circ Res* **107**, 1185-1197 (2010). https://doi.org:10.1161/CIRCRESAHA.110.227033
113 Medamana, J., Clark, R. A. & Butler, J. Platelet-Derived Growth Factor in Heart Failure. *Handb Exp Pharmacol* **243**, 355-369 (2017). https://doi.org:10.1007/164_2016_80
114 Cheng, M., Park, H., Engelmayr, G. C., Moretti, M. & Freed, L. E. Effects of regulatory factors on engineered cardiac tissue in vitro. *Tissue Eng* **13**, 2709-2719 (2007). https://doi.org:10.1089/ten.2006.0414
115 Vantler, M. *et al.* PDGF-BB protects cardiomyocytes from apoptosis and improves contractile function of engineered heart tissue. *J Mol Cell Cardiol* **48**, 1316-1323 (2010). https://doi.org:10.1016/j.yjmcc.2010.03.008
116 McGrath, M. F., de Bold, M. L. & de Bold, A. J. The endocrine function of the heart. *Trends Endocrinol Metab* **16**, 469-477 (2005). https://doi.org:10.1016/j.tem.2005.10.007
117 Ding, K., Gui, Y., Hou, X., Ye, L. & Wang, L. Transient Receptor Potential Channels, Natriuretic Peptides, and Angiotensin Receptor-Neprilysin Inhibitors in Patients With Heart Failure. *Front Cardiovasc Med* **9**, 904881 (2022). https://doi.org:10.3389/fcvm.2022.904881

118 Ong, S. G. & Hausenloy, D. J. Hypoxia-inducible factor as a therapeutic target for cardioprotection. *Pharmacol Ther* **136**, 69-81 (2012). https://doi.org:10.1016/j.pharmthera.2012.07.005

119 Kubin, T. *et al.* The Role of Oncostatin M and Its Receptor Complexes in Cardiomyocyte Protection, Regeneration, and Failure. *Int J Mol Sci* **23** (2022). https://doi.org:10.3390/ijms23031811

120 Wang, P. *et al.* The alteration of Hippo/YAP signaling in the development of hypertrophic cardiomyopathy. *Basic Res Cardiol* **109**, 435 (2014). https://doi.org:10.1007/s00395-014-0435-8

121 Horn, M. A. & Trafford, A. W. Aging and the cardiac collagen matrix: Novel mediators of fibrotic remodelling. *J Mol Cell Cardiol* **93**, 175-185 (2016). https://doi.org:10.1016/j.yjmcc.2015.11.005

122 Baiocchini, A. *et al.* Extracellular Matrix Molecular Remodeling in Human Liver Fibrosis Evolution. *PLoS One* **11**, e0151736 (2016). https://doi.org:10.1371/journal.pone.0151736

123 Shangzu, Z. *et al.* Aquaporins: Important players in the cardiovascular pathophysiology. *Pharmacol Res* **183**, 106363 (2022). https://doi.org:10.1016/j.phrs.2022.106363